Architecture
and the
Built environment

#12
2018

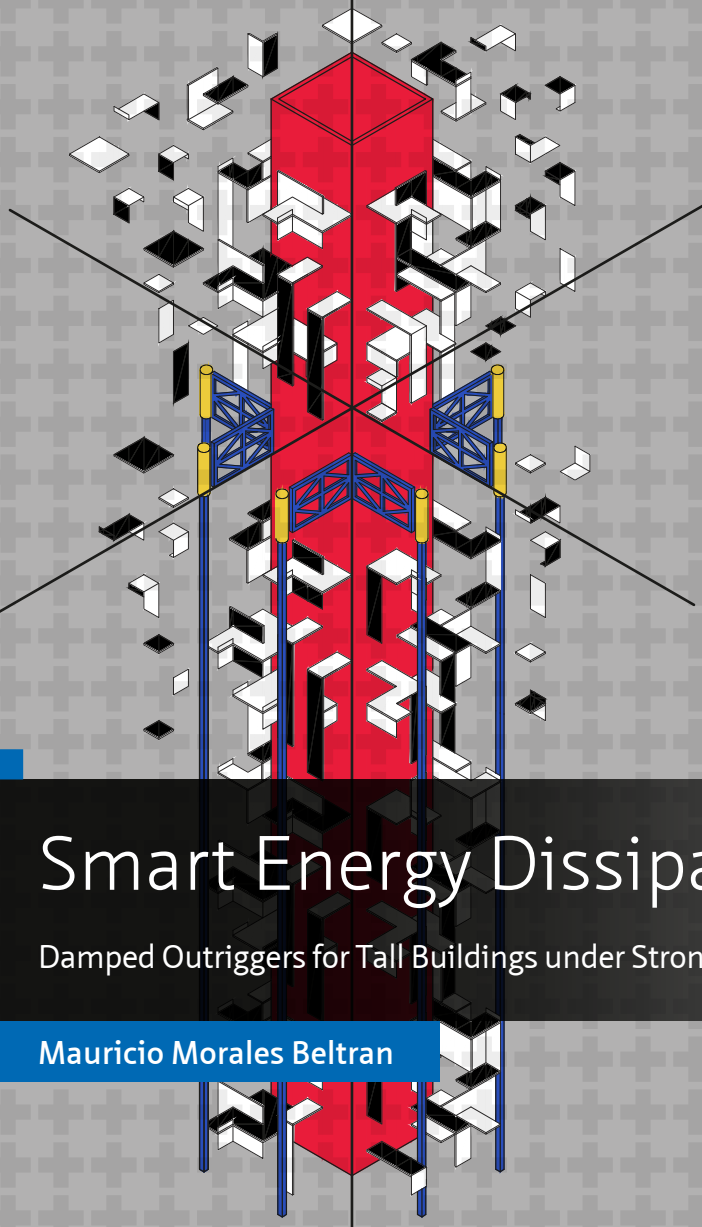

Smart Energy Dissipation

Damped Outriggers for Tall Buildings under Strong Earthquakes

Mauricio Morales Beltran

Smart Energy Dissipation

Damped Outriggers for Tall Buildings under Strong Earthquakes

Mauricio Morales Beltran
Delft University of Technology, Faculty of Architecture and the Built Environment, Department of Architectural Engineering + Technology

Architecture
and the
Built environment

abe.tudelft.nl

Design: Sirene Ontwerpers, Rotterdam

Cover image: Designed by Irem Bozdağlı and Mauricio Morales Beltran, the cover image conceptually represents a tall building with damped outriggers dissipating seismic energy. The drawing, which is based on one of the several FE models developed in the course of this research, displays the colours and geometrical patterns explored by De Stijl movement.

ISBN 978-94-6366-042-6
ISSN 2212-3202

© 2018 Mauricio Morales Beltran

All rights reserved. No part of the material protected by this copyright notice may be reproduced or utilized in any form or by any means, electronic or mechanical, including photocopying, recording or by any information storage and retrieval system, without written permission from the author.

Unless otherwise specified, all the photographs in this thesis were taken by the author. For the use of illustrations effort has been made to ask permission for the legal owners as far as possible. We apologize for those cases in which we did not succeed. These legal owners are kindly requested to contact the publisher.

To my son Facundo

**"...earthquake is supposed to be a natural disaster, but it's not natural.
It's a one man-made disaster, because people are not killed by earthquakes.
People are killed by the collapse of the building,
so that is our responsibility as architects..."**

*Shigeru Ban, Pritzker Architecture Prize, acceptance speech
Rijksmuseum, Amsterdam, June 14, 2014.*

Acknowledgements

I want to express my sincere gratitude to Rob Nijsse for his pragmatic supervision during these last months. I would also like to thank former supervisors Joop Paul and Patrick Teuffel for their guidance during the previous years of research. I also thank Gürsoy Turan for his constant willingness to revise my work for improvement.

I would like to thank the committee members Sevil Sariyildiz, Patrick Teuffel, Simon Wijte, Fred Veer and Andy van den Dobbelsteen for reading this dissertation and commenting on it. Special thanks to Sevil and Andy for their support and encouragement.

Special thanks to Andrew Charleson, Tomas Guendelman, Sergio Tapia, and Thaleia Konstantinou for their helpful review of some of the chapters of this dissertation. I would like to thank Peter Eigenraam, for the great support when setting models and analyses in Diana and kindly translating the summary of this dissertation to Dutch.

I would like to thank my colleagues at the Faculty of Architecture, Yaşar University, for giving me the opportunity to continue practicing my passion as an instructor and for providing me a hectic environment for writing this dissertation. My deepest gratitude to Elif Esra Aydin for her joyful encouragement. A big thank to Nur Yemişçi, Pinar Adanir and Irem Bozdağli for their great help with some of the drawings used in this dissertation.

I would like to thank Véro Crickx for turning these highly unformatted scribbles into a handsome book.

The support from colleagues and friends at TU Delft is been always very much appreciated. Many thanks to Alejandro and Luz Maria for providing me a nice place to stay, every time I was back in Delft, during the past four years. Many thanks too to Bo for her cheerful help through all these years. Special thanks to Michela and Thaleia for the support and keeping me connected with the rest of the world during my biking trips. Many thanks to the Persian Army: Pirouz, Sama and Sina for the good times and dreams about a better world.

I am grateful to my former colleagues at the Faculty of Architecture, *Universidad Catolica del Norte*, Carlos Miranda and Jose Guerra, for their honest interest in the development of my research. Special thanks to Emilia and Jacqueline for their always cheerful messages.

Foremost, I want to express my deepest gratitude to my family for their love and constant encouragement (*besos, abrazos, palmetazos por doquier y cabezaso a cabezoncito*).

Finally, I am truly indebted to James Hetfield, Mikael Akerfeldt, David Gilmour, Roger Waters, and Mike Patton for providing me with inspiration and peace of mind during these seven years of hard work.

Contents

List of Tables 20
List of Figures 22
List of symbols and abbreviations 29
Summary 33
Samenvatting 39

1 Introduction to the research 45

1.1 Research motivation 45

1.1.1 Smart integration of damping devices in tall buildings for reducing structural response 45
1.1.2 Strong earthquake energy dissipation in tall buildings through damped outriggers 47

1.2 Problem statement 48

1.2.1 How much seismic energy is dissipated by the dampers? 48

1.3 Research Objectives 49

1.3.1 Main research question 49
1.3.2 Secondary research questions 49
1.3.3 Hypothesis 50

1.4 Scope 50

1.4.1 Type of dampers used in the damped outriggers 50
1.4.2 Less is more: integration is understood as obtaining better performance with fewer devices 51
1.4.3 Tall buildings under strong earthquakes 51

1.5 Approach and methodology 54

1.5.1 Dissipation of seismic energy in tall buildings equipped with damped outriggers 54
1.5.2 Numerical Investigations using MATLAB 56
1.5.3 Finite Element Models in DIANA 56

1.6 Thesis outline 57

2 State of the Art in the Design of Damped Outriggers 61

2.1 Summary 61

2.2 Introduction 61

2.3 Conventional outrigger system (fixed) 62

2.4 The damped outrigger concept 65

2.4.1 Passive damped outriggers 65
2.4.2 Semiactive damped outriggers 67

2.5 Design of damped outriggers 68

2.5.1 Intrinsic damping in tall buildings versus additional damping 68
2.5.2 Purpose of the damped outrigger system 72
2.5.3 Optimal location of the outriggers 74
2.5.4 Damping coefficient 77
2.5.5 Stiffness core-to-column ratio 79
2.5.6 Stiffness core-to-outrigger ratio 81

2.6 Conclusions 83

3 Energy-based Design Methods 87

3.1 Summary 87

3.2 Introduction 87

3.3 Absolute and relative energy equations for a SDOF system 89

3.3.1 Derivation of absolute energy equation 90
3.3.2 Derivation of relative energy equation 91

3.4 Relative energy balance equation of a MDOF system 91

3.4.1 Use of the relative energy equation in this thesis 91
3.4.2 Derivation of relative energy balance equation for a MDOF system 93

3.5 Energy-based design of buildings 95

3.5.1 Towards an energy-based design of tall buildings with supplemental damping devices 96
3.5.2 Ratios of damping-to-input energy and hysteretic-to-input energy as indicators of structural performance 97
3.5.3 Assessment of the hysteretic energy 98

3.6 Computations of energy using a FE model 99

3.6.1 Normalized Cumulative Energy in Diana 99
3.6.2 Strain and hysteretic energy stored by elements under axial forces 101
3.6.3 Strain and hysteretic energy stored by elements under bending moments 102
3.6.4 Cumulative absorbed energy by a structure subjected to a transient loading 104

3.7 Conclusions 107

4 Parametric study on optimal outrigger structures 111

4.1 Summary 111

4.2 Introduction 112

4.3 Preliminary static design of tall buildings with outriggers 114

4.3.1 Simplified analysis using wind-loading 114
4.3.2 Simplified analysis using earthquake loading 115
4.3.3 Prototype model in Diana 118
4.3.4 Comparison of results 119

4.4 Outrigger design 120

4.4.1 Design force 121
4.4.2 Outrigger definition 122
4.4.3 Modelling assumptions 124
4.4.4 Outrigger design proposals 125
4.4.5 Nonlinear static analysis (pushover) 127

4.5 Nonlinear time-history response analyses 130

4.5.1 Finite element (FE) models with conventional and damped outriggers 131
4.5.2 Nonlinear setting and plasticity models for core and outrigger elements in Diana 134
4.5.3 Modal response and inherent damping ratios 136
4.5.4 Long-period earthquakes 138
4.5.5 Consideration of lateral confinement and uniform distribution of longitudinal reinforcement in the modelling of the core 139

4.6 Factors affecting the performance of damped outriggers 142

4.6.1 Frequency versus height of the building 142
4.6.2 Outrigger location (λ) 143
4.6.3 Optimal dampers' damping coefficient (C_d) 147
4.6.4 Stiffness core-to-outrigger ρ_{cto} and core-to-column ρ_{ctc} ratios 150

4.7 Conclusions 155

5 Seismic energy distribution in passive single damped outriggers 159

5.1 Summary 159

5.2 Introduction 159

5.3 Assessment of the distribution of seismic energy in a tall building 161

5.3.1 Methodology 163
5.3.2 Long-period earthquakes 164

5.4 Energy dissipation under different levels of ground motion 167

5.4.1 Outrigger systems subjected to small - moderate earthquakes 167
5.4.2 Outrigger systems subjected to strong earthquakes 169
5.4.3 Outrigger systems subjected to severe earthquakes 172

5.5 Inherent and supplemental damping versus hysteresis energy ratios 176

5.5.1 Elastic response 176
5.5.2 Inelastic response 177

5.6 Seismic energy distribution per element 180

5.6.1 Core 180
5.6.2 Outriggers 182

5.7 Comparative performance fixed – damped outrigger systems 184

5.7.1 Inter-storey drift 184
5.7.2 Peak accelerations 184
5.7.3 Base shear 185
5.7.4 Overturning moment versus yielding stress 186

5.8 Discussion 188

5.8.1 Distribution of energy in conventional and damped outriggers 188
5.8.2 Distribution of energy under strong earthquakes 190
5.8.3 Hysteretic energy and frequency content of the ground motions 193
5.8.4 Comparative performance between fixed and damped outriggers 196

5.9 Conclusions 197

6 Energy dissipation and performance assessment of double damped outriggers in tall buildings under strong earthquakes 199

6.1 Summary 199

6.2 Introduction 200

6.3 Methodology 201

6.3.1 Analytical models 201
6.3.2 Optimal increase of inherent damping ratio (ζ) through free vibration analyses 202
6.3.3 Energy balance equations 203
6.3.4 Assessment of the distribution of seismic energy in a tall building 204
6.3.5 Earthquake Levels 205

6.4 Optimal damping ratio (ζ) under fee vibration 207

6.4.1 Single damped outrigger 207
6.4.2 Double damped outriggers 208
6.4.3 Double fixed outriggers 209
6.4.4 Combined damped and fixed outriggers 210
6.4.5 Combined fixed and damped outriggers 211

6.5 Energy dissipation under strong earthquakes 212

6.5.1 Single damped outriggers 212
6.5.2 Double damped outriggers 213
6.5.3 Combined damped and fixed outriggers 215

6.6 Decrease in structural response 216

6.6.1 Peak inter-storey drift 216
6.6.2 Peak accelerations 217
6.6.3 Base shear 217
6.6.4 Stresses and overturning moment 218

6.7 Simplified economic evaluation 221

6.7.1 Results of economic evaluation 223
6.7.2 Pushover Analyses 226

6.8 Discussion 228

6.8.1 Optimal configurations for increasing the inherent damping ratio ζ 228
6.8.2 Optimal configurations for reducing the hysteretic energy 228
6.8.3 Hysteretic energy and frequency content of the ground motions 230
6.8.4 Optimal configurations for reducing the overall structural response 232

6.9 Conclusions 235

7 Integrated discussion: towards an energy-based seismic design of tall buildings with damped outriggers 237

7.1 Summary 237

7.2 Introduction 237

7.3 Parameters influencing the distribution of energy in an outrigger system 239

7.3.1 Damping coefficient of the dampers 239
7.3.2 Number and position of the outriggers 240
7.3.3 Modal damping and damping ratios 241
7.3.4 Stiffness core-to-columns and core-to-outriggers ratios 241
7.3.5 Feasibility of supplying the required control force 242
7.3.6 Optimal design of damped outriggers 243

7.4 Assessment of the energy demands due to strong-earthquake induced motion 244

7.5 Assessment of the energy capacity of tall buildings with damped outriggers 246

7.5.1 Energy dissipated by the core 246
7.5.2 Energy dissipated by the outrigger 247
7.5.3 Energy dissipated by the perimeter columns 247
7.5.4 Energy dissipated by the dampers 248

7.6 Research question revisited: design for elasticity? 249

7.6.1 Damping (f)or damage? 249
7.6.2 Strategies to extend the elastic response threshold of viscous damped outrigger systems 251

7.7 Slenderness and plan design of tall buildings with damped outriggers 252

7.7.1 Slenderness and aspect ratio of tall buildings 252
7.7.2 Building plan incorporating outriggers 253

7.8 Conclusions 254

8 Conclusions 257

8.1 Summary 257

8.2 Introduction 257

8.3 Conclusions from the parametric analyses 258

8.3.1 Optimal damping coefficient C_d and optimal location λ are the most influential design parameters 258
8.3.2 There is no optimal design for all the cases 259
8.3.3 The distribution of energy is determined by the type of nonlinear modelling 259

8.4 Conclusions from the analyses of viscous damped outrigger systems 260

8.4.1 Viscous damped outrigger systems reduce the damage potential under strong earthquakes 260
8.4.2 No optimal damped outrigger configuration can reduce completely the damage during strong earthquakes 261
8.4.3 The main source of hysteretic energy dissipation is the core 261

8.5 Conclusions from the analyses of double damped outrigger systems 262

8.5.1 Under certain conditions, double damped outriggers overpass the performance of single damped outriggers 262
8.5.2 Optimal double damped outrigger systems offer flexibility of design and cost-saving 263

8.6 Recommendations 263

8.6.1 Large scale experimental testing 264
8.6.2 Architectural considerations 264
8.6.3 Topology optimization of damped outriggers 265

Appendix A Strain and hysteretic energy stored by elements under shear forces 267
Appendix B Comparative floor-by-floor seismic equivalent lateral forces 269
Appendix C Matlab scripts 271
Appendix D Diana files 291
Appendix E Peak responses – Single, double and combined damped outrigger systems 297
Appendix F Average distance between central core and perimeter columns in Chilean office buildings 305

Curriculum Vitae 307
List of publications 309

List of Tables

3.1 Preliminary results 106

4.1 Properties of model elements and materials used in the Diana model 119

4.2 Top storey displacement responses and axial forces with columns=0.4m^2, chords=0.04 m^2, and braces=0.03 m^2 120

4.3 Top storey displacement responses and axial forces with columns=0.8m^2, chords=0.20 m^2, and braces=0.15 m^2 120

4.4 Strength demand of the outrigger 121

4.5 Frequencies obtained for both models 124

4.6 Steel profiles used in each of the outrigger designs (in mm) 126

4.7 Summary of results showing designs arranged according to their linear stiffness 127

4.8 Results of nonlinear analyses 129

4.9 Expected gravity load for determining the storey mass applied on the model (all values are in kN) 132

4.10 Effective mass participation in X direction 136

4.11 Effective mass participation in Y direction 137

4.12 Scaled PGA-PGV of four earthquake levels of El Centro ground motion record 138

4.13 Correlation of modelling parameters organized per model 140

5.1 Selected ground motions and factors chosen to scale them to the four earthquake levels used in this study. 165

5.2 Distribution of seismic energy [kN-m] in the studied outrigger configurations 189

5.3 Energy Ratios of the damped and fixed outrigger systems 192

5.4 Ground motions organized from most to less damaging and their corresponding hysteretic and input energies. F and D are fixed and damped outrigger systems, respectively. 195

5.5 % of damping energy absorbed by the outrigger in the studied configurations 196

6.1 Selected ground motions and factors chosen to scale them to the four earthquake levels used in this study. 205

6.2 Effective modal mass participation in X direction 222

6.3 Effective modal mass participation in Y direction 222

6.4 Required *horizontal* reinforcement steel values in the building core 223

6.5 Required *vertical* reinforcement steel values in the building core 224

6.6 Supply of dampers according to the required damping coefficients (C_d's) 225

6.7 Comparative cost analysis among structural design alternatives 225

6.8 Peak energy dissipation ratios (trend line-based), for each configuration under all earthquake levels. 230

6.9 Ground motions organized from most to less damaging and their corresponding hysteretic and input energies. F, D, d, and c are fixed, damped, double, and combined outrigger systems, respectively. 231

6.10 Average Normalized Peak Inter-storey Drifts 232

6.11 Average Normalized Peak Accelerations 233

6.12 Average Normalized Peak Base Shear 233

6.13 Average Normalized Peak Stresses 234

6.14 Average Normalized Peak Overturning Moment 234

7.1 Comparative core sizes in 200m office buildings, located in Chile, Germany and USA. 253

7.2 Usable space depth according to the location of the building 254

List of Figures

1.1 Viscous dampers integrated in a braced frame system (left) and a tuned mass damper hanging from the Taipei 101 building's roof (right). Sources: *engineeringfeed.com* and *civil-engg-world.blogspot.nl*, respectively. 46

1.2 Damped Outrigger concept, as originally proposed by Smith & Willford (2007) - Reprinted with permission of the publisher 47

1.3 Tall buildings in selected cities located in seismic regions around the world. Source: Skyscraperpage.com 53

1.4 Relative top storey lateral displacement of a 200 m tall building under Izmit-Kocaeli Earthquake, without outriggers (cantilever), with conventional outriggers (fixed), and with damped outriggers (damped). 54

1.5 Thesis outline 58

2.1 Main elements of an outrigger structural system (a); its structural behaviour under wind loading (b); with its resultant deflections (c) and core moments (d) [adapted from Smith and Coull (1991)] 63

2.2 Alternative outriggers - core configurations: outriggers at only one side of the core in a 200m 40-storey office building (left) and outriggers extending in diagonal on the building's corners in a 200m 42-storey building (right). Both located in Izmir, Turkey (Photographies by the author) 63

2.3 Damped Outrigger concept, as originally proposed by Smith and Willford (2007) - Reprinted with permission of the publisher 66

2.4 Common types of damper devices: (a) oil, (b) viscous, (c) viscoelastic and (d) steel damper (adapted from Kibayashi *et al.* (2004)) 66

2.5 Damping measurements of (a) steel buildings, (b) steel-reinforced concrete buildings, (c) reinforced concrete buildings and (d) reinforced concrete chimneys. Image source: Smith *et al.*, 2010 - Reused with permission of the publisher. 70

2.6 Identified damping ratios for the fundamental mode versus building height, compared to some proposed recommendations: (a) steel buildings; (b) reinforced concrete buildings. Image source: Cruz and Miranda, 2017 - With permission from ASCE 71

2.7 Damping force versus damper velocity for BDH oil viscous damper (source: Kayaba System Machinery Co. Ltd) 73

2.8 Analytical model of a conventional outrigger system 74

2.9 Optimal outrigger location for one-outrigger-system as proposed by Smith and Coull (1991) 75

2.10 Optimal location of outrigger at different outrigger span *b*, according to Zhou *et al.* (2016) 76

2.11 Example of the use of pipelines and service areas located at the outrigger storey (50-storey building in Izmir; photography by the author) 77

2.12 Cantilever beam with damped outriggers. Adapted from Chen *et al.* (2010) 78

2.13 (a) simplified model and (b) general rotational stiffness model. Adapted from Tan *et al.* (2014) 79

2.14 Different configurations of damped (a), undamped (d) and combined damped and undamped outrigger systems (b-c). Adapted from Fang *et al.* (2015) 80

2.15 The criteria discussed for the selection of the racking shear stiffness of the outrigger 82

3.1 Analytical model of a SDOF system subjected to ground motion. Adapted from Uang and Bertero (1990) 90

3.2 Typical energy distribution of an inelastic system with viscous damper under strong ground motions 96

3.3 Step-wise computation of energy 100

3.4 Strain energy for an inelastic system defined by F-Δ (left) and the equivalent σ - ε (right) 101

3.5 Analytical model of an element subjected to bending moments 103

3.6 Strain energy for an inelastic system defined by M - θ 104

3.7 Example of the computation of the cumulative energy in a structure subjected to a transient loading 105

4.1 36m square building plan, based on a 9m grid. Note that the outriggers are not loading all the perimeter columns. 114

4.2 Comparative floor-by-floor seismic equivalent lateral forces according to NCh433 and UBC1994 including (a) 60 storeys; (b) between 51st and 59th storey; and, (c) the first 50 storeys 117

4.3 Structural components and 3D model utilized in Diana 118

4.4 Feasible configurations of the truss-girder outrigger with one bay (a); two bays (b); three bays (c); and selected configuration displaying overall dimensions (d). 123

4.5 K-braced (left) and X-braced (right) truss girder outriggers 123

4.6 Loading and support conditions of the outrigger model (left) and FE model (right) 125

4.7 Outrigger elements 126

4.8 Correlation between pushover curve and the steps in the nonlinear analysis for node 21 (at the end of the outrigger) 128

4.9 Plasticity status distribution in the outrigger: first at the braces (red circles), second at horizontal chords (blue circles), and finally at vertical chords (green circles) 130

4.10 Typical plan for the fixed (a) and damped (b) outrigger building models 133

4.11 Structural elements used in the nonlinear modelling of the damped outrigger in Diana-FEA 135

4.12 Conversion scheme box-to-I shape cross section of the core. Integration/stress points are depicted for each integration zone. 135

4.13 Predominant mode shapes of the fixed (upper row) and damped (lower row) outrigger system depicting variations due to the combined influence of outrigger location and core-to-outrigger and core-to-column stiffness ratios (9x5x5 parameters = 225 modal shapes in each plot). 137

4.14 Scaled strong ground motion of 1940 El Centro used in this study and its associated energy input spectra. Displayed accelerations (strong level) caused damage to the building. 139

4.15 Comparison between maximum inter-storey drift ratios of the four core modelling parameters –depicted in pairs- under four intensity levels of 1940 El Centro earthquake, at different outrigger locations (λ). Under strong and severe levels, the response is inelastic. 140

4.16 Input energy in the outrigger structure, modelled with combined core parameters, when subjected to four intensity levels of 1940 El Centro earthquake. 141

4.17 Δ_e (%) between energy distributions obtained with a non-uniform (*n*) and uniform (*u*) distribution of longitudinal reinforcement under strong and severe intensity levels of 1940 El Centro earthquake. Note that vertical scale is different for each plot. 141

4.18 IBC 2006 design response spectrum 142

4.19 Acceleration response spectrum for Mexico Earthquake - component NW 143

4.20 Increased ζ due to the combined influence of λ (0.1– 0.9) and dampers size, under free vibration. 144

4.21 Normalized (actual/peak) drift, velocity and lateral accelerations for different outrigger locations (λ=0.4 – 0.9), of the damped outrigger building (ζ=2%, C_d=1.18E+05kN-s/m) subjected to four intensity levels of 1940 El Centro earthquake 145

4.22 Normalized (actual/peak) base shear and overturning moments of the damped outrigger building (ζ=2%, C_d=1.18E+08kN-s/m), subjected to four intensity levels of 1940 El Centro earthquake, with different outrigger locations (λ=0.4 – 0.9). 145

4.23 Normalized (actual/maximum) energy distributions of the outrigger structure (ζ=2% - C_d=1.18E+05kN-s/m) according to outrigger location (λ=0.4 – 0.9) under four intensity levels of 1940 El Centro earthquake. 146

4.24 Frequency-based vertical displacements of the nodes outrigger-damper (nOD) and damper-column (nDC) for different damping coefficients of the viscous damper (in kN-s/m). 148

4.25 Optimal ζ according to values of λ between 0.4 and 0.9 149

4.26 Configuration of eight outriggers with one (a), two (b), and four (c) dampers 149

4.27 Distribution of ζ (in %) according to variable parameters ρ_{ctc}=1 – 4, C_d = 2.40E+04 – 6.72E+05 kN-s/m, and λ = 0.4 – 0.9, under free vibration. Inherent ζ = 2% 151

4.28 Distribution of ζ (in %) according to initial ζ = 1.5, 2.0, and 2.5%; ρ_{ctc}, ρ_{cto} = 1 – 4; λ= 0.7 under free vibration. 152

4.29 Shifts in 1st mode period due to the combined effect of ρ_{cto} and ρ_{ctc} on the fixed and 1.18E+05kN-s/m damped outrigger structure; λ=0.7 and ζ=1.5%. 153

4.30 Influence of λ on the period shifts of the fixed and damped outrigger. Data points correspond to couples ρ_{cto}=ρ_{ctc} = 1, 2.5, and 4. 153

4.31 Variations of the Normalized Input Energy ($E_I\rho/E_{Imax}$), according to combined effect of ρ_{cto} and ρ_{ctc}, under different earthquake levels of 1940 El Centro earthquake; C_d= 1.18E+05kN-s/m, λ=0.7 and ζ=1.5%. 154

5.1 Five (out of eight) scaled ground motion records used in this study. Displayed accelerations, corresponding to strong earthquake level, caused damage to the single damped outrigger structure. 165

5.2 Two (out of eight) scaled ground motion records used in this study. Displayed accelerations, corresponding to severe earthquake level, caused damage to the single damped outrigger structure. 166

5.3 One of the eight scaled ground motion records used in this study. Displayed accelerations, corresponding to severe earthquake level, did not cause damage to any of the outrigger structures. 166

5.4 Input energy (E_I) of damped and fixed outrigger systems under moderate earthquake levels 167

5.5 Damping energy (E_D) and hysteretic energy (E_H) of damped and fixed outrigger systems under moderate earthquake levels 168

5.6 Dampers energy ($E_{dampers}$) of damped outrigger systems under moderate earthquake levels 168

5.7 Strain elastic energy (E_S) and kinetic energy (E_K) of damped and fixed outrigger systems under moderate earthquake levels 170

5.8 Input energy (E_I) of damped and fixed outrigger systems under strong earthquake levels 170

5.9 Damping energy (E_D) and hysteretic energy (E_H) of damped and fixed outrigger systems under strong earthquake levels 171

5.10 Dampers energy ($E_{dampers}$) of damped outrigger systems under strong earthquake levels 171

5.11 Strain elastic energy (E_S) and kinetic energy (E_K) of damped and fixed outrigger systems under strong earthquake levels 172

5.12 Input energy (E_I) of damped and fixed outrigger systems under severe earthquake levels 173

5.13 Dampers energy ($E_{dampers}$) of damped outrigger systems under severe earthquake levels 173

5.14 Damping energy (E_D) and hysteretic energy (E_H) of damped and fixed outrigger systems under severe earthquake levels 174

5.15 Strain elastic energy (E_S) and kinetic energy (E_K) of damped and fixed outrigger systems under severe earthquake levels 175

5.16 Energy ratios of the outrigger systems under small earthquake levels 176

5.17 Energy ratios of the outrigger systems under moderate earthquake levels 177

5.18 Energy ratios of the outrigger systems under strong earthquake levels 178

5.19 Energy ratios of the outrigger systems under severe earthquake levels 179

5.20 Distribution of the hysteretic energy dissipated by the core of the damped outrigger 180

5.21 Distribution of the hysteretic energy dissipated by the core of the fixed outrigger 181

5.22 Normalized hysteretic energy dissipated by the core under severe level of Izmit-Kocaeli, 1940 El Centro, and New Zealand earthquakes. The five core elements displayed dissipated up to 50, 51 and 41% of the total hysteretic energy for each earthquake, respectively. (C_d= 1.18E+05kN-s/m, λ=0.7 and ζ=2.0%) 181

5.23 Damping energy (in %) dissipated only by the outriggers, under the combined influence of λ and different earthquake levels of 1940 El Centro earthquake; C_d= 1.18E+05kN-s/m and ζ=2.0%. 182

5.24 Damping energy dissipated by the outrigger in the damped (left) and fixed (right) system 183

5.25 Percentage of the total damping energy that is dissipated by the outrigger in the damped (left) and fixed (right) system 183

5.26 Normalized peak inter-storey drifts of the studied outrigger configurations 184

5.27 Peak accelerations of the studied outrigger configurations 185

5.28 Normalized base shear (V/W) of the studied outrigger structures subjected to four earthquake levels of all ground motions 185

5.29 Normalized *core* stress (σ/σ_{yield}) to normalized overturning moment ($M\theta/M\theta_{-max}$) of the damped outrigger configurations subjected to four earthquake levels of all ground motions 186

5.30 Normalized *core* stress (σ/σ_{yield}) to normalized overturning moment ($M\theta/M\theta_{-max}$) of the fixed outrigger configurations subjected to four earthquake levels of all ground motions 187

5.31 Normalized *outrigger* stress (σ/σ_{yield}) to normalized overturning moment ($M\theta/M\theta_{-max}$) of the studied outrigger configurations subjected to four earthquake levels of all ground motions 187

5.32 Normalized *column* stress (σ/σ_{yield}) to normalized overturning moment ($M\theta/M\theta_{-max}$) of the studied outrigger configurations subjected to four earthquake levels of all ground motions. 188

5.33 Energy distribution of the fixed and 1.18E+05kN-s/m damped outrigger structures under small and moderate levels of Izmit-Kocaeli earthquake (λ=0.7 and ζ=2.0%). 189

5.34 Energy distribution of the fixed and 1.18E+05kN-s/m damped outrigger structures under strong and severe levels of Izmit-Kocaeli earthquake (λ=0.7 and ζ=2.0%). 190

5.35 Energy ratios based on E_I and $E_D+E_{dampers}+E_H$, for the damped outrigger under strong earthquake level of 1940 El Centro earthquake; C_d= 1.18E+05kN-s/m, λ=0.7 and ζ=2.0%. 191

5.36 Energy Ratios of the damped outrigger (C_d= 1.18E+05kN-s/m, λ=0.7 and ζ=2.0%), under strong and severe levels of 1940 El Centro and New Zealand – Greendale earthquakes 192

6.1 Analytical outrigger building models: (a) single damped; (b) double damped; (c) double fixed; (d) combined damped and fixed; and, (e) combined fixed and damped. 201

6.2 Five (out of eight) scaled ground motion records used in this study. Displayed accelerations, corresponding to strong earthquake level, caused damage to the single damped outrigger structure. 206

6.3 Two (out of eight) scaled ground motion records used in this study. Displayed accelerations, corresponding to severe earthquake level, caused damage to the single damped outrigger structure. 206

6.4 One of the eight scaled ground motion records used in this study. Displayed accelerations, corresponding to severe earthquake level, did not cause damage to any of the outrigger structures. 207

6.5 Optimal ζ in absolute values under a single damped outrigger configuration 208

6.6 Optimal ζ (absolute values) under a double damped outrigger configuration (C_d outrigger 1 = 1.68E+05kN-s/m) and C_d distribution according to optimal λ combinations. 209

6.7 Optimal ζ (absolute values) under a double fixed outrigger configuration 210

6.8 Optimal ζ (absolute values) under a combined damped (λ_1) and fixed outrigger (λ_2) configuration and C_d distribution according to optimal λ combinations 210

6.9 Optimal ζ (absolute values) under a combined fixed (λ_1) and damped outrigger (λ_2) configuration and C_d distribution according to optimal λ combinations 211

6.10 Energy dissipation ratios of the *single* damped outrigger under strong (upper row) and severe (lower row) levels of the selected eight earthquakes. 213

6.11 Energy dissipation ratios of the *double* damped outrigger under strong (upper row) and severe (lower row) levels of the selected eight earthquakes. 214

6.12 Energy dissipation ratios of the *combined* damped and fixed outrigger under strong (upper row) and severe (lower row) levels of the selected eight earthquakes. 215

6.13 Normalized peak inter-storey drifts of the studied outrigger configurations. 216

6.14 Normalized peak accelerations of the studied outrigger configurations. 217

6.15 Normalized base shear (V/W) of the studied outrigger structures subjected to four earthquake levels of all ground motions. 218

6.16 Normalized *core* stress (σ/σ_{yield}) to normalized overturning moment ($M\theta/M\theta_{-max}$) of the single (upper row), double (middle row) and combined (lower row) outrigger configurations subjected to four earthquake levels of all ground motions. 219

6.17 Normalized *outrigger* stress (σ/σ_{yield}) to normalized overturning moment ($M\theta/M\theta_{-max}$) of the studied outrigger configurations subjected to four earthquake levels of all ground motions. 220

6.18 Normalized *column* stress (σ/σ_{yield}) to normalized overturning moment ($M\theta/M\theta_{-max}$) of the studied outrigger configurations subjected to four earthquake levels of all ground motions. 220

6.19 SRSS modal storey shear and OTM moment envelopes for the three configurations of outriggers. 222

6.20 Pushover (PO) curves for Mode 1 with and without P-Delta effects 227

6.21 Comparison between pushover (PO) curves - Modes 1 & 2, without P-Delta effect 227

7.1 Typical arrangement of frame outrigger used in this research (a) and possible combinations of dampers (b). 240

7.2 Scaled ground motions and their corresponding input energy (E_I), displaying the three main periods of the structures studied. 245

7.3 Normalized *column* stress (σ/σ_{yield}) to normalized overturning moment ($M\theta/M\theta_{max}$) of the studied outrigger configurations subjected to four earthquake levels of all ground motions. 248

7.4 Distribution of seismic input energy in the cantilever, fixed, and damped outrigger models 250

7.5 Floor plans of Titanium (a), Messeturm (b), and Nations Bank Plaza (c) buildings. 253

List of symbols and abbreviations

SYMBOL	DESCRIPTION
C	damping matrix
C_d	damping coefficient of the dampers
E_A	absorbed energy
EA_c	axial stiffness of the perimeter column
E_D	damping energy
$E_{dampers}$	dampers energy
E_H	hysteretic energy
E_I	input energy
EI_c	bending stiffness of the core
EI_r	bending stiffness of the outrigger
E_K	kinetic energy
E_S	strain energy
fs	restoring force
H / h	height of the building
h_s	storey height
k	exponent (damping force)
K	stiffness matrix
M	mass matrix
M_x / Mθ	restoring moment
r	distance end of the outrigger to centroid of the core
T	period
V	shear forces
W	seismic mass
Wn	cumulative energy in Diana
x	displacement
$\dot{x}$	velocity
$\ddot{x}$	acceleration
$\ddot{x}_g$	ground acceleration
Γ	vector containing the locations where the ground acceleration affect the structural response
Δ_e	difference between peak energies
ζ	damping ratio
θ_c	cantilever rotation
λ	outrigger location height to total height ratio

>>>

SYMBOL	DESCRIPTION
Λ	vector containing the locations of the dampers
ρ_{ctc}	stiffness core-to-column ratio
ρ_{cto}	stiffness core-to-outrigger ratio
σ	stress

ABBREVIATION	DESCRIPTION
2D	two dimensional
3D	three dimensional
DOF	degree of freedom
FE	finite element
FEA	finite element analysis
L6BEN	linear structural element (Diana)
L7BEN	nonlinear structural element (Diana)
MDOF	multi-degree of freedom
MR	magneto-rheological
nDC	node connection damper-column
nOD	node connecting outrigger-damper
OTM	overturning moment
PGA	peak ground acceleration
PGV	peak ground velocity
PO	pushover
PT3T	point mass (Diana)
SDOF	single-degree of freedom
SP2TR	discrete damping point (Diana)
SRSS	square root of sum of squares
TX	X direction
TY	Y direction

Summary

The use of outriggers in tall buildings is a common practice to reduce response under dynamic loading. Viscous dampers have been implemented between the outrigger and the perimeter columns, to reduce vibrations without increasing the stiffness of the structure. This damped outrigger concept has been implemented for reducing vibrations produced by strong winds. However, its behaviour under strong earthquakes has been not yet properly investigated. Strong earthquakes introduces larger amount of energy into the building's structure, compared to moderate earthquakes or strong winds. In tall buildings, such seismic energy is dissipated by several mechanisms including bending deformation of the core, friction between structural and non-structural components, and eventually, damage.

This research focuses on the capability of tall buildings equipped with damped outriggers to undergo large deformations without damage. In other words, when the ground motion increases due to strong earthquakes, the dampers can be assumed to be the main source of energy dissipation whilst the host structure displays an elastic behaviour. These investigations are based on the assessment of both the energy demands due to large-earthquake induced motion and the energy capacity of the system, i.e. the energy capacity of the main components, namely core, outriggers, perimeter columns and dampers. The objective of this research is to determine if the energy dissipated by hysteresis can be fully replaced by energy dissipated through the action of passive dampers.

This research is based on finite element (FE) models developed in Diana-FEA software. These analytical models consider the use of nonlinear settings throughout almost the whole FE model. The numerical investigations on passive damped outriggers are based on master Matlab scripts, which run combined parametric analysis within Diana.

Parametric analyses – Chapter 4

This chapter answers the question: Which parameters influence the distribution of seismic input energy through a tall building structure equipped with damped outriggers?

The numerical investigations focus on the aspects of the modelling and the structural parameters influencing the behaviour of tall building equipped with fixed and viscous damped outriggers. This chapter also provides a parametric study to assess

the distribution of seismic energy in tall buildings equipped with viscous damped outriggers, i.e. with outriggers that have one or more viscous dampers installed between their ends and the perimeter columns. The aim of this explorative study is to determine which parameters influence (a) the structural response and (b) the distribution of seismic input energy through the building structure. First, this chapter describes a parametric study that addresses the influence of natural period of the building, position of the outriggers, damping coefficient, and stiffness core-to-outrigger and core-to-columns ratios in the control performance of the outrigger structures. Indirectly, it provides the basis for exploring which strategies will extend the elastic response threshold of a tall building equipped with viscous dampers and subjected to strong earthquake ground motions. The optimization of these parameters define pseudo-optimal configurations, which are further are assessed in terms of response reduction, namely displacement, acceleration, base shear, base moment and stress distribution; and, in terms of energy distributions. The strategy to assess the distribution of earthquake energy in tall buildings equipped with viscous damped outriggers and subjected to strong motions is based on the numerical study of 60-storey buildings equipped with conventional and damped outriggers, respectively. Secondly, this chapter describes the inter-dependency between structural properties of tall buildings equipped with damped outriggers and ground motion characteristics, which is examined under small, moderate, strong, and severe levels of the 1940 El Centro earthquake record.

Single passive damped outrigger system – Chapter 5

This chapter provides answers to the questions: How such energy is eventually dissipated by both the host structure and the viscous dampers? To which extent can hysteretic energy be completely overcome by the energy dissipated by the action of dampers?

The objective of the study presented in this chapter is to determine if the energy dissipated by hysteresis (damage) can be fully replaced by energy dissipated through the action of passive viscous dampers. More precisely, the goal is to determine whether it is correct to assume that main structural components will remain elastic during the entire strong earthquake response of a tall building, as well as which parameters mainly affect the response of damped outrigger structures and how such influence is exerted. In order to determine to which extent the use of viscously damped outriggers would avoid damage, both the host structure's hysteretic behaviour and the dampers' performance need to be evaluated in parallel. First, the time-history responses of fixed and damped outrigger structures, subjected to different levels of peak ground accelerations (PGA) of a suite of eight earthquake records, are obtained using 2D finite

element (FE) models. Using these results, the nonlinear behaviour of the outrigger system with and without viscous dampers is examined under small, moderate, strong and severe long-period earthquakes to assess the hysteretic energy distribution through the core and outriggers. Next, the distribution of seismic energy in the structures is assessed by means of the damping-to-input (E_D/E_I), dampers' damping-to-input ($E_{DAMPERS}/E_I$), and hysteretic-to-input (E_H/E_I) energy ratios; the concept of *optimal* configuration is therefore discussed in terms of reducing the hysteresis energy ratio of the structure. This assessment gives insights on which strategies will extend the elastic response threshold of a tall building equipped with viscous dampers and subjected to strong earthquake ground motions. The results show that, as the ground motion becomes stronger, viscous dampers effectively reduce the potential of damage in the structure if compared to conventional outriggers. However, the use of dampers cannot entirely prevent damage under critical excitations.

Double conventional and damped outrigger system – Chapter 6

This chapter answers the question: Which strategies will extend the elastic response threshold of a tall building equipped with viscous dampers and subjected to strong earthquake ground motions?

The use of a set of outriggers equipped with oil viscous dampers increases the damping ratio of tall buildings in about 6-10%, depending on the loading conditions. However, if a single damped outrigger structure is designed for an optimal damping ratio, could this ratio still be increased by the addition of another set of outriggers? Should this additional set be equipped with dampers too? In order to answer these questions, several double damped outrigger configurations for tall buildings are investigated and compared to an optimally designed single damped outrigger, located at elevation 0.7 of the total building's height (*h*). Using free vibration analyses, double outrigger configurations increasing damping up to a ratio equal to the single-based optimal are identified. Next, selected configurations are subjected to small, moderate, strong, and severe earthquake levels of eight ground motions to compare their capability for dissipating energy and thus avoiding damage under critical excitations. Last, a simplified economic analysis highlights the advantages of each optimal configuration in terms of steel reinforcement savings versus damper cost. The results show that combining a damped outrigger at 0.5 h with a conventional outrigger at 0.7 *h* is more effective in reducing hysteretic energy ratios and economically viable if compared to a single damped outrigger solution.

Conclusions

From the *parametric analyses* using FE models with conventional and damped outrigger systems, under free vibration, it is concluded that optimal damping coefficient C_d and optimal location λ have a major influence in the optimal damping ratio ζ. This optimal damping ratio may not necessarily imply a significant reduction in the overall response of the outrigger structure. Nevertheless, when λ and C_d approximate to the optimal values, the effect of ρ_{ctc} may imply an overall ζ increase in 7%. This suggests that if required damper sizes are not available, a modification in the ratio ρ_{ctc} will help to increase the overall damping ratio. It should be noted that such increase occurs only if ρ_{ctc} decreases.

Complementary modification of the stiffness ratios may help to improve the effect of the viscous damped outriggers in the reduction of response of the building. For example, both λ and ρ_{ctc} exert their influence by modifying the building's natural frequency. The fact that ρ_{cto} does modifies the response but not the frequency, suggests that its influence is closely related to the effect of the viscous dampers. None of the parameters under discussion, namely λ, ρ_{ctc} and ρ_{cto}, have any influence on the frequency shift of the damped outrigger, when $\lambda<0.6$. Frequency shifts become more significant as the outrigger approaches the roof.

From the numerical analyses under El Centro earthquake, it is concluded that when the outrigger is flexible (ρ_{cto} =4), E_I is comparatively large under all earthquake levels except by severe. This condition is not affected by the value of ρ_{ctc}. Under severe earthquakes, the use of a rigid outrigger (ρ_{cto} =1) implies larger amount of input energy in the system. This shift may be the result of large damping forces being linearly amplified by the high velocities of the severe motions.

From all the parametric analyses, it is concluded that regardless the optimal C_d, λ < 0.4 has less effect on improving the overall damping ratio of the building, if compared to values of λ >= 0.4. This suggests that optimal λ is somewhere between 0.4 and 0.9. Nevertheless, the optimal damping varies with the mode, so no single outrigger location will lead to reduce the response of all the modes to its minimum.

From the numerical analyses using FE models with conventional and viscous damped outrigger systems, subjected to four levels of ground motions, it was concluded that as the ground motion becomes stronger, viscous dampers effectively reduce the potential of damage in the structure if compared to conventional outriggers. The results confirm that increasing dynamic stiffness by using dampers is more effective than simply increasing stiffness by adding outriggers to reduce the overall response of core structures. The use of dampers in the outrigger seems to be effective in reducing

both kinetic and strain energies, which also explains the overall decrease in the accelerations.

In addition, the use of viscous damped outriggers under optimal design conditions, reduces the overturning moments and stresses of the main components of the system, i.e. core, outriggers and perimeter columns, under strong earthquakes –if compared to a conventional outrigger.

From the numerical analyses using FE models with conventional and viscous damped outrigger systems, subjected to four levels of ground motions, it was concluded that inter-storey drifts, peak accelerations and base shear are not substantially reduced with the addition of viscous dampers to the outriggers. These results reinforce the conclusion that no optimal configuration can be considered optimal for reducing all structural responses.

From the numerical analyses using FE models with conventional and damped outrigger systems, subjected to four levels of ground motions, it was concluded that damped outriggers cannot reduce completely the structural damage under critical earthquakes because the peak E_H/E_I usually precedes the peak $E_{dampers}/E_I$. On the other hand, since dampers increase the dissipative action of energy by damping, the energy that must be absorbed by hysteresis of the structure is reduced.

Hysteretic energy is concentrated in the core, whose damage is provoked by the overpass of the tensile strength. Hence, the core is the main dissipative source of both damping and hysteretic energy. With the addition of viscous dampers the outrigger has a minor load-bearing role. The main advantage of adding viscous dampers to the outriggers is the overall reduction of stress in the members, thus increasing ductility in the structure.

From the analyses of several configurations of double damped and combined fixed+damped outrigger systems described in Chapter 6, under free vibration, it is concluded that only a double set of damped outriggers and the combined damped and fixed outriggers (attaching viscous dampers in the lower set of outriggers) display larger increase of ζ than the 8% of the single damped outrigger. Optimized ζ of the former two are 8.8 and 8.6%, respectively.

Despite this increase of ζ, double and combined outrigger solutions do not present further reduction of peak inter-storey drifts when compared with the single configuration. This seems to suggest that configurations with optimal ζ might not be further optimized for inter-storey drifts reductions. From these results it is not possible to conclude which configuration seems to be the optimal to reduce the overall structural response.

From the analyses of optimal double set of damped outriggers and the combined damped and fixed outriggers, subjected to eight different ground motions, it is concluded that these configurations reduced the hysteretic energy ratio (E_H/E_I). In addition, the double damped outrigger is more effective for reducing the damage in the structure when subjected to strong and severe earthquake levels. However, such reduction in the hysteretic energy provided by the supplemental damping is not significant.

From all the time-history analyses using a set of eight earthquake records, it can be concluded that viscous damper outrigger structures exhibit a comparatively improved performance if the use of two outriggers matches the predominance of the 2nd mode of vibration, given by the ground motion frequency.

From the simplified economic analyses of optimal double set of damped outriggers and the combined damped and fixed outriggers, it is concluded that the extra costs due to the double damped are about 50% more expensive than the single damped solution. This is valid within the framework given by the C_d values involved in these optimal designs, and assuming the building costs mostly influenced by the amount of reinforcement steel and viscous dampers. To the contrary, the additional costs due to the combined damped and fixed solutions are about 16% cheaper than the single damped solution.

Samenvatting

De toepassing van vakwerkconstructies is gebruikelijk in hoogbouw om de reactie ten gevolge van dynamische belasting te verminderen. Viskeuze dempers worden toegepast tussen het vakwerk en de kolommen in de omtrek van het gebouw om trillingen te verminderen zonder de stijfheid van de constructie te verhogen. Dit concept van gedempte vakwerken wordt toegepast om de trillingen ten gevolge van sterke wind te verminderen. Het gedrag van deze constructies ten gevolge van zware aardbevingen is nog niet grondig onderzocht. Zware aardbevingen introduceren een grotere hoeveelheid energie in de constructie van het gebouw vergeleken met belasting door gematigde aardbevingen of sterke wind belasting. In hoogbouw wordt deze energie opgenomen door verschillende mechanismen waaronder buiging van de kern, wrijving tussen constructieve en niet-constructieve componenten en uiteindelijk schade.

Dit onderzoek richt zich op de capaciteit van hoge gebouwen uitgerust met gedempte vakwerken zodat deze veel kunnen vervormen voordat schade ontstaat. In andere woorden, tijdens beving van de grond, door een zware aardbeving, nemen voornamelijk de dempers de energie op waardoor de constructie zich als geheel elastisch gedraagt. Verschillende studies zijn gebaseerd op de beoordelingen van zowel de vereisten voor de energie geïntroduceerd door zware aardbevingen en de capaciteit van het systeem. In het bijzonder de capaciteit van de belangrijkste onderdelen, zoals de kern, het vakwerk, de kolommen in de omtrek van het gebouw en de dempers. Het doel van dit onderzoek is te bepalen of energie opname door schade kan worden vervangen door opname van energie door passieve dempers.

Dit onderzoek is gebaseerd op eindig elementen (EE) modellen ontwikkeld in Diana-FEA software. Deze analytische modellen zijn niet-lineair in bijna alle onderdelen van het EE model. Deze numerieke studies van passief gedempte vakwerken zijn gebaseerd op Matlab scripts welke verschillende parametrische analyses berekenen binnen Diana.

Parametrische analyse – Hoofdstuk 4

Dit hoofdstuk beantwoord de volgende vraag: Welke parameters beïnvloeden de verdeling van de seismische energie in hoogbouw welke is uitgerust met gedempte vakwerken?

De numerieke studies richten zich op de aspecten van modellering en de constructieve parameters welke invloed hebben op het gedrag van hoogbouw uitgerust met gefixeerde en viskeus gedempte vakwerken. Dit hoofdstuk beschrijft ook een parametrische studie ter beoordeling van de verdeling van de seismische energie in hoogbouw uitgerust met viskeus gedempte vakwerken. Bijvoorbeeld vakwerken met een of meer viskeuze dempers geïnstalleerd tussen het vakwerk en de kolommen in de gevel. Het doel van deze verkennende studie is om te bepalen welke parameters invloed hebben op (a) het constructieve gedrag en (b) de verdeling van seismische energie door de constructie. Als eerste beschrijft dit hoofdstuk een parametrische studie welke zich richt op de invloed van de eigen periode van het gebouw, positie van de vakwerken, dempingscoëfficiënt, kern-naar-vakwerk en kern-naar-kolom stijfheid verhouding in de prestatie van met vakwerk uitgeruste hoogbouw. Indirect geeft dit de basis voor de verkenning van strategieën voor verbeteren van het elastisch gedrag van hoogbouw uitgerust met viskeuze dempers en belast met zware grond beving. De optimalisatie van deze parameters definieert een pseudo-optimale configuratie welke verder wordt beoordeeld in termen van reactie reductie, namelijk verplaatsing, versnelling, afschuiving aan de basis, basis moment en spanningsverdeling. En in termen van energie verdeling. De strategie voor het beoordelen van de verdeling van aardbeving energie in hoogbouw uitgerust met viskeus gedempte vakwerken en belast met zware bevingen is gebaseerd op een numerieke studie van een 60 verdiepingen hoog gebouw uitgerust met gebruikelijke en gedempte vakwerken. Als tweede beschrijft dit hoofdstuk de onderlinge afhankelijkheid tussen constructieve eigenschappen van hoogbouw uitgerust met gedempte vakwerken en grond beving. Dit is onderzocht voor kleine, gematigde, sterke en zeer zware niveaus van de 1940 El Centro beving.

Passive gedempte enkelvoudige vakwerkconstructies – Hoofdstuk 5

Dit hoofdstuk beantwoord de vraag: Hoe deze energie uiteindelijk wordt opgenomen door zowel de hoofdconstructie en de viskeuze dempers? Tot welk niveau kan hysteretische energie worden opgenomen door bijdrage van de dempers?

Het doel van de studie gepresenteerd in dit hoofdstuk is te bepalen of de energie opgenomen als hysteretische energie (schade) volledig kan worden opgenomen door de actie door passief viskeuze dempers. Ook wel, het doel is te bepalen of het terecht is aan te nemen dat de componenten van de hoofdconstructie zich elastisch gedragen gedurende een zware aardbeving en reactie van hoogbouw daarop. En welke parameters hoofzakelijk invloed hebben op de reactie van constructie met gedempte vakwerken en hoe deze invloed is uitgeoefend. Om te bepalen tot hoe ver de viskeus gedempte vakwerken schade voorkomen worden zowel het hysteretische gedrag van de hoofdconstructie en de prestatie van de dempers parallel geëvalueerd. Als eerste de

tijd-historische reactie van gefixeerde en gedempte vakwerk constructies onderworpen aan verschillende niveaus van grondversnelling (peak ground acceleration, PGA) van een collectie van 8 bevingsopnames welke zijn verkregen door 2D EE modellen. Met behulp van deze resultaten is het niet-lineaire gedrag van gedempte en niet-gedempte vakwerken onderzocht voor kleine, gematigde, sterke en langdurig zware aardbevingen. Dit om de hysteretische energie opname door de kern en de vakwerken te beoordelen. Vervolgens is de opname van seismische energie in de constructie beoordeeld door middel van de energie verhoudingen demping-tot-invoer (damping-to-input, E_D/E_I), deze verhouding voor de dempers ($E_{DAMPERS}/E_I$) en hysteretisch-tot-invoer (hysteretic-to-input, E_H/E_I); het concept van een optimale configuratie is daarbij besproken in termen van vermindering van de hysteretische energie verhouding van de constructie zal vergroten. De resultaten tonen dat, wanneer de grond beving zwaarder wordt, viskeuze dempers effectief zijn bij de vermindering van potentiele schade in de constructie vergeleken met gebruikelijke vakwerken. Het gebruik van dempers kan schade niet volledig voorkomen voor kritische belasting.

Gebruikelijk en gedempte dubbele vakwerkconstructies – Hoofdstuk 6

Dit hoofdstuk beantwoord de vraag: Welke strategieën verbeteren de elastische reactie grens van hoogbouw uitgerust met viskeus dempers en belast met sterke aardbeving?

Het gebruik van een set vakwerken uitgerust met olie viskeuze dempers verbeterd de demping verhouding van hoogbouw met ongeveer 6-10%, afhankelijk van de belasting condities. Echter blijft de vraag of, wanneer een enkelvoudig gedempt vakwerk is ontworpen voor een optimale demping verhouding, deze verhouding nog kan verbeteren door toevoeging van een tweede set? En, zou deze set ook moeten worden uitgerust met dempers? Om deze vragen te beantwoorden zijn verschillende configuraties voor hoogbouw uitgerust met gedempte vakwerken onderzocht en vergeleken met een configuratie welke is ontworpen voor optimale demping verhouding, welke is gepositioneerd op 0.7 van de totale gebouw hoogte (h). Configuraties met dubbel vakwerk zijn geïdentificeerd, door vrije trilling analyse, welke de demping verhouding verbeteren tot het niveau van een geoptimaliseerd enkel vakwerk configuratie. Vervolgens zijn deze configuraties belast met niveaus van kleine, gematigde, sterke en zeer zware bevingen door 8 verplaatsingen om de capaciteit voor energie opname te vergelijken en daarmee schade te voorkomen tijdens kritische belasting. Als laatst belicht een vereenvoudigde economische analyse de voordelen van elke optimale configuratie in termen van staal wapening besparing vergeleken met de kosten voor de dempers. De resultaten tonen dat een vakwerk op 0.5 h gecombineerd met een vakwerk op 0.7 h effectiever is voor het verminderen van de hysteretische energie verhouding en economisch haalbaarder vergeleken met een enkel gedempt vakwerk.

Conclusies

Uit de parametrische analyse met behulp van EE modellen van gebruikelijke en gedempte vakwerken, belast met trillingen, kan worden geconcludeerd dat de optimale dempingscoëfficiënt C_d en optimale locatie λ een grote invloed hebben op de demping ratio ζ. Deze optimale demping ratio impliceert niet een significante vermindering van reactie van de constructie met vakwerk. Niettemin, wanneer λ and C_d bijna optimaal zijn, impliceert het effect van ρ_{ctc} mogelijk een toename van ζ van 7%. Dit suggereert dat wanneer de benodigde afmeting van de dempers niet beschikbaar is een aanpassing van de verhouding ρ_{ctc} zal helpen de dempingscoëfficiënt te vergroten. Een dergelijke vergroting zal alleen optreden als ρ_{ctc} kleiner wordt.

Aanpassing van de stijfheid verhoudingen kan helpen het effect van de viskeus gedempte vakwerken, om de reactie van het gebouw te verkleinen, te verbeteren. Bijvoorbeeld, het aanpassen van zowel λ als ρ_{ctc} zal de eigen frequentie van het gebouw beïnvloeden. Het feit dat aanpassen van ρ_{ctc} de reactie veranderd maar niet de eigen frequentie suggereert dat de invloed gerelateerd is met de viskeuze dempers. Geen van de besproken parameters, λ, ρ_{ctc} en ρ_{cto}, beïnvloeden de frequentie verandering van gedempte vakwerken, wanneer $\lambda<0.6$. De frequentie verandering wordt significanter wanneer het vakwerk de hoogte van het dak benaderd.

Vanuit numerieke analyse met belasting door El Centro aardbeving is geconcludeerd dat wanneer het vakwerk flexibel is ($\rho_{cto}=4$), E_I relatief is groot voor alle niveaus van belasting. Deze conditie is niet beïnvloed door ρ_{cto}. Het gebruik van stijve vakwerken ($\rho_{cto}=1$) impliceert een grotere hoeveelheid energie in het system. Deze verschuiving zou het resultaat kunnen zijn van grote demping krachten welke lineair worden vergroot door de hoge snelheid van zware bevingen.

Vanuit alle parametrische analyses is geconcludeerd dat ongeacht de optimale C_d, $\lambda<0.4$ minder effect heeft op het verbeteren van de algehele demping verhouding van het gebouw, wanneer vergeleken met de waarde $\lambda>=0.4$. Dit suggereert dat de optimale λ ergens ligt tussen 0.4 en 0.9. Niettemin, de optimale demping verschilt per mode, een enkel vakwerk configuratie zal de reactie niet voor alle modus verminderen tot een minimum.

Vanuit de numerieke analyse door EE modellen van gebruikelijke en viskeus gedempte vakwerken, belast met vier niveaus van grond beving, is geconcludeerd dat wanneer de beving sterker wordt, viskeuze dempers efficiënt de potentiele schade in de constructie verminderen vergeleken met gebruikelijke vakwerken. De resultaten bevestigen dat de vergroting van de dynamische stijfheid door gebruik van dempers efficiënter is dan het vergroten van de stijfheid door extra vakwerken toe te voegen om de reactie van de

constructie te verminderen. Het gebruik van dempers lijkt effectief bij het verminderen van zowel de kinetische als de rek energie, dit verklaard ook de algehele vermindering van versnellingen.

Daarbij verminderd het gebruik van viskeus gedempte vakwerken in optimaal ontwerp het moment en spanningen van de hoofd componenten van het systeem. Bijvoorbeeld de kern, het vakwerk en de kolommen in de omtrek van het gebouw. Dit is het geval voor zware aardbevingen vergeleken met gebruikelijke vakwerken.

Vanuit de numerieke analyse door EE modellen van gebruikelijke en viskeus gedempte vakwerken belast met vier niveaus van grond beving is geconcludeerd dat de onderlinge verplaatsing van de verdiepingen (inter-storey drifts), piek versnellingen (peak accelerations) en afschuiving aan de basis (base shear) niet substantieel verminderd door het toepassen van viskeus gedempte vakwerken. Deze resultaten bekrachtigen de conclusie dat geen enkele optimale configuratie kan worden gezien als het optimum voor vermindering van de reactie van de constructie.

Vanuit de numerieke analyse door EE modellen van gebruikelijke en gedempte vakwerk systemen, belast met vier niveaus van grond beving, is geconcludeerd dat gedempte vakwerken schade niet volledig voorkomen voor kritisch aardbevingen omdat de piek E_H/E_I eerder optreed dan de piek $E_{dampers}/E_I$. Aan de andere kant is de energie die wordt opgenomen door hysterese verminderd doordat de dempers de verdeling van de energie vergroten.

Hysteretische energie is geconcentreerd in de kern. De schade is veroorzaakt door het overschrijden van de trekspanning. De kern absorbeert de grootste hoeveelheid energie door zowel demping als hysteretische energie. Door toevoeging van de viskeuze dempers hebben de vakwerken een kleine rol in de draagkracht. Het grootste voordeel van het toevoegen van viskeuze dempers aan de vakwerken is de algehele vermindering van spanningen in de onderdelen en daarmee de buigzaamheid.

Uit analyse van verschillende configuraties van dubbel gedempte en gecombineerd gefixeerd+gedempte vakwerken zoals beschreven in hoofdstuk 6, in vrije trilling, is geconcludeerd dat alleen een dubbele set van gedempte en de gecombineerd gedempte en gefixeerde vakwerken (het plaatsen van viskeuze dempers in de onderste set van vakwerken) een vergroting van ζ van 8% van een enkel gedempt vakwerk vertonen. Geoptimaliseerde waarden van ζ zijn 8.8 en 8.6% respectievelijk.

Ondanks deze toename van ζ vertonen de dubbel en gecombineerde vakwerken geen vermindering van de piek van onderlinge verplaatsing van verdiepingen wanneer deze wordt vergeleken met een enkele configuratie. Dit lijkt te suggereren dat configuraties

met een optimale ζ niet verder geoptimaliseerd kunnen worden voor vermindering van onderlinge verplaatsing van verdiepingen. Uit deze resultaten is het niet mogelijk te concluderen welke configuratie het optimum is voor de algehele reactie van de constructie.

Uit de analyse van optimale dubbele set van gedempte vakwerken en de gecombineerd gedempte en gefixeerde vakwerken, welke zijn belast met acht verschillende grond bevingen, is geconcludeerd dat deze configuraties de hysteretische energie verhouding (E_H/E_I) verminderen. Daarbij is het dubbel gedempte vakwerk efficiënter in het verminderen van schade in de constructie wanneer deze is belast met sterke en zeer zware aardbevingen. Echter is degelijke vermindering van de hysteretische energie verkregen door extra demping niet significant.

Uit alle tijd-historie analyses met een set van 8 aardbeving opnames kan worden geconcludeerd dat viskeus gedempte vakwerken een vergelijkbare verbeterde prestatie leveren wanneer het gebruik van dubbele vakwerken overeenkomt met de overheersende 2^e mode van trilling, gegeven door de grond beving frequentie.

Vanuit een vereenvoudigde economische analyse van een optimale dubbele set van gedempte vakwerken en gecombineerd gedempte en gefixeerde vakwerken is geconcludeerd dat de extra kosten voor de dubbel gedempte vakwerken ongeveer 50% hoger zijn dan de enkel gedempte oplossing. Dit is valide binnen een kader gegeven door C_d waarden benodigd voor een optimaal ontwerp en ervan uitgaande dat de bouwkosten vooral worden beïnvloed door de hoeveelheid wapening en de viskeuze dempers. Daarentegen zijn de extra kosten voor de gecombineerd gedempte en gefixeerde oplossing ongeveer 16% goedkoper dan een enkel gedempte oplossing.

1 Introduction to the research

§ 1.1 Research motivation

§ 1.1.1 Smart integration of damping devices in tall buildings for reducing structural response

Excessive lateral deformation of buildings is often avoided by increasing stiffness. In tall and slender buildings, the increase of stiffness is not only insufficient but also undesirable as it leads to increase vibrations that disrupt the users' comfort. A less disrupting solution is the addition of supplemental damping to the system by means of installing damping devices. Such supplemental damping helps the reduction of the structural response of tall buildings subjected to wind or earthquake loadings, without increasing the stiffness. The damping characteristics of a system have a major effect over the structural response to ground motions because small amount of damping significantly reduces maximum deflections due to resonant response. As a direct consequence, increased supplemental damping reduces the inelastic energy demand on the structural members.

Supplemental damping increment may be achieved by using passive, active or semiactive control devices[1]. Among the passive control devices available to increase structural damping, viscous dampers are usually preferred as they do not add mass into the system, if compared to tuned mass dampers (Figure 1.1), and thus the host structure do not need to increase in size, saving space and also material costs. In addition, integration of dampers into the host structure seems to be more feasible (if compared with mass dampers), as they are used along the main axis of the lateral-force resisting system. Because of being 'hidden' in the structure, viscous dampers

1 Passive control devices do not require electric power to produce a damping force; active control requires a power supply to provide a control force. Semiactive control requires little power to modify the device properties; its advantage is then that it combines the adaptability of an active systems and the reliability of a passive device control.

are less invasive than a mass damper. The use of viscous dampers is, in synthesis, a cost-savings solution, and easy to integrate into the structural system and thus in the architecture of the building.

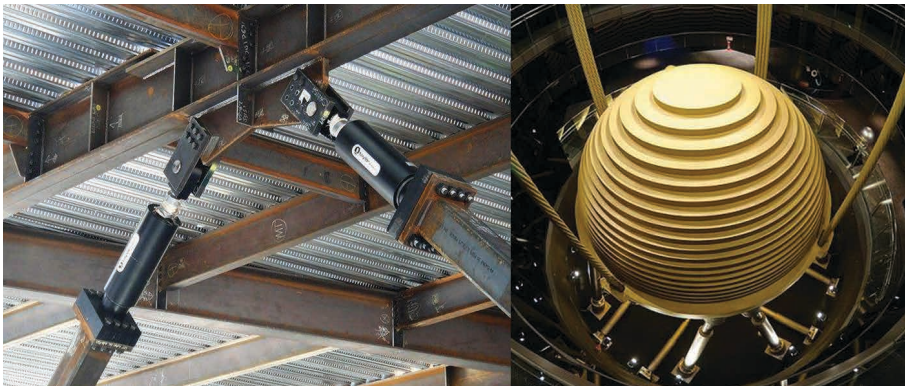

FIGURE 1.1 Viscous dampers integrated in a braced frame system (left) and a tuned mass damper hanging from the Taipei 101 building's roof (right). Sources: *engineeringfeed.com* and *civil-engg-world.blogspot.nl*, respectively.

The physical integration of damping devices into the lateral force-resisting system is desirable as the first step towards the realization of smart structures. However, such integration also requires optimal locations for the dampers to be installed. In this sense, viscous dampers –being velocity-dependant- display a better performance if they connect parts of the structure that otherwise will present large differential motion. This principle led to the damped outrigger concept (Smith and Willford, 2007), where only few viscous dampers are installed between the outriggers cantilevering from the core and the perimeter columns (Figure 1.2). When subjected to lateral loading, the dampers will help to reduce both lateral deflections and vibrations. The variation in the position of the outrigger along the height of the building (location) will influence this reduction in the structural response. The optimal location of the dampers and its embedding into the host structure makes the damped outrigger system an integrated damping system.

The achievement of smart building structures also relies on the use of adaptive control strategies (Morales-Beltran and Teuffel, 2013). Adaptive means that the structure can adapt to changes in the loading conditions. This is feasible through the use of sensors -for monitoring the loading action and/or the performance of the structure, a controller – which command the response, and actuators or semiactive dampers. Adaptive control requires, nonetheless, the use of an external power supply. This power

supply is used to exert the control force in active system) or to modify local properties of a device or structural member in semiactive systems. In general, the use of semiactive devices is preferred over the active devices, for two reasons: (1) active devices introduce control forces into the system that may lead to instability of the structure, whereas semiactive devices only introduce damping forces, and (2) in case of power failure, active devices become useless; semiactive devices relies on the passive component to continue working, hence they are more reliable.

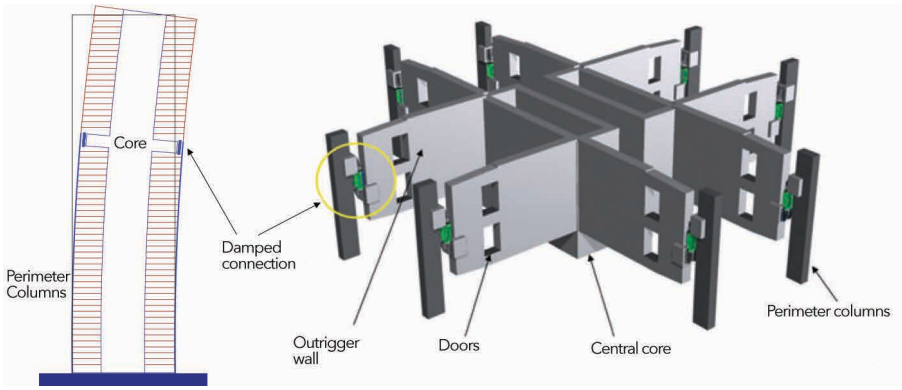

FIGURE 1.2 Damped Outrigger concept, as originally proposed by Smith & Willford (2007) - Reprinted with permission of the publisher

§ 1.1.2 Strong earthquake energy dissipation in tall buildings through damped outriggers

Damped outriggers have been used in few tall buildings applications for controlling wind response (Smith, 2016). Experimental and numerical research studies have been conducted to extend the application of damped outriggers to seismic control (Asai *et al.*, 2013; Chang *et al.*, 2013; Deng *et al.*, 2013; Gamaliel, 2008; Kim and Kang, 2017; Wang *et al.*, 2010; Ying Zhou and Li, 2013; Ying Zhou *et al.*, 2017) . Earthquakes are the sudden release of energy that has been stored in the form of cumulative strain between tectonic plates. This seismic energy is inevitably transmitted to the buildings, which are designed to dissipate energy through vibration. The stronger the earthquake is, the higher the energy that is introduced in the building. However, for tall buildings equipped with viscous damped outriggers, the capability of the structure to undergo large deformations without damage has been assumed. In other words, with the

increase in the ground motion given by strong earthquakes, the dampers are assumed to be the main source of energy dissipation whilst the host structure displays an elastic behaviour. This is questionable. Strong earthquakes introduces larger amount of energy into the building's structure, compared to moderate earthquakes or strong winds. In tall buildings, such seismic energy is dissipated by several mechanisms including bending deformation of the core, friction between structural and non-structural components, and eventually, damage. The stronger the earthquake is, the larger the chance that such energy will be dissipated by structural damage, even in a building equipped with damped outriggers.

§ 1.2 Problem statement

On the one hand, when modelling buildings with supplemental damping the assumption is that dampers behave nonlinearly whereas the host structure remains linear. This assumption is not valid in the context of strong earthquakes and hence investigations of the nonlinear behaviour of the structure along the dampers' performance are highly needed.

On the other hand, given the high chance of damage under strong earthquakes, conventional seismic design codes enlarge the structural elements to guarantee that such damage will not pose a life risk to occupants. Evidently, the enlargement of structural elements represents additional costs of building construction. With the addition of outriggers with dampers, the structural response is reduced and the need of a superstructure eliminated (Infanti *et al.*; Smith and Willford, 2007; Willford and Smith, 2008). Hence it is more accurate to assume that, during strong earthquakes, ***part*** of the seismic energy is dissipated by the dampers installed in the outriggers (Zhou *et al.*, 2014). Therefore, a damped outrigger aims to indirectly prevent damage during the occurrence of a large earthquake.

§ 1.2.1 How much seismic energy is dissipated by the dampers?

Assuming that in an outrigger structure equipped with dampers and subjected to seismic motion, dampers will actually dissipate part of the seismic energy, the question that arises is how much of that seismic energy will be dissipated by the dampers?

Moreover, if under strong earthquakes structures often present some degree of damage, how much of that damage can be prevented by adding viscous dampers? Would it be possible to reduce completely the structural damage by dissipating seismic energy through the dampers?

§ 1.3 Research Objectives

The objective of this research is to determine if the energy dissipated by hysteresis (damage) can be fully replaced by energy dissipated through the action of passive dampers. More precisely, the goal is to determine whether it is correct to assume that main structural components will remain elastic during the entire strong earthquake response of a tall building, as well as which parameters mainly affect the response of damped outrigger structures and how such influence is exerted.

§ 1.3.1 Main research question

To which extent is it possible to reduce the level of damage in a tall building subjected to strong earthquake motion, if equipped with damped outriggers?

§ 1.3.2 Secondary research questions

- Which parameters influence the distribution of seismic input energy through a tall building structure equipped with damped outriggers?
- How such energy is eventually dissipated by both the host structure and the viscous dampers?
- To which extent can hysteretic energy be completely overcome by the energy dissipated by the action of dampers?
- Which strategies will extend the elastic response threshold of a tall building equipped with viscous dampers when subjected to strong earthquake ground motions?

§ 1.3.3 Hypothesis

Compared with a conventional outrigger system (i.e. without dampers), it is possible to reduce the damage in a tall building subjected to strong motion by using viscous damped outriggers.

§ 1.4 Scope

The scope of this research is in the field of seismic design of buildings, specifically seismic design of tall buildings with viscous dampers. Computational-based performance and programming are also covered here, as the research is based on computational models and simulations which were all elaborated by the author.

It is worth to mention here that architectural matters, related to the subject, were of particular interest of the author at the beginning of this research. Nevertheless, due to the required in-depth direction of the research, such architectural aspects are unfortunately not covered here.

Due to the extent of the research, some subjects addressed in this investigation have been simplified. Descriptions of these subjects and their scopes are given as follows.

§ 1.4.1 Type of dampers used in the damped outriggers

Although the concept of damped outriggers (sometimes called damping outrigger system) includes the use of any damping device, say, viscous, viscous-elastic, hysteretic, tuned-mass, magneto-rheological, etc., in this research there is only one type: oil viscous dampers. When applied to the outrigger structure, the system including a viscous damper will be addressed indistinctly as oil viscous, viscous or passive damped outrigger.

§ 1.4.2 Less is more: integration is understood as obtaining better performance with fewer devices

The concept of integrated control devices in buildings follows a twofold approach. One is *integration* as design strategy in the sense of using non-disrupting distributions, optimal placements or by the utilization of parts of the building itself as control mechanisms, i.e., the degree of integration is inversely proportional to the distribution and amount of new attachments to the main structure. Second approach supports *integration* as a goal for economic savings, using the simple assumption that the reduction of a superstructure, otherwise needed if no dampers are attached, will reduce the costs of building construction. In this research, *integration* is thus understood as a design strategy that (1) minimizes the number of devices by finding optimal locations of the damped outriggers, and (2) implies economic savings in the building construction by reducing the size of the host structure. However, economic savings are not the focus of the studies and they are aimed only as an indirect benefit of finding optimal designs from the perspective of a better structural performance.

§ 1.4.3 Tall buildings under strong earthquakes

Tall building is a slippery definition. According to the *Council of Tall Buildings and Urban Habitat*[2], a tall building is considered as such when it features relevant height relative to the context, slender proportions, or embraces technologies relevant to tall buildings. For the *Structural Design of Tall and Special Buildings Journal*[3], tall building can be defined as 'a structure that is equal to or greater than 50 meters (165 feet) in height, or 14 storeys or greater.'

In the context of this research, however, the concept of tall building is derived as follows.

Since a tall building will likely present a fundamental long period, the effectiveness of the damped outriggers to decrease the building response under earthquake motion was a question mark from the beginning. The first concern rises from the fact that a building with a 5 or 6 s period, checked against any seismic code spectra, will present

2 http://ctbuh.org/TallBuildings/HeightStatistics/Criteria/tabid/446/language/en-US/Default.aspx

3 http://onlinelibrary.wiley.com/journal/10.1002/(ISSN)1541-7808/homepage/ProductInformation.html

a very low response to the ground accelerations, and thus, wind loading will become the predominant state of loading. However, the performance of viscous damper-based outriggers under wind loading is out of the scope of this study and it is only addressed, for comparison purposes, during the preliminary studies described in Chapter 4. The aforementioned concern seems to suggest, nevertheless, that even under exclusively consideration of earthquake loading the reductive effect of the viscous dampers on the overall building response will increase as the building height decreases. Evidently, a lower building will naturally be more affected by the acceleration of the ground. Since the aim of this research is determine the bounds for the effectiveness of damped outriggers under strong earthquakes, tall buildings are considered here in the range of 200 meters.

It is worth to note as well that buildings of 200 m high are a common landscape in important cities located on seismic regions around the world (Figure 1.3).

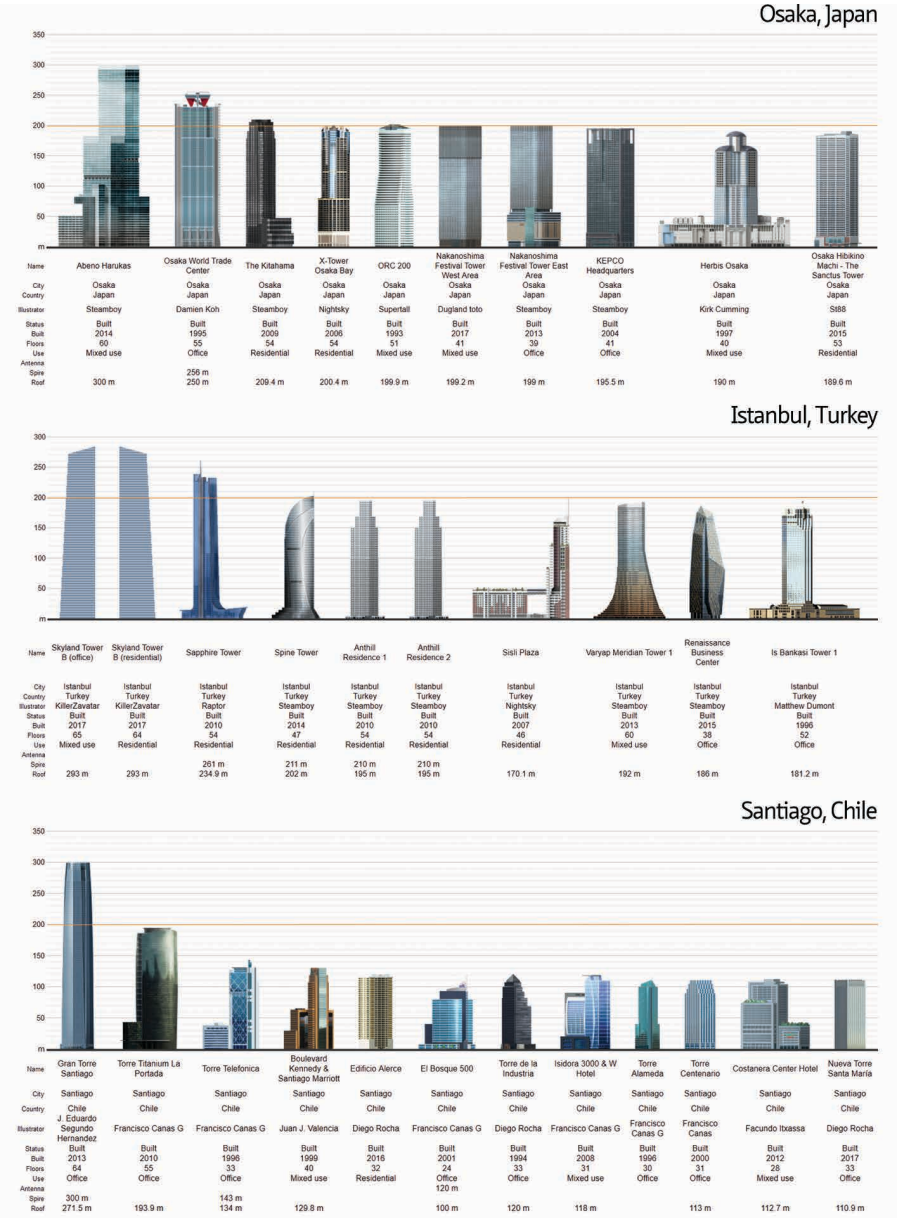

FIGURE 1.3 Tall buildings in selected cities located in seismic regions around the world. Source: Skyscraperpage.com

§ 1.5 Approach and methodology

§ 1.5.1 Dissipation of seismic energy in tall buildings equipped with damped outriggers

To illustrate the risks of evaluating the structural response exclusively in terms of peak responses, observe the displacement responses displayed in Figure 1.4. There, it can be noticed that near the 10 s of the motion, peak displacements are reached for the three structural systems evaluated. Also, that the difference between these three peak responses is relatively small compared to the peak displacement. If we observe now the responses in the region near the 50 s, one can notice that the use of damped outriggers have reduced in half the response given by the use of conventional outriggers, whilst the building without outriggers does not show a decrease in the response at all. It is obvious then that considering only the peak values at 10 s would lead to assume a rather ineffective use of both conventional and damped outriggers. Evaluation of the response along the entire history of the motion is therefore required.

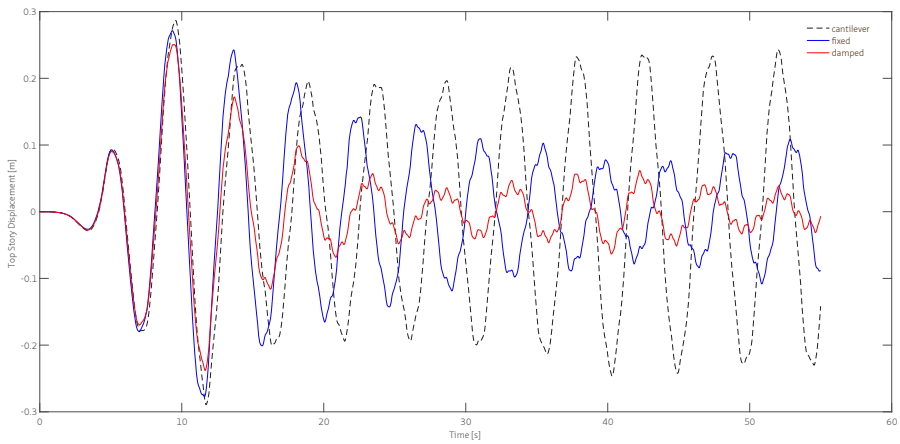

FIGURE 1.4 Relative top storey lateral displacement of a 200 m tall building under Izmit-Kocaeli Earthquake, without outriggers (cantilever), with conventional outriggers (fixed), and with damped outriggers (damped).

Seismic events worldwide have served as empirical proof that structures designed by using design forces derived from its linear behaviour, have resisted higher earthquake forces due to its ductility. However, such codes are based on the quantification of the response demand in terms of peak values. The design of earthquake-resistant structures is not only a function of the peak response demand but also a function of the time history response demand. Hence the effectiveness of the supplemental damping given by the outrigger to the overall building response reduction needs to be evaluated along the entire history of the motion and not only in terms of peak response values. In addition to the reduction of the response in terms of peak values, the combined influence of the intensity, frequency content, and duration of strong earthquakes in the control performance of the damped outriggers need to be evaluated.

Energy-based design methods have the potential to address both the effect of the duration of the earthquakes and the hysteretic behaviour of the structure. Hence the use of an energy-based assessment of the building response by which the damage potential can be quantified. An energy-based design method is based on the premise that the energy demand during an earthquake can be predicted as the energy supplied by the structure can be therefore defined (Uang and Bertero, 1990). The balance among the mechanisms of energy dissipation required to cope with the demand of input energy derived from an earthquake is expressed in terms of the energy balance equation, given as:

$$E_K + E_D + E_{dampers} + E_S + E_H = E_I \tag{1.1}$$

where E_K, E_D, $E_{dampers}$, E_S, E_H, and E_I are the kinetic, damping, dampers, strain, hysteretic and input energies, respectively.

According to Eq. 1.1, the distribution of seismic energy is based on the demand of total input energy – E_I. In addition, kinetic and elastic strain energies tend to zero at the end of the vibration, thus it is valid to assume that, by the end of the motion, E_I is mostly defined by the combined effect of E_D, $E_{dampers}$ and E_H. In the case of tall buildings equipped with damped outriggers, the hysteretic behaviour of the host structure needs to be evaluated along the dampers' performance in order to determine how the earthquake input energy is distributed through all the components. Insights on how these energies are related can be obtained by evaluating (a) the hysteresis energy ratio E_H/E_I; (b) the inherent viscous damping energy ratio E_D/E_I; and (c) the supplemental damping ratio $E_{dampers}/E_I$.

§ 1.5.2 Numerical Investigations using MATLAB

The numerical investigations on passive damped outriggers are based on master Matlab scripts (see Appendix C). These scripts are written to (a) output a file to be read by Diana, containing all the parameters required for a given analyses; (b) run a non-stopping loop of combined parametric analysis by commanding time-history analyses in Diana, and retrieving the output data; and (c) compute the energy distributions resulting from a specific time-history analysis.

Several sets of simulations were studied. The combined work Matlab-Diana required reducing the size of the output files by a careful selection of relevant nodes and/or reducing the amount of data points of the time-history ground motion. All Matlab files to read and process Diana outputs were optimized for decreasing computational time.

§ 1.5.3 Finite Element Models in DIANA

All the analytical models used in this research are based on the existing Shangri-La building in Manila, Philippines. Both core and outrigger were modelled using nonlinear settings, as they are expected to be the major sources of hysteretic energy dissipation. Perimeter columns, on the contrary, were modelled with elastic elements. The analytical model considers the use of general nonlinear material models throughout almost the whole finite element model as specified by Diana-FEA software (2014). The basic 2D model comprises 255 DOF (see Appendix D).

Despite its apparent simplicity, the nonlinear FE model of damped outrigger structure implemented in Diana-FEA can effectively account for the post-yield behaviour of the structure and thus the conclusions derived from the results are fully reliable within the boundaries of the presented study.

§ 1.6 Thesis outline

This thesis manuscript is distributed in nine chapters, organized in four main sections (Figure 1.5) apart from the introduction to the research, which is given in Chapter 1.

The first section delivers background information: Chapter 2 aims to deliver specific information of the state-of-the-art of applications, experimental, and analytical research on damped outrigger structures; Chapter 3 aims to deliver information about energy-based design methods.

The second section discusses both the modelling and structural parameters that influence the behaviour of tall building equipped with fixed and damped outriggers. In particular, Chapter 4 explains which parameters affect the performance of damped outrigger structure and how such influence is exerted.

The third section addresses the analytical and numerical studies developed in this research: Chapter 5 discusses to which extent the use of passive viscous damped outriggers can avoid damage of the host structure when subjected to strong earthquake motion; Chapter 6 discusses the benefit of using multiple viscous damped outriggers and explores the performance of combined configurations using conventional and damped outriggers.

The last section sets an integrated discussion, following the results obtained in the previous numerical studies, and draws some conclusions: Chapter 7 discusses the main aspects of a design method for outrigger structures using passive viscous dampers, by integrating the results obtained in the analyses described in chapters 4, 5, and 6; Chapter 8 remarks some conclusions and recommendations.

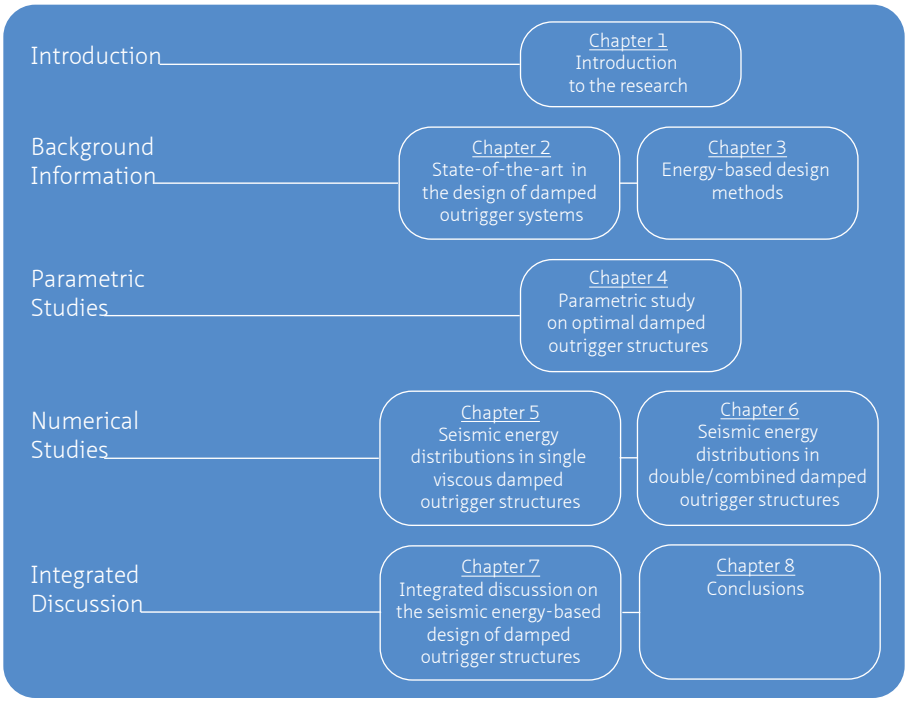

FIGURE 1.5 Thesis outline

References

Asai, T., Chang, C.-M., Phillips, B. M. and Spencer Jr, B. F. 2013. Real-time hybrid simulation of a smart outrigger damping system for high-rise buildings. Engineering Structures. 57: 177-188. http://dx.doi.org/10.1016/j.engstruct.2013.09.016

Chang, C.-M., Wang, Z., Spencer Jr, B. F. and Chen, Z. 2013. Semi-active damped outriggers for seismic protection of high-rise buildings. Smart Structures and Systems. 11: 435-451.

Deng, K., Pan, P., Lam, A. and Xue, Y. 2013. A simplified model for analysis of high-rise buildings equipped with hysteresis damped outriggers. The Structural Design of Tall and Special Buildings. 10.1002/tal.1113n/a-n/a. 10.1002/tal.1113

Gamaliel, R. 2008. Frequency-based response of damped outrigger systems for tall buildings

Infanti, S., Robinson, J. and Smith, R. 2008. Viscous dampers for high-rise buildings

Kim, H.-S. and Kang, J.-W. 2017. Semi-active Outrigger Damping System for Seismic Protection of Building Structure. Journal of Asian Architecture and Building Engineering. 16: 201-208. 10.3130/jaabe.16.201

Morales-Beltran, M. and Teuffel, P. 2013. Towards smart building structures: adaptive structures in earthquake and wind loading control response–a review. Intelligent Buildings International. 5: 83-100.

Smith, R. 2016. The Damped Outrigger-Design and Implementation. International Journal of High-Rise Buildings. 5: 63-70.

Smith, R. J. and Willford, M. R. 2007. The damped outrigger concept for tall buildings. The Structural Design of Tall and Special Buildings. 16: 501-517. 10.1002/tal.413

Uang, C.-M. and Bertero, V. V. 1990. Evaluation of seismic energy in structures. Earthquake Engineering & Structural Dynamics. 19: 77-90. 10.1002/eqe.4290190108

Wang, Z., Chang, C.-M., Spencer Jr, B. F. and Chen, Z. 2010. Controllable outrigger damping system for high rise building with MR dampers

Willford, M. and Smith, R. 2008. Performance based seismic and wind engineering for 60 story twin towers in Manila

Zhou, Y. and Li, H. 2013. Analysis of a high-rise steel structure with viscous damped outriggers. The Structural Design of Tall and Special Buildings. 23: 963-979. 10.1002/tal.1098

Zhou, Y., Zhang, C. and Lu, X. 2017. Seismic performance of a damping outrigger system for tall buildings. Structural Control and Health Monitoring. 24: e1864-n/a. 10.1002/stc.1864

Zhou, Y., Zhang, C. Q. and Lu, X. L. 2014. Earthquake resilience of a 632-meter super-tall building with energy dissipation outriggers

2 State of the Art in the Design of Damped Outriggers

§ 2.1 Summary

This chapter provides general descriptions of outrigger systems including the use of dampers, commonly known as damped outriggers, in the context of tall buildings. It describes the physical behaviour of the outriggers and it introduces the comparative advantages of adding dampers. This chapter also emphasizes the aspects related to the location of the outriggers, stiffness core-outrigger-perimeter columns ratios, supplemental versus inherent damping, and building's natural frequency versus earthquakes' frequency content. From the studies revised in this literature review, it is concluded that the most influential parameters in the design of damped outrigger systems are the outrigger location, damping coefficient, and stiffness core-to-column and core-to-outrigger ratios. Moreover, the optimization of outrigger location or damper size mostly follows a roof displacement reduction criterion. Few studies consider reducing other parameters, such as inter-storey drifts, base shear or moments. Finally, it seems that there are few implementations of viscous damped outriggers in tall buildings and none of semiactive damped outriggers.

§ 2.2 Introduction

In buildings taller than 40-storeys, usually the stiffness of the core is not enough to reduce lateral drifts to acceptable limits during both wind and seismic events (Taranath, 1998). Among several structural typologies available to provide sufficient strength and stiffness, including tube structures, bundled tubes, etc., a well extended method to increase lateral stiffness is the use of outriggers to tie the core to the perimeter columns. An outrigger system then, consists of a series of cantilever truss beams or shear walls connecting the building core with the perimeter columns. As a result, the axial forces acting at the end of the outriggers help the reduction of the total

deflection of tall buildings by increasing the restoring moment. The use of outriggers, thus, helps to reduce the drift response without increasing the core stiffness.

Dampers have been introduced between the perimeter columns and the outriggers, resulting in an increase in the overall damping of the building, instead of an increase of static stiffness and strength (Smith and Willford, 2007). The first worldwide implementation of this system in twin 60-storey buildings was reported in Willford and Smith (2008). The authors reported that, by using damped outriggers, the 210 m high reinforced concrete residential buildings achieved a 7.5% total damping. Park *et al*. (2010) reported the installation of damped outriggers in a 68-storey tower in South Korea. In a recent review, Smith (2016) reported two more applications of damped outriggers in tall buildings: Another 225 m hotel building in Manila, where a damped outrigger was installed (only in one direction), adding a 3% supplementary damping to the building. A 40-storey office building in New York, to which a damped outrigger located at the top of the building, added a 2% supplementary damping (Jackson and David, 2010). All the authors point out that the addition of supplementary damping systems not only reduced the overall vibration response, but also construction costs due to the reduction of the overall super-structure.

This chapter provides general descriptions of outrigger systems including the use of dampers, commonly known as damped outriggers. It introduces the physical behaviour of the outriggers and the comparative advantages of adding dampers. This chapter also emphasizes the aspects related to the location of the outriggers, stiffness core-outrigger-perimeter columns ratios, supplemental versus inherent damping, and building's natural frequency versus earthquakes' frequency content. These issues, as design parameters, play a fundamental role in the overall performance of the damped outrigger -in any of its variants- and they have been subjected to constant research and modification by lessons learned in practice, which is reviewed next.

§ 2.3 Conventional outrigger system (fixed)

In order to fully understand the concept of the damped outrigger, let us first to revisit the principles that govern the physical behaviour of a conventional or fixed outrigger system. An outrigger structure consists of a main core connected to the exterior columns by flexurally stiff horizontal cantilevers, called outriggers (see Figure 2.1a). When horizontal loading acts on the building, say wind loading (Figure 2.1b), the tied columns help the outriggers to resist the rotation of the core. The resulting restoring

couple reduces both the lateral deflections and bending moments in the core (Figure 2.1 c-d). The core, which can be either a reinforced-concrete shear wall or a braced-steel frame (Hoenderkamp and Bakker, 2003), is often located between the column lines with outriggers extending on both sides. Other configurations are also possible. For example, outriggers at only one side of the core (Figure 2.2-left) or outriggers extending in diagonal on the building's corners (Figure 2.2-right). Buildings with traditional outriggers are typically best suited for heights between 150 and 400 m (Smith, 2016).

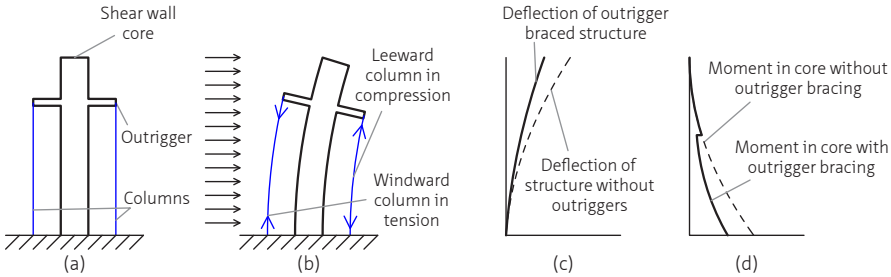

FIGURE 2.1 Main elements of an outrigger structural system (a); its structural behaviour under wind loading (b); with its resultant deflections (c) and core moments (d) [adapted from Smith and Coull (1991)]

FIGURE 2.2 Alternative outriggers - core configurations: outriggers at only one side of the core in a 200m 40-storey office building (left) and outriggers extending in diagonal on the building's corners in a 200m 42-storey building (right). Both located in Izmir, Turkey (Photographies by the author)

According to Choi *et al.* (2012), the main benefits of an outrigger system applied to tall buildings are:

1. Reduction in deformation: Up to 40% reduction in core overturning moment, compared to a free cantilever, and a relatively significant reduction in drift depending on both core and outriggers stiffness (Lame, 2008 as cited in Choi *et al.* (2012));
2. Efficiency: Since perimeter columns have been already sized for gravity load, minimal changes in size or reinforcement may be necessary for the columns to be able to resist outrigger forces. Due to the decrease in the overturning moments, material quantities in core can be significantly reduced by a small increase in outrigger or columns material quantities.
3. Foundation forces: Since outriggers help to distribute overturning loads on foundations, there is an advantage in force reduction at core foundations that makes the design economical or more practical, if compared with foundation of a core-only lateral system.

Outriggers present the disadvantage that when the building is subjected to severe earthquakes, the shear force and moment are prone to change abruptly at the outrigger-located floors (Zhou *et al.*, 2017). While the outrigger system is very effective in increasing the structure's flexural stiffness, it does not increase its resistance to shear, which has to be carried mainly by the core (Smith and Coull, 1991; Taranath, 1998). Moreover, in order to make the outriggers and belt girder[4] adequately stiff in flexure and shear, they are made at least one, and often two, storeys deep. Consequently, to minimize the obstruction they cause, they are usually located at plant levels. A building can be stiffened effectively by a single level of outriggers or by using multiple outriggers. However, each additional level of outriggers increases the lateral stiffness by a smaller amount than the previous additional level. Up to four outrigger levels may be used in very tall buildings.

Despite outrigger systems have been widely applied in tall building all over the world, for at least 30 years, the debate on the optimal parameters affecting its response, namely flexural stiffness and location, has not concluded. A good overview on current research can be found in Zhou *et al.* (2016). Late references to optimal location of outriggers can be found in Chen and Zhang (2017) and Kamgar and Rahgozar (2017).

4 When the intention is to use perimeter columns that are not the end of the outriggers, the use of a deep spandrel girder or 'belt' will help those columns to restrain the outriggers.

§ 2.4 The damped outrigger concept

§ 2.4.1 Passive damped outriggers

Supplemental damping increment may be achieved by using passive, active or semiactive control devices. Among the passive control devices available to increase structural damping, viscous dampers are usually preferred as they do not add mass to the system, and thus the host structure do not need to increase in size, which saves space and material costs. In addition, dampers can be integrated into the host structure as they are used along the main axis of the lateral-force resisting system. However, such integration also requires of optimal locations for installing the dampers (Morales-Beltran and Teuffel, 2013). In this sense, viscous dampers –being velocity-dependant- display a better performance if they connect parts of the structure that otherwise will present large differential motion. Dampers should be placed between disconnect elements presenting high stiffness, to avoid that larger damping forces may overpass the strength capacity of the surrounding structure. In addition, such stiff elements should present a high relative movement when they are unconnected. Suitable connections are at the ends of outriggers, between shear walls and in diagonal braces. This principle led to the damped outrigger concept (Smith and Willford, 2007), where only few viscous dampers are installed between the outriggers cantilevering from the core and the perimeter columns (Figure 2.3). When subjected to lateral loading, the dampers will help to reduce both lateral deflections and vibrations. The variation in the position of the outrigger along the height of the building will influence this reduction in the structural response.

An outrigger equipped with viscous dampers is considered passive control because no external power is required by the dampers to dissipate energy. Although the initial concept design and most of its further developments comprise the use of viscous dampers, the damped outrigger can be realized with all types of dampers, such as friction, visco-elastic (Ahn *et al.*, 2008), hysteresis (Deng *et al.*, 2013; Ying Zhou *et al.*, 2017), and buckling restrained bracing (BRB) (Jiang *et al.*, 2017; Ying Zhou *et al.*, 2017). A good overview of the different types of dampers can be found in Kibayashi *et al.* (2004), from where Figure 2.4 was originally taken. Magneto-rheological (MR) dampers have been also used in outrigger but as they are dependent on external power, they are reviewed in the next section.

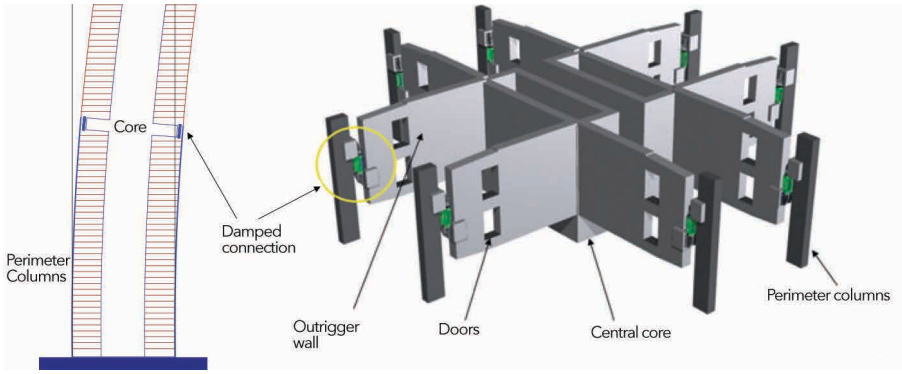

FIGURE 2.3 Damped Outrigger concept, as originally proposed by Smith and Willford (2007) - Reprinted with permission of the publisher

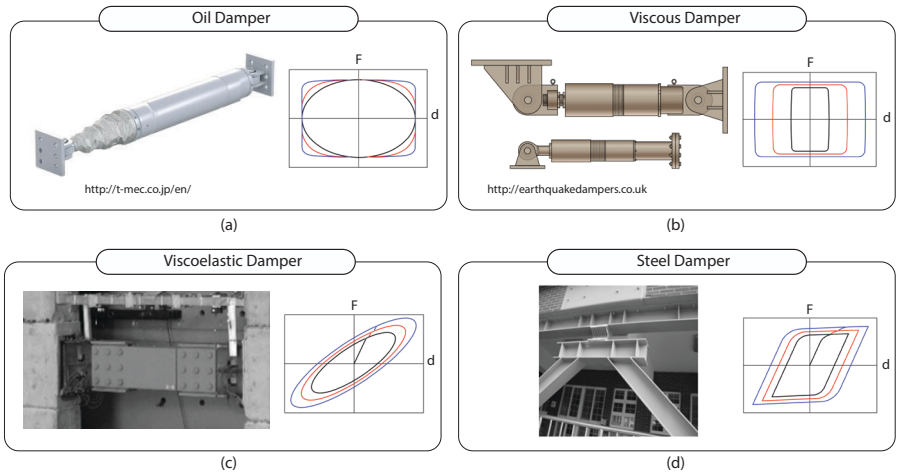

FIGURE 2.4 Common types of damper devices: (a) oil, (b) viscous, (c) viscoelastic and (d) steel damper (adapted from Kibayashi *et al.* (2004))

BRB outriggers have been studied and proposed in the design of a 632m high building (Ying Zhou *et al.*, 2017). This damping outrigger system uses BRB instead of typical diagonal steel members. The system not only provides additional damping but also stiffness to the structure. BRB is been described as a system that 'is much more familiar to structural engineers and much more easier to design' (Black *et al.*, 2004 as cited in Yang *et al.* (2016)). However, as pointed out by Smith (2016), 'since these systems rely upon yielding of steel, the energy dissipation (i.e. damping) can only occur when there is higher drift within the building'. Consequently, in the presence of small earthquakes

or any type of wind loading, the system provides no damping. Note that even when the system may effectively protect the host structure from severe damage under strong or sever earthquakes, the braces need to be replaced.

Damped outriggers have been used in few tall buildings for controlling wind response (Smith, 2016). Numerical and experimental studies have been conducted to extend the use of damped outriggers towards an improved reduction of the dynamic response under wind loading (Fang *et al.*, 2015; Huang and Takeuchi, 2017; Park *et al.*, 2010; Ping Tan *et al.*, 2014). However, because viscous dampers are reliable and can absorb energy at all ranges of motion this system is particularly beneficial in areas of high seismicity (Jackson and David, 2010). Hence experimental and analytical research studies have been conducted to extend the application of damped outriggers to seismic control (Asai *et al.*, 2013; Chang *et al.*, 2013; Deng *et al.*, 2013; Gamaliel, 2008; Kim and Kang, 2017; O'Neill, 2006; Wang *et al.*, 2010; Ying Zhou and Li, 2013; Ying Zhou *et al.*, 2017; Y. Zhou *et al.*, 2014). Among these studies, nevertheless, few explore the performance of damped outriggers under strong earthquake motion. Generally, studies are based on the use of peak ground acceleration (PGA) values up to 0.4g whereas strong earthquakes may exhibit PGAs of about 1.0g. At the same time, most of the research studies have focused on the reduction of the response in terms of peak values. Only few studies consider the combined influence of the intensity, frequency content, and duration of these strong earthquakes in the control performance of the damped outriggers. Hence the need of an energy-based assessment of the building response by which the damage potential can be quantified.

§ 2.4.2 Semiactive damped outriggers

A viscous damped outrigger, as any other passive damping system, cannot adapt to changes in the loading conditions nor in the host structure. Moreover, as pointed out by Wang *et al.* (2010), the optimal viscous damper size is mainly designed for the first mode, whereas seismic motions may excite higher modes of the structure, hence limiting the effectiveness of the viscous damper outrigger. In order to extend the control performance of damped outriggers, semi-active schemes including the use of magneto-rheological (MR) dampers have been proposed (Asai *et al.*, 2013; Chang *et al.*, 2013; Kim and Kang, 2017). MR dampers are classified as controllable fluid devices, as their damping force can be controlled by modifying the rheological fluid by means of the application of a magnetic field. Through experimental and analytical research, MR dampers have demonstrated a superior performance to that of comparable passive systems (Yi *et al.*, 2001). Chang *et al.* (2013) verified the efficacy of semiactive damped

outrigger systems to reduce building displacements and overturning moments, through numerical simulation. Their study was based on the use of Linear Quadratic Gaussian (LQG)/clipped-optimal control to reduce the structural response of a 210m high building against El Centro and Kobe earthquakes. Asai *et al*. (2013) provided an experimental verification of the previous theoretical studies, through real-time hybrid simulation of a MR-damped outrigger model. Results proved that semi-active controller, compared to passive and bare[5] versions, provided the best control performance in terms of both relative displacements and base shear. Kim and Kang (2017) studied a semi-active outrigger damping system installed in a 200m high building subjected to an artificial earthquake. A fuzzy logic controller was optimized to generate the command voltage sent to the MR damper. Although a passive damped outrigger was not included in this numerical study, the authors showed that a semi-active damped outrigger can reduce both displacement and acceleration responses compared to a conventional outrigger system.

§ 2.5 Design of damped outriggers

There are several factors involved in the design of damped outriggers. Despite the fact that they are closely interconnected and therefore its influence on the performance also depends on parallel definitions, these factors will be revised separately for convenience.

§ 2.5.1 Intrinsic damping in tall buildings versus additional damping

It is been said that dampers introduce additional damping in the system, but what is the typical damping ratio of a tall building? Unfortunately, there is no precise answer to this question and engineers do not agree on the use of default values, neither. For example, some engineers argue that damping levels on very tall buildings may be as

5 A bare version refers to that building without outriggers, usually modelled as a simple cantilever beam.

low as 0.5% (Willford *et al.*, 2008), whilst others consider that 'typical damping levels for tall buildings and high earthquake intensity may reach higher values than 1.5%'[6].

Whereas mass and stiffness properties can be easily obtained from the structural geometry of a building, damping is harder to estimate within a range of adequate certainty. The sources of damping in buildings may include material damping, friction or slip at structural connections, soil-structure interaction, interaction with non-structural components, hysteresis of yielding components and aerodynamic damping (Smith *et al.*, 2010). Damping is therefore difficult not only to estimate but to model mathematically due to the different principles that govern each of the previously mentioned sources. Hence the only reliable way to estimate damping is through measurements on existing buildings (Cruz and Miranda, 2017; Smith and Willford, 2007; Seymour and Kareem, 2014). Damping measurements presented by Smith *et al.* (2010) and Cruz and Miranda (2017) are shown in Figure 2.5 and Figure 2.6, respectively. Although scatter data can be observed in all plots, the trends in the damping ratio show that:

1. Damping ratios decrease with increasing building height. The investigation of Seymour and Kareem (2014) suggests , nonetheless, that is rather the predominant lateral deformation mechanism –given by the selected structural system, the one that gives a good predictive parameter on the damping capacity of a tall building ;
2. Buildings higher than 150 m have damping ratios lower than 2.5%, which is the usual value used in seismic design (Cruz and Miranda, 2017);
3. There are virtually no measurements above 1% in buildings over 250 m (Smith *et al.*, 2010);
4. Whereas there is no clear correlation between damping ratio and material type in Figure 2.5, damping ratios in concrete structures are higher than those in steel structures in Figure 2.6. This contradiction exemplifies the difficulty of obtaining reliable damping estimates even from actual measurements.

An additional issue of interest is the relationship between damping and amplitude of motion. The aforementioned measurements were made in buildings under relative small amplitudes (Cruz and Miranda, 2017; R. Smith *et al.*, 2010). In the study presented by Smith *et al.* (2010), a small increase in damping is associated with increasing amplitude. However, they also evidence that damping may decrease at greater amplitudes and that the highest damping can occur at relative small

6 Unknown reviewer, personal communication on Referee' Comments to Author, as part of the decision on the submitted manuscript "Distribution of strong earthquake input energy in tall buildings equipped with damped outriggers" to The Structural Design of Tall and Special Buildings, February 16, 2017.

amplitudes. Cruz and Miranda (2017) studied this relationship addressing changes in the damping ratio as a function of the peak roof drift ratio. They found that in most cases the damping ratio remains approximately constant even with tenfold increase in peak roof drift ratios, concluding that the saturations in damping ratios with increased amplitude due to earthquake loading are consistent with previous studies on wind-induced amplitudes. It is been suggested as well, that for strong motions, the effect of the damping is limited; the damped outrigger performs much better for wind loading and a more frequent earthquake because the starting level of damping is much lower[7].

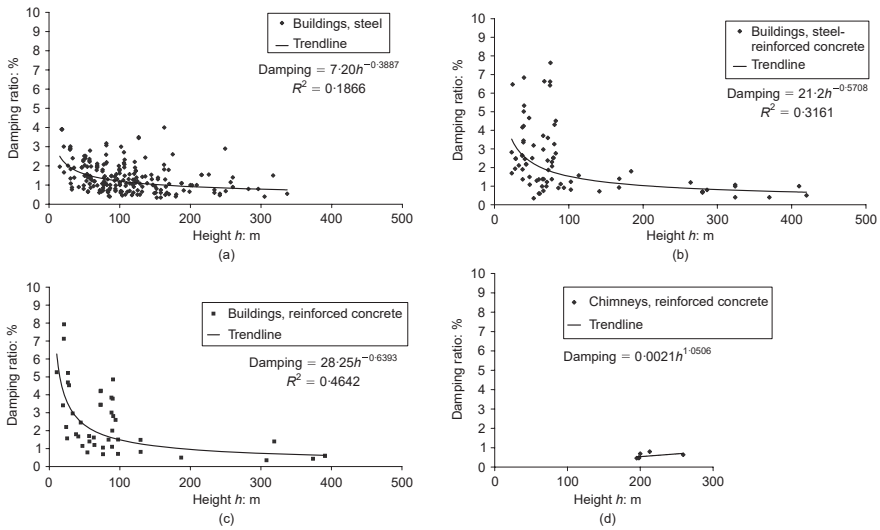

FIGURE 2.5 Damping measurements of (a) steel buildings, (b) steel-reinforced concrete buildings, (c) reinforced concrete buildings and (d) reinforced concrete chimneys. Image source: Smith *et al.*, 2010 - Reused with permission of the publisher.

In the first implementation of a damped outrigger, the engineers considered 1% of intrinsic damping for a 210m 60-storey residential building subjected to wind loading. On the other hand, analytical studies using the same benchmark-building model have proposed 2% damping ratio. Rob Smith -one of the engineers who designed and implemented the damped outrigger in the building in discussion- suggested[8] the

7 Rob Smith, personal communication, April 14, 2017

8 Idem

use of 2.0 – 2.5% as a pre-yielding equivalent viscous damping, citing as references the guidelines provided by the ATC-PEER (2010) and LATBSDC(2014). This latter document states that 'The effective additional modal or viscous damping shall not exceed 2.5% of critical for the primary modes of response.'

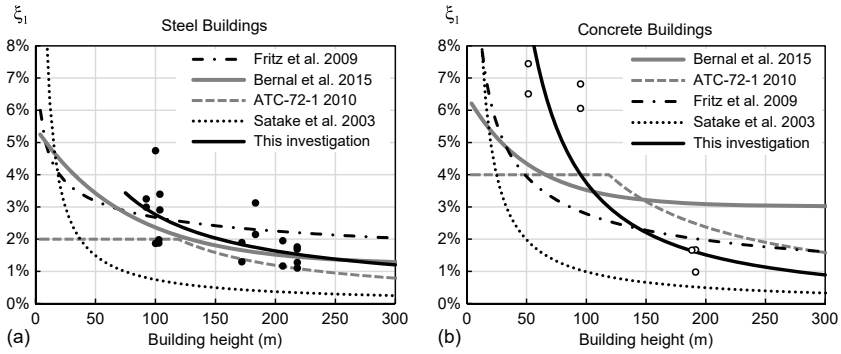

FIGURE 2.6 Identified damping ratios for the fundamental mode versus building height, compared to some proposed recommendations: (a) steel buildings; (b) reinforced concrete buildings. Image source: Cruz and Miranda, 2017 - With permission from ASCE

A brief but precise review on methods to compute the available damping is provided by Smith (2016). Time-history analysis is the recommended one, although suggested for final calculations, whereas simplified frequency ratio checks are suggested for the initial assessments of available damping. Methods involving 'normal modes' should be avoided as they cannot account for discrete damping elements within a structure (Smith and Willford, 2007).

Reports on additional damping provided by viscous dampers show that a maximum of 11.2% additional damping (100-year wind) was achieved in the 210m 60-storey building in Manila (Smith and Willford, 2007). The available or additional damping, nonetheless, is highly dependent on several factors associated with the components of the damped outrigger and its interaction with other main structural elements of the tall buildings, such as the core and perimeter columns. These factors, for convenience of the explanation, are described separately in the following sections.

§ 2.5.2 Purpose of the damped outrigger system

Since the engineer chooses the amplitude of most importance for a high-rise building response, the question is which amplitude will be more useful to consider for the design, given the characteristics of the building and its location. The first variable is building height versus material, as the transition from earthquake to wind dominant loading –in seismically active regions, it is at about 150 m for steel buildings (Connor and Laflamme, 2014; Taranath, 1998) and 250 m for concrete buildings (Connor and Laflamme, 2014). The second variable relates to the slenderness of the building; as previously mentioned, a large relative motion between perimeter columns and outrigger is necessary for the dampers to dissipate energy. Slenderness guarantees that the building's design is controlled by bending and axial stress rather than by shear deformation. The aspect ratio, i.e. the height/width ratio of the building, should be equal or larger than 5, in order to obtain a slender structure. There is no agreement about this value though; Smith and Coull (1991), in the context of the use of dynamic methods in wind loading analysis, and citing UBC, pointed out the validity of such methods for "exceptionally tall, slender, or vibration-prone buildings. Those may be defined (...) as those of height greater than 400ft (123m), or of a height greater than five times their width, or those with structures that are sensitive to wind-excited oscillations".

Some authors suggest that damping wind loading, even in high seismic regions, is more useful than damping seismic loading (Smith, 2016). However, this assumption responds to the need of reducing accelerations to meet serviceability criteria, whereas tall buildings in seismic regions may be exposed to severe ground motions that may pose challenges to meet safety criteria. Although the predominant loading condition may influence the assumed inherent damping ratio, (Smith *et al.*, 2010) argue that 'damping values nearer to those adopted in wind design are in fact more appropriate for seismic design of high-rise buildings'. The two 210 m tall residential buildings in Manila used as benchmark case study in this research, are located in a seismic region (UBC-97 Zone 4), but they were designed for damping vibrations induced by typhoon-strength winds (Willford and Smith, 2008). A feasible earthquake-exclusive scenario could only be observed in countries where hazards due to strong winds are not comparable, neither in frequency nor in level of damages, to those derived from the occurrence of earthquakes. For instance, in Chile there is no statistical data about strong winds, neither an official method for calculating wind forces in function of the building height. The reason seems to be the complete absence of such strong winds in the country. However, for the design of the two tallest buildings in Chile, *Titanium* (200 m) and *Costanera Center* (300 m), wind tunnel tests were required to assess the influence of the neighbour buildings over the wind pressure in the respective buildings. According to these studies it was concluded that the response is mixed: stress

and loading in foundations is dominated by the seismic action, while in the upper third of the building height, results from the application of seismic and wind loading are similar. Consequently, lateral displacements due to wind action should not be neglected[9].

The selection of the predominant amplitude or loading conditions will influence the type of damper to be used. The force produced by the dampers is dependent on the size and the velocity across the damper, modified by an exponent *k*. This exponent *k* can be varied between 0.15 and 2, depending on the damper manufacturer's specifications (Infanti *et al.*, 2008; Smith, 2016). The use of *k* =1, implies that the damping forces provided by the damper will be linearly proportional to the velocity. The use of ~=2 implies high forces at lower velocities, whereas the opposite occurs when lower values of k are used. It is been suggested that the selection of the exponent *k* depends on the purpose of the damped outrigger system. For example, a linear exponent (*k*=1) is been suggested optimal for wind applications (Smith, 2016). Under strong earthquake motions, the use of lower exponent might lead to the insensitivity of the dampers to low velocities, whereas the use of a linear exponent might lead to excessive damping forces, if compared to the wind damping (Smith, 2016; Willford and Smith, 2008). Referring to the study of Zhou and Li (2013), the amplitude dependence may be explained by the use of non-linear dampers with an exponent=0.2 (Smith, 2016). Often in commercially available viscous dampers, a relief valve helps to avoid excessive damping forces. A relief valve allows the damper to work in a linear pattern until a relief load or pressure value is reached (Figure 2.7). At higher velocities then, the damper exerts low forces without affecting its performance at lower velocities.

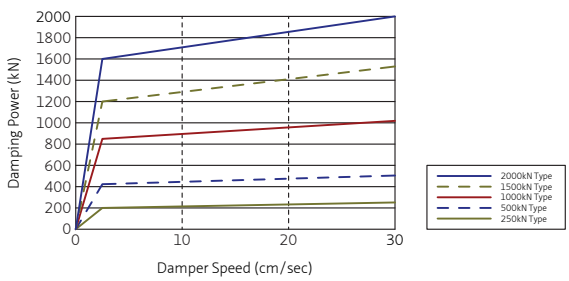

FIGURE 2.7 Damping force versus damper velocity for BDH oil viscous damper (source: Kayaba System Machinery Co. Ltd)

9 Guendelman, Tomas, personal communication, April 12, 2014

§ 2.5.3 Optimal location of the outriggers

For introducing this section, let the following model (Figure 2.8) be representative of a tall building with conventional outriggers, subjected to a lateral uniform loading:

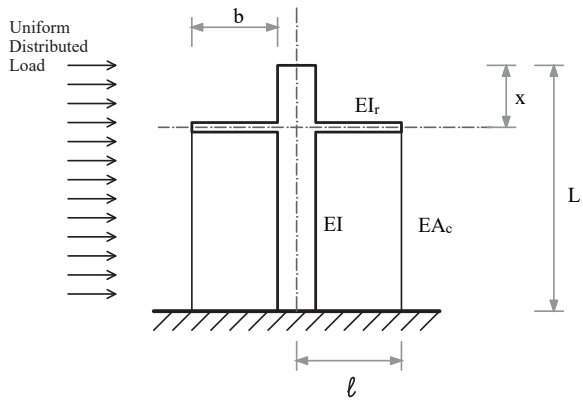

FIGURE 2.8 Analytical model of a conventional outrigger system

Aiming the preliminary design of buildings with conventional outriggers, Taranath (1998) defined a location of 0.545 of the total height as optimal for a single outrigger system to reduce the top drift. According to Taranath's simplified model, this optimal solution is a function of maximizing both the stiffness of the equivalent spring and the magnitude of the rotation of the cantilever at the spring location due to external loads. The stiffness decreases proportionally to the distance of the outrigger to the base; the rotation of the cantilever varies parabolically from a maximum value –at the top of the structure- to zero –at the bottom. Hence the optimal value is in between the maximum stiffness –bottom- and maximum rotation control –top. This is expressed by the restoring moment due to outrigger restraint $M_{x,}$ that is given by:

$$M_X = \frac{\theta_c}{\frac{1}{K_X} + \frac{L-x}{EI_C}} \tag{2.1}$$

where θ_c is the cantilever rotation at a distance x from the top (expressed as $L - x$) -due to a uniformly distributed load; EI_C is the bending stiffness of the core; and, K_X is the

equivalent spring stiffness of the perimeter columns at *x*, i.e. depending on the cross sectional area of the columns *A*.

Although Eq. 2.1 might be helpful for the preliminary design of the outrigger system, the optimal location obtained is the result of highly simplified assumptions that are unrealistic from a practical point of view. For example, the assumption that the intensity of lateral load remains constant for the whole height or that outriggers are flexurally rigid, may not reflect the actual structural behaviour. As it can be noted in Eq. 2.1, the outrigger stiffness is not included since it is assumed as an infinitively rigid truss. However, it might be necessary to introduce the outrigger flexibility in the analyses to obtain insights on how influential are the outrigger design parameters on the overall performance of the system. With this purpose, Smith and Coull (1991) proposed a compatibility analysis to determine the optimal location of outrigger systems to reduce roof drifts for a building under static uniform lateral loading. Despite it is also based on the building modelled as a cantilever beam, the method considered the stiffness properties of core, columns and outriggers by introducing the parameter ω, as defined by

$$\omega = \frac{\beta}{12(1+\alpha)} \tag{2.2}$$

where α and β are nondimensional parameters representing the stiffness core-to-column and core-to-outrigger ratios, respectively (as further revised in sections 2.4.5 and 2.4.6). Hence the optimal location for a single outrigger varied between 0.65 h –for a very stiff structure or small ω - and 0.79 h – for a very flexible structure or large ω (Figure 2.9).

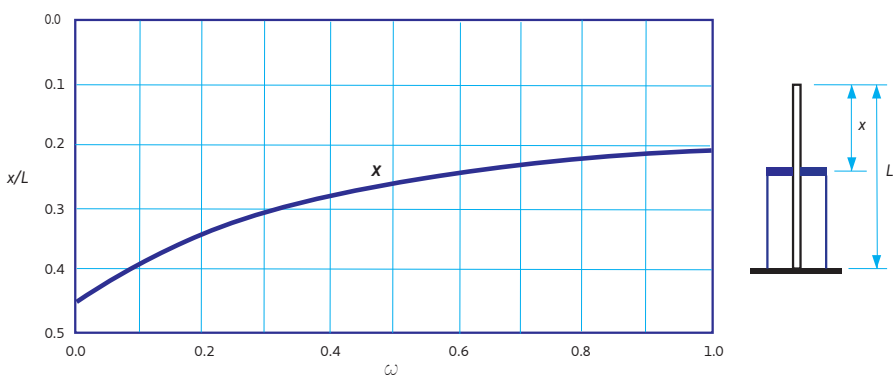

FIGURE 2.9 Optimal outrigger location for one-outrigger-system as proposed by Smith and Coull (1991)

Similar compatibility methods have been developed in order to determine optimal outrigger locations when account for foundations parameters in modelling shear-walls (Hoenderkamp, 2004; Hoenderkamp *et al*., 2003); or, when aiming the reduction of the base moment in core of multi-outriggers in tall building structures (Wu and Li, 2003). The influence of two outriggers in shear-wall buildings has been studied by Hoenderkamp (2008).

According to the studies reviewed, it seems that reducing structural roof deflection under consideration of static or quasi-static loading conditions will tend to determine an optimal location at about 0.5 h. According to Gamaliel (2008), the optimal location of a single outrigger is one that achieves a balanced moment design. This means that the reduction of moment due to the outrigger conveys a base moment equal to the moment at the level just above the outrigger. Accordingly, the core can be designed uniformly throughout the height providing adequate amount of bending stiffness. Under a quasi-static wind loading condition, such optimal location is found at 0.52 of the building's height. However, if the inter-storey drift is targeted for response reduction under the influence of an optimal location, such location approximately rises up to 0.63 (Zhou *et al*., 2016). This optimal height varies depending on the flexural rigidity of the outrigger defined by the parameter *b*, which is the distance between the core and perimeter column (Figure 2.10)

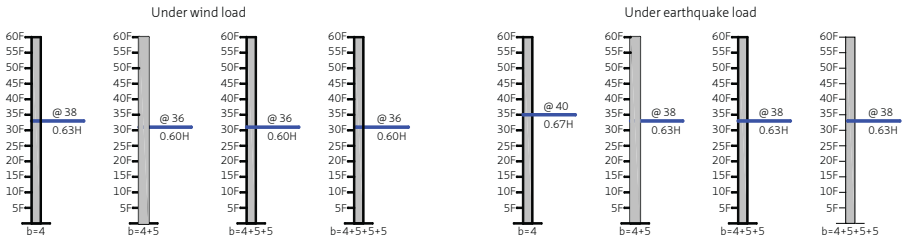

FIGURE 2.10 Optimal location of outrigger at different outrigger span *b*, according to Zhou *et al*. (2016)

Finally, from a functional perspective, outriggers are often placed within mechanical rooms in high rise buildings (Smith, 2016). These areas are used to locate compressors for air conditioning, general air handling equipment and other machinery (Figure 2.11). This makes it also possible to use facade riggers as there will be no office workers

or apartment dwellers present, i.e. no need of any windows[10]. All in all, the final location of the outriggers depends on both the availability of space and the influence of the outrigger members' size (Choi and Joseph, 2012).

FIGURE 2.11 Example of the use of pipelines and service areas located at the outrigger storey (50-storey building in Izmir; photography by the author)

§ 2.5.4 Damping coefficient

In order to provide an optimal supplemental damping, the optimal size or damping coefficient need to be found. The study of Chen *et al.* (2010), provided an approximate method to determine optimal location and size (damping coefficient) of the dampers, under free vibration, using a uniform straight cantilever beam with intermediate viscous dampers (Figure 2.12). In this study, the damper's effect was adding into a general partial differential motion equation under Bernoulli-Euler beam theory. Subsequent analytical solutions were derived, from which –through numerical iteration, eigenvalues of any order could be obtained. Optimal damping coefficients of the dampers (C_d) and corresponding maximum damping ratios of systems with different damper locations (αL, where L=building's height) were obtained for the first five modes. Moreover, the authors provided validated empirical equations to

10 Hoenderkamp, Hans, personal communication, May 21, 2014

estimate optimal damper locations for the first mode. According to a given formula, the maximum modal damping ratio for the first mode is achieved when the dampers are located at 0.51 of the beam's length. However, this analytical solution does not consider the axial deformation of the perimeter columns, nor the bending stiffness of the outriggers ($E_0I_0=\infty$). Without accounting for this influence, the location of the damped outriggers can only be considered sub-optimal in terms of modal damping increase, as it will be further discussed in sections 2.4.5 and 2.4.6.

Huang and Takeuchi (2017), developed an eigenvalue analysis method to obtain complex mode shapes and damping ratios for single-damped-outrigger systems. Outrigger stiffness and damper size indexes were introduced to determine optimal outrigger location and damper size. From this parametric study, the authors concluded that both outrigger location and damper size are the most influencing parameters in the response, as the damping ratio is most sensitive to these parameters. Moreover, the results reinforced the idea that optimal outrigger location –for a single-damped – outrigger- falls somewhere between 0.5 and 0.8h.

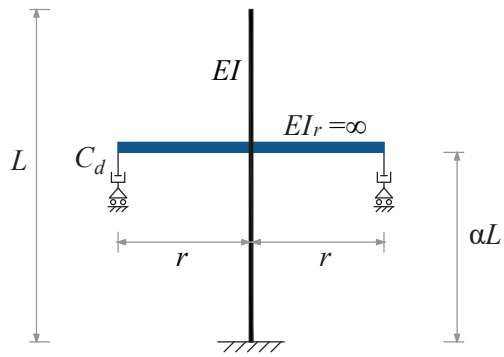

FIGURE 2.12 Cantilever beam with damped outriggers. Adapted from Chen *et al.* (2010)

§ 2.5.5 Stiffness core-to-column ratio

The non-dimensional stiffness core-to-column ratio is defined as follows (Smith and Coull, 1991)

$$\rho_{cto} = \frac{2EIr}{(EI)_O H} \tag{2.3}$$

where *EI* and $(EA)_c$ represent core and column rigidities, respectively; *r* is the distance between the centroid of the core and the perimeter columns.

The influence of the axial stiffness of the perimeter columns in the optimal location of a single outrigger was studied by Tan *et al.* (2014). The analytical model proposed there simulated the action of the damped outrigger as a general rotational spring (Figure 2.13). The equivalent rotational spring incorporated the combined effects of the dynamic stiffness of the dampers and the axial stiffness of the perimeter columns. A parametric study was conducted to address the combined influence of the stiffness core-to-column ratio, location of the damped outrigger and damping coefficient. Regarding the optimal location of the damped outriggers, the study concluded that the optimal position varies with the stiffness core-to-column ratio and damper's damping coefficient. In addition, the authors pointed out that the number of optimal positions is equal to the mode order. This means that a single damped outrigger can be optimally located to increase modal damping of the first mode only. Despite the authors found that the stiffness core-to-column ratio significantly affects the modal damping ratio, yet the optimal location was set at 0.51 of the building's height (h), for the first mode.

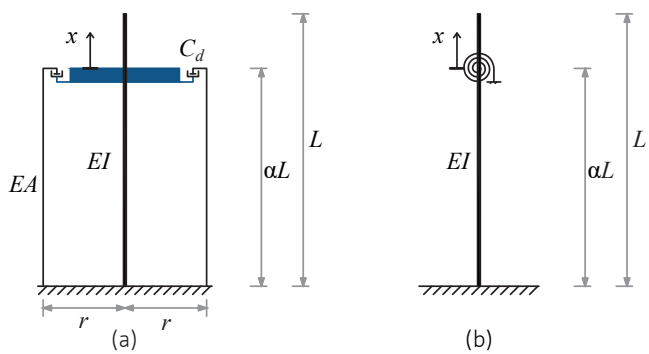

FIGURE 2.13 (a) simplified model and (b) general rotational stiffness model. Adapted from Tan *et al.* (2014)

The general rotational spring model proposed in the aforementioned study was combined with dynamic stiffness method for application to multiple damped outriggers and verified in comparison with a finite element (FE) model in Tan *et al.* (2015). It was found that the corresponding optimal positions are around 0.5h at the first mode, 0.18 – 0.82h at the second mode, and 0.1 – 0.48 – 0.9h at the third. The same method was improved by adding the influence of stiffness core-to-outrigger ratio into the formulation of the general rotational stiffness, in the study of Fang *et al.* (2015). Two-outrigger configurations, combining damped and undamped (conventional) outriggers, were investigated through four FE models: two damped outriggers, bottom damped outrigger, top damped outrigger, and two conventional outriggers (Figure 2.14). Results showed that maximum modal damping is achieved when locations for the two damped outriggers and bottom damped outrigger are, respectively, around 0.42h and 0.45h at the first mode, 0.21h and 0.22h at the second mode, and 0.5h and 0.5h at the third. However, in these simulations the contribution of the stiffness core-to-outrigger ratio was not considered.

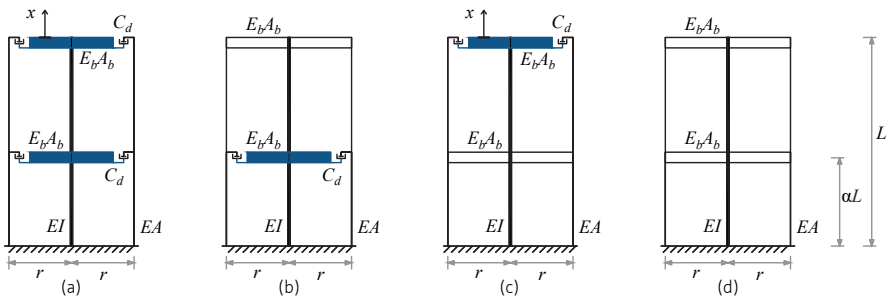

FIGURE 2.14 Different configurations of damped (a), undamped (d) and combined damped and undamped outrigger systems (b-c). Adapted from Fang *et al.* (2015)

In the study of Chang *et al.* (2012), semi-active damped outriggers were modelled inspired in the existing 60-storey building with viscous damped outriggers, and two simplified numerical models were developed; either with or without the contribution of the perimeter columns. The MR damped outrigger without perimeter columns was later experimentally verified through real-time hybrid simulation for validation. The results showed that for the MR damped outrigger with perimeter columns, the optimal location is 0.9h and damper size is 80-90MN-sec/m. The optimallocation of the MR damped outrigger without the contribution of the perimeter columns is 0.7h and damper size is half of the previous one.

§ 2.5.6 Stiffness core-to-outrigger ratio

The stiffness core-to-outrigger ratio is a non-dimensional parameter given by Smith and Coull (1991)

$$\rho_{ctc} = \frac{EI}{2(EA)_C r^2} \tag{2.4}$$

where $(EI)_O$ is the effective flexural rigidity of the outrigger, and H is the building's height.

Hoenderkamp (2004) proposed a compatibility method which replaces the equivalent column spring stiffness, by the bending and shear stiffness of the outrigger. Consequently, this method is similar to that of Taranath (Eq. 2.1), except in the way the restoring moment due to outrigger restraint M_x is computed. This is now given by:

$$M_X = \frac{\theta_c}{\frac{L-x}{EI_C} + \frac{b}{24\alpha^2 EI_r} + \frac{1}{h\alpha^2 GA_r}} \tag{2.5}$$

where α is the ratio of the distance of the exterior column - centre line of the core (*l*) to the outrigger length (*b*); EI_r is the bending stiffness of the outrigger, which accounts for the cross-sectional area of the top and bottom chords of the outrigger; *h* is the outrigger's height; and, GA_r is a parameter accounting for the individual racking shear stiffness of all the bracing segments in the outrigger. In simple words, the second term in the divisor in Eq. 2.5 represents the rotation due to bending at the outrigger interface, whereas the third term represents the rotation due to racking shear resulting from the strain in the diagonals.

The racking shear stiffness is dependent on the type of bracing used in the outrigger. Since two separate models with outriggers of one and two storeys high are under study, the criterion for the calculation of the racking shear stiffness required a decision as to whether the bracing should be taken as X or K type (Figure 2.15). Hoenderkamp suggested the use of the X-bracing type (option 1):

'The reason is that the racking shear stiffness of K-bracing assumes the inclusion of the beam stiffness. This comes from the generally accepted basic analytical model for bracing segments where the shear force at story level is split equally between the two nodes at the top of the columns. This causes axial forces in the beams with K-bracing. For the analysis of X-braced segments the forces go directly into the diagonals.

That's why the cross-sectional area of the floor beam is omitted in the equation for its racking shear stiffness.' [11]

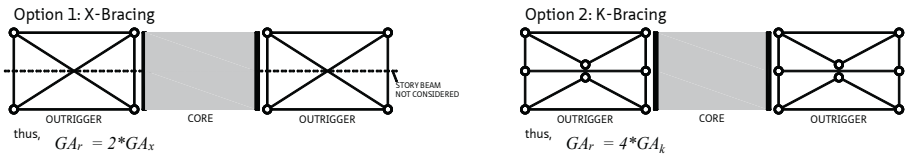

FIGURE 2.15 The criteria discussed for the selection of the racking shear stiffness of the outrigger

Since the outriggers increase the restoring moment of the core against lateral loads, a stiff outrigger cantilever is desirable as it simplifies the analysis by assuming its behaviour to be closed to a rigid body. Consequently, outriggers are commonly designed to include two storeys, so that the large depth helps to increase the moment of inertia of the system and thus, its bending and shear stiffness. Although the original outrigger used in Shangri-la building is composed of shear walls (called outrigger walls or deep beam outriggers), in this study we selected a truss girder model for the outrigger configuration due to the achievement of 'a high effective stiffness due to the utilization of axially loaded members' (O'Neill, 2006).

11 Hoenderkamp, Hans, personal communication, May 2, 2014.

§ 2.6 Conclusions

From the studies revised in this literature research, it is possible to conclude that

- Although conventional outrigger systems have been studied and implemented thoroughly, there are a few implementations of viscous damped outriggers and none of semi-active damped outriggers. Research studies seem to follow the same trend.
- Outrigger systems can be applied for reducing dynamic response under both wind and earthquake loading.
- The most influential parameters in the design of damped outrigger systems are the outrigger location, damping coefficient, and stiffness core-to-column and core-to-outrigger ratios.
- The optimization of these parameters, say outrigger location or damper size, is influenced by the selected response to be reduced. Most of the studies concentrated on reducing roof displacements. Few studies consider other parameters, such as inter-storey drifts, base shear or moments.

References

Ahn, S.-K., Min, K.-W., Park, J.-H., Lee, S.-H., Lee, D.-G., Oh, J.-K., Kim, K.-S. and Lee, S.-K. 2008. Practical issues and solutions on installation of viscoelastic dampers in a 46-story reinforced concrete building structure. The Structural Design of Tall and Special Buildings. 17: 231-243. 10.1002/tal.353

Asai, T., Chang, C.-M., Phillips, B. M. and Spencer Jr, B. F. 2013. Real-time hybrid simulation of a smart outrigger damping system for high-rise buildings. Engineering Structures. 57: 177-188. http://dx.doi.org/10.1016/j.engstruct.2013.09.016

ATC-PEER, Applied Technology Council - Pacific Earthquake Engineering Research Center. 2010. Modeling and acceptance criteria for seismic design and analysis of tall buildings.

Chang, C.-M., Asai, T., Wang, Z., Spencer Jr, B. F. and Chen, Z. 2012. Smart outriggers for seismic protection of high-rise buildings

Chang, C.-M., Wang, Z., Spencer Jr, B. F. and Chen, Z. 2013. Semi-active damped outriggers for seismic protection of high-rise buildings. Smart Structures and Systems. 11: 435-451.

Chen, Y., McFarland, D., Wang, Z., Spencer, B. and Bergman, L. 2010. Analysis of Tall Buildings with Damped Outriggers. Journal of Structural Engineering. 136: 1435-1443. 10.1061/(ASCE)ST.1943-541X.0000247

Chen, Y. and Zhang, Z. 2017. Analysis of outrigger numbers and locations in outrigger braced structures using a multiobjective genetic algorithm. The Structural Design of Tall and Special Buildings. 10.1002/tal.1408e1408-n/a. 10.1002/tal.1408

Choi, H. S., Ho, G., Joseph, L. and Mathias, N. 2012. Outrigger design for high-rise buildings. Council on Tall Buildings and Urban Habit

Choi, H. S. and Joseph, L. 2012. Outrigger system design considerations. International Journal of High-Rise Buildings. 1: 237-246.

Connor, J. and Laflamme, S. 2014. Structural motion engineering. Springer:

Cruz, C. and Miranda, E. 2017. Evaluation of Damping Ratios for the Seismic Analysis of Tall Buildings. Journal of Structural Engineering. 143: 04016144. 10.1061/(ASCE)ST.1943-541X.0001628

Deng, K., Pan, P., Lam, A. and Xue, Y. 2013. A simplified model for analysis of high-rise buildings equipped with hysteresis damped outriggers. The Structural Design of Tall and Special Buildings. 10.1002/tal.1113n/a-n/a. 10.1002/tal.1113

Fang, C. J., Tan, P., Chang, C. M. and Zhou, F. L. 2015. A general solution for performance evaluation of a tall building with multiple damped and undamped outriggers. The Structural Design of Tall and Special Buildings. 24: 797-820. 10.1002/tal.1212

Gamaliel, R. 2008. Frequency-based response of damped outrigger systems for tall buildings

Hoenderkamp, J. 2004. Shear wall with outrigger trusses on wall and column foundations. The structural design of tall and special buildings. 13: 73-87.

Hoenderkamp, J. C. D. 2008. Second outrigger at optimum location on high-rise shear wall. The Structural Design of Tall and Special Buildings. 17: 619-634. 10.1002/tal.369

Hoenderkamp, J. C. D. and Bakker, M. C. M. 2003. Analysis of high-rise braced frames with outriggers. The Structural Design of Tall and Special Buildings. 12: 335-350. 10.1002/tal.226

Hoenderkamp, J. C. D., Bakker, M. C. M. and Snijder, H. H. 2003. Preliminary design of high-rise outrigger braced shear wall structures on flexible foundations. Heron. 48: 81-98.

Huang, B. and Takeuchi, T. 2017. Dynamic Response Evaluation of Damped-Outrigger Systems with Various Heights. Earthquake Spectra. 33: 665-685. 10.1193/051816EQS082M

Infanti, S., Robinson, J. and Smith, R. 2008. Viscous dampers for high-rise buildings

Jackson, M. and Scott David, M. 2010. Increasing Efficiency in Tall Buildings by Damping

Jiang, H., Li, S. and Zhu, Y. 2017. Seismic performance of high-rise buildings with energy-dissipation outriggers. Journal of Constructional Steel Research. 134: 80-91. https://doi.org/10.1016/j.jcsr.2017.03.013

Kamgar, R. and Rahgozar, R. 2017. Determination of optimum location for flexible outrigger systems in tall buildings with constant cross section consisting of framed tube, shear core, belt truss and outrigger system using energy method. International Journal of Steel Structures. 17: 1-8. 10.1007/s13296-014-0172-8

Kibayashi, M., Kasai, K., Tsuji, Y., Kikuchi, M., Kimura, Y., Kobayashi, T., Nakamura, H. and Matsuba, Y. 2004. JSSI manual for building passive control technology. Part-2 Criteria for implementation of energy dissipation devices

Kim, H.-S. and Kang, J.-W. 2017. Semi-active Outrigger Damping System for Seismic Protection of Building Structure. Journal of Asian Architecture and Building Engineering. 16: 201-208. 10.3130/jaabe.16.201
LATBSDC. 2014. An Alternative Procedure for Seismic Analysis and Design of Tall Builings Located in the Los Angeles Region.
Morales-Beltran, M. and Teuffel, P. 2013. Towards smart building structures: adaptive structures in earthquake and wind loading control response–a review. Intelligent Buildings International. 5: 83-100.
O'Neill, J. C. 2006. Application of damping in high-rise buildings
Park, K., Kim, D., Yang, D., Joung, D., Ha, I. and Kim, S. 2010. A comparison study of conventional construction methods and outrigger damper system for the compensation of differential column shortening in high-rise buildings. International Journal of Steel Structures. 10: 317-324. 10.1007/BF03215840
Smith, B. S. and Coull, A. 1991. Tall building structures: analysis and design.
Smith, R. 2016. The Damped Outrigger-Design and Implementation. International Journal of High-Rise Buildings. 5: 63-70.
Smith, R., Merello, R. and Willford, M. 2010. Intrinsic and supplementary damping in tall buildings. Proceedings of the Institution of Civil Engineers - Structures and Buildings. 163: 111-118. 10.1680/stbu.2010.163.2.111
Smith, R. J. and Willford, M. R. 2007. The damped outrigger concept for tall buildings. The Structural Design of Tall and Special Buildings. 16: 501-517. 10.1002/tal.413
Spence Seymour, M. J. and Kareem, A. 2014. Tall Buildings and Damping: A Concept-Based Data-Driven Model. Journal of Structural Engineering. 140: 04014005. 10.1061/(ASCE)ST.1943-541X.0000890
Tan, P., Fang, C. and Zhou, F. 2014. Dynamic characteristics of a novel damped outrigger system. Earthquake Engineering and Engineering Vibration. 13: 293-304. 10.1007/s11803-014-0231-3
Tan, P., Fang, C. J., Chang, C. M., Spencer, B. F. and Zhou, F. L. 2015. Dynamic characteristics of novel energy dissipation systems with damped outriggers. Engineering Structures. 98: 128-140. https://doi.org/10.1016/j.engstruct.2015.04.033
Taranath, B. S. 1998. Steel, concrete, & composite design of tall buildings.
Wang, Z., Chang, C.-M., Spencer Jr, B. F. and Chen, Z. 2010. Controllable outrigger damping system for high rise building with MR dampers
Willford, M. and Smith, R. 2008. Performance based seismic and wind engineering for 60 story twin towers in Manila
Willford, M., Smith, R., Scott, D. and Jackson, M. 2008. Viscous dampers come of age. STRUCTURE magazine. 6: 15-18.
Wu, J. R. and Li, Q. S. 2003. Structural performance of multi-outrigger-braced tall buildings. The Structural Design of Tall and Special Buildings. 12: 155-176. 10.1002/tal.219
Yang, Q., Lu, X., Yu, C. and Gu, D. 2016. Experimental study and finite element analysis of energy dissipating outriggers. Advances in Structural Engineering. 20: 1196-1209. 10.1177/1369433216677122
Yi, F., Dyke, S., J., Caicedo, J., M. and Carlson, J. D. 2001. Experimental Verification of Multiinput Seismic Control Strategies for Smart Dampers. Journal of Engineering Mechanics. 127: 1152-1164. 10.1061/(ASCE)0733-9399(2001)127:11(1152)
Zhou, Y. and Li, H. 2013. Analysis of a high-rise steel structure with viscous damped outriggers. The Structural Design of Tall and Special Buildings. 23: 963-979. 10.1002/tal.1098
Zhou, Y., Zhang, C. and Lu, X. 2016. An inter-story drift-based parameter analysis of the optimal location of outriggers in tall buildings. The Structural Design of Tall and Special Buildings. 25: 215-231. 10.1002/tal.1236
Zhou, Y., Zhang, C. and Lu, X. 2017. Seismic performance of a damping outrigger system for tall buildings. Structural Control and Health Monitoring. 24: e1864-n/a. 10.1002/stc.1864
Zhou, Y., Zhang, C. Q. and Lu, X. L. 2014. Earthquake resilience of a 632-meter super-tall building with energy dissipation outriggers

3 Energy-based Design Methods

§ 3.1 Summary

This chapter aims to give background information about energy-based design methods for earthquake-resistant buildings. Through a literature review, the derivation of the energy balance equation is described first, as the use of relative terms for its definition in this thesis is also addressed. Next, energy-based methods applied to seismic design of buildings are reviewed; emphasis is given to the assessment of both energy demands – defined by the earthquake motion, and energy capacity – defined by elastic and plastic mechanism of energy dissipation. Despite the advantages of energy-based design methods, there are few precedents of studies on seismic energy distributions in outrigger structures and on tall buildings with long periods. Similarly, studies addressing the use of viscous dampers to increase the energy capacity of tall buildings subjected to earthquake motion are rare. Hence, based on both the literature reviewed and the specific case of tall buildings with damped outriggers, the evaluation of the energy capacity of the system is proposed on the basis of energy ratios: damping (inherent and supplemental) and hysteresis to input energy.

§ 3.2 Introduction

Within an ideal scenario, structures behave elastically. In practice though, hence in structural design, structures are intended to partially respond in the inelastic range, which makes them more economical. This inelastic threshold, especially in seismic design, is determined by a cost-saving approach that does not compromise structural safety. Seismic events worldwide have served as empirical proof that structures designed by using design forces derived from its linear behaviour, have resisted higher earthquake forces due to its ductility. Seismic design codes, either force- or displacement-based, have accounted for these effects, by introducing modification factors to reduce seismic force and over strength demands depending on the structural system and the aimed ductility. However, such codes are based on the quantification

of the response demand in terms of peak values. The design of earthquake-resistant structures is not only a function of the peak response demand but also a function of the time history response demand. Moreover, the effectiveness of supplemental damping provided by, say a damped outrigger, to reduce the building response needs to be evaluated along the entire history of the seismic motion and not only in terms of peak response values.

The peak response might not provide enough information about the nonlinear behaviour of the structure during a seismic motion; Parameters accounting for the cumulative nonlinear response, such as plastic energy, represent an effective quantity to evaluate time history response. This is a good indication of how the plastic energy has been absorbed by the structural components, or in simple words, as an indicator of the damage suffered by the structure. For instance, under earthquake loadings, a reinforced concrete structure is weakened or damaged by a combination of stress reversals and high stress excursions; consequently, any damage criterion should include not only the maximum response, but also the effect of repeated cyclic loadings (Gosain, *et al*., 1977; Banon, *et al*., 1980 as cited in Park *et al*. (1984)). Since, in addition to the reduction of the response in terms of peak values, the combined influence of the intensity, frequency content, and duration of strong earthquakes on the time-history response of the structure need to be evaluated, energy-based design methods seems to be more suitable. Energy-based design methods have the potential to address both the effect of the duration of the earthquakes and the hysteretic behaviour of the structure (Khashaee *et al*., 2003). As stated by Uang and Bertero (1990), an energy-based design method is based on the premise that the energy demand during an earthquake can be predicted as the energy absorbed and dissipated by the structure can be therefore defined. A correct design implies therefore that an energy-dissipating mechanism provides the structure with the ability to absorb and dissipate large amounts of seismic energy. The capacity to absorb and dissipate energy of a structure must be larger than the input energy introduced during a strong ground motion, in order to ensure that such structure will efficiently resist earthquakes.

In the case of tall buildings equipped with damped outriggers, a correct design also relies on the arguable assumption that the dampers will absorb the total earthquake energy while the rest of the structure remains elastic during the seismic event. Nevertheless, under strong or severe earthquake-induced motion some plastic hinges or failures may be produced in the structure before the dampers can dissipate the total input energy. Therefore, the hysteretic behaviour of the host structure needs to be evaluated along the dampers' performance in order to determine how the earthquake input energy is distributed through all the components.

This chapter aims to give background information about energy-based design methods for earthquake-resistant buildings. Derivation of the energy balance equation is described, addressing the use of relative terms for its definition in this thesis. A short literature review is given next, where energy-based methods applied to seismic design of buildings are reviewed. Emphasis is given on how the design method is based on the assessment of both energy demands – defined by the earthquake motion, and energy capacity – defined by elastic and plastic mechanism of energy dissipation. Based on both the literature reviewed and the specific case of tall buildings with damped outriggers, the evaluation of the energy capacity of the system is proposed on the basis of energy ratios: damping (inherent and supplemental) and hysteresis energy.

§ 3.3 Absolute and relative energy equations for a SDOF system

Housner (1956), as cited in Terapathana (2012), proposed the study of the seismic response of the structures in energy terms. The underlying idea is that after transferring the total input energy to the structure, part of it will be dissipated by the motion of structure, called kinetic energy. Some part will be absorbed by deformation of structural members, known as strain energy. The rest of the input energy will be dissipated through damping and plastic deformation. Based on this principle, 'he inferred that the safe design could be obtained if the sum of elastic energy and plastic energy which is considered as energy supply is greater than or equal to the total input energy which considered as energy demand.' (Terapathana, 2012). Based on Housner's idea, researchers suggested the use of an energy balance equation to improve the estimation of the maximum input energy (for example, see Akiyama (1988)). However, Uang and Bertero (1990) remarked that an equation of motion of a system can be formulated in terms of either absolute or relative terms. Hence they noted that the definition of both input and kinetic energy depend on which equation is used to derive the energy equation. Specifically, they noted that the equation of motion of a single degree of freedom (SDOF) system can be formulated as either

$$m\ddot{x}_t + c\dot{x} + f_s = 0 \tag{3.1}$$

$$m\ddot{x} + c\dot{x} + f_s = -m\ddot{x}_g \tag{3.2}$$

where m=mass, c=damping, f_s=kx (linear elastic system) = restoring force, $x_t = x + x_g$ = absolute displacement of the mass, x = relative displacement of the mass w.r.t the ground, and x_g = earthquake ground displacement. Whilst Eq. 3.1 describes a system where the restoring plus damping force is equal to the force applied to the structure foundation (Figure 3.1a), Eq. 3.2 describes the equivalent system with a fixed based and subjected to an effective horizontal dynamic force of magnitude $-m\ddot{x}g$ (Figure 3.1b).

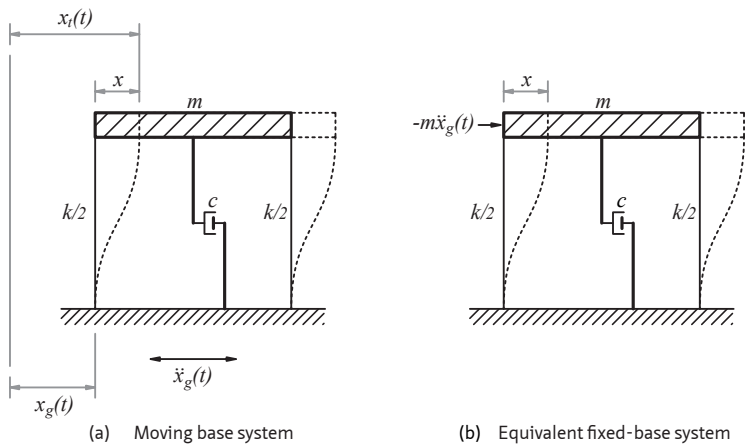

FIGURE 3.1 Analytical model of a SDOF system subjected to ground motion. Adapted from Uang and Bertero (1990)

§ 3.3.1 Derivation of absolute energy equation

Following Uang and Bertero (1990), integrating Eq.3.1 w.r.t the displacement x over the duration of the ground motion and replacing x by ($x_t - x_g$) in the resulting first term, yields

$$\frac{m(\dot{x}_t)^2}{2} + \int c\dot{x}dx + \int f_s dx = \int m\ddot{x}_t dx_g \tag{3.3}$$

where the first, second and third terms of the above equation represent the *absolute* kinetic, damping and absorbed energies, respectively. The absorbed energy is composed of the elastic strain energy and plastic hysteretic energy. The right-hand-side term is the *absolute* input energy, which represents the work done by the total base shear at the foundation on the foundation displacement.

§ 3.3.2 Derivation of relative energy equation

Integrating Eq. 3.2 w.r.t displacement *x*, yields

$$\frac{m(\dot{x})^2}{2} + \int c\dot{x}dx + \int f_s dx = -\int m\ddot{x}_g dx \tag{3.4}$$

where the first term represents the *relative* kinetic energy. The second and third terms remain unchanged, hence damping and absorbed energies are calculated in the same way regardless if relative or absolute terms are used. The right-hand-side term is the *relative* input energy, which represents the work done by the static equivalent lateral force on the equivalent fixed-base system, i.e. neglecting the effect of rigid body translation of the structure (Uang and Bertero, 1990).

§ 3.4 Relative energy balance equation of a MDOF system

§ 3.4.1 Use of the relative energy equation in this thesis

Absolute- and relative-based energy balance equations differ only in the way they define kinetic and input energy. Since (1) damping energy, strain energy, and hysteretic energy terms are uniquely defined, irrespective of which method is used, and (2) input energy (E_I) is equal to the sum of kinetic plus all the other energies, we can conclude that the difference between the two methods lies on how kinetic energy is defined. In fact, absolute kinetic energy is based on the absolute velocity, which in turn is the sum of the relative velocity (used to calculate relative kinetic energy) and the ground velocity. Hence, as expressed by Bruneau and Wang (1996) '*the relative kinetic energy could be considered as just a subset of the absolute one*'.

According to Bruneau and Wang (1996) and Chopra (1995) as cited in Khashaee *et al.* (2003), the computation of the earthquake 'input energy in terms of the relative motion is more meaningful than the input energy in terms of absolute motion since internal forces within a structure are computed using relative displacements and velocities'. Such recommendation is followed in this study. Other researchers,

nevertheless, support the use of absolute energy input. In Wong and Johnson (2009), the use of tuned mass dampers (TMD's) to reduce the structural response is proposed. According to the studies, TMDs are able to store large elastic energy to be further released in the form of damping energy. This leads to the reduction of plastic energy dissipated by the host structure, during a seismic event. Since the stored elastic energy is the sum of kinetic and strain energies, the use of whether absolute or relative terms to define the kinetic energy there becomes crucial. The authors then justify the use of absolute kinetic energy by referring to the seminal study of Uang and Bertero (1990), where the authors concluded that '*the use of an "absolute" energy equation rather than a "relative" energy equation has the advantage that the physical energy input is reflected*'.

When the energy capacity of a structure is based on the increasing storing energy, the definition –and discussion- of which method must be used to quantify the energy demand becomes fundamental. However, when the increase of the energy capacity of a structure is not based on the increase of storing elastic energy but the damping energy given by the viscous dampers ($E_{DAMPERS}$), the definition of which type of method we use to assess the energy distribution is less relevant. In the study described in the next chapters, given the interest on quantifying only the hysteretic and damping energies – including that derived from the dampers as well, the distinction between absolute and relative energy methods become less critical (Bruneau and Wang, 1996; Khashaee *et al.*, 2003). Nevertheless, Uang and Bertero (1990) point out that the use of the relative input energy may lead to inaccurate computations of the input energy for long period structures –which is the case in this research-, as the methods to select the time in which the input energy is evaluated 'may significantly underestimate the maximum input energy that may occur early in the ground motion shaking'.

Finally, regardless of the energy balance equation being defined in relative or absolute terms, it is worth noting that results obtained by either method are certainly interchangeable by modifying the respective parameters. This does not compromise, therefore, the validity of the observations made by one or the other method.

§ 3.4.2 Derivation of relative energy balance equation for a MDOF system

The equation governing dynamic response of a multi-degree of freedom (MDOF) system, such as a tall building, can take the form

$$M\ddot{x} + C\dot{x} + Kx = -M\Gamma\ddot{x}_g \tag{3.5}$$

where *M* and *K* are the diagonal lumped mass and stiffness matrices, respectively; *C* is the damping matrix computed considering Rayleigh damping; *x* is the column vector of relative displacements of the node mass with respect to ground; $\ddot{x}_g$ is the one-dimensional ground acceleration; and Γ is the influence vector that accounts for the effect of ground excitation on a specific degree of freedom of the structure (Chopra, 2012). If Eq. 3.5 is multiplied by the transpose of the relative velocity vector $\dot{x}(t)$, and integrated over the entire duration of the ground motion (*0-t*), the equation of motion can be expressed in terms of the energy balance equation as follows

$$\int_0^t \dot{x}^T M\ddot{x}dt + \int_0^t \dot{x}^T C\dot{x}dt + \int_0^t \dot{x}^T Kxdt = -\int_0^t \dot{x}^T M\Gamma\ddot{x}_g dt \tag{3.6}$$

The first term in Eq. 3.6 is the relative kinetic energy (E_K), which can be written as

$$E_K = \int_0^t \dot{x}^T M\ddot{x}\ dt = \frac{1}{2}\dot{x}^T M\dot{x} \tag{3.7}$$

The second term in Eq. 3.6 is the damping energy of the structure ($E_{DAMPING}$) and it can be written as

$$E_{DAMPING} = \int_0^t \dot{x}^T C\dot{x}\ dt \tag{3.8}$$

Since viscous dampers are attached to the outrigger structure, $E_{DAMPING}$ includes also the energy dissipated by these passive devices, so that the total damping energy becomes

$$E_{DAMPING} = E_D + E_{dampers} = \int_0^t \dot{x}^T C\dot{x}\ dt + \int_0^t \dot{x}^T \Lambda C_d \dot{x}_d^{\kappa}\ dt \tag{3.9}$$

where E_D represents the energy dissipated by inherent structural damping (also called equivalent viscous damping); Λ is the location matrix of the dampers –associated to the outrigger location λ, C_d is the damping coefficient of the damper, $\dot{x}_d$ is the velocity

across the damper and κ is the exponent value that controls the linear/nonlinear behaviour of the damper.

The third term in Eq. 3.6 is the total absorbed energy (E_A), defined as

$$E_A = \int_0^t \dot{x}^T K x \, dt \tag{3.10}$$

Since the structure absorbs energy by a combination of elastic and inelastic mechanisms, E_A can also be defined as

$$E_A = E_S + E_H \tag{3.11}$$

where E_S and E_H are the elastic strain and hysteretic energy, respectively. By considering [K] as the pre-yield stiffness matrix of the structure, E_S can be written as

$$E_S = \frac{1}{2} \dot{x}^T K x \tag{3.12}$$

The hysteretic energy E_H is given by

$$E_H = E_{H-axial} + E_{H-bending} + E_{H-shear} \tag{3.13}$$

where $E_{H\text{-axial}}$, $E_{H\text{-bending}}$, and $E_{H\text{-shear}}$ are the hysteretic energies due to axial, bending, and shear stresses, respectively. However, due to the assumption of a Bernoulli beam in the modelling of the core, stresses and strains derived from shear forces can be neglected and thus E_H is reduced to

$$E_H = \int f_s(x - x_{yield}) \, dx + \int M_b(\theta - \theta_{yield}) \, d\theta \tag{3.14}$$

where f_s is the restoring force, M_b is the bending moment, and θ is the associated angle of rotation. The formulations to derive the strain and hysteretic energy are given in section 3.5. Although they are not included in the computations, the formulations to derive energies from shear forces are given in Appendix A: Strain and hysteretic energy stored by elements under shear forces, for completeness.

Finally, the last term in the Eq. 3.6 is the total energy introduced in the system as a consequence of the ground motion produced by an earthquake. This energy is equivalent to the energy input at foundation of the building as given by

$$E_I = -\int_0^t \dot{x}^T M \ddot{x}_g \, dt \tag{3.15}$$

Finally Eq. 3.6 can be rewritten as the energy balance equation for a MDOF system is given by

$$E_K + E_D + E_{dampers} + E_S + E_H = E_I \tag{3.16}$$

§ 3.5 Energy-based design of buildings

In an energy-based design of buildings, the first five terms in Eq. 3.16 are considered the energy capacity of the structure, whereas the right-hand-side term is considered the energy demand. From a seismic design perspective, it is obvious that the capacity of the structure should be larger than the response demand, i.e. energy capacity > energy demand. For a non-linear system subjected to ground motions (Figure 3.2), strain and kinetic energies are relatively small and at the end of the response, both E_K and E_S become zero (Bulent Akbas *et al.*, 2006; Nariyuki and Hirao, 1988) . Thus, Eq. 3.16 becomes

$$E_D + E_{dampers} + E_H = E_I \tag{3.17}$$

Whereas E_D and $E_{dampers}$ can be easily obtained from the structural and damper parameters, both E_H and E_I are more difficult to obtain; the seismic energy demand on the structure due to the design earthquake (E_I) depends on several parameters. Akiyama (1988) computed that the parameters that affected earthquake input energy were mainly the mass and the fundamental period of the structure, whereas strength and stiffness characteristics scarcely affected the total input energy. Sucuoğlu and Nurtuğ (1995) studied the sensitivity of seismic energy dissipation to ground motion and system characteristics. It is found that peak ground acceleration, peak ground velocity to acceleration (V/A), dominant period of ground excitation and effective response duration are closely correlated with the energy dissipated by a SDOF system. Ductility ratio and damping ratio have no significant influence on the energy dissipation.

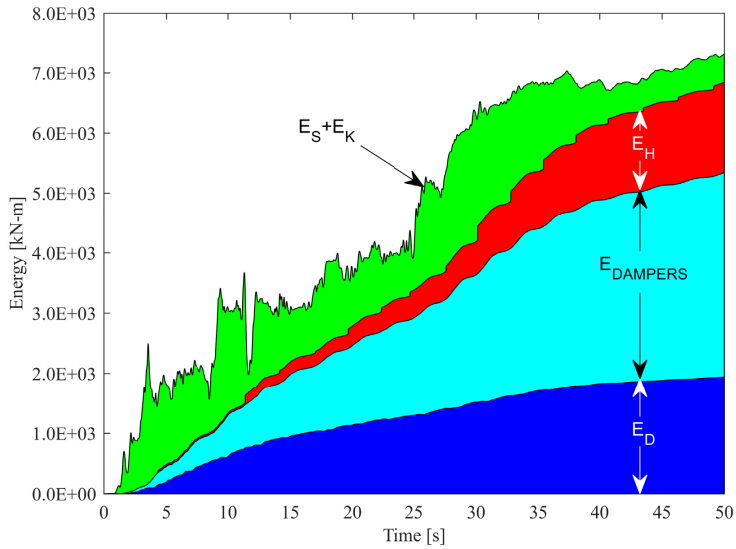

FIGURE 3.2 Typical energy distribution of an inelastic system with viscous damper under strong ground motions

Apart from estimating the energy demand, the mechanism of dissipation of the input energy in structural elements by the hysteretic action is of primordial importance. Due to the fact that multi-storey MDOF systems can be modelled as SDOF system, extensive research have been developed on methods to estimate the distribution of hysteretic energy along storeys, using simplified models (Nakashima *et al*., 1996; Wang and Yi, 2012). A method for estimating a storey-wise hysteretic energy distribution in steel moment frame buildings up to 10-storeys is presented in Shen and Akbas (1999)and up to 20-storeys is presented in Prasanth *et al*. (2008). Hysteretic energy distributions in shear buildings up to 10-storeys are studied in Papazafeiropoulos *et al*. (2017).

§ 3.5.1 Towards an energy-based design of tall buildings with supplemental damping devices

Energy-based design directly accounts for the influence of the duration of strong motion and for the hysteretic behaviour of the structure and is suited for seismic design of structures with supplemental damping devices. Energy-based design of buildings with supplemental damping devices have been addressed by considering hysteretic

dampers (Benavent-Climent, 2011; Foti *et al.*, 1998; Nakashima *et al.*, 1996); tuned mass dampers (Wong and Johnson, 2009); and active mass dampers and tendon systems (Yanik *et al.*, 2014). Studies on seismic energy distribution in tall buildings can also be found in related literature –see for example (Beiraghi *et al.*, 2016; Lu *et al.*, 2014; Zhou *et al.*, 2014). Most of the reviewed research on seismic energy distributions concentrates on buildings with natural periods up to 4s (B. Akbas *et al.*, 2001; Decanini and Mollaioli, 2001).

An energy-based seismic design method of tall buildings with damped outriggers is based on the assessment of both the energy demands due to large-earthquake induced motion the energy capacity of the system, i.e. the energy capacity of the main components, namely core, outriggers, (perimeter) columns and dampers. In addition, the design of damped outriggers for seismic control applications seems to rely on the assumption that the total earthquake energy will be absorbed by damping and elastic mechanisms of energy dissipation (E_K+E_S). In other words, it is assumed that the structure's behaviour remains elastic during the seismic event. Nevertheless, under large or severe earthquake-induced motion, some plastic hinges or failures may be produced in the structure before the dampers are able to dissipate the total input energy. Therefore, hysteretic behaviour of the host structure need to be evaluated along the dampers' performance in order to determine how the earthquake input energy is distributed by all the components.

§ 3.5.2 Ratios of damping-to-input energy and hysteretic-to-input energy as indicators of structural performance

In an energy-based design approach, once the energy demand for a structure is estimated from the earthquake ground motion, the damage potential can be quantified by a combination of response and energy parameters (Khashaee *et al.*, 2003). These relationships can be expressed by (a) the ratio of hysteretic-to-input energy, defined as the hysteresis energy ratio E_H/E_I; (b) the ratio of damping-to-input energy, defined as the inherent viscous damping energy ratio E_D/E_I; and (c) the ratio of dampers-to-input energy, defined as the supplemental damping ratio $E_{dampers}/E_I$. Whereas $E_H/E_I = 1$ implies that the total change in input energy is dissipated by extended damage and/or failure of the structure, a value of zero implies no structural damage (Bojórquez *et al.*, 2010). Furthermore, $E_H/E_I = 0$ implies elastic behaviour in all the elements of the structure, during the entire ground motion. Since this latter case is highly unlikely under strong and severe earthquake levels, the purpose of the following studies is to determine which

outrigger configurations extend the threshold where energy dissipation due to hysteresis can be fully replaced by energy dissipated through the action of viscous dampers.

Strength and stiffness demands aside, the following aspects are proposed for consideration in an energy-based design for structures with viscous dampers (adapted from Ye *et al.*(2009)):

1. Demand of total input energy - E_I;
2. Hysteresis energy ratio E_H/E_I;
3. Damping energy ratio E_D/E_I, including supplemental damping ratio $E_{dampers}$ / E_I;
4. Distribution of hysteresis energy in the structure;
5. Evaluation of the component damage.

§ 3.5.3 Assessment of the hysteretic energy

The inelastic component of the absorbed energy (E_H=E_A-E_S) is a function of the hysteretic behaviour of the structure. When studying SDOF systems, such hysteretic behaviour can be accounted by using suitable hysteresis models. However, in practice, structures are MDOF systems and hence the difficulty in obtaining reliable hysteretic energy quantities. A great effort has been put forward to the simplification of MDOF into SDOF system, in order to obtain reliable models of energy distribution. It is generally accepted as accurate enough that if the global parameters, namely damping ratio(ξ), ductility (μ), and natural period (T_0) of the SDOF and MDOF are identical, the input energy to inelastic SDOF systems $E_{i,SDOF}$ is approximated to that to inelastic MDOF systems $E_{i,MDOF}$ (Ye *et al.*, 2009), such as

$$E_{i,MDOF} = E_{i,SDOF}\left(\xi, \mu, T_0\right) \tag{3.18}$$

Nakashima *et al.* (1996) investigated the energy behaviour of structures having hysteretic dampers, which are characterized by a large ratio of the post-yielding stiffness to the initial elastic stiffness (α). Results showed that the total input energy and hysteretic energy for MDOF systems are approximately the same as those of the equivalent SDOF system, and the hysteretic energy can be distributed uniformly over the storeys provided that α is large. Hernandez-Montes *et al.* (2004) proposed an energy-based displacement that is equivalent to the spectral displacement obtained by conventional pushover analysis methods within the linear elastic domain. Manoukas *et al.* (2011), proposed an energy-based pushover procedure to determine the characteristics of the equivalent SDOF by equating the external work of the lateral loads

acting on a MDOF system under consideration to the strain energy of the SDOF system. A remarkable aspect of this study is that the procedure uses the strain energy, which depends on the values of all forces acting to the structure as well as on the values of the displacements of all the system's degrees of freedom. Shargh and Hosseini (2011) proposed an optimal distribution of stiffness along the height of multi-storey shear buildings (up to 20 storeys), through which the seismic input energy is minimized – when using energy spectra. This optimal distribution implies both linear modal displacements and maximum drifts in all storeys; hence, a parabolic- or bell-shaped optimal distribution is likely to occur.

The hysteretic energy dissipation can be, nonetheless, accurately determined from nonlinear time-history analysis of the structure subjected to a suite of ground motions. The computation time involved in these analyses is relative to the number of DOF modelled, thus computing the hysteretic energy demand is a trade-off between the complexity of the model and the intended accuracy in the results.

§ 3.6 Computations of energy using a FE model

§ 3.6.1 Normalized Cumulative Energy in Diana

In Diana environment, the normalized cumulative energy (E_A) can be calculated if the total strain crack model is used to characterize the nonlinear behaviour of concrete. This constitutive model is based on total strain and describes the tensile and compressive behaviour of a material with one stress–strain relationship. This model is very well suited for Serviceability Limit State and Ultimate Limit State analyses which are predominantly governed by cracking or crushing of the material (TNO-DIANA, 2014).

The normalized cumulative energy W_n at step n is calculated incrementally by the following equation:

$$W_n = W_{n-1} + \frac{1}{2f}(\sigma_{ij}^{n-1} + \sigma_{ij}^{n})(\varepsilon_{ij}^{n} - \varepsilon_{ij}^{n-1}) \tag{3.19}$$

where W_{n-1} is the normalized cumulative energy in the previous step, f is the maximum stress that the material can resist under compressive loading and σ_{ij} and ε_{ij} are the stress tensor and strain tensor in the previous and current step, respectively.

Leaving out the maximum stress f (required to normalize the output) and reordering the stress and strain tensors, the cumulative energy W_n at step n is formulated as

$$W_n = W_{n-1} + \frac{1}{2}(\sigma_{ij}^{n-1}\varepsilon_{ij}^{n} - \sigma_{ij}^{n-1}\varepsilon_{ij}^{n-1} + \sigma_{ij}^{n}\varepsilon_{ij}^{n} - \sigma_{ij}^{n}\varepsilon_{ij}^{n-1}) \tag{3.20}$$

where the quantities expressed by the terms

$$\sigma_{ij}^{n-1}\varepsilon_{ij}^{n} - \sigma_{ij}^{n-1}\varepsilon_{ij}^{n-1}$$

and

$$\sigma_{ij}^{n}\varepsilon_{ij}^{n} - \sigma_{ij}^{n}\varepsilon_{ij}^{n-1}$$

can be expressed geometrically as the areas A and B in Figure 3.3, respectively, hence the increment to the cumulative energy W_{n-1} at step n is equal to

$$\frac{A+B}{2} \tag{3.21}$$

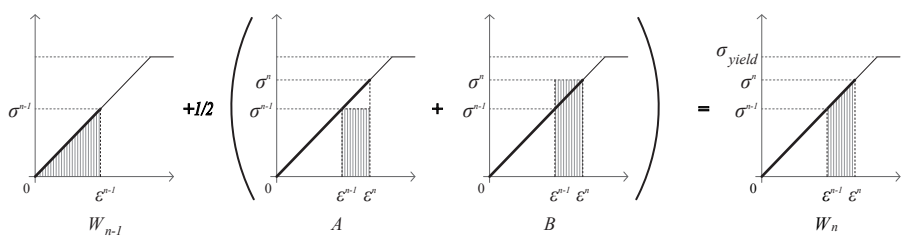

FIGURE 3.3 Step-wise computation of energy

§ 3.6.2 Strain and hysteretic energy stored by elements under axial forces

For a given element *ele* using a bilinear or elastic-perfectly-plastic model, the hysteretic (irrecoverable) strain energy is defined by the area OABD as the elastic (recoverable) strain energy is defined by the area DBC (Figure 3.4).

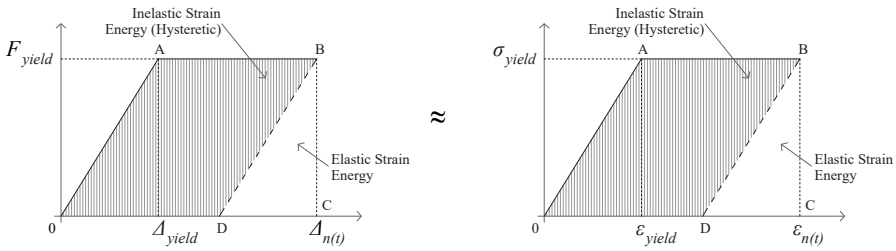

FIGURE 3.4 Strain energy for an inelastic system defined by F-Δ (left) and the equivalent σ - ε (right)

The elastic strain energy stored by an element subjected to axial forces (F) is given as

$$ds = \frac{F}{2} * \Delta \tag{3.22}$$

where Δ is the associated axial elongation. Using the following relationships

$$E = \frac{\sigma}{\varepsilon} \qquad \sigma = \frac{F}{A_s} \qquad \varepsilon = \frac{\Delta}{l_n} \tag{3.23}$$

where A_s is the cross-sectional area of the element and l_n its length, the strain energy can be formulated as

$$ds = \frac{F}{2} * \frac{Fl_n}{EA_s} \Rightarrow \frac{F^2 l_n}{2EA_s} \Rightarrow \frac{\sigma^2 A_s l_n}{2E} \tag{3.24}$$

Since Diana can deliver the values of elastic and plastic strains separately, it is more convenient to formulate the elastic strain energy in terms of stresses (σ) and strains (ε)

$$ds = \frac{\sigma\varepsilon A_s l_n}{2} \qquad \text{if } \sigma < \sigma_{yield} \tag{3.25}$$

Thus, the total elastic strain energy stored by a structure under axial forces is equal to

$$E_s = \sum \frac{\sigma \varepsilon A_s l_n}{2} \tag{3.26}$$

According to Eq. 3.11, energy will be dissipated by plastic hinges occurring in the elements so that the total energy absorbed E_A by the structure corresponds to the sum of the elastic strain energy E_S and the inelastic hysteretic energy E_H. Hence, in the presence of nonlinearities, the inelastic strain energy dissipated by damage (hysteresis) of an element under axial forces can be computed as

$$ds_P = F_{yield}(\Delta - \Delta_{yield}) \tag{3.27}$$

Since plastic hinges appear when yielding is reached, the corresponding yield stress and strain can be introduced in the equation such that

$$ds_p = A_s \sigma_{yield}(\varepsilon_{n(t)} l_n - \varepsilon_{yield} l_n) \Rightarrow ds_p = A_s l_n \sigma_{yield}(\varepsilon_{n(t)} - \varepsilon_{yield}) \tag{3.28}$$

Thus, the total hysteretic energy dissipated by a structure under axial forces is equal to

$$E_H = \sum A_s l_n \sigma_{yield}(\varepsilon_{n(t)} - \varepsilon_{yield}) \tag{3.29}$$

§ 3.6.3 Strain and hysteretic energy stored by elements under bending moments

The elastic strain energy stored by an element subjected to bending moments (M) is given as

$$ds = \frac{M}{2} * d\theta \tag{3.30}$$

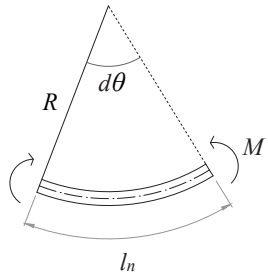

FIGURE 3.5 Analytical model of an element subjected to bending moments

where θ is the associated angle of rotation. Using the following relationships

$$d\theta = \frac{l_n}{R} \qquad \frac{M}{I} = \frac{E}{R} \tag{3.31}$$

where R is the radius of rotation, E is the material modulus of elasticity, I is the second moment of inertia of the element and l_n its length. Consequently, the strain energy can be formulated as

$$ds = \frac{M}{2} * \frac{Ml_n}{EI} \Rightarrow \frac{M^2 l_n}{2EI} \tag{3.32}$$

Thus, the total elastic strain energy stored by a structure under bending moments is equal to

$$E_s = \sum \frac{M^2 l_n}{2EI} \tag{3.33}$$

When subjected to strong ground motions, structure will undergo inelastic moment – rotations (Figure 3.6). The resulting inelastic strain energy dissipated by damage (hysteresis) of an element under bending moments can be computed as

$$ds_P = M_{yield}(\theta - \theta_{yield}) \tag{3.34}$$

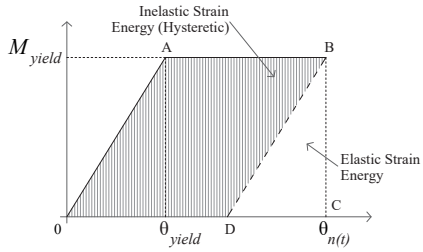

FIGURE 3.6 Strain energy for an inelastic system defined by M - θ

Thus, the total hysteretic energy dissipated by a structure under bending moment is equal to

$$E_H = \sum M(\theta - \theta_{yield}) \tag{3.35}$$

§ 3.6.4 Cumulative absorbed energy by a structure subjected to a transient loading

When the structure is subjected to a time-history loading, such as an earthquake, the cumulative energy absorbed by an element at a time step *n* is given by

$$ds_n = ds_{n-1} + \Delta_n \tag{3.36}$$

where du_{n-1} is the cumulative absorbed energy at the previous step and Δ_n is the energy increment given by the transient loading at step t. When the structure deforms elastically, Eq.3.36 is used to compute the cumulative strain energy, i.e. the increment in the elastic strain energy is formulated as

$$\Delta_n = \frac{A_s l_n}{2}(\sigma_{ij}^{n-1}\varepsilon_{ij}^{n} - \sigma_{ij}^{n-1}\varepsilon_{ij}^{n-1} + \sigma_{ij}^{n}\varepsilon_{ij}^{n} - \sigma_{ij}^{n}\varepsilon_{ij}^{n-1}) \tag{3.37}$$

Nevertheless, when the structure experiences nonlinear deformations, the stress-strain relationship is no longer linear and hence the increment must be evaluated to include both the energy dissipated by hysteresis of the structure and the stored elastic strain energy. The hysteretic behaviour of a structural element depends primarily on the

plastic characteristics of the material, which in this research is simulated by an elastic-perfectly-plastic model[12].

In order to deduce the equation to compute the energy increment when the structure presents nonlinear response, consider the example depicted in Figure 3.7. In this example, the cumulative energy in a structure subjected to a transient loading at the previous step *n-1*, is equals to 8 [J] ($A_s l_n = 1m^3$). Under elastic behaviour (left), the structure will experiment an elastic strain ε^n due to σ^n at step *n*, so the energy increment computed by Eq.3.7 is equal to 90, and the total cumulative energy is 98 [J]. The energy due to nonlinear behaviour nonetheless (middle), using a bilinear plasticity model with a yield stress (σ^{yield}) equals to 6 [kN/m^2], Eq.3.37 fails to predict the increment and the cumulative energy at step *n*, which is 66 [J].

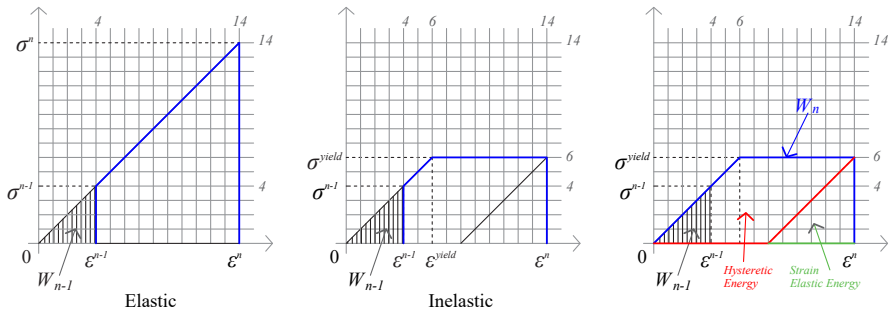

FIGURE 3.7 Example of the computation of the cumulative energy in a structure subjected to a transient loading

Consequently, yield stress must be introduced in the formulation of the increment in the cumulative absorbed energy, at step *n*, as it follows

$$\Delta_n = A_s l_n (\sigma_{ij}^{yield}(\varepsilon_{ij}^n - \varepsilon_{ij}^{n-1}) - \frac{(\sigma_{ij}^{yield} - \sigma_{ij}^{n-1})(\varepsilon_{ij}^{yield} - \varepsilon_{ij}^{n-1})}{2}) \tag{3.38}$$

so that the cumulative absorbed energy W_n, at step *n*, is given by

12 This plasticity model is generally accepted as a conservative approach in the design of structures.

$$W_n = W_{n-1} + A_s l_n (\sigma_{ij}^{yield} (\varepsilon_{ij}^{n} - \varepsilon_{ij}^{n-1}) - \frac{(\sigma_{ij}^{yield} - \sigma_{ij}^{n-1})(\varepsilon_{ij}^{yield} - \varepsilon_{ij}^{n-1})}{2}) \tag{3.39}$$

Moreover, the strain elastic and inelastic (hysteretic) portions of the cumulative energy can be calculated by

$$W_{elastic} = \frac{A_s l_n \sigma_{ij}^{yield} \varepsilon_{ij}^{yield}}{2} \tag{3.40}$$

$$W_{inelastic} = A_s l_n \sigma_{ij}^{yield} (\varepsilon_{ij}^{n} - \varepsilon_{ij}^{yield}) \tag{3.41}$$

$$W_n = W_{elastic} + W_{inelastic} \tag{3.42}$$

Applying Eq.3.38-42 to the previous example (third image to the right), the results are (Table 3.1)

STEP	W PREVIOUS STEP	Δ_n	W CUMULATIVE	$W_{elastic}$	$W_{inelastic}$
W_{n-1}	0	8	8	8	0
W_n	8	58	66	18	48

TABLE 3.1 Preliminary results

Since DIANA computes the values of stresses and strains from the combined effects of axial forces and bending moments (see Appendix A: Strain and hysteretic energy stored by elements under shear forces), Eq. 3.38 – 3.41 are applicable for computing the total hysteretic energy (E_h) and total elastic strain energy (E_s) of a structure under a transient loading. Thus,

$$E_s = W_{elastic} \qquad E_h = W_{inelastic} \qquad E_a = E_s + E_h = W_n \tag{3.43}$$

§ 3.7 Conclusions

From the studies reviewed in this chapter it is possible to conclude that

- There are few precedents of studies on energy distributions in outrigger structures. The reasons may be related to the fact that a building with outriggers cannot be modelled as a SDOF system. Most energy-based design methods rely on simplifications which are not applicable to a model of an outrigger structure, e.g. distribution of the hysteretic energy along the height is not uniform;
- Energy-based studies focus mostly on the design of buildings with periods up to 4s, i.e. low-rise and high-rise buildings with less than 40 storeys (150 meters approx.). The reason may be regarded to a wrong assumption, derived from the use of seismic code-based spectra, that long-period tall buildings will not be affected by earthquakes;
- There are few studies on energy distributions of structures using supplemental damping, and almost none, addressing the use of viscous dampers to increase the energy capacity of tall buildings subjected to earthquake motion;
- The damage potential can be quantified by energy ratios: hysteretic-to-input energy (E_H/E_I); damping-to-input energy (E_D/E_I); and dampers-to-input energy ($E_{dampers}/E_I$).

References

Akbas, B., Shen, J. and Hao, H. 2001. Energy appproach in peformance-based seismic design of steel moment resisting frames for basic safety objective. The Structural Design of Tall Buildings. 10: 193-217. 10.1002/tal.172

Akbas, B., Shen, J. and Temiz, H. 2006. Identifying the hysteretic energy demand and distribution in regular steel frames. Steel and Composite Structures. 6: 479.

Akiyama, H. 1988. Earthquake resistant design based on the energy concept

Beiraghi, H., Kheyroddin, A. and Kafi, M. A. 2016. Energy dissipation of tall core-wall structures with multi-plastic hinges subjected to forward directivity near-fault and far-fault earthquakes. The Structural Design of Tall and Special Buildings. 25: 801-820. 10.1002/tal.1284

Benavent-Climent, A. 2011. An energy-based method for seismic retrofit of existing frames using hysteretic dampers. Soil Dynamics and Earthquake Engineering. 31: 1385-1396. https://doi.org/10.1016/j.soildyn.2011.05.015

Bojórquez, E., Reyes-Salazar, A., Terán-Gilmore, A. and Ruiz, S. 2010. Energy-based damage index for steel structures. Steel and Composite Structures. 10: 331-348.

Bruneau, M. and Wang, N. 1996. Some aspects of energy methods for the inelastic seismic response of ductile SDOF structures. Engineering Structures. 18: 1-12. http://dx.doi.org/10.1016/0141-0296(95)00099-X

Chopra, A. K. 1995. Dynamics of structures. Prentice Hall:

Decanini, L. D. and Mollaioli, F. 2001. An energy-based methodology for the assessment of seismic demand. Soil Dynamics and Earthquake Engineering. 21: 113-137. http://dx.doi.org/10.1016/S0267-7261(00)00102-0

Foti, D., Bozzo, L. and López-Almansa, F. 1998. Numerical efficiency assessment of energy dissipators for seismic protection of buildings. Earthquake Engineering & Structural Dynamics. 27: 543-556. 10.1002/(SICI)1096-9845(199806)27:6<543::AID-EQE733>3.0.CO;2-9

Hernandez-Montes, E., Kwon, O.-S. and Aschheim, M. A. 2004. An energy-based formulation for first-and multiple-mode nonlinear static (pushover) analyses. Journal of Earthquake Engineering. 8: 69-88. 10.1080/13632460409350481

Khashaee, P., Mohraz, B., Sadek, F., Lew, H. and Gross, J. L. 2003. Distribution of earthquake input energy in structures. U.S. Department of Commerce

Lu, X., Lu, X., Sezen, H. and Ye, L. 2014. Development of a simplified model and seismic energy dissipation in a super-tall building. Engineering Structures. 67: 109-122. http://dx.doi.org/10.1016/j.engstruct.2014.02.017

Manoukas, G., Athanatopoulou, A. and Avramidis, I. 2011. Static Pushover Analysis Based on an Energy-Equivalent SDOF System. Earthquake Spectra. 27: 89-105. 10.1193/1.3535597

Nakashima, M., Saburi, K. and Tsuji, B. 1996. Energy input and dissipation behaviour of structures with hysteretic dampers. Earthquake Engineering & Structural Dynamics. 25: 483-496. 10.1002/(SICI)1096-9845(199605)25:5<483::AID-EQE564>3.0.CO;2-K

Nariyuki, Y. and Hirao, K. 1988. Effect of Structural and Hysteretic Characteristics on Distribution of Input and Hysteretic Energy of MDOF Systems subjected to Seismic Excitation

Papazafeiropoulos, G., Plevris, V. and Papadrakakis, M. 2017. A New Energy-Based Structural Design Optimization Concept under Seismic Actions. Frontiers in Built Environment. 3: 44.

Park, Y. J., Ang, A. H.-S. and Wen, Y. K. 1984. Seismic Damage Analysis and Damage-LImiting Design of R.C. Buildings.

Prasanth, T., Ghosh, S. and Collins, K. R. 2008. Estimation of hysteretic energy demand using concepts of modal pushover analysis. Earthquake Engineering & Structural Dynamics. 37: 975-990. 10.1002/eqe.802

Shargh, F. H. and Hosseini, M. 2011. An optimal distribution of stiffness over the height of shear buildings to minimize the seismic input energy. Journal of Seismology and Earthquake Engineering. 13: 25.

Shen, J. and Akbas, B. 1999. Seismic energy demand in steel moment frames. Journal of Earthquake Engineering. 3: 519-559. 10.1080/13632469909350358

Sucuoğlu, H. and Nurtuğ, A. 1995. Earthquake ground motion characteristics and seismic energy dissipation. Earthquake Engineering & Structural Dynamics. 24: 1195-1213. 10.1002/eqe.4290240903

Terapathana, S. 2012. An Energy Method for Earthquake Resistant Design of RC Structures

TNO-DIANA 2014. Analysis Procedures

Uang, C.-M. and Bertero, V. V. 1990. Evaluation of seismic energy in structures. Earthquake Engineering & Structural Dynamics. 19: 77-90. 10.1002/eqe.4290190108

Wang, F. and Yi, T. 2012. A Methodology for Estimating Seismic Hysteretic Energy of Buildings

Wong Kevin, K. and Johnson, J. 2009. Seismic Energy Dissipation of Inelastic Structures with Multiple Tuned Mass Dampers. Journal of Engineering Mechanics. 135: 265-275. 10.1061/(ASCE)0733-9399(2009)135:4(265)

Yanik, A., Aldemir, U. and Bakioglu, M. 2014. Energy Distributions In Actively And Passively Controlled Nonlinear Structures. International Journal of Computational Methods and Experimental Measurements. 2: 14-29. 10.2495/CMEM-V2-N1-14-29

Ye, L., Cheng, G. and Qu, Z. 2009. Study on energy-based seismic design method and the application for steel braced frame structures

Zhou, Y., Zhang, C. Q. and Lu, X. L. 2014. Earthquake resilience of a 632-meter super-tall building with energy dissipation outriggers

4 Parametric study on optimal outrigger structures

§ 4.1 Summary

This chapter discusses both the modelling and structural parameters that influence the behaviour of tall buildings equipped with fixed and damped outriggers. It introduces core-to-column and core-to-outrigger stiffness ratios, location and number of the outriggers, viscous damping coefficients of the dampers, natural frequency of the building, and frequency content of the seismic motion as the main parameters to be studied. Through sensitivity analyses the separate and combined influence of these parameters on the building response are evaluated. In addition, pseudo-optimal configurations are assessed in terms of reduction of displacement, velocity, acceleration, base shear, base moment and stress distribution. Preliminary studies on energy distribution are addressed to widen the comparison framework for either modelling or design parameters. Finally, optimal design parameters are proposed for further investigation of the behaviour of damped outrigger structures. The results show that both the optimal damping coefficient C_d and the optimal location λ have a major influence on the optimal damping ratio ζ and, thus, on the overall response of the outrigger structure. If supplemental damping is required but not achievable in practice, modification of the stiffness ratios ρ_{cto} and ρ_{ctc} may help to reduce the gap between damping demand and supply of supplemental damping.

Chapter 4 is partially based on the parametric study presented in D*istribution of strong earthquake input energy in tall buildings equipped with damped outriggers*, published in 'The Structural Design of Tall and Special Buildings'.

§ 4.2 Introduction

Since the research targets tall buildings about 200m high, namely long-period structures, the effectiveness of the damped outriggers to decrease the building response under earthquake motion was a question mark from the beginning. The first concern rises from the fact that a 200 m building –with 50 or 60 storeys- will roughly have a period of about 5-6 s. Checked against any code-based earthquake-acceleration spectra, this period will be associated with low ground accelerations, and thus, wind loading most probably the predominant state of loading. The performance of viscous damper-based outriggers under wind loading is out of the scope of this study as reports of its implementation in the Shangri-La building can be found in Willford and Smith (2008). However, the aforementioned concern seems to suggest that, even under exclusive consideration of earthquake loading, the reductive effect of the viscous dampers on the overall building response will increase as the building fundamental period decreases.

A second concern arises from the role of the outrigger position in the reduction of the response. According to Taranath (1998), by using simplified models to represent a building with outriggers, and under static loading, the optimal position of a single fixed outrigger (without dampers) is at 0.55 of the total building height (h). With the addition of dampers, such an optimal position is moved nearby to 0.50h if only the first mode of vibration is accounted for, and there is only one outrigger attached to the core[13]. However, it is also acknowledged that the optimal outrigger location will vary depending on the desired performance objective: an outrigger located at mid building height may be optimal for reducing displacements but not necessarily accelerations (Chang *et al.*, 2013; Chen *et al.*, 2010). Moreover, it also generally accepted that outriggers must be located near the top in order to minimize the drift, whereas maximum reduction in base moment is achieved when outriggers are located near the base (Smith and Coull, 1991). Nonetheless, a rather powerful reason for evaluating the optimal outrigger position is the fact that the modification of the outrigger location influences the building natural frequency. The changes in the axial stiffness of the columns due the variations in the outrigger position are the cause of this shift in the frequency. This frequency shift will increase or decrease the response according the frequency content of the input ground motions, and thus frequency and outrigger position are mutually affected.

13 There is only one optimal position to reduce the first mode response; two outriggers are required to reduce the second mode response, three for the third mode and so on. For a more comprehensive explanation, see Tan, P., Fang, C. and Zhou, F. 2014. Dynamic characteristics of a novel damped outrigger system. Earthquake Engineering and Engineering Vibration. 13: 293-304. 10.1007/s11803-014-0231-3

A third issue to be included in the parametric analysis, because it is also related to the frequency shifts, is the core-to-column and core-to-outrigger stiffness ratios. According to Smith and Coull (1991), comparatively large drift reduction can be obtained if a building is designed with rigid outriggers and perimeter columns with increased sectional areas (small core-to-outrigger and large core-to-column stiffness ratios). In the study by Chang *et al*. (2013), two analytical models of a building with damped outriggers were compared. The models differ in whether the dynamics of the perimeter columns are included in the building performance. The results showed that the use of an oversimplified model, i.e. without considering columns, leads to overestimation of the response (in this case acceleration) and larger demands of supplemental damping.

The fourth and last parameter to be considered in the parametric study is the damping coefficient, which is a measure of the force the damper can actually produce. The importance of studying the influence and interaction of the damping coefficient with other parameters comes from two facts. First, the extra damping provided by the viscous dampers may help to decrease the lateral displacements but simultaneously increase the accelerations, provoking a problem in terms of serviceability. Secondly, commercially available viscous dampers produce a force no larger than 3000 kN, thus defining a supplemental damping capacity threshold.

This chapter also provides a parametric study to assess the distribution of seismic energy in tall buildings equipped with viscous damped outriggers, i.e. with outriggers that have one or more viscous dampers installed between their ends and the perimeter columns. The aim of this explorative study is to determine which parameters influence (a) the structural response and (b) the distribution of seismic input energy through the building structure. First, a parametric study addresses the influence of natural period of the building, position of the outriggers, damping coefficient, and core-to-outrigger and core-to-columns stiffness ratios in the control performance of the outrigger structures. Indirectly, it provides the basis for exploring which strategies will extend the elastic response threshold of a tall building equipped with viscous dampers and subjected to strong earthquake ground motions. The strategy to assess the distribution of earthquake energy in tall buildings equipped with viscous damped outriggers and subjected to strong motions is based on the numerical study of 60-storey buildings equipped with conventional and damped outriggers, respectively. Secondly, the inter-dependency between structural properties of tall buildings equipped with damped outriggers and ground motion characteristics is examined under small, moderate, strong, and severe levels of the 1940 El Centro earthquake record.

§ 4.3 Preliminary static design of tall buildings with outriggers

§ 4.3.1 Simplified analysis using wind-loading

The preliminary lateral forces system design considered the main wind pressures, calculated according ASCE 7-95 wind loading provisions as described in Taranath (1998). Building parameters were 210m high, 60 storeys, 36m square plan including outriggers of 9 m long (Figure 4.1), and a damping ratio = 0.015. The building model was sub-divided in sections of ~40m high (excluding a 5m high base portion) to account for partial wind loading. The building exposure was taken as A - Heavily built-up urban locations. Building structure was classified as slender because its aspect ratio is larger than 5; building is higher than 152m (500ft), and building natural frequency is less than 1. Building importance factor I = 1.00. The basic wind speed V = 90 MPH (145km/h).

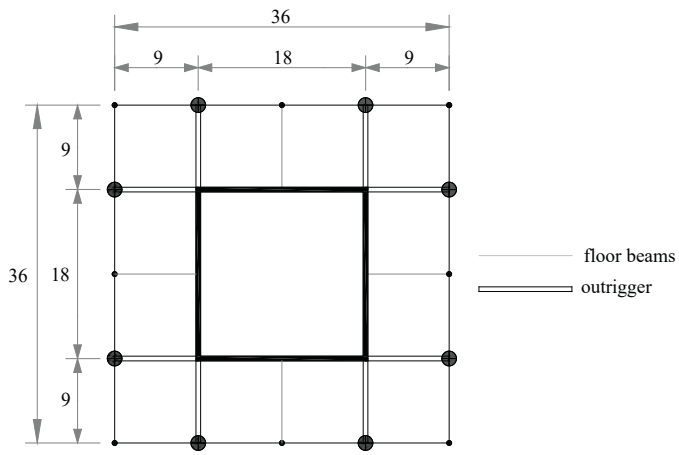

FIGURE 4.1 36m square building plan, based on a 9m grid. Note that the outriggers are not loading all the perimeter columns.

Following design approaches developed by Tan *et al*. (2014), Taranath (1998), and Smith and Coull (1991), outriggers were preliminarily located at mid-height of the building, i.e. at the 30th storey. The building is modelled under the assumption that the

cross sections of both perimeter columns and core are uniform throughout the height. Similarly, the intensity of lateral load is considered constant for the whole height. The core is rigidly fixed at the base; shear deformation is neglected. Floor girders are assumed to be pinned to the core and to the columns so that frame action is precluded (Rutenberg and Tal, 1987). Finally, the structure is assumed linearly elastic.

The two compatibility methods described in Chapter 3 are used to compute the peak deflections. The first method – proposed by Taranath (1998)-allows the computation of the resulting drift at the top of the structure, which is modelled as a cantilever beam. The outriggers are flexurally rigid and induce only axial forces in the columns. Hence, the lateral resistance is provided only by the bending resistance of the core and the tiedown action of the exterior columns. Accordingly, the restoring moment due to outrigger restraint is a function of the cantilever rotation due to a uniformly distributed load, the bending stiffness of the core, and the equivalent spring stiffness of the perimeter columns. As previously noted, the outrigger stiffness is not included in the compatibility method proposed by Taranath, so an alternative computation is defined according to the method proposed by Hoenderkamp (2004). This compatibility method replaces the equivalent spring stiffness given by the columns, by the bending and shear stiffness of the outrigger. Consequently, the methods are dissimilar only in the way the restoring moment due to outrigger restraint is now also a function of the bending stiffness of the outrigger.

§ 4.3.2 Simplified analysis using earthquake loading

As in the wind loading analyses, Taranath's and Hoenderkamp's methods are used to calculate the building deflection under seismic loading. In order to determine the building seismic mass (*W*), dead loads were obtained by considering materials' density and the volume of structural elements. Steel is used in beams, columns and outriggers (density = 78 kN/m^3). Preliminary steel cross-sections are 0.4m^2 for columns; 0.04m^2 and 0.03m^2 for outrigger frame's chords and braces, respectively; and, 0.035m^2 for all beams. Reinforced concrete is used in the core (density = 24 kN/m^3). Slabs are using composite RC and steel. Core and slabs have 0.55 and 0.15 m thickness, respectively. An additional uniform distributed dead load of 2.71 kN is added, due to non-structural elements such as ceiling (0.1) flooring (1.65), and partition walls (0.96). Live load equivalent to a typical office floor -2.4 kN/m^2 according to (1991-1-1, 2002), is also considered.

The earthquake design loads are calculated first according to the static method of the 1994 UBC Equivalent Lateral Force Procedure, as described in Taranath (1998). There, the design base shear V is given as:

$$V = Z \times I \times C \times W / R_W \tag{4.1}$$

where W is the total seismic mass previously determined; R_w is the response modification factor, which in this case is defined as 7; Z is the effective PGA of a region. In this case we set a value of 0.4g and then 0.8g, this later corresponding to a strong earthquake[14]; I is the importance factor = 1.0, since the building function is office, I=1.0; C is coefficient depending on the building period T and the site coefficient depending on the type of soil S. Since the soil profile is unknown, the norm suggests using 1.5. The fundamental period of vibration of the structure[15] is T=5.2 s.

Earthquake design loads were also calculated according to the static method of Chilean Seismic Design Code NCh433.of96 – revised in 2010 after the M8.8 El Maule Earthquake (INN-Chile, 2009). There, the design base shear Q_o is given by:

$$Q_0 = I \times C \times P \tag{4.2}$$

where P is total seismic dead load; I is the importance factor =1.0. The seismic coefficient C depends on the effective PGA of a region A_0 = 0.4; the response modification factor R, depending on the type of structure and adopted as 7; the fundamental period of vibration of the structure T, which for simplicity is assumed as previously computed, i.e. 5.2 s; and several parameters depending on the type of soil, which is defined as medium dense or medium firm soils as for the UBC method. The lower bound for C is defined as $A_o/4$ (for R=7), hence C_{min}=0.067.

The resulting equivalent seismic forces are displayed in Figure 4.2(a). As it can be noted in the distribution of forces resulting from NCh433 – 0.4g and from UBC1994 -0.8g, they are relatively equal at the top storey. At 59th floor (Figure 4.2b) the application of NCH433-0.4g produces a force almost five times larger than that from the UBC1994-

14 The UBC only uses a maximum ground acceleration of 0.4g. However, for comparative purposes with the Chilean Seismic Code, a higher value of 0.8g was introduced in the procedure as it is more representative of the strong earthquakes occurring in Chile and Japan.

15 The fundamental period of vibration of the structure is calculated by T=0.02*[(*ns**4/0.3048)^(3/4)], where *ns* is the number of storeys

0.8g. Towards mid height, both vertical distributions decrease their difference, which becomes zero at 21st floor (Figure 4.2c). Finally, at the base, the force derived from NCh433-0.4g is more than 10 times larger than that of the UBC1994-0.8g. The reason for the relative similitude between the equivalent seismic forces with 0.4g (NCH433) and 0.8g (UBC1994), and the large differences at the base and 59th floor, may be attributable to the fact that the NCH433 static method is suitable only for low- to mid-rise buildings. These building typologies, with lower periods than a tall building, are more susceptible to resonance with the high frequency content of the average Chilean earthquake. Hence the application of a normative intended for low rises, to high-rise buildings, may create disproportionate seismic demands, compared to the actual ground accelerations. However, given the lack of a specific normative for the design of high-rises in Chile, the results discussed here have been considered for the purposes of the preliminary design of a tall building. Numerical data of these results are given in Appendix B: Comparative floor-by-floor seismic equivalent lateral forces.

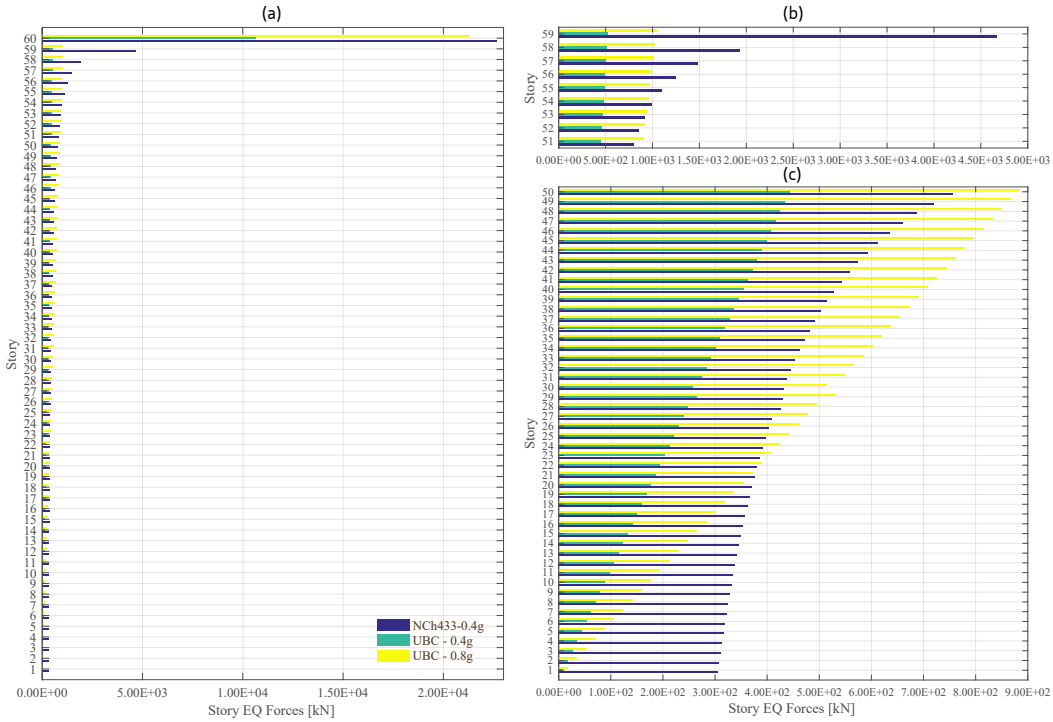

FIGURE 4.2 Comparative floor-by-floor seismic equivalent lateral forces according to NCh433 and UBC1994 including (a) 60 storeys; (b) between 51st and 59th storey; and, (c) the first 50 storeys

§ 4.3.3 Prototype model in Diana

A 3D model was built in Rhinoceros (McNeel, 2017) and then imported into Diana (FEA, 2014). The process of modelling in Diana consists of the meshing process including the definition of boundary conditions, and the attachment of geometrical properties and materials to the finite element mesh. Three sets were created in the case of the simplified tie-down model: walls (core), columns (perimeter) and outrigger (Figure 4.3). Materials used are steel and reinforced concrete, as described in Table 4.1. The model considered the following assumptions: (1) the sectional properties of the core, columns and outriggers are constant through their height; (2) the outriggers are hinged to the columns and the columns are hinged to the foundation; (3) the influences of the horizontal members are neglected except in the outriggers; (4) the structure is linearly elastic; and, (5) Totally rigid floor diaphragms are assumed at each level. Similarly to the previous calculations, there are four analyses: two per each loading case (wind and EQ), each using two different outrigger heights (1 and 2-storey).

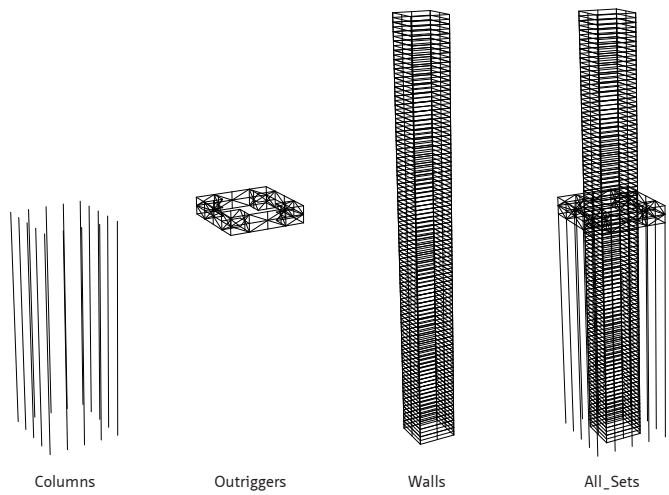

FIGURE 4.3 Structural components and 3D model utilized in Diana

ELEMENT	MODEL ELEMENT	MATERIAL	PROPERTIES	SECTIONS – 1st DESIGN	SECTIONS – 2nd DESIGN
columns	line	steel	E=2.1E+11 N/m^2; Poisson ratio v=0.3; mass density = 7.8E+03 kg/m^3	0.40m^2	0.80m^2
outrigger chords	pipe*			0.04m^2	0.20m^2
outrigger braces	pipe*			0.03m^2	0.15m^2
core	plane	concrete	E=2.2E+10 N/m^2; Poisson ratio v=0.2; mass density = 2.4E+03 kg/m^3	0.55m thickness	0.55m thickness

** Pipe sections are used to avoid the axis orientation the 'profile' may exert on the total restoring moment of inertia of the outrigger. Since in pipe sections X and Y axis are equal, so are their transvers moments of inertias.*

TABLE 4.1 Properties of model elements and materials used in the Diana model

§ 4.3.4 Comparison of results

According to the results for the design case 1 and 2 -displayed in Table 4.2 and Table 4.3 respectively, Hoenderkamp's method seems to be more accurate than Taranath's one to predict the behaviour of a tall building equipped with outriggers. Especially, if the results obtained for a single-storey outrigger under wind loading using 3D FEM in Diana and 2D Hoenderkamp's method are compared. The consideration of the outrigger stiffness might explain the relative similitude between the results obtained by these two methods, henceforth refered as FE and Hoenderkamp methods. In addition, since increasing the outrigger's height from 1- to 2- storey reduces the top storey displacements, the use of a 2- storey outrigger is also justified by the stiffness increment and simultaneous reduction of axial stresses in truss members. Finally, the outrigger building structure is consequently designed to meet the target performance objectives for a 0.4g strong earthquake-induced motion, as defined by the Equivalent Static Lateral Force method described in the Chilean Seismic Code - NCh.433 (INN-Chile, 2009).

			Δ TOP	N COLUMNS	N OUTRIGGER
Taranath (outrigger not considered)		W	0.23	3.24E+07	
		EQ	0.97	1.11E+08	
1- storey outrigger	Hoenderkamp	W	0.39	1.26E+07	3.10E+07
		EQ	1.53	4.37E+07	1.08E+08
	Diana	W	0.39	1.27E+06	4.86E+06
		EQ	1.99	6.36E+06	2.43E+07
2- storey outrigger	Hoenderkamp	W	0.29	2.47E+07	3.72E+07
		EQ	1.19	8.51E+07	1.28E+08
	Diana	W	0.35	1.74E+06	2.63E+06
		EQ	1.74	8.72E+06	1.36E+07

TABLE 4.2 Top storey displacement responses and axial forces with columns=0.4m^2, chords=0.04 m^2, and braces=0.03 m^2

			Δ TOP	N COLUMNS	N OUTRIGGER
Taranath (outrigger not considered)		W	0.16	4.05E+07	
		EQ	0.75	1.39E+08	
1- storey outrigger	Hoenderkamp	W	0.23	3.26E+07	8.02E+07
		EQ	0.97	1.12E+08	2.75E+08
	Diana	W	0.33	2.09E+06	8.81E+06
		EQ	1.64	1.04E+07	4.40E+07
2- storey outrigger	Hoenderkamp	W	0.14	4.35E+07	6.54E+07
		EQ	0.66	1.50E+08	2.26E+08
	Diana	W	0.27	2.64E+06	4.17E+06
		EQ	1.34	1.32E+07	2.20E+07

TABLE 4.3 Top storey displacement responses and axial forces with columns=0.8m^2, chords=0.20 m^2, and braces=0.15 m^2

§ 4.4 Outrigger design

This section describes the factors considered in the design of the steel braced outriggers of the benchmark 60- storey building model. It also addresses the linear and nonlinear (static) analysis of a few design proposals, using Diana, in order to assess their performance and thus determine their suitability for further integrating a damper-based outrigger system.

§ 4.4.1 Design force

The restoring moment created by the outriggers decreases the maximum displacement of the building as axial forces are developed in the perimeter columns. Such axial force represents, therefore, the strength demand for the outrigger design. Moreover, the outrigger system with viscous dampers must remain in the elastic range while the building is subjected to strong seismic motion. Hence, the force generated by the viscous dampers must be smaller than that required to yield the outrigger; i.e. the strength of the outrigger must be larger than the force produced by the damper. In order to determine the design force, a criterion based on either a practical or a conservative approach can be introduced. The practical approach sets the force produced by a single, commercially-available, and average size oil viscous damper as a *lower bound* to determine the outrigger's required strength. The conservative approach, instead, sets an *upper bound* according to the static analysis results described in the previous section. This latter approach is conservative as design forces obtained through Hoenderkamp's method are 25 times larger than the force capacity of a regular viscous damper (Table 4.4).

TOTAL FORCE REQUIRED [N]	ACCORDING TO:	FORCE PER SINGLE DAMPER [N]	TYPE OF APPROACH
	Average commercially-available viscous damper	1.50E+06	Practical
1.50E+08	Hoenderkamp method (strong EQ*)	3.75E+07	Conservative

** Strong earthquake motions were defined as 0.4g according to NCH.433 –of.2010 (Chilean Seismic Code) and as 0.8 according to UBC 1994 – USA*

TABLE 4.4 Strength demand of the outrigger

In order to ensure that the outrigger will not yield when subjected to the force produced by the damper, the strength demand must be equal to the damper force amplified by a safety factor, such that

$$\text{Strength demand} > no * \Phi * f_d \tag{4.3}$$

where Φ = safety factor, no=numbers of dampers attached to the outrigger, and f_d = single damper force = 1.50E+06 N.

In engineering practice, a safety factor of 1.25 is acceptable to increase the elastic threshold of steel structures. However, due to the uncertainty produced by the large differences in the outrigger's strength demands obtained by each approach, a safety factor of 2 is used. This implies that only 50% of the outrigger's strength capacity is required to cope with the forces produced by the action of the dampers. Thus, the outrigger strength demand (or minimum outrigger yielding force) must be larger than 3.00E+06 N for a single damper. Accordingly, the strength demands are 6.00E+06 and 1.20E+7 N for two and four dampers installed between the outrigger and the perimeter column[16]. Finally, the acceptable yielding loading for the outrigger is, therefore, between 3.00E+06 and 3.75E+07 N.

§ 4.4.2 Outrigger definition

Although the original outrigger used in the Shangri-La building is composed of shear walls (called outrigger walls or deep beam outriggers), in this study we selected a truss girder model for the outrigger configuration due to the following advantages:

- The achievement of 'a high effective stiffness due to the utilization of axially loaded members' (O'Neill, 2006);
- A simpler connection to core-outrigger design;
- More available space in the truss for functional use, such as spatial continuity, pipeline distribution, ventilation uses, etc.

Following the previous results, a two-storey deep design was selected to provide adequate bending and shear stiffness to the outriggers. In the proposed model, the two-storey deep (7 m) outriggers are distributed in pairs at each side of the building core (Figure 4.1). The location of braces was defined according to the positioning of feasible openings allowing functional connectivity within the storey where the outrigger is attached to. Figure 4.4 displays feasible schemes for the outrigger (a-c) and the selected configuration (d).

16 See Optimal dampers' damping coefficient (C_d) for further discussion on the number of dampers attached to the outrigger.

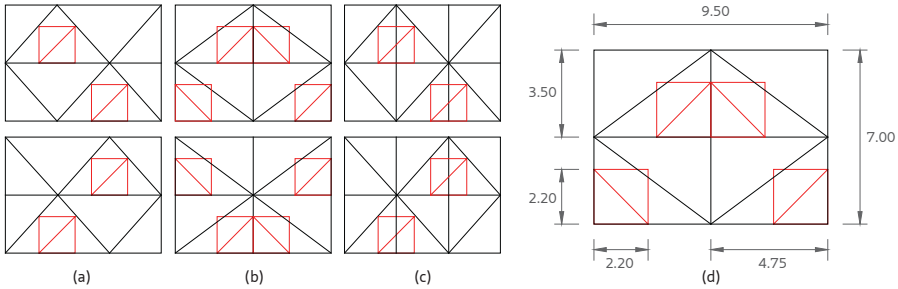

FIGURE 4.4 Feasible configurations of the truss-girder outrigger with one bay (a); two bays (b); three bays (c); and selected configuration displaying overall dimensions (d).

Since the outriggers impose architectural constraints to the floor where they are installed, a modification of the K-braced outrigger was further investigated and compared. Both 2-bays 2-storey K- and X-braced truss-girder outriggers (Figure 4.5) are very alike in terms of design, so the aim of the linear analyses was to determine any difference in terms of structural performance. Nonlinear analyses were performed for completeness of the study. Eigen frequency analyses showed that predominant modes are almost the same (Table 4.5). According to the linear static results, X-braced outrigger is slightly stiffer than the K-braced. From the nonlinear static analyses results, nonetheless, it is concluded that both configurations yield under the same load force (1.05E+07 N). Both plastic hinges appear first at the braces due to similar level of axial stress. Therefore, it is valid to assume both configurations as equal in terms of initial plastic behaviour. However, since a larger displacement (about 10 times larger) must be reached in the further cyclic loading analysis, K-braced outrigger remains as the subject of analysis.

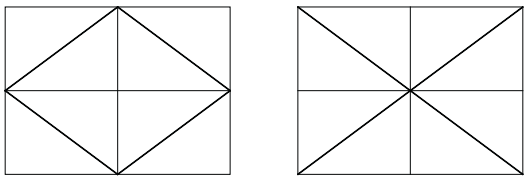

FIGURE 4.5 K-braced (left) and X-braced (right) truss girder outriggers

MODE	FREQUENCIES [HZ]	
	K - braced	X - braced
1	12.2	12.0
2	15.9	17.4
3	23.6	25.3
4	27.7	26.2
5	41.6	41.1
6	45.0	45.3
7	48.6	49.4
8	49.2	51.5
9	56.5	54.8
10	58.1	55.2

TABLE 4.5 Frequencies obtained for both models

§ 4.4.3 Modelling assumptions

The outrigger was modelled as a 3-D truss girder beam cantilevering from the core. A 3D model is preferred as it helps to detect out-of-plane bending deformations that might become significantly influential in the response of the outrigger. Similarly, the use of H-profiles with height to width ratio (h/b) close to 1 obeys the principle of giving enough second moment of inertia to the outrigger in the out-of-plane axis, so that the main deformations remain in the plane of interest for the analysis. Since a vertical force will be applied at the end of the cantilever during the analysis, the outrigger model is clamped (fixed) to the core. It is free to displace in vertical direction at the loaded end (Figure 4.6). The FE model developed in Diana contains 118 elements and 229 nodes. Elements are modelled as CL18B nonlinear structural elements. The initial load force of 1.50E+06 N will be divided by 21 (number of nodes in the loaded vertical component) and applied evenly to each node.

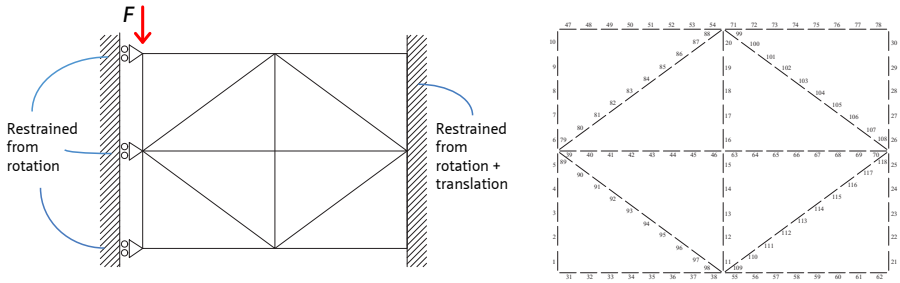

FIGURE 4.6 Loading and support conditions of the outrigger model (left) and FE model (right)

Physically and geometrically nonlinear effects were considered in the analysis in Diana (TNO-DIANA, 2014a) because large rotations at the nodes needed to be accounted for. Moreover, stresses are concentrated around the buckled deformation of the braces. Properties of steel are S355; modulus of elasticity (E) is 2.1E+11 N/m^2; Poisson ratio (ν) is 0.32; mass density (ρ) is 7800 kg/m^3. For the nonlinear analysis, two models of plasticity are considered: ideal elastoplastic (also called elastic-perfectly-plastic) or bilinear model, and the other including a strain hardening slope. Both were defined under the considerations given by Eurocode 3 (1993-1-1, 2004). In both models yield stress (fy) is 3.55E+08 N/m2 and nonlinear behaviour is assessed by using Von Mises plasticity models. The reason for using these two models is that bilinear models allows for an initial assessment of the steel stress-strain relationship without the extra reserve of ductility given by the post-yield hardening and thus increasing the safety factor in the design. For instance, results using similar modelling parameters but different material definition (bilinear and strain hardening) showed that outrigger's strength increased with the addition of the post-yield strain hardening, whereas the force-displacement curve maintained the same shape. Nevertheless, strain hardening was finally taken into account for evaluating the hysteretic behaviour of the outrigger. Since research studies prove that the use of post-yield strain hardening slope improves the correlation between tested and modelled results (ATC-PEER, 2010), the reliability of the simulations was increased.

§ 4.4.4 Outrigger design proposals

Four outrigger designs using several steel profile sections were tested in order to explore the ductile capabilities of the structure under a force of about 3.75E+07 N. In addition, the nonlinear incursion of the structure by the formation of either shear or flexural hinges was addressed by testing different plastic hinge locations either in the braces or chords (Figure 4.7).

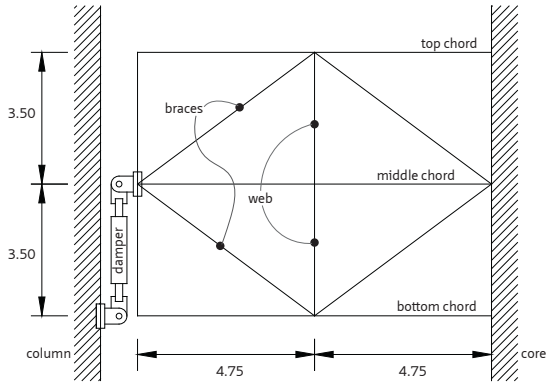

FIGURE 4.7 Outrigger elements

While the actual building referenced in this study (60-storey Shangri-La) possesses wall-type or deep beam outriggers, the proposed profile sections had to be compared with existing truss-girder outriggers in order to validate the feasibility of its preliminary design (Table 4.6). Design no.3 thus uses the same profile sections used in the construction of the outrigger installed in Shanghai Tower (632m)(Lu *et al.*, 2014), whereas design no.4 does so with reference to the outriggers installed in a 50-storey building located in Izmir, Turkey.

DESIGN	CHORDS	BRACES	WEB
1	H390 x 300 x 10 x 16	H400 x 408 x 21 x 21	H300 x 300 x 10 x 15
2	H498 x 432 x 55 x 88	H498 x 432 x 45 x 70	H458 x 417 x 30 x 50
3	H498 x 432 x 45 x 70	H400 x 408 x 21 x 21	H498 x 432 x 45 x 70
4	H300 x 300 X 10 X 15	H400 x 300 x 10 x 16	H300 x 300 X 10 X 15

TABLE 4.6 Steel profiles used in each of the outrigger designs (in mm)

Linear static analyses were performed in Diana in order to investigate the initial yield strength of the proposed outriggers. The results displayed in Table 4.7, were obtained from the peak vertical displacement of the end of the outrigger, under the loading force previously described. The results show that all the proposed configurations yield under forces larger than the minimum required one (3.00E+06 N), although none of them reached the desirable strength of 3.75E+07 N. According to the AISC seismic provisions for structural steel buildings (ANSI, 2005), members subjected to cyclic loadings need to be loaded up to rotational values of 0.04 radians (for instance, beam to column moment connections) or of about 0.038 m displacement, in the specific case of the

outrigger studied. The design no.3 presents a comparatively larger displacement, hence it is selected. Although this latter feature does not guarantee necessarily the best choice, a larger displacement may indicate a larger energy dissipation capability and hence the interest to also explore the ductile behaviour of the selected outrigger configuration. The selected design exhibits a preliminary yield strength of 1.62E+07 N.

DESIGN	YIELDING*		STIFFNESS (K) = (V/D) [N/M]	CLASSIFICATION
	force (V) [N]	displacement (D) [m]		
2	2.68E+07	0.0396	6.77E+08	stiff
3	1.62E+07	0.0535	3.03E+08	medium
1	5.12E+06	0.0334	1.53E+08	flexible
4	4.44E+06	0.0438	1.01E+08	very flexible

** determined by linear interpolation*

TABLE 4.7 Summary of results showing designs arranged according to their linear stiffness

§ 4.4.5 Nonlinear static analysis (pushover)

A pushover analysis is required to determine the ductile properties of the proposed outrigger configuration. The main objective thus is to determine the yield and ultimate strength of the structure. The outrigger is designed mainly to resist the bending moment and the shear forces during an earthquake. Because the bending moment is primarily resisted by the upper and lower horizontal members (chords) while the shear forces are generally withstood with diagonal members, the location where the plastic hinges (fuses) are firstly formed will indicate whether the design is governed by the bending or shear behaviour of the structure. Finally, in order to validate the consistency of the analysis, the resulting curve force-deformation is plotted and compared to bilinear steel model. The plot is expected to exhibit the same elastic-perfectly-plastic (EPP) behaviour of the material model. Since Rayleigh damping is required for including viscous damping effects in the analysis, damping ratio was defined as 5%, following recommended damping percentages given by Chopra (2007).

The results show that the outrigger structure began to yield under a load of 1.04E+07 N, due to the axial stress in one of the brace members (Table 4.8). However, the redistribution of stresses through the other components of the outrigger, maintain the overall behaviour in the linear range till the load force reaches 1.22E+07 N or step 22

in Figure 4.8. Under this load force all brace elements already exhibit plastic behaviour. The first plasticity in a horizontal chord element occurs under a load of 1.35E+07 N (step 31). Finally, the structure behaviour reaches the yield plateau under a load of 1.46E+07 N (step 38), after that some vertical chords members entered the plastic region as well. For practical purposes, the yield strength of the outrigger is therefore assumed as 1.04E+07 N. It is worth noticing that, comparatively, in the Shangri-La tower test simulation (Lu *et al.*, 2014), a maximum reaction force damper –when subjected to average seismic loading, was 2.54E+06 N, as in Willford and Smith (2008) the predicted damper peak force reached 2.2E+06 N for a damped-outrigger installed in a 60- storey building. Finally, as originally intended, the plastic hinges take place first at the braces and then in the chords member of the frame (Figure 4.9)

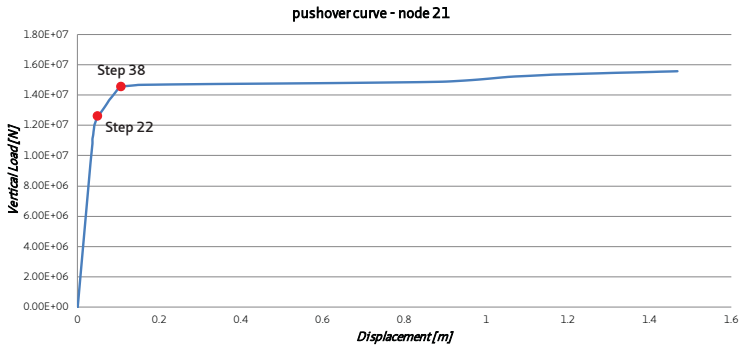

FIGURE 4.8 Correlation between pushover curve and the steps in the nonlinear analysis for node 21 (at the end of the outrigger)

STEP	LOAD FACTOR	FORCE	TYDY NODE 21	PLASTICITY STATUS			OBSERVATION
				Group	Element	Plasticity New	
1	0.600	9.00E+06	-0.030				*initial load step*
10	0.690	1.04E+07	-0.035	Brace 4	118	6	1st Plasticity in the outrigger
11	0.700	1.05E+07	-0.035	Brace 4	118	12	
12	0.710	1.07E+07	-0.036	Brace 1	79	36	
				Brace 2	108		
				Brace 4	117 - 118		
13	0.720	1.08E+07	-0.036	Brace 1	79 - 80	87	*All braces in plastic behaviour*
				Brace 3	89 - 90		
				Brace 2	106 - 108		
				Brace 4	116 - 117		
22	0.810	1.22E+07	-0.043	Braces	79, 82 - 83, 85 - 95, 104 - 106, 109, 116 - 117	318	*change in the stiffness slope*
31	0.900	1.35E+07	-0.074	Upper Chord	78	3	1st Plasticity in the frame (horizontal)
32	0.910	1.37E+07	-0.077	Lower Chord	62	3	
35	0.940	1.41E+07	-0.091	Vertical Chord	11	3	1st Plasticity in the frame (vertical)
38	0.970	1.46E+07	-0.106	Braces	92, 94, 97	42	*change in the stiffness slope*
				Horizontal Chords	31, 39, 46, 62, 70, 77	42	
				Vertical Chords	11, 20	6	
106	1.038	1.56E+07	-1.482				
107	1.039	1.56E+07					*No convergence*

TABLE 4.8 Results of nonlinear analyses

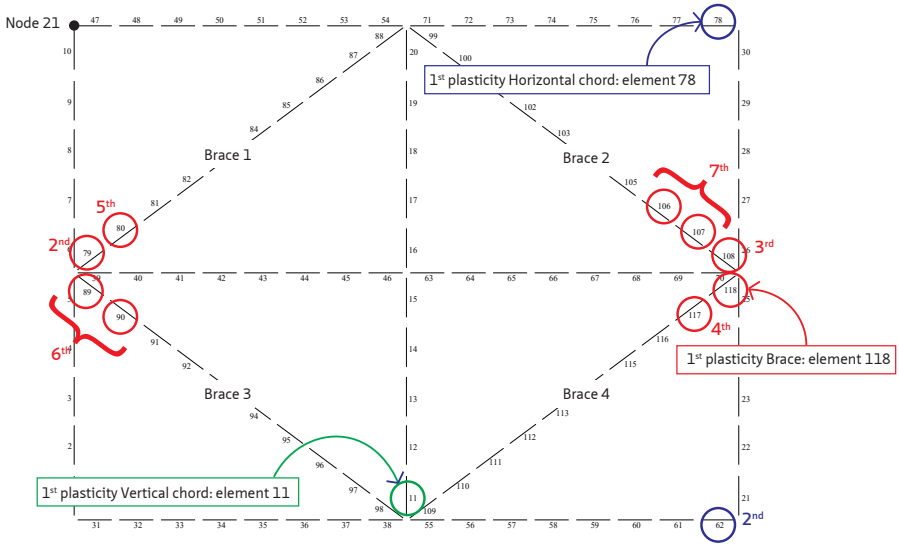

FIGURE 4.9 Plasticity status distribution in the outrigger: first at the braces (red circles), second at horizontal chords (blue circles), and finally at vertical chords (green circles)

§ 4.5 Nonlinear time-history response analyses

Since the dampers used in this study are velocity-dependant, they only work under the presence of motion. Unlike other types of damping such as friction, hysteretic, and visco-elastic devices, fluid viscous dampers vary their outputs with stroke velocity. In equivalent static wind or earthquake loading design, damped outriggers are not considered as part of the lateral stiffness system. This means that static loading design methods fail to introduce the supplemental damping in the reduction of the building response, and thus the displacement of a building with damped outriggers will be higher than an equivalent building with conventional outriggers. This means that the benefit of the increased damping is only included in calculating the dynamic loads (Jackson and David, 2010). Time-history methods directly account for the influence of the supplemental damping in the response reduction.

Another reason for the use of (nonlinear) time-history analyses, instead of simplified static loading methods, is the fact that the damping force is completely out of phase with stresses due to flexing of the columns[17]. In other words, velocity and displacement are out of phase. This is explained by Gamaliel (2008):

'Consider an example of a building with viscous dampers mounted in the diagonal bracings. During a seismic event, the columns reach its maximum stress when the building has displaced a maximum amount from its original position. At this point, the velocity is zero; therefore no force is generated in the viscous damper. When the building flexes back in the opposite direction, maximum velocity is reached at the point of zero displacement from the original position, meaning the building is upright. At this time, the exact opposite is observed. The viscous damper is giving out its maximum output while the stresses in the columns due to bending are zero.'

§ 4.5.1 Finite element (FE) models with conventional and damped outriggers

The analytical models used in this study are based on the existing Shangri-La building in Manila, Philippines, as described by Willford and Smith (2008). The Shangri-La building possesses eight two storey -deep outriggers distributed in pairs at each side. The 2D finite element (FE) model described here considers two outriggers per side, each pair modelled as a single 7 meters high outrigger. In the model, both building plan and distribution of resistant elements are symmetrical so the lateral stiffness in two orthogonal directions is assumed to be equal. Equally assumed is the lack of significant torsional effects, and therefore a planar model is used for simplification purposes.

While the actual 60- storey Shangri-La building features wall-type or deep beam outriggers, a truss girder model for the outrigger configuration is proposed in this study as it enables a more efficient use of the space for functional purposes. In terms of modelling, outriggers are usually defined as infinite rigid and mass less (Tan *et al.*, 2014; Taranath, 1988; Wang *et al.*, 2010). This simplifies the analyses because it is assumed that by attaching an infinitely rigid outrigger to the main core, both will rotate the same amount. However, there are two main reasons for the present study not following this assumption: (a) the outriggers are designed with a larger

17 Hence reducing building deflections and the column stresses instead of increasing the loads in them

stiffness compared to the other storeys, whose effect provokes changes of stiffness in the building and thus make it more vulnerable under strong earthquakes (Zhou and Li, 2013). Assuming an infinitely rigid outrigger may lead to incorrect results of the building's behaviour during nonlinear transient analyses; and (b) the assumption of an infinitely rigid outrigger is incompatible with a seismic energy distribution-based analysis. Moreover, it has been suggested that the outrigger may be the major plastic energy dissipation component in tall buildings with conventional outriggers (Lu *et al.*, 2014). Hence the stiffness of the outrigger is considered in this study.

The core is an 18m x 18m reinforced concrete tube, with a constant thickness of 0.75m. The FE model of the core is modelled as a Bernoulli-Euler cantilever beam type, due to the fact that the potential failure of the core tube is dominated by bending deformation. The core was modelled as a rectangular tubular beam divided in a number of segments equal to the number of storeys of the building. The material properties correspond to reinforced concrete (RC): Young's modulus E=3.4E+10 N/m^2; Poisson's ratio ν = 0.2; and mass density ρ = 2.4E+03 kg/m^3.

Storey masses equivalent to the sum of the unfactored dead load and the 20% of the live load[18] were added as lumped masses in the nodes corresponding to each storey in the model. Since the mass of the core will be calculated directly in the analysis, the dead load only considers slabs, beams and columns (for gravity load bearing) and distributed load due to ceiling, flooring and partition walls (0.1, 1.65, and 0.96 kN/m^2 respectively). Live load accounts for typical office floor (2.4 kN/m^2). Under consideration of the recommendations given in (ATC-PEER, 2010), the storey mass applied for each floor in the model was 7.77E+06 N as briefly described in Table 4.9, However, the contribution of these secondary structural components to the total lateral stiffness of the structure was not considered in the model.

STRUCTURE SELF-WEIGHT*	ARCHITECTURAL FINISHES**	D STOREY	L STOREY	1.0*D	0.2*L	EXPECTED GRAVITY LOAD
4314	2935	7249	2599	7249	520	7769

** excluding self-weight of the core, outriggers and perimeter columns; ** including partitions, exterior wall, floor and ceiling finishes*

TABLE 4.9 Expected gravity load for determining the storey mass applied on the model (all values are in kN)

18 According to ATC-PEER. 2010. Modeling and acceptance criteria for seismic design and analysis of tall buildings. , `The live load should be reduced from the nominal design live load to reflect: (1) the low probability of the nominal live load occurring throughout the building; and (2) the low probability of the nominal live load and earthquake occurring simultaneously'. Generally, the combination of these two effects can be considered by applying a net load factor equal to 0.2

Reinforced concrete perimeter columns are also modelled following the design of the existing 60- storey building in Manila. The material properties correspond to reinforced concrete (RC): Young's modulus E=2.2E+10 N/m^2; Poisson's ratio ν = 0.2; and mass density ρ = 2.4E+03 kg/m^3. In summary, the model comprises 255 DOF.

Finally, two types of building models were used for the analyses: one building with conventional outrigger systems and the other with damped outriggers (Figure 4.10). The first model, hereafter called *fixed outrigger* comprises the core, the outriggers and the perimeter columns. The second model, hereafter called *damped outrigger* comprises the core, outriggers, perimeter columns and viscous dampers installed between the outriggers and the columns. The use of two analytical models offers a comparative framework, wherein the improvements provided by the addition of dampers may be compared – and thus validated.

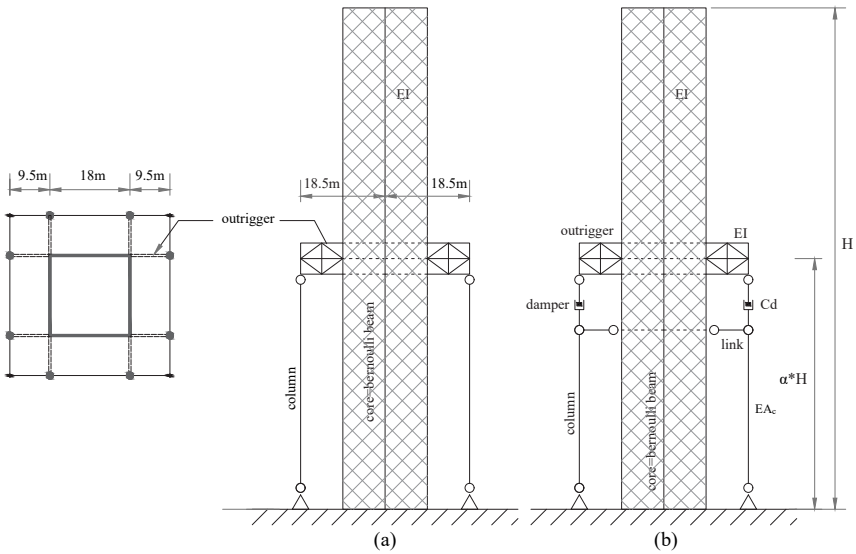

FIGURE 4.10 Typical plan for the fixed (a) and damped (b) outrigger building models

§ 4.5.2 Nonlinear setting and plasticity models for core and outrigger elements in Diana

Both core and outrigger were modelled using nonlinear settings, as they are expected to be the major sources of hysteretic energy dissipation. Perimeter columns, on the contrary, were modelled with elastic elements. Unless the use of a small cross-sectional area is combined with a large core bending deformation, column strength demand can be safely expected to be smaller than 70% of the yielding strength, even under severe earthquake loading, and thus remaining within the elastic threshold. The modelling of the core wall requires the definition of plastic regions, usually located at the base zone. However, related studies have pointed out the formation of plastic hinges in other places, such as at the mid height (Panagiotou and Restrepo, 2009) or at the regions adjacent to outriggers (Beiraghi and Siahpolo, 2017). By modelling some portions of the structure with elastic elements, the energy dissipation associated with yielding and cracking might not be captured. Moreover, the study in Beiraghi *et al.* (2016) demonstrated that the distribution of inelastic energy up the building's height is strongly related to the amount of plastic hinges used in the modelling of the core. The analytical model described here, therefore, considers the use of general nonlinear material models throughout almost the whole finite element model as specified by Diana-FEA software (TNO-DIANA).

The main structural elements used for the modelling in Diana-FEA are depicted in Figure 4.11, wherein only half of the model is showed for simplification. For modelling both core and outrigger, the L7BEN nonlinear structural element was used as it accounts for geometric and physical nonlinearities in the analysis. Diana-FEA calculates strains and stresses in the so-called 'stress points' of beam elements. In L7BEN elements the stress points are equivalent with the integration points (Figure 4.12). Despite the core modelled as a box, in 2D settings Diana-FEA merges the integration zones parallel to the analysed direction (X in the figure), so the beam presents an I-shape cross-section. Each quadrilateral integration zone contains three integration points. At any given node, the stress produced by axial forces is accounted for at integration point (*intp*) 8 whilst the tensile/compressive stresses produced by bending moment are considered at *intp* 3 and *intp* 4. In addition to these nonlinear settings, node masses were modelled using PT3T; the columns and the storey beam required for equilibrium conditions with L6BEN; and the viscous damper with SP2TR.

The total strain crack model is used to define the nonlinear behaviour of the concrete, which is characterized by tensile cracking and compressive crushing. This constitutive model is based on total strain and describes the tensile and compressive behaviour of the concrete based on a bi-linear stress-strain relationship as defined in Eurocode 2 (1992-1-1, 2004). Concrete strength class is C35/45 and reinforcement steel bars are 400MPa.

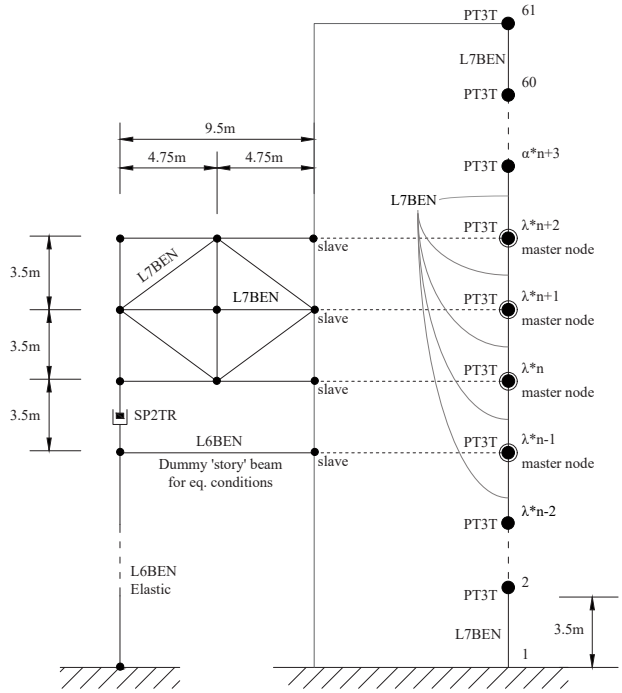

FIGURE 4.11 Structural elements used in the nonlinear modelling of the damped outrigger in Diana-FEA

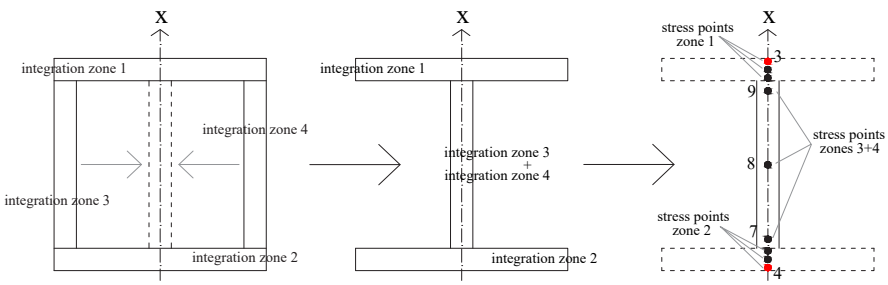

FIGURE 4.12 Conversion scheme box-to-I shape cross section of the core. Integration/stress points are depicted for each integration zone.

For the outrigger, the plasticity model of Von Mises is used to define the nonlinear properties of the steel. An elasto-plastic model is considered for its constitutive behaviour, i.e. strain hardening effect is not taken into account. The reserve of ductility given by the hardening post-yield is considered as a safe increase in the design. Properties of the steel are derived from Eurocode 3 (1993-1-1, 2004)

§ 4.5.3 Modal response and inherent damping ratios

Following design approaches developed by Smith and Coull (1991); Tan *et al.* (2014); and Taranath (1988), outriggers were preliminarily located at mid-height of the building, i.e. at the 30th storey. However, the effective mass participation in the X direction (Table 4.10) shows that the building with outriggers behaves similarly to fixed-free beam under bending vibration, wherein the effective modal mass of the first and second modes are 0.6131 and 0.1883 of the total mass, respectively. This suggests that, given the predominance of the first mode, the optimal position of the outrigger to reduce the lateral displacements is at 0.66H, i.e., at the effective modal height. For convenience, the initial location was set at 0.7H.

When the effective mass participation in the Y direction is considered (Table 4.11), the third mode has more than 81% of the effective mass participation becoming the predominant mode of the response in the vertical direction. Modal shapes of 17 modes (up to 30Hz) of the building with fixed and damped outriggers were obtained using Diana-FEA. Since frequency content of the earthquakes larger than 30 Hertz does not significantly affect the response, only Eigen-frequencies within that range were further considered. The modal shapes depicted in Figure 4.13 correspond to the predominant ones for parametric variations in the outrigger location and core-to-column and core-to-outrigger stiffness ratios. These parametric variations will be addressed in the next sections.

	PERIOD (S)		EFF. MASS TX		CUMULATIVE %	
MODE	Fixed	Damped	Fixed	Damped	Fixed	Damped
1	4.99	5.10	4.98E+07	4.94E+07	61.4	61.3
2	0.85	0.82	1.53E+07	1.53E+07	80.3	80.3
4	0.30	0.29	5.09E+06	5.13E+06	86.6	86.7
5	0.16	0.15	2.49E+06	2.54E+06	89.7	89.8
7	0.10	0.12	3.26E+04	2.27E+01	89.7	89.8
9	0.09	0.09	1.48E+06	1.39E+06	91.5	91.6

TABLE 4.10 Effective mass participation in X direction

	PERIOD (S)		EFF. MASS TY		CUMULATIVE %	
MODE	Fixed	Damped	Fixed	Damped	Fixed	Damped
3	0.39	0.38	6.52E+07	6.50E+07	80.5	80.7
6	0.13	0.13	7.57E+06	7.23E+06	89.9	89.7
8	0.10	0.12	2.97E+05	5.54E+05	90.2	90.4

TABLE 4.11 Effective mass participation in Y direction

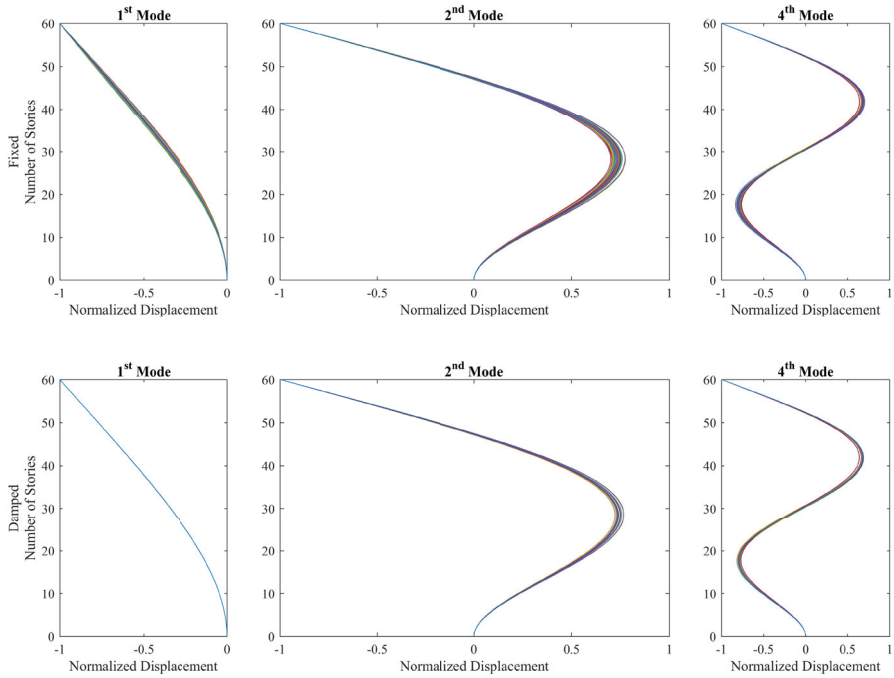

FIGURE 4.13 Predominant mode shapes of the fixed (upper row) and damped (lower row) outrigger system depicting variations due to the combined influence of outrigger location and core-to-outrigger and core-to-column stiffness ratios (9x5x5 parameters = 225 modal shapes in each plot).

§ 4.5.4 Long-period earthquakes

Since this study focuses on tall buildings, transient response analyses are considered more meaningful to provide insights regarding the response if the structure is subjected to long-period earthquakes. An empirical way to obtain these is by computing the peak ground acceleration (PGA) to peak ground velocity (PGV) ratio, which should be smaller or equal to eight[19]. Although at least seven or more ground motions records are required to obtain reliable conclusions, in this parametric study only one ground motion was considered for two reasons: (1) by using only one input ground motion, effects on the performance and distribution of seismic energy are clearly differentiable, and (2) the analytical models herein discussed are further subjected to a comprehensive set of eight ground motions, as described in the Chapter 5. The 6.9Mw El Centro earthquake (18.05.1940), component 270, as registered in the station No.117 is selected because it is a very well-known record, commonly used in earthquake engineering. The 1940 El Centro earthquake presents a PGA of 2.10 m/s^2 and a PGV of 0.36 m/s (Table 4.12). These values were scaled up in order to critically asses the distribution of seismic input energy in the structure (Figure 4.14). The scaling was based on the earthquakes' PGV, which is more meaningful for the assessment of structures whose expected improved performance relies on the addition of velocity-dependant devices. The elastic threshold was set at velocity amplitudes up to 0.9 m/s and classified as moderate earthquakes, whereas velocity amplitudes less than 0.5 m/s were classified as small earthquakes; velocity amplitudes between 1.0 and 1.5 m/s as strong earthquakes; and, velocity amplitudes beyond 1.5 m/s, as severe earthquakes. This earthquake record was downloaded via the Strong-motion Virtual Data Center (CESMD, 2014).

	SMALL	MODERATE	STRONG	SEVERE
factors	1.25	2.50	4.00	6.70
PGA (m/s^2)	2.63	5.25	8.41	14.08
PGV (m/s)	0.46	0.92	1.48	2.47
PGA/PGV	5.69	5.69	5.69	5.69

TABLE 4.12 Scaled PGA-PGV of four earthquake levels of El Centro ground motion record

19 Dicleli, Murat, personal communication, July 2, 2015.

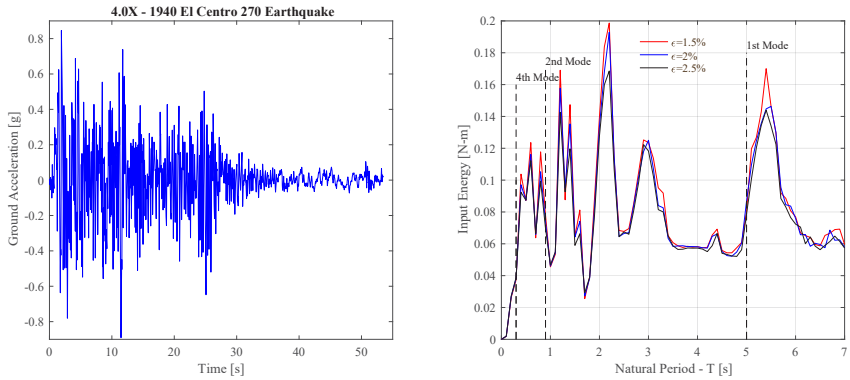

FIGURE 4.14 Scaled strong ground motion of 1940 El Centro used in this study and its associated energy input spectra. Displayed accelerations (strong level) caused damage to the building.

§ 4.5.5 Consideration of lateral confinement and uniform distribution of longitudinal reinforcement in the modelling of the core

Initially, the influences of neither the lateral confinement nor the lateral cracking were considered in the reduction of strength after cracking. The resulting increase in ductility due to the confinement was considered as an extra safety margin. Nevertheless, the use of this model may fail to define to what extent the non-accounted increase of the wall strength would influence the energy dissipation mechanisms of the structure, especially after cracking. Therefore, a second model considering the effect of both lateral confinement and lateral cracking was developed. In Diana-FEA, the lateral confinement is modelled 'through a pre-strain concept in which the lateral expansion effects are accounted for with an additional external loading on the structure' (TNO-DIANA, 2014b), according to the work of Selby and Vecchio (as cited in (TNO-DIANA, 2014b)). To test the influence of these modelling assumptions, results of nonlinear analyses using both models –with and without lateral confinement- had to be compared.

In a similar approach, the influence of the distribution of longitudinal steel reinforcement of the core up the height on the nonlinear performance of the outrigger structure was studied by proposing two models. One with 1% vertical reinforcement, uniformly distributed up the height, and another, where the maximum longitudinal reinforcement was provided only over the lower section of the building (six floors) and decreased towards the upper levels. This distribution was defined following the capacity flexural strength design envelope as proposed by Boivin and Paultre

(2012), with a minimum reinforcement ratio = 0.25% (ATC-PEER, 2010). All models considered the reduction of the Poisson effect after cracking.

Four numerical models were then developed (Table 4.13) to represent the 60- storey building with a single damped outrigger with a damper's damping coefficient equalling to 1.5E+08 Ns/m. Inherent damping ratio = 2%. Analyses included the modification of outrigger location between 0.4 and 0.9H.

MODEL DENOMINATION	LATERAL CONFINEMENT?	UNIFORM DISTRIBUTION OF LONGITUDINAL REINFORCEMENT?
lu	yes	yes
ln	yes	no
nu	no	yes
nn	no	no

TABLE 4.13 Correlation of modelling parameters organized per model

Figure 4.15 is representative of the storey drifts under outrigger locations between 0.4 and 0.9. According to the results obtained, it is possible to conclude that there is no difference in the response of the outrigger structure under four different earthquake magnitudes, in terms of considering lateral confinement (or not) in the modelling of the core. By contrast, the use of non/uniform distribution of longitudinal steel bar reinforcement modifies the response, although not substantially (variation < 2%).

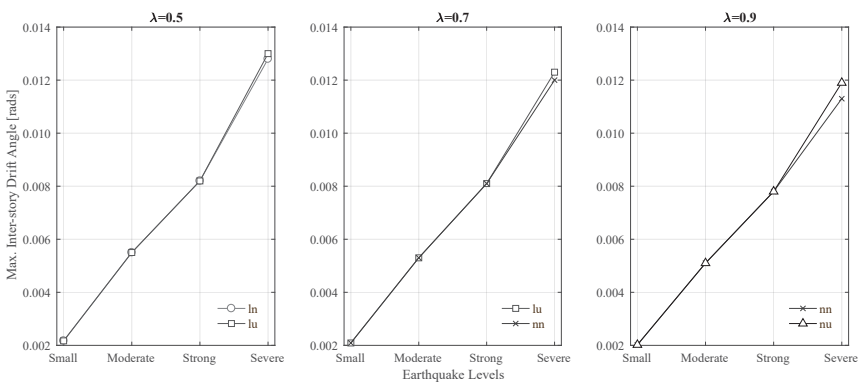

FIGURE 4.15 Comparison between maximum inter-storey drift ratios of the four core modelling parameters –depicted in pairs- under four intensity levels of 1940 El Centro earthquake, at different outrigger locations (λ). Under strong and severe levels, the response is inelastic.

A similar trend is observed when energy distribution is considered. For example, in Figure 4.16, it can be noticed that the use of lateral confinement does not substantially modify the distribution of input energy (variation < 0.0000001%). Nevertheless, the same plot shows that modelling the core with and without a uniform distribution of longitudinal reinforcement does affect the energy distribution (variation < 12%). Since the modification of these modelling parameters makes no difference when the response is elastic, in Figure 4.17 only the inelastic response is shown. Here, the variation of the energy distributions is accounted by Δ_e, which is equal to the difference between the peak energy values of the structure with non-uniform (*n*) and with uniform (*u*) longitudinal reinforcement distribution, i.e. Δ_e = Peak E_n – Peak E_u. The time-history analyses were performed with the outrigger at locations between 0.4 and 0.9H. Under strong earthquake levels, Δ_e between dampers and damping energies remains within a 0.5%, whereas input and hysteretic energies display variations in the order of 2.0%. Under severe earthquake level, damping and input energies display a difference of about 10%, dampers energy almost 20% and hysteretic energy, a difference larger than 25%.

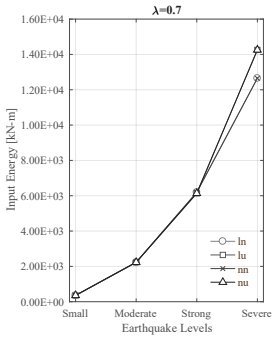

FIGURE 4.16 Input energy in the outrigger structure, modelled with combined core parameters, when subjected to four intensity levels of 1940 El Centro earthquake.

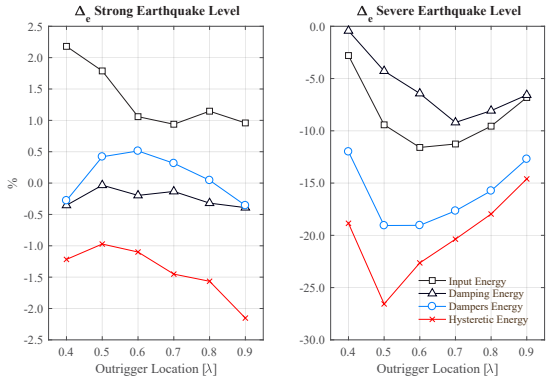

FIGURE 4.17 Δ_e (%) between energy distributions obtained with a non-uniform (*n*) and uniform (*u*) distribution of longitudinal reinforcement under strong and severe intensity levels of 1940 El Centro earthquake. Note that vertical scale is different for each plot.

Given the aforementioned results, the FE models described in this study, unless stated otherwise, do consider the contribution of lateral confinement and use a non-uniform distribution of longitudinal reinforcement in the modelling of the core.

§ 4.6 Factors affecting the performance of damped outriggers

The following parametric study was set by modification of the core-damping ratio (ζ); outrigger location (λ) and core-to-outrigger stiffness ratio (ρ_{cto}); dampers' damping coefficient (C_d); and, core-to-column stiffness ratio (ρ_{ctc}). Models including combinations of these parameters were subjected to small, moderate, strong, and severe earthquake levels of the 1940 El Centro ground motion.

§ 4.6.1 Frequency versus height of the building

Evaluated against any typical seismic design response spectrum –see for example Figure 4.18, it is clear that reducing the building period implies an increase of accelerations, and hence the assumption that dampers –being velocity dependent- will perform in full capacity, or at least better, if attached to buildings with shorter periods. Nonetheless, if ground motion records are observed in detail, it can be clearly noticed that a decrease in the period not always implies an increase in the acceleration. In the long-period ground motion record displayed in Figure 4.19, it can be observed that if a building has a period equals to 2.2 s, either the increase or decrease of the period implies an increase in the accelerations. Inversely, if the base period is 2 s, a shift in the building's frequency, either up or down, will invariably decrease the acceleration response.

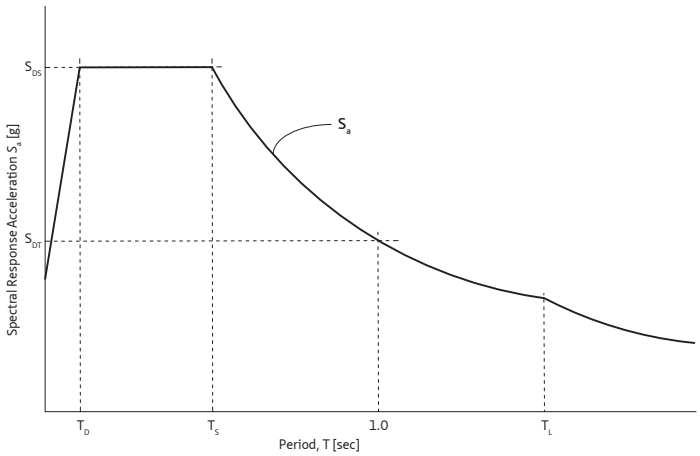

FIGURE 4.18 IBC 2006 design response spectrum

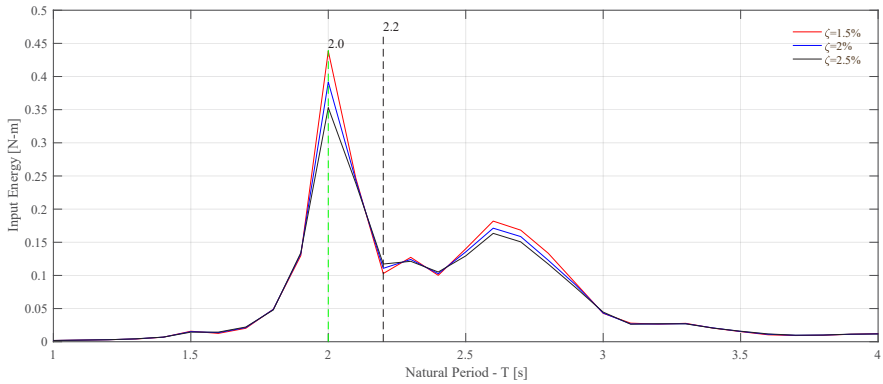

FIGURE 4.19 Acceleration response spectrum for Mexico Earthquake - component NW

§ 4.6.2 Outrigger location (λ)

The influence of the outrigger location on the increase of the inherent damping ratio **ζ** was studied by assuming a range of locations between 0.1 and 0.9 of the total height of the building, under free-vibration analyses. The outrigger location is described in terms of a non-dimensional parameter **λ**, such that location of the outrigger = **λ***H, hence **λ**=0.1 – 0.9. The inherent damping ratio **ζ**, assumed as equivalent viscous damping coefficient, was calculated using Rayleigh damping with values = 1.5, 2.0, and 2.5%. Then the optimal damping ratio ζ_{OPT} was computed under free vibration using logarithmic decrement technique. The case of the damped outrigger with **ζ**=2% is shown in (Figure 4.20). Considering optimal dampers size, ζ_{OPT} are displayed when **λ**=0.6 – 0.8. However, before and beyond the region defined by the optimal dampers' damping coefficients (C_d), the use of **λ**=0.4 – 0.9 display similar trends. In addition, regardless of the dampers size (damping coefficient), **λ** < 0.4 has less effect on improving the overall damping ratio of the building, if compared to values of **λ** >= 0.4. This observation is in agreement with the study of Huang and Takeuchi (2017), and suggests that λ_{OPT} is somewhere between 0.4 and 0.9. It should be noticed, nevertheless, that the optimal damping varies with the mode, so no single outrigger location will simultaneously reduce the response of all the modes (Chen *et al.*, 2010). Hence this optimal range of **λ** is hereafter considered assuming first mode predominance.

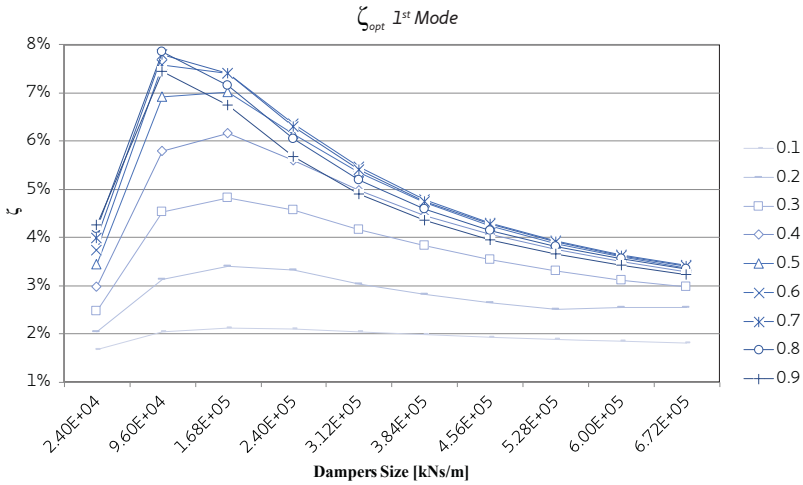

FIGURE 4.20 Increased ζ due to the combined influence of λ (0.1– 0.9) and dampers size, under free vibration.

Although it is been suggested that the damping ratio may exert a larger influence on the structural performance (Huang and Takeuchi, 2017), peak responses may not be optimally reduced by assuming an optimal location of the outrigger (λ_{OPT}) based on the increase of the damping ratio. If, for a given earthquake level, the peak inter- storey drift at each of the selected range of outrigger locations λ is plotted, then the inter-storey drift is reduced as λ increases (Figure 4.21a). A similar trend is displayed when the peak inter-storey velocities are accounted for, considering the first mode as predominant (Figure 4.21c). In the case of the building drift (Figure 4.21b), a shift of the optimal location between λ=0.8 and λ=0.6 can be noticed when the response goes from elastic (λ=0.8) to inelastic (λ=0.7 and 0.6, for strong and severe earthquake levels, respectively). Peak lateral accelerations are comparatively reduced when λ=0.5, for the elastic case and under strong earthquake level. A shift to λ=0.6 occurs under severe motion (Figure 4.21d). Although drift responses are valid performance targets, in some cases it is more significant to control base forces or moments. For example, Wu and Li (2003) argue that an outrigger that is been designed stiff with the aim of reducing the top drift of a tall building, may create weak floors near the outrigger level. This may shift the 'optimal location' from a top drift-based control to an overturning moment-based control. In Figure 4.22(right), it can be noticed that the overturning moment is comparatively reduced when λ=0.5, except for the severe level, where the optimal location is at λ=0.7. For reducing base shear (Figure 4.22, left), λ=0.7 is the optimal location for the linear cases (small and moderate earthquake levels); λ=0.8 and 0.5 are the optimal locations under strong and severe motion, respectively. Although in apparent randomness, these observations reinforce the idea that λ_{OPT} is somewhere between 0.5 and 0.8 – and that the definition of 'optimal' is strongly related to the target performance.

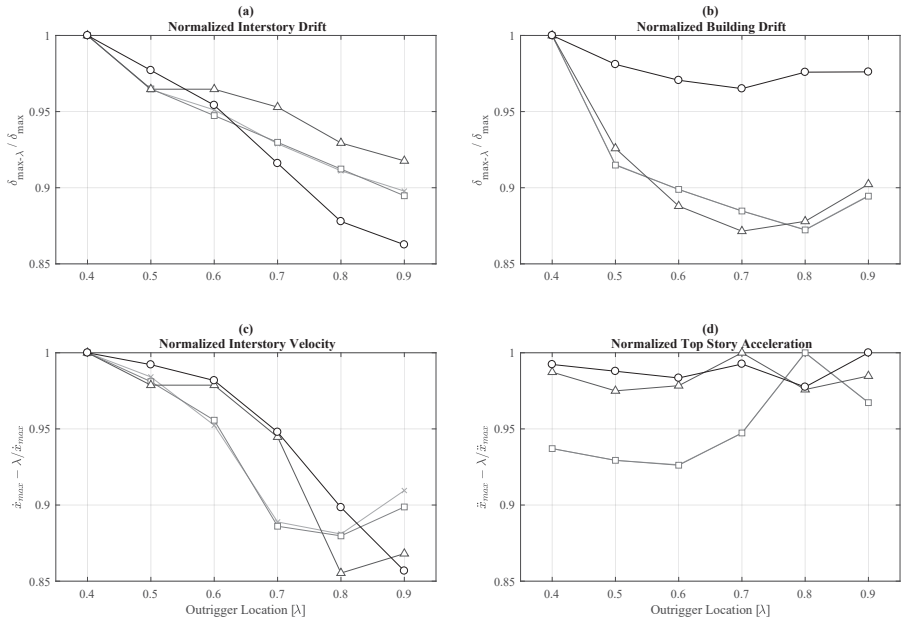

FIGURE 4.21 Normalized (actual/peak) drift, velocity and lateral accelerations for different outrigger locations (λ=0.4 – 0.9), of the damped outrigger building (ζ=2%, C_d=1.18E+05kN-s/m) subjected to four intensity levels of 1940 El Centro earthquake

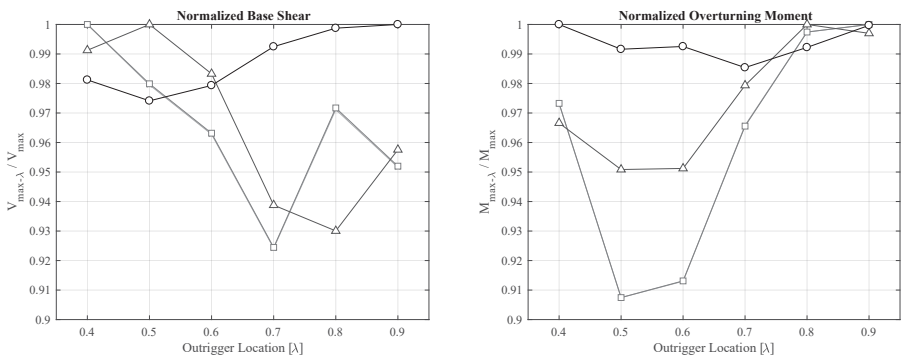

FIGURE 4.22 Normalized (actual/peak) base shear and overturning moments of the damped outrigger building (ζ=2%, C_d=1.18E+08kN-s/m), subjected to four intensity levels of 1940 El Centro earthquake, with different outrigger locations (λ=0.4 – 0.9).

In Figure 4.23, the plots of input energy, damping, dampers and hysteretic energies are separately displayed. Although the study of the energies alone cannot truly represent the way they are distributed through the structure, neither how they are dissipated, the observation of these individual distributions gives insights over the influence of λ on the global behaviour of the structure. For instance, when λ=0.6, the structure displays the lowest E_D if compared to the E_{Dmax}, for the first three earthquake levels. In addition, λ=0.6 implies the lowest E_I even in the presence of hysteretic energy dissipation due to a strong earthquake. However, when λ=0.6 the energy dissipated by hysteresis is fairly closed to its peak occurring when the outrigger is located at λ=0.7. This means that an outrigger located at λ=0.6, will help to decrease the input energy, but if nonlinearities occur, most of that input energy may be dissipated by damage and not by damping. Furthermore, λ=0.6 is not an optimal location from the perspective of an efficient use of the viscous dampers either, during an elastic response. Under inelastic response, on the contrary, the peak energy dissipation by dampers takes place when λ=0.7, i.e. dampers and hysteresis energy follow the same trend. This means that either the use of viscous dampers increases the damage in the structure, or given the reduction of E_I, dampers are indeed accounting for energy that otherwise would be dissipated by damage. These hypotheses are discussed in Chapter 5.

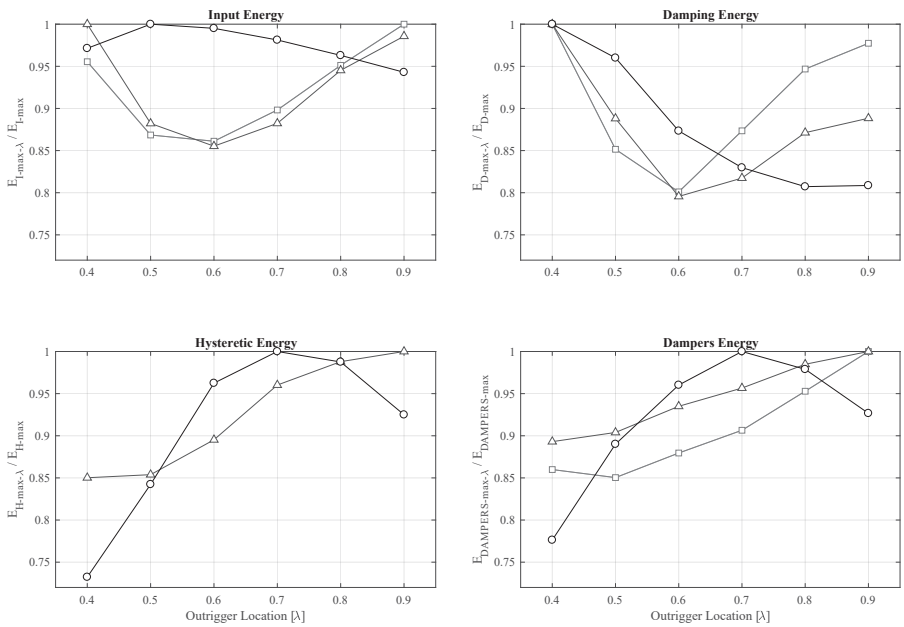

FIGURE 4.23 Normalized (actual/maximum) energy distributions of the outrigger structure (ζ=2% - C_d=1.18E+05kN-s/m) according to outrigger location (λ=0.4 – 0.9) under four intensity levels of 1940 El Centro earthquake.

§ 4.6.3 Optimal dampers' damping coefficient (C_d)

According to energy equations derived in Chapter 3, the energy dissipated by the dampers is proportional to the product of C_d and the velocity across the damper, modified by the exponent κ. This exponent can be varied between 0.15 and 2, depending on the damper manufacturer's specifications (Smith, 2016). The use of κ=1, which is been suggested optimal for wind applications (Infanti *et al.*, 2008; Smith, 2016), implies that the damping forces provided by the damper will be proportional to the velocity. The use of κ~=2 implies high forces at lower velocities, whereas the opposite occurs when lower values of κ are used. Under strong earthquake motions, the use of a lower exponent might lead to the insensitivity of the dampers to low velocities, whereas the use of a linear exponent might lead to excessive damping forces, if compared to the wind damping (Smith, 2016). In this parametric study, however, *k* is taken equals to one since comparatively excessive damping forces may help to understand the role of the outrigger's bending and shear stiffness in the distribution of seismic energy in the building structure. If, as a result of this assumption, the damping forces are indeed excessive, the use of a relief valve may help to avoid them. A relief valve allows the damper to work in a linear pattern till a relief load or pressure value is reached. At higher velocities then, the damper exerts low forces without affecting its performance at lower velocities.

In order to assess the performance of the oil viscous dampers attached to the outriggers, frequency response analyses were executed using damping coefficients ranging between 1.5E+02 and 1.5E+8kNs/m. These values are arbitrary and were found by conducting sensitive analyses through a process of trial and error. It was observed that when C_d < 1.5E+02, the system remains only damped by the core, i.e. without any contribution of the outrigger whatsoever. Beyond 1.5E+8 the structure behaves the same as with fixed outriggers. The observation of the vertical displacement response of the outrigger-damper (*nOD*) and damper-column (*nDC*) nodes in Figure 4.24, shows that when C_d=1.5E+03, the dynamic stiffness of the dampers is not enough to combine the axial stiffness given by the columns and the bending stiffness created by the core. Whereas *nOD* displays a large vertical displacement, same displacement of *nDC* is almost zero, indicating that they practically work separate from one another. When C_d=1.5E+06, the high dynamic stiffness 'ties' the column to the outrigger so vertically they displace the same amount, i.e. as if the structure had only conventional outriggers. Furthermore, the use of a low C_d values introduces large stresses in the core and not in the perimeter column. In contrast, the use of large C_d values not only leads to large stresses in the columns but also in the vertical chords of the outrigger frame (Morales Beltran *et al.*, 2017). In Figure 4.24 it can also be noticed that the frequency shift is insignificant if compared with the large variation of the C_d values, and hence it can be neglected (Huang and Takeuchi, 2017).

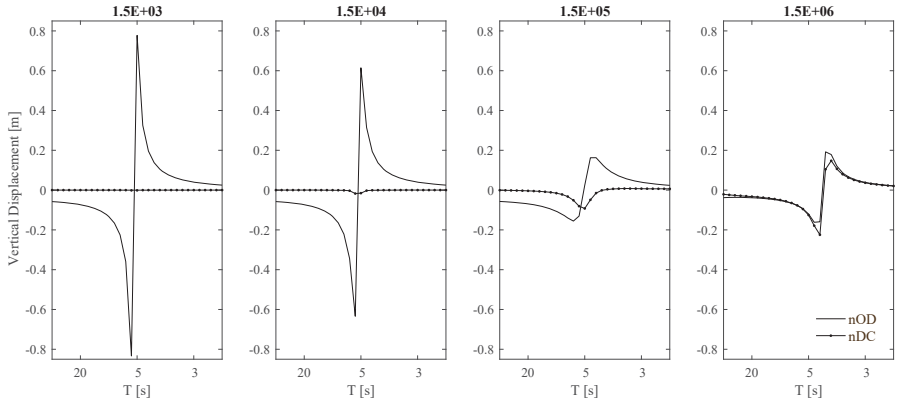

FIGURE 4.24 Frequency-based vertical displacements of the nodes outrigger-damper (nOD) and damper-column (nDC) for different damping coefficients of the viscous damper (in kN-s/m).

Based on the previous free vibration analyses, and according to the results displayed in Figure 4.25, for a damped outrigger structure with ζ=2%, the combined influence of λ and C_d will optimally increase the initial damping ratio when λ=0.7 and C_d=1.18E+05 kN-s/m. Although this value may vary between different case studies, a numerical result is used here to illustrate the practical implications associated with providing the demanded supplemental damping. For example, commercially-available viscous dampers are insufficient as they feature C_d values in the order of 1.5E+03 kN-s/m. Alternatively, the number of dampers could be increased according to the space availability in the outrigger (Figure 4.26). If two dampers are installed per outrigger, C_d increases up to 2.4E+04 (eight outriggers with two dampers); and up to 4.8E+04 if four dampers are installed at each outrigger arm. Since the number of dampers per outrigger cannot be likely increased beyond eight, the available supplemental damping may not match the optimal supplemental damping. However, the available-optimal gap could be reduced by modifying the stiffness properties of the key elements of the system, namely, core, outriggers and perimeter columns.

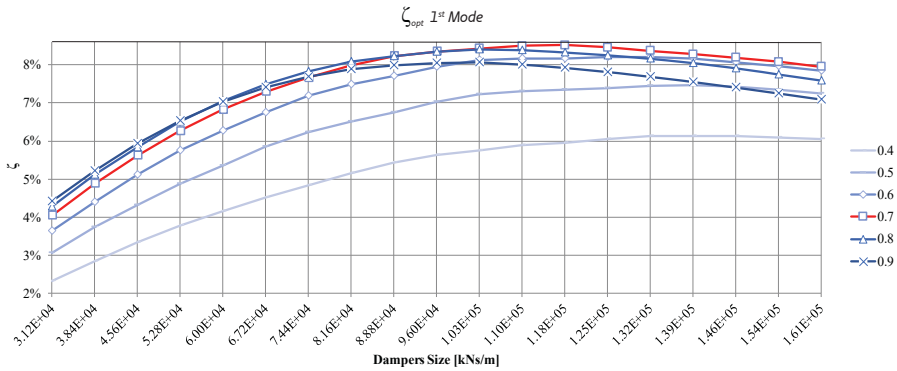

FIGURE 4.25 Optimal ζ according to values of λ between 0.4 and 0.9

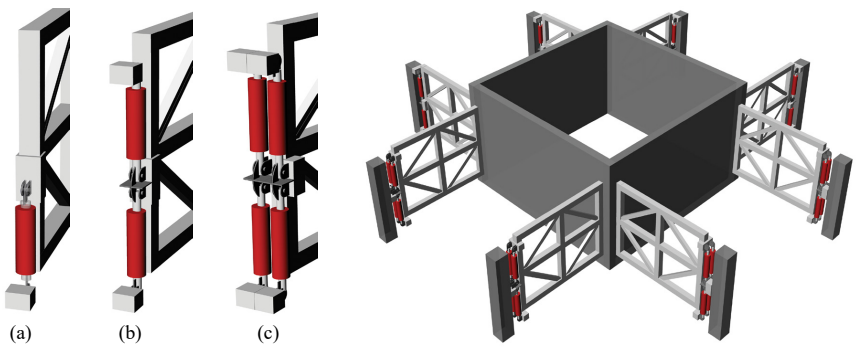

FIGURE 4.26 Configuration of eight outriggers with one (a), two (b), and four (c) dampers

Finally, it should be noted that with the additional viscous dampers, results obtained by modal analysis are no longer fully reliable because damping may not be evenly distributed under any modal shape. analyses involving normal modes should not be used 'because they cannot account for discrete damping elements within a structure' (Smith and Willford, 2007). Furthermore, model analysis cannot be used because nonlinear response is expected. Since dampers add an important percentage of damping, the response must be therefore evaluated by a full single analysis, such as a complete time-history analysis using direct solution methods, directly solve the dynamic equations of motion from the mass, stiffness and damping matrices.

§ 4.6.4 Stiffness core-to-outrigger ρ_{cto} and core-to-column ρ_{ctc} ratios

In order to provide insights over their influence on the energy distribution and seismic response, the stiffness-based core-to-outrigger and core-to-perimeter column relationships are studied through stiffness ratios. The core-to-outrigger stiffness ratio is a non-dimensional parameter given by Smith and Coull (1991)

$$\rho_{cto} = \frac{2EIr}{(EI)_O H} \tag{4.4}$$

where EI represents the core rigidity; $(EI)_O$ is the effective flexural rigidity of the outrigger; *r* is the distance between the centroid of the core and the perimeter columns; and, H is the building's height.

The also non-dimensional core-to-column stiffness ratio is defined as follows (Smith and Coull, 1991)

$$\rho_{ctc} = \frac{EI}{2(EA)_C r^2} \tag{4.5}$$

where $(EA)_c$ represents the column rigidity.

The initial FE model included a core design about 2.5 times stiffer than the combined bending and shear stiffness of the outrigger, i.e. ρ_{cto} ~=2.5. The core bending stiffness is about 2.25 times stiffer than the axial stiffness of the perimeter columns, i.e. ρ_{ctc} ~= 2.3. In order to study the damping ratio sensitivity to the variation of the ρ_{cto} and ρ_{ctc} stiffness ratios, these values were extended over a range between one and four. This is because values of ρ_{ctc} smaller than one, although possible, are not practical from an implementation point of view, as they would require the use of columns with comparatively large cross sections in combination with a core of comparatively small wall dimensions. Values of $\rho_{ctc} > 4$, on the other hand, imply that the axial stiffness of perimeter columns is less than 25% of the bending stiffness of the core. Moreover, according to the study of Tan *et al.* (2014), ρ_{ctc} 'should not be larger than four to achieve a supplementary 5% damping level'.

The results of analyses exploring the damping ratio sensitivity of the damped outrigger, to the combined effect of λ, C_d and ρ_{ctc} are displayed in Figure 4.27. It can be seen that effect of ρ_{ctc} is limited to a general 1% increase of ζ, for a given λ and C_d. However, when λ and C_d approximate to the optimal values, the effect of ρ_{ctc} may imply an overall ζ increase of 7%.

This suggests that given the fact that required dampers size may not be available, a modification in the ratio ρ_{ctc} will help to increase the overall damping ratio. It should be noted that such an increase will only occurs if ρ_{ctc} decreases.

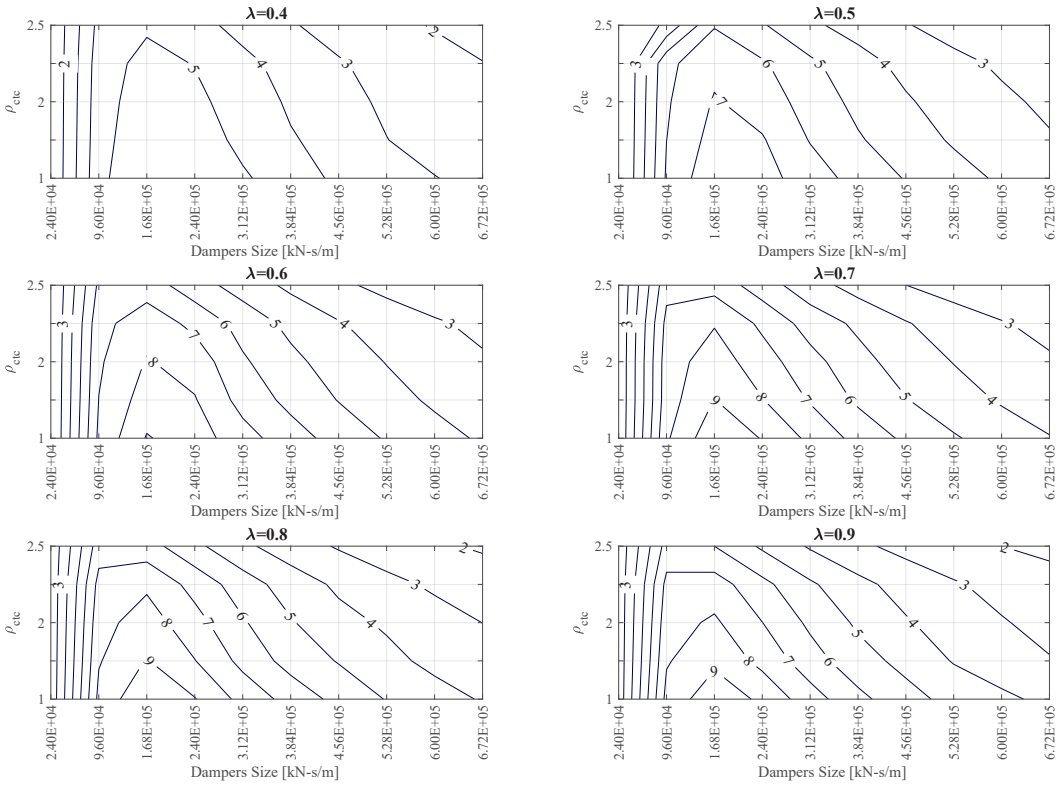

FIGURE 4.27 Distribution of ζ (in %) according to variable parameters ρ_{ctc}=1 – 4, C_d = 2.40E+04 – 6.72E+05 kN-s/m, and λ = 0.4 – 0.9, under free vibration. Inherent ζ = 2%

The combined influence of ρ_{cto} and ρ_{ctc} displayed in Figure 4.28, given an optimal λ=0.7, shows that the damping ratio can be further increased by 1%. In addition, and as expected, peaks for each ζ show that the increase is proportional to the inherent damping ratio: 9.73% for a $\zeta_{inherent}$=1.5%, 10.29% for a $\zeta_{inherent}$=2%, and 10.82% for a $\zeta_{inherent}$=2.5%.

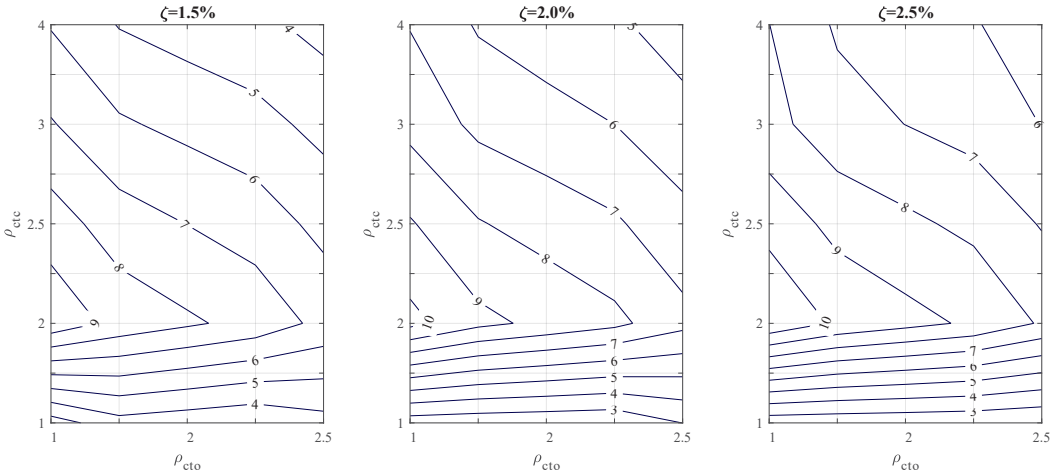

FIGURE 4.28 Distribution of ζ (in %) according to initial ζ = 1.5, 2.0, and 2.5%; ρ_{ctc}, ρ_{cto} = 1 – 4; λ= 0.7 under free vibration.

In order to understand to which extent the influence of the combined parameters ρ_{cto} and ρ_{ctc} is depending on either the integrated action of the viscous dampers or the modification of the fundamental building's frequency, Eigen-frequency analyses were conducted using fixed and damped outriggers. In Figure 4.29, the results show that the frequency shift is larger in the fixed outrigger (about 0.10Hz), compared to that of the damped outrigger (about 0.6Hz). In addition, in the case of the damped outrigger, the influence of ρ_{cto} is almost none and the frequency shift is due almost exclusively to the variation of ρ_{ctc}. With the increase in λ, the outrigger exerts a major influence in the frequency shift, reaching its maximum around λ=0.8-0.9 in both fixed and damped outriggers (Figure 4.30). It is interesting to note that none of the parameters currently under discussion, namely λ, ρ_{ctc} and ρ_{cto}, have any influence on the frequency of the damped outrigger, when λ<0.6. The fact that frequency shifts become more significant as the outrigger approaches the roof, and that only ρ_{ctc} has influence on such frequency shifts, supports the conclusion that both λ and ρ_{ctc} exert their influence by modifying the building's natural frequency. The fact that ρ_{cto} does modify the response but not the frequency, suggests that its influence is closely related to the effect of the viscous dampers.

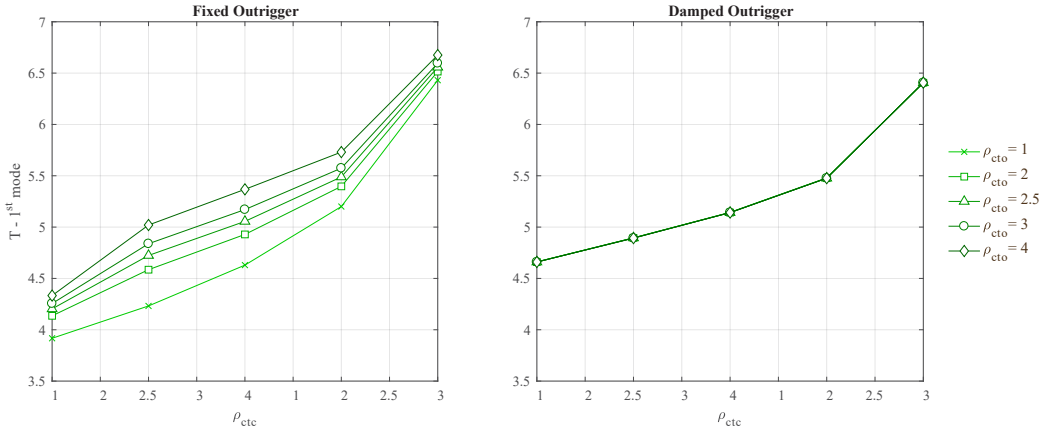

FIGURE 4.29 Shifts in 1st mode period due to the combined effect of ρ_{cto} and ρ_{ctc} on the fixed and 1.18E+05kN-s/m damped outrigger structure; λ=0.7 and ζ=1.5%.

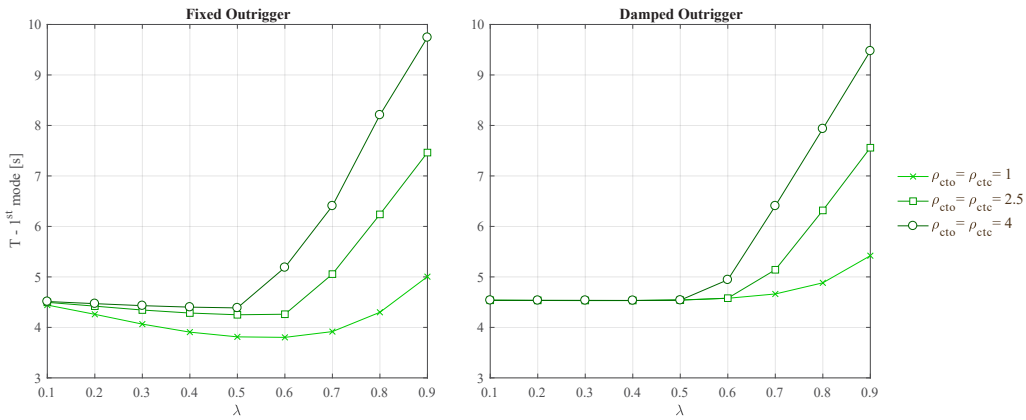

FIGURE 4.30 Influence of λ on the period shifts of the fixed and damped outrigger. Data points correspond to couples ρ_{cto}=ρ_{ctc} = 1, 2.5, and 4.

Finally, the influence of the combined parameters ρ_{cto} and ρ_{ctc} on the seismic energy distributions was studied through time-history analyses of the damped outrigger. The results displayed in Figure 4.31 show that when the outrigger is flexible (ρ_{cto} =4), E_I is comparatively large regardless the modification of ρ_{ctc}, under all earthquake levels except severe. Under this last one, the use of a rigid outrigger (ρ_{cto} =1) implies larger amount of input energy in the system. This sudden shift may be related to the assumption of the linear behaviour of the dampers: under small, moderate, and strong earthquakes, the velocities across the damper might not be large and hence the

damping forces benefit from a rigid outrigger. Under severe earthquakes, the damping forces will be proportionally increased to the now large velocities and hence damping forces are amplified by the effect of a rigid outrigger.

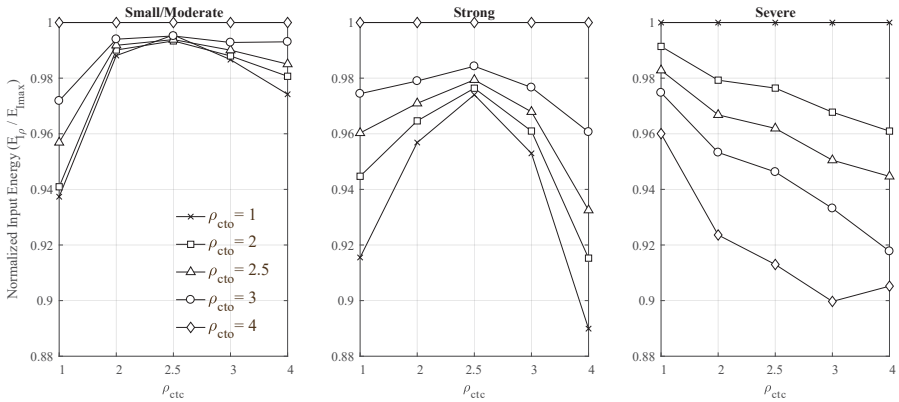

FIGURE 4.31 Variations of the Normalized Input Energy ($E_I\rho/E_{Imax}$), according to combined effect of ρ_{cto} and ρ_{ctc}, under different earthquake levels of 1940 El Centro earthquake; C_d = 1.18E+05kN-s/m, λ=0.7 and ζ=1.5%.

§ 4.7 Conclusions

An explorative study on the parameters that influence the distribution of seismic energy in outrigger structures is been presented. General observations can be derived from the described numerical studies as follows:

- Modelling the core with and without a uniform distribution of longitudinal reinforcement affects the energy distribution. Under severe earthquake levels, damping energy (E_D) and input energy (E_I) vary by 10%, dampers energy ($E_{dampers}$) by almost 20% and hysteretic energy (E_H), more than 25%.
- The optimal damping coefficient C_d and the optimal location λ have a major influence in the optimal damping ratio ζ and, thus, in the overall response of the outrigger structure.
- Regardless of C_d, $\lambda < 0.4$ has less effect on improving the overall damping ratio of the building, if compared to values of $\lambda >= 0.4$. This suggests that the optimal λ is somewhere between 0.4 and 0.9.
- The optimal damping varies with the mode, so no single outrigger location will lead to reduce the response of all the modes to their minimum.
- When λ and C_d approximate to the optimal values, the effect of ρ_{ctc} may imply an overall ζ increase of 7%. This suggests that if required damper sizes are not available, a modification in the ratio ρ_{ctc} will help to increase the overall damping ratio. It should be noted that such increase occurs only if ρ_{ctc} decreases.
- None of the parameters under discussion, namely λ, ρ_{ctc} and ρ_{cto}, have any influence on the frequency shift of the damped outrigger, when $\lambda<0.6$. Frequency shifts become more significant as the outrigger approaches the roof.
- Both λ and ρ_{ctc} exert their influence by modifying the building's natural frequency. The fact that ρ_{cto} does modify the response but not the frequency, suggests that its influence is closely related to the effect of the viscous dampers.
- When the outrigger is flexible (ρ_{cto} =4), E_I is comparatively large regardless of ρ_{ctc}, under all earthquake levels except by severe. Under this latter, the use of a rigid outrigger (ρ_{cto} =1) implies larger amount of input energy in the system. This shift may be the result of large damping forces being linearly amplified by the high velocities of the severe motions.

References

1991-1-1, E. 2002. Eurocode 1: Actions on structures - Part 1-1: General actions - Densities, self-weight, imposed loads for buildings

1992-1-1, E. 2004. Eurocode 2: Design of concrete structures - Part 1-1: General rules and rules for buildings

1993-1-1, E. 2004. Eurocode 3: Design of steel structures - Part 1-1: General rules and rules for buildings

ANSI, A. 2005. AISC 341-05''Seismic provisions for structural steel buildings.''American Institute of Steel Construction.

ATC-PEER, Applied Technology Council - Pacific Earthquake Engineering Research Center. 2010. Modeling and acceptance criteria for seismic design and analysis of tall buildings.

Beiraghi, H., Kheyroddin, A. and Kafi, M. A. 2016. Energy dissipation of tall core-wall structures with multi-plastic hinges subjected to forward directivity near-fault and far-fault earthquakes. The Structural Design of Tall and Special Buildings. 25: 801-820. 10.1002/tal.1284

Beiraghi, H. and Siahpolo, N. 2017. Seismic assessment of RC core-wall building capable of three plastic hinges with outrigger. The Structural Design of Tall and Special Buildings. 26: e1306-n/a. 10.1002/tal.1306

Boivin, Y. and Paultre, P. 2012. Seismic force demand on ductile reinforced concrete shear walls subjected to western North American ground motions: Part 2 — new capacity design methods. Canadian Journal of Civil Engineering. 39: 738-750. 10.1139/l2012-044

CESMD 2014. Strong-motion Virtual Data Center

Chang, C.-M., Wang, Z., Spencer Jr, B. F. and Chen, Z. 2013. Semi-active damped outriggers for seismic protection of high-rise buildings. Smart Structures and Systems. 11: 435-451.

Chen, Y., McFarland, D., Wang, Z., Spencer, B. and Bergman, L. 2010. Analysis of Tall Buildings with Damped Outriggers. Journal of Structural Engineering. 136: 1435-1443. 10.1061/(ASCE)ST.1943-541X.0000247

Chopra, A. K. 2007. Dynamics of structures: theory and applications to earthquake engineering. Prentice-Hall:

Council, A. T. 2010. Modeling and acceptance criteria for seismic design and analysis of tall buildings.

DIANA FEA Release 10.1 TNO - DIANA FEA BV Delft, the Netherlands

Gamaliel, R. 2008. Frequency-based response of damped outrigger systems for tall buildings

Hoenderkamp, J. 2004. Shear wall with outrigger trusses on wall and column foundations. The structural design of tall and special buildings. 13: 73-87.

Huang, B. and Takeuchi, T. 2017. Dynamic Response Evaluation of Damped-Outrigger Systems with Various Heights. Earthquake Spectra. 33: 665-685. 10.1193/051816EQS082M

Infanti, S., Robinson, J. and Smith, R. 2008. Viscous dampers for high-rise buildings

INN-Chile 2009. NCh 433-of. 96 Diseño sísmico de edificios.

Jackson, M. and Scott David, M. 2010. Increasing Efficiency in Tall Buildings by Damping

Lu, X., Lu, X., Sezen, H. and Ye, L. 2014. Development of a simplified model and seismic energy dissipation in a super-tall building. Engineering Structures. 67: 109-122. http://dx.doi.org/10.1016/j.engstruct.2014.02.017

Rhinoceros 5

Morales Beltran, M., Turan, G. and Yildirim, U. 2017. Distribution of large-earthquake input energy in viscous damped outrigger structures

O'Neill, J. C. 2006. Application of damping in high-rise buildings

Panagiotou, M. and Restrepo, J. I. 2009. Dual-plastic hinge design concept for reducing higher-mode effects on high-rise cantilever wall buildings. Earthquake Engineering & Structural Dynamics. 38: 1359-1380. 10.1002/eqe.905

Rutenberg, A. and Tal, D. 1987. Lateral load response of belted tall building structures. Engineering Structures. 9: 53-67. https://doi.org/10.1016/0141-0296(87)90041-1

Smith, B. S. and Coull, A. 1991. Tall building structures: analysis and design.

Smith, R. 2016. The Damped Outrigger-Design and Implementation. International Journal of High-Rise Buildings. 5: 63-70.

Smith, R. J. and Willford, M. R. 2007. The damped outrigger concept for tall buildings. The Structural Design of Tall and Special Buildings. 16: 501-517. 10.1002/tal.413

Tan, P., Fang, C. and Zhou, F. 2014. Dynamic characteristics of a novel damped outrigger system. Earthquake Engineering and Engineering Vibration. 13: 293-304. 10.1007/s11803-014-0231-3

Taranath, B. S. 1988. Structural analysis and design of tall buildings. McGraw-Hill: New York

Taranath, B. S. 1998. Steel, concrete, & composite design of tall buildings.
TNO-DIANA 2014a. Analysis Procedures
TNO-DIANA 2014b. Element Library
Wang, Z., Chang, C.-M., Spencer Jr, B. F. and Chen, Z. 2010. Controllable outrigger damping system for high rise building with MR dampers
Willford, M. and Smith, R. 2008. Performance based seismic and wind engineering for 60 story twin towers in Manila
Wu, J. R. and Li, Q. S. 2003. Structural performance of multi-outrigger-braced tall buildings. The Structural Design of Tall and Special Buildings. 12: 155-176. 10.1002/tal.219
Zhou, Y. and Li, H. 2013. Analysis of a high-rise steel structure with viscous damped outriggers. The Structural Design of Tall and Special Buildings. 23: 963-979. 10.1002/tal.1098

5 Seismic energy distribution in passive single damped outriggers

§ 5.1 Summary

This chapter discusses to which extent the use of passive viscous damped outriggers can avoid damage of the host structure when subjected to strong earthquake motion. The distribution of seismic energy and responses between fixed and damped outrigger structures, subjected to different levels of peak ground accelerations (PGA), is comparatively evaluated. Moreover, damping-to-input (E_D/E_I), dampers' damping-to-input ($E_{DAMPERS}/E_I$), and hysteretic-to-input (E_H/E_I) energy ratios are proposed as parameters for the energy distribution assessment. The concept of *optimal* configuration is therefore discussed in terms of reducing the total input energy introduced in the structure by an earthquake. The results show that passive damped outriggers improve the building seismic performance if compared to its counterpart the fixed outriggers. In addition, results show that by means of passive viscous dampers, outrigger structures cannot avoid damage in the building core when subjected to strong earthquake motion.

Chapter 5 is based on the study presented in '*Distribution of strong earthquake input energy in tall buildings equipped with damped outriggers*'.

§ 5.2 Introduction

Damped outriggers have been used in few tall buildings applications for controlling wind response (Smith, 2016). Experimental and numerical research studies have been conducted to extend the application of damped outriggers to seismic control (Asai *et al.*, 2013; Chang *et al.*, 2013; Zhou and Li, 2013). However, in these studies the capability of the structure to undergo large deformations without damage has been assumed. In other words, with the increase in the ground motion given by strong

earthquakes, the dampers are assumed to be the main source of energy dissipation whilst the host structure displays an elastic behaviour. This is questionable. Strong earthquakes introduces larger amount of energy into the building's structure, compared to moderate earthquakes or strong winds. In tall buildings, such seismic energy is dissipated by several mechanisms including bending deformation of the core, friction between structural and non-structural components, and eventually, damage. The stronger the earthquake is, the larger the chance that such energy will be dissipated by structural damage, even in a building equipped with damped outriggers.

On the other hand, given the high chance of damage under strong earthquakes, conventional seismic design codes enlarge the structural elements to guarantee that such damage will not pose a life risk to occupants. Evidently, the enlargement of structural elements represents additional costs of building construction. With the addition of outriggers with dampers, the structural response is reduced and the need of a superstructure eliminated. Hence it is more accurate to assume that, when subjected to strong earthquakes, ***part*** of the seismic energy is dissipated by the dampers installed in the outriggers. However, if a damped outrigger aims to prevent damage during the occurrence of a large earthquake by dissipating a portion of the input energy, the question that arises is how much of that seismic energy will be dissipated by the dampers? Moreover, if under strong earthquakes structures often present some degree of damage, how much of that damage can be prevented by adding viscous dampers? Would it be possible to reduce completely the structural damage by dissipating seismic energy through the dampers?

The objective of the study presented in this chapter is to determine if the energy dissipated by hysteresis (damage) can be fully replaced by energy dissipated through the action of passive viscous dampers. More precisely, the goal is to determine whether it is correct to assume that main structural components will remain elastic during the entire strong earthquake response of a tall building, as well as which parameters mainly affect the response of damped outrigger structures and how such influence is exerted. In order to determine to which extent the use of viscously damped outriggers would avoid damage, both the host structure's hysteretic behaviour and the dampers' performance need to be evaluated in parallel. First, the time-history responses of fixed and damped outrigger structures, subjected to different levels of peak ground accelerations (PGA) of a suite of eight earthquake records, are obtained using 2D finite element (FE) models. Therefore, the nonlinear behaviour of the outrigger with and without viscous dampers is examined under small, moderate and strong long-period earthquakes to assess the hysteretic energy distribution through the core and outriggers. Next, the distribution of seismic energy in the structures is assessed by means of the damping-to-input (E_D/E_I), dampers' damping-to-input ($E_{DAMPERS}/E_I$), and hysteretic-to-input (E_H/E_I) energy ratios. The concept of *optimal* configuration is

therefore discussed in terms of reducing the hysteresis energy ratio of the structure. This assessment gives insights on which strategies will extend the elastic response threshold of a tall building equipped with viscous dampers and subjected to strong earthquake ground motions. The results show that, as the ground motion becomes stronger, viscous dampers effectively reduce the potential of damage in the structure if compared to conventional outriggers. However, the use of dampers cannot entirely prevent damage under critical excitations.

§ 5.3 Assessment of the distribution of seismic energy in a tall building

The equation governing dynamic response of a multi-degree of freedom (MDOF) system, such as a tall building, can take the form

$$M\ddot{x} + C\dot{x} + Kx = -M\Gamma\ddot{x}_g \tag{5.1}$$

where *M* and *K* are the diagonal lumped mass and stiffness matrices, respectively; C is the damping matrix computed considering Rayleigh damping; *x* is the column vector of relative displacements of the node mass with respect to ground; $\ddot{x}_g$ is the one-dimensional ground acceleration; and Γ is coefficient vector for ground accelerations. If Eq. 5.1 is multiplied by the transpose of the relative velocity vector $\dot{x}(t)$, and integrated over the entire duration of the ground motion (0-t), the equation of motion can be expressed in terms of the energy balance equation as follows

$$\int_0^t \dot{x}^T M\ddot{x}dt + \int_0^t \dot{x}^T C\dot{x}dt + \int_0^t \dot{x}^T Kxdt = -\int_0^t \dot{x}^T M\Gamma\ddot{x}_g dt \tag{5.2}$$

The first term in Eq. 5.2 is the relative kinetic energy (E_K), which can be written as

$$E_K = \int_0^t \dot{x}^T M\ddot{x}\ dt = \frac{1}{2}\dot{x}^T M\dot{x} \tag{5.3}$$

The second term in Eq. 5.2 is the inherent damping energy of the structure (E_D) and it can be written as

$$E_D = \int_0^t \dot{x}^T C\dot{x}\ dt \tag{5.4}$$

Since viscous dampers are attached to the outrigger structure, E_D includes also the energy dissipated by these passives devices, so that the total damping energy becomes

$$E_{D_total} = E_D + E_{dampers} = \int_0^t \dot{x}^T C\dot{x}\ dt + \int_0^t \dot{x}^T \Lambda C_d \dot{x}_d^{\ \kappa}\ dt \tag{5.5}$$

where Λ is the location matrix of the dampers –associated to the outrigger location λ, C_d is the damping coefficient of the damper, $\dot{x}_d$ is the velocity across the damper and κ is the exponent value that controls the linear/nonlinear behaviour of the damper.

The third term in Eq. 5.2 is the total absorbed energy (E_A), defined as

$$E_A = \int_0^t \dot{x}^T Kx\ dt \tag{5.6}$$

Since the structure absorbs energy by a combination of elastic and inelastic mechanisms, E_A can also be defined as

$$E_A = E_S + E_H \tag{5.7}$$

where E_S and E_H are the elastic strain and hysteretic energy, respectively. By considering [*K*] as the pre-yield stiffness matrix of the structure, E_S can be written as

$$E_S = \frac{1}{2}\dot{x}^T Kx \tag{5.8}$$

The hysteretic energy E_H is given by

$$E_H = E_{H-force} + E_{H-bending} + E_{H-shear} \tag{5.9}$$

where $E_{H\text{-force}}$, $E_{H\text{-bending}}$, and $E_{H\text{-shear}}$ are the hysteretic energies due to axial, bending, and shear stresses, respectively. However, due to the assumption of a Bernoulli beam in the modelling of the core, stresses and strains derived from shear forces can be neglected and thus E_H is reduced to

$$E_H = \int f_s(x - x_{yield})\ dx + \int M_b(\theta - \theta_{yield})\ d\theta \tag{5.10}$$

where f_s is the restoring force, M_b is the bending moment, and θ is the associated angle of rotation.

Finally, the last term in the Eq. 5.2 is the total energy introduced in the system as a consequence of the ground motion produced by an earthquake. This energy is equivalent to the energy input at foundation of the building as given by

$$E_I = -\int_0^t \dot{x}^T M \ddot{x}_g \, dt \tag{5.11}$$

Replacing Equations 5.3, 5.5, 5.6, 5.7 and 5.11 in Equation 1, the energy balance equation for a MDOF system is given by

$$E_K + E_D + E_{dampers} + E_S + E_H = E_I \tag{5.12}$$

As noted, the energy balance equation has been defined in relative terms instead of absolute ones. According to Uang and Bertero (1990), damping energy, strain energy, and hysteretic energy terms are uniquely defined, irrespective of what method is used. Given the interest on quantifying only the hysteretic and damping energies –including that derived from the dampers as well, the distinction between absolute and relative energy methods become less critical (Bruneau and Wang, 1996; Khashaee *et al.*, 2003). In addition, the authors believe that the use of relative energy terms instead of absolute ones is more meaningful for engineering applications. Chopra (2007) and Bruneau and Wang (1996), as cited in Khashaee *et al.* (2003), support this approach as 'internal forces within a structure are computed using relative displacements and velocities'.

§ 5.3.1 Methodology

According to Eq. 5.12, the distribution of seismic energy is based on the demand of total input energy – E_I. Nonetheless, kinetic and elastic strain energies tend to zero at the end of the vibration, whilst its maximum values take place at the beginning of the earthquake motion. Hence, they are not affected by the duration of strong motion (Khashaee *et al.*, 2003) and it is valid to assume that, by the end of the motion, E_I is mostly defined by the combined effect of damping energies (E_D + $E_{dampers}$) and hysteretic energy (E_H) dissipation. On the other hand, maximum damping and hysteretic energies permit to evaluate the energy dissipation capacity to limit structural damage. Therefore, insights on how these energies are related may be more significant for the

assessment of the seismic energy distribution in the damped outriggers, than spotting single-based performances. These relationships can be expressed by (a) the hysteretic-to-input energy $\xi_{hyst\text{-}to\text{-}inp}$ ratio, defined as the hysteresis energy ratio E_H/E_I; (b) the damping-to-input energy $\xi_{damp\text{-}to\text{-}inp}$ ratio, defined as the inherent viscous damping energy ratio E_D/E_I; and (c) the dampers-to-input energy $\xi_{dampers\text{-}to\text{-}inp}$ ratio, defined as the supplemental damping ratio $E_{dampers}/E_I$. Whereas $E_H/E_I = 1$ implies that the total input energy is dissipated by extended damage and/or failure of the structure, a value of zero implies no structural damage (Bojórquez *et al.*, 2010). Furthermore, $E_H/E_I = 0$ implies elastic behaviour in all the elements of the structure, during the entire ground motion. Since this latter case is highly unlikely under strong and severe earthquake levels, the purpose of the following studies is not only determining which parameters mainly affects the seismic response of damped outrigger structures, but also how such influence is exerted. The ultimate goal, nevertheless, is to determine if the energy dissipation due to hysteresis can be fully replaced by energy dissipated through the action of viscous dampers.

§ 5.3.2 Long-period earthquakes

Eight earthquake records were used in the analysis. These records were scaled down/up based on peak-ground-velocity (PGV) rather than on peak-ground-acceleration (PGA). This is because a velocity-based assessment framework is more meaningful for structures whose expected improved performance relies on the addition of velocity-dependent devices. The elastic threshold was set at velocity amplitudes around 0.9 m/s. Ground velocity amplitudes up to 0.5, 1.0, 1.5 m/s and beyond, were classified as small, moderate, strong and severe earthquakes, respectively (Table 5.1). Strong levels of five ground motions that induced damage in the structures are displayed in Figure *5.1*. Severe levels of the remaining three ground motions are displayed in Figure 5.2 and Figure 5.3. Note that the latter earthquake did not produce any damage to the structures at all. These earthquake records were downloaded via the Strong-motion Virtual Data Center (CESMD).

NO	EVENT/STATION/COMPONENT	PGA (G)	PGV (M/S)	PGA/PGV	FACTORS TO SCALE EARTHQUAKES TO:			
					Small	Moderate	Strong	Severe
1	Izmit-Kocaeli, Yarimca, 90	0.230	0.91	2.54	0.50	1.00	1.50	2.50
2	Michoacan, SCT1, N90W	0.158	0.57	2.76	0.80	1.60	2.50	4.00
3	El Centro, No.117, 270	0.210	0.37	5.69	1.25	2.50	4.00	6.70
4	El Maule, Concepcion, Long.	0.393	0.68	5.81	0.70	1.40	2.20	3.60
5	Northridge, Newhall - County Fire, 90	0.580	0.75	7.75	0.65	1.25	2.00	3.30
6	New Zealand, Greendale, N55W	0.738	0.95	7.81	0.50	1.00	1.50	2.50
7	Kobe, KJMA, 90	0.600	0.74	8.07	0.65	1.25	2.00	3.30
8	El Centro, No.117, 180	0.342	0.33	10.22	1.40	2.80	4.40	7.00

TABLE 5.1 Selected ground motions and factors chosen to scale them to the four earthquake levels used in this study.

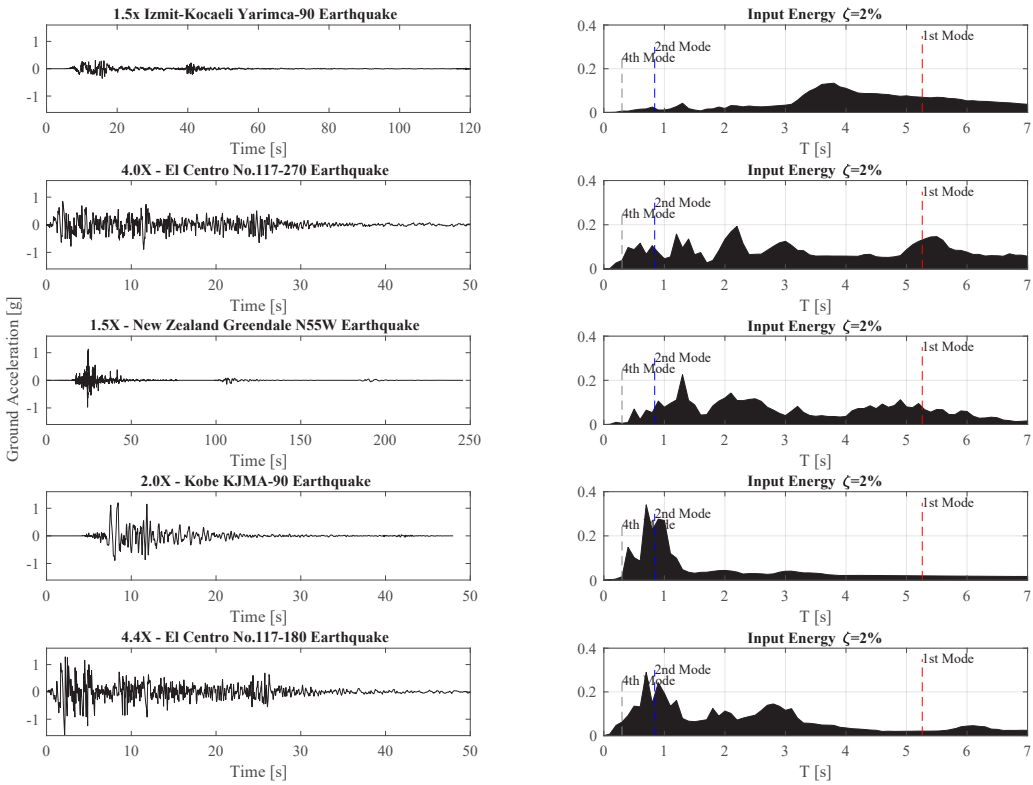

FIGURE 5.1 Five (out of eight) scaled ground motion records used in this study. Displayed accelerations, corresponding to strong earthquake level, caused damage to the single damped outrigger structure.

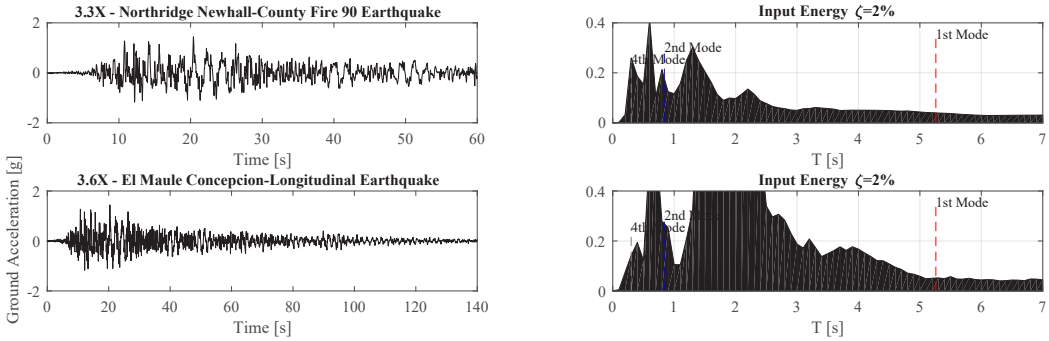

FIGURE 5.2 Two (out of eight) scaled ground motion records used in this study. Displayed accelerations, corresponding to severe earthquake level, caused damage to the single damped outrigger structure.

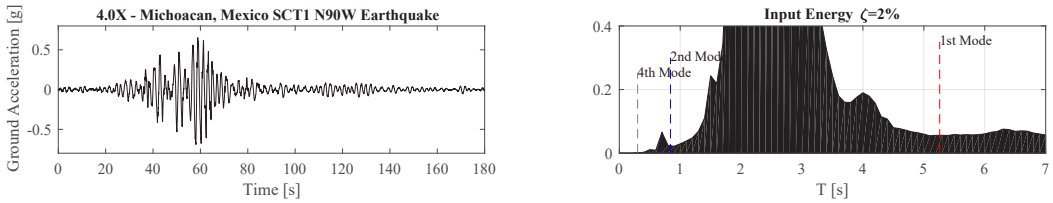

FIGURE 5.3 One of the eight scaled ground motion records used in this study. Displayed accelerations, corresponding to severe earthquake level, did not cause damage to any of the outrigger structures.

§ 5.4 Energy dissipation under different levels of ground motion

§ 5.4.1 Outrigger systems subjected to small - moderate earthquakes

Given the linear increase in the ground accelerations from small to moderate levels, the increase trend in the elastic response of the outrigger systems does not vary unless there is damage. For this reason, only energy responses to moderate levels are showed. In Figure 5.4 it can be noticed that for both outrigger systems, E_I does not vary substantially. However, E_D in the case of the damped systems is smaller (Figure 5.5), which is explained by the energy dissipated by the dampers (Figure 5.6). Under small levels the outrigger systems did not experience any damage, thus E_H is zero.

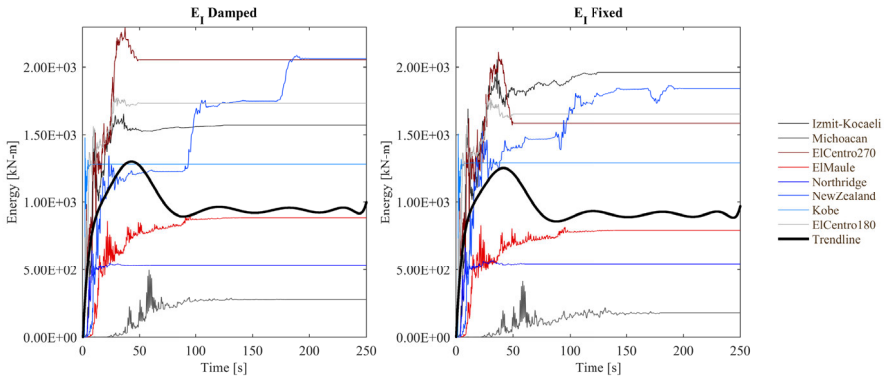

FIGURE 5.4 Input energy (E_I) of damped and fixed outrigger systems under moderate earthquake levels

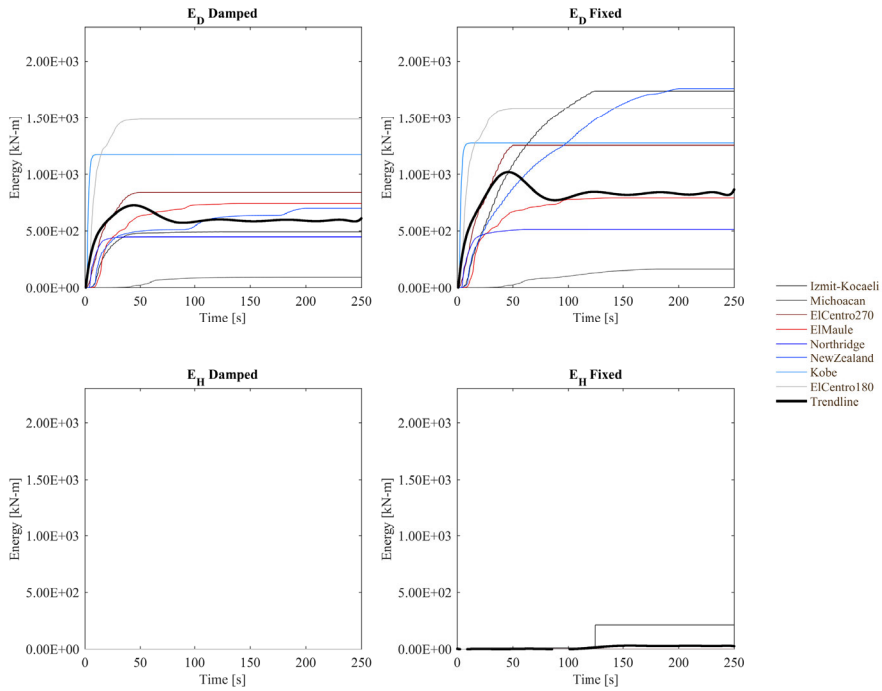

FIGURE 5.5 Damping energy (E_D) and hysteretic energy (E_H) of damped and fixed outrigger systems under moderate earthquake levels

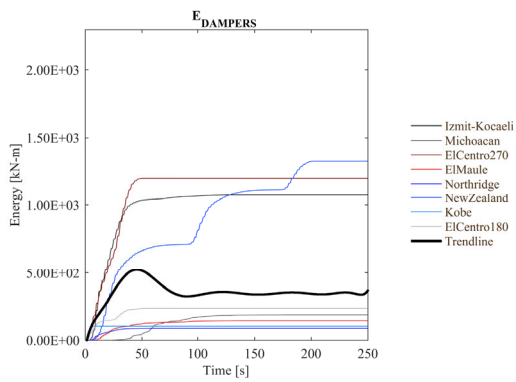

FIGURE 5.6 Dampers energy ($E_{dampers}$) of damped outrigger systems under moderate earthquake levels

Due to the increase in lateral stiffness provided by the link between outriggers and perimeter columns in the conventional design of outriggers, herein called fixed, the energy dissipated by motion is quite important (Figure 5.7). Although this may appear as an advantage from the energy dissipation perspective, in fact, it means that the building with fixed outrigger will experience a larger horizontal motion, i.e. accelerations, compared with the damped outrigger system.

§ 5.4.2 Outrigger systems subjected to strong earthquakes

From the plots displayed in Figure 5.8, it can be noted that E_I is fairly similar in both cases, except by El Centro 270 and New Zealand earthquakes. This seems to suggest that (a) structural properties have no major influence in the input energy definition, and (b) characteristics of the ground motions may be of more importance in defining noticeable variations in such input energy.

Since both E_I are similar, the distribution or dissipation of the seismic energy may be observed in different mechanisms of energy dissipation. Since the hysteresis mechanisms are again similar (Figure 5.9), the balance is created by adding $E_D+E_{dampers}$ (Figure 5.10), on the side of the damped configuration, and only E_D, on the side of the fixed configuration. This clearly explains the reduction of E_D in this latter configuration. Moreover, elastic strain and kinetic energy are slightly larger in the case of the fixed outrigger (Figure 5.11), due to its larger lateral stiffness.

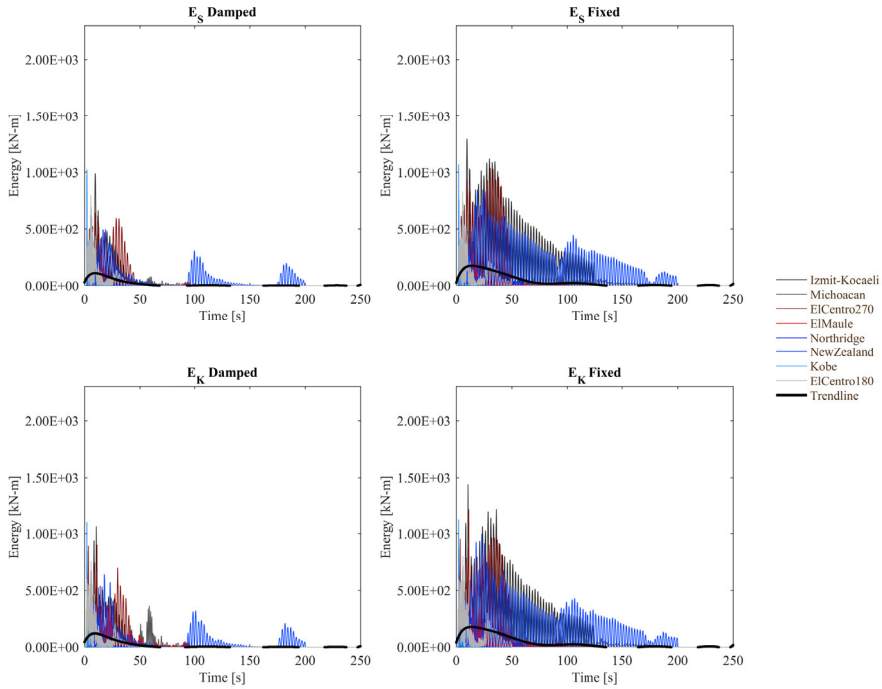

FIGURE 5.7 Strain elastic energy (E_S) and kinetic energy (E_K) of damped and fixed outrigger systems under moderate earthquake levels

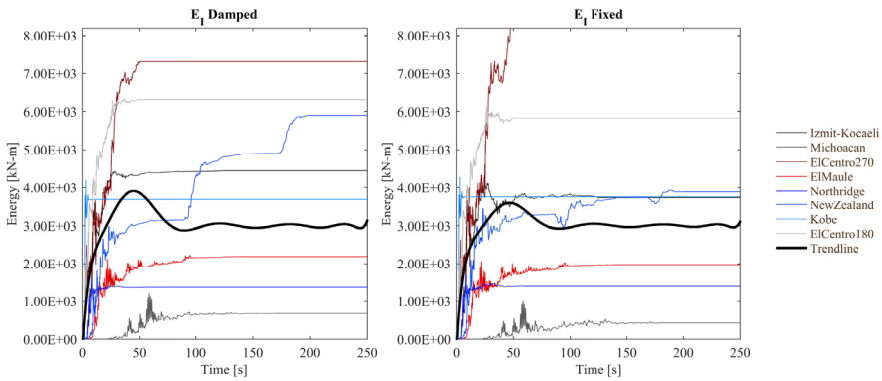

FIGURE 5.8 Input energy (E_I) of damped and fixed outrigger systems under strong earthquake levels

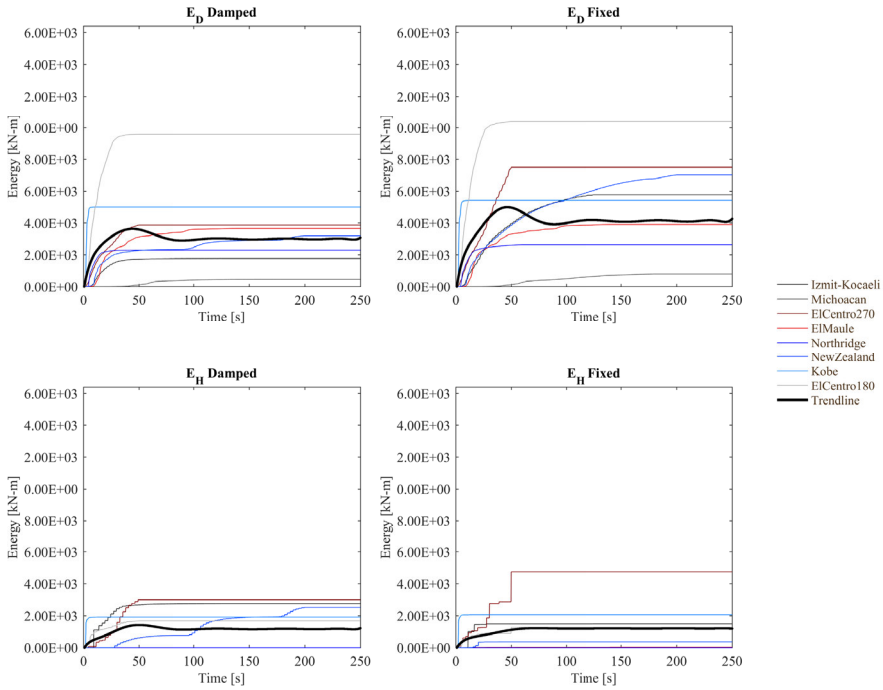

FIGURE 5.9 Damping energy (E_D) and hysteretic energy (E_H) of damped and fixed outrigger systems under strong earthquake levels

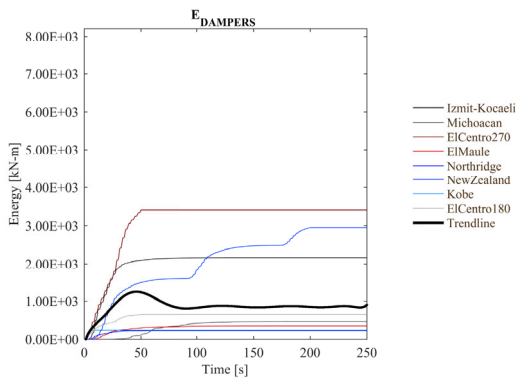

FIGURE 5.10 Dampers energy ($E_{dampers}$) of damped outrigger systems under strong earthquake levels

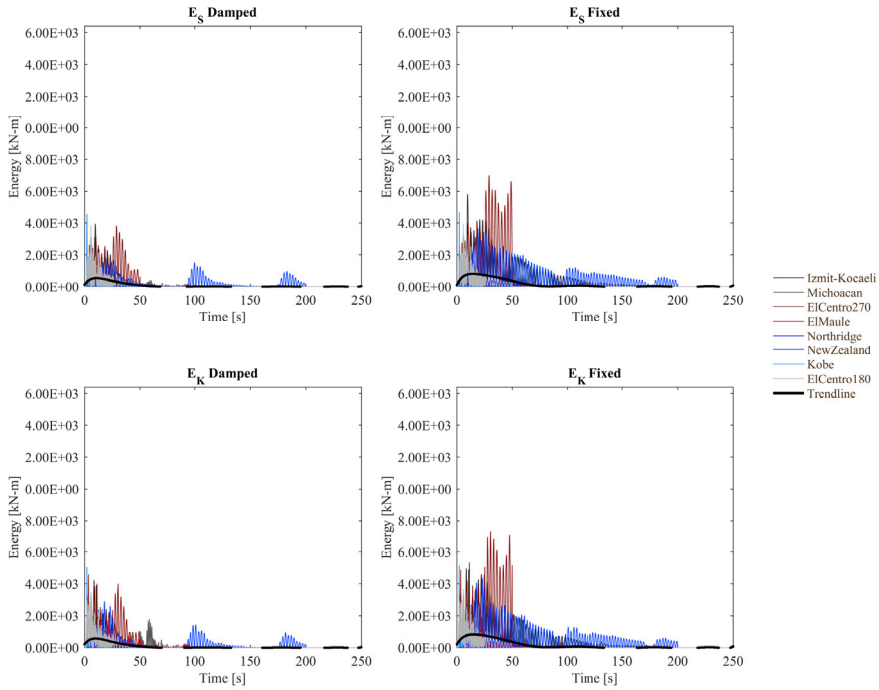

FIGURE 5.11 Strain elastic energy (E_S) and kinetic energy (E_K) of damped and fixed outrigger systems under strong earthquake levels

§ 5.4.3 Outrigger systems subjected to severe earthquakes

Under severe ground motions, the input energy of the damped outrigger is smaller than that of the fixed outrigger (Figure 5.12). The reason seems to be associated with the fairly increase in the energy dissipated by the dampers (Figure 5.13).

Although the hysteretic energy is comparatively reduced, compared to the strong level case, both outriggers systems seem to undergo a similar level of damage (Figure 5.14). This assumed even hysteresis needs to be investigated by revising the hysteretic distribution in the core –reviewed in the next section. Once more, the larger stiffness of the fixed configuration implies larger amount of kinetic and strain energy dissipated (Figure 5.15).

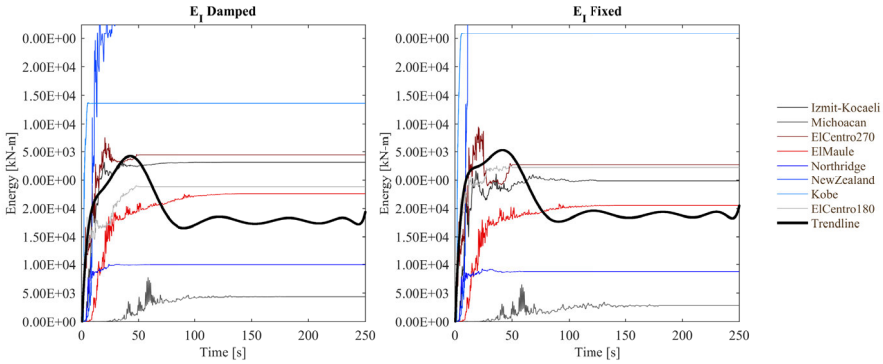

FIGURE 5.12 Input energy (E_I) of damped and fixed outrigger systems under severe earthquake levels

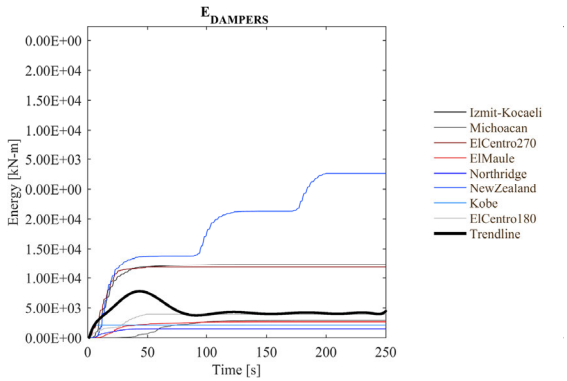

FIGURE 5.13 Dampers energy ($E_{dampers}$) of damped outrigger systems under severe earthquake levels

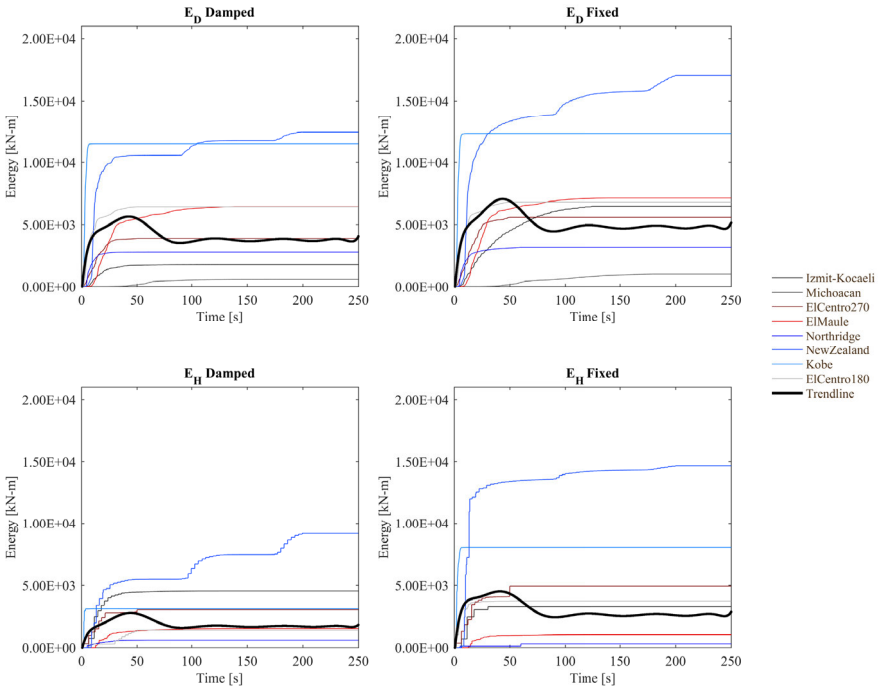

FIGURE 5.14 Damping energy (E_D) and hysteretic energy (E_H) of damped and fixed outrigger systems under severe earthquake levels

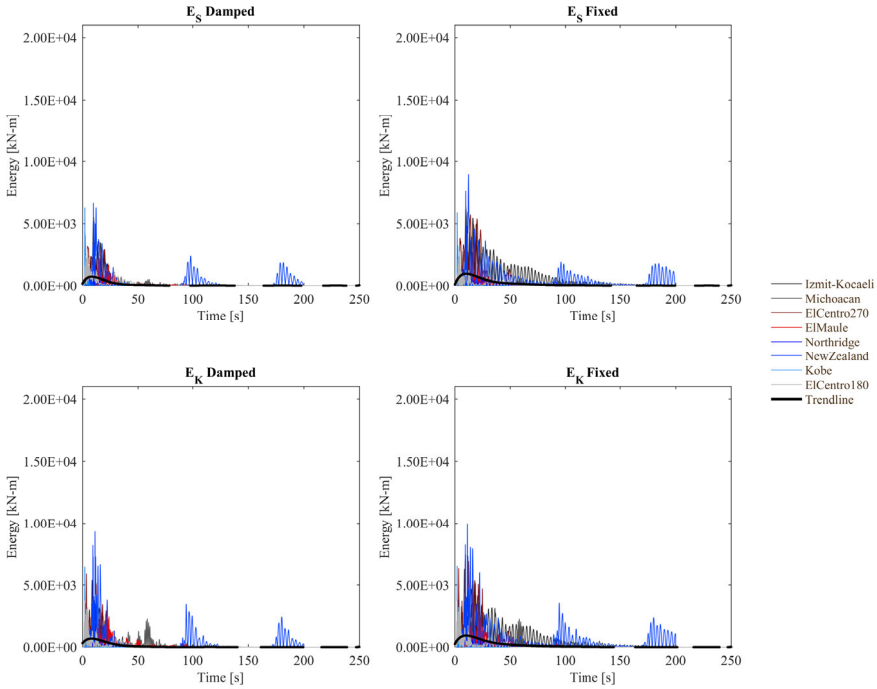

FIGURE 5.15 Strain elastic energy (E_S) and kinetic energy (E_K) of damped and fixed outrigger systems under severe earthquake levels

§ 5.5 Inherent and supplemental damping versus hysteresis energy ratios

§ 5.5.1 Elastic response

The study of the energy ratios within the elastic region (Figure 5.16-Figure 5.17) shows that (a) the ratios, as expected, remain linear if the variation in the ground motion is also linear, and (b) that dampers can effectively reduce the energy dissipated by inherent damping –mostly given by the core

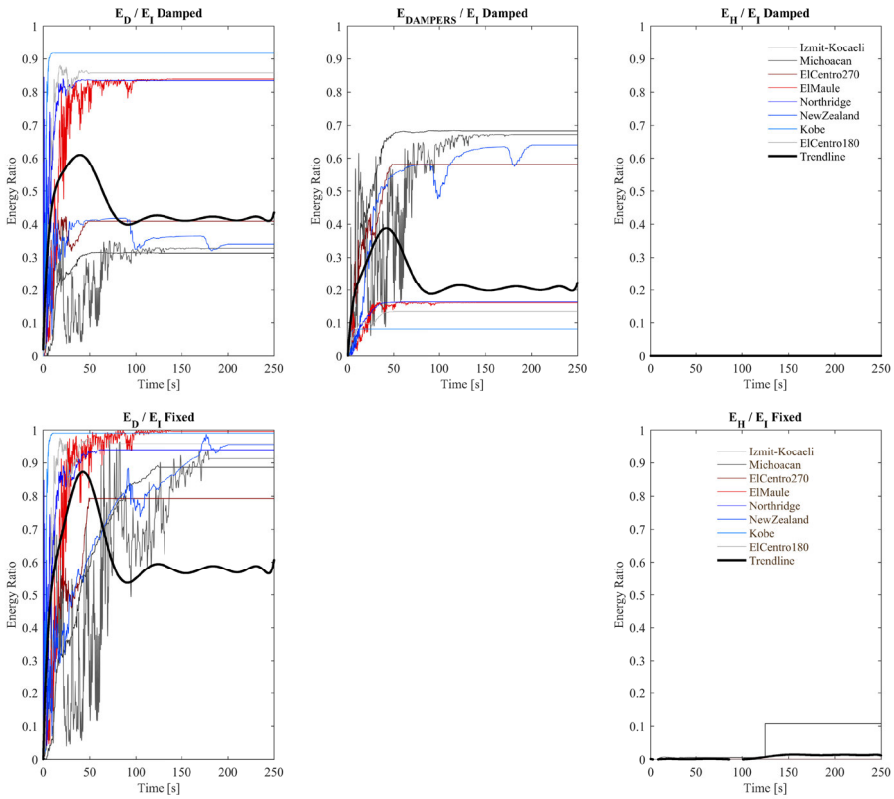

FIGURE 5.16 Energy ratios of the outrigger systems under small earthquake levels

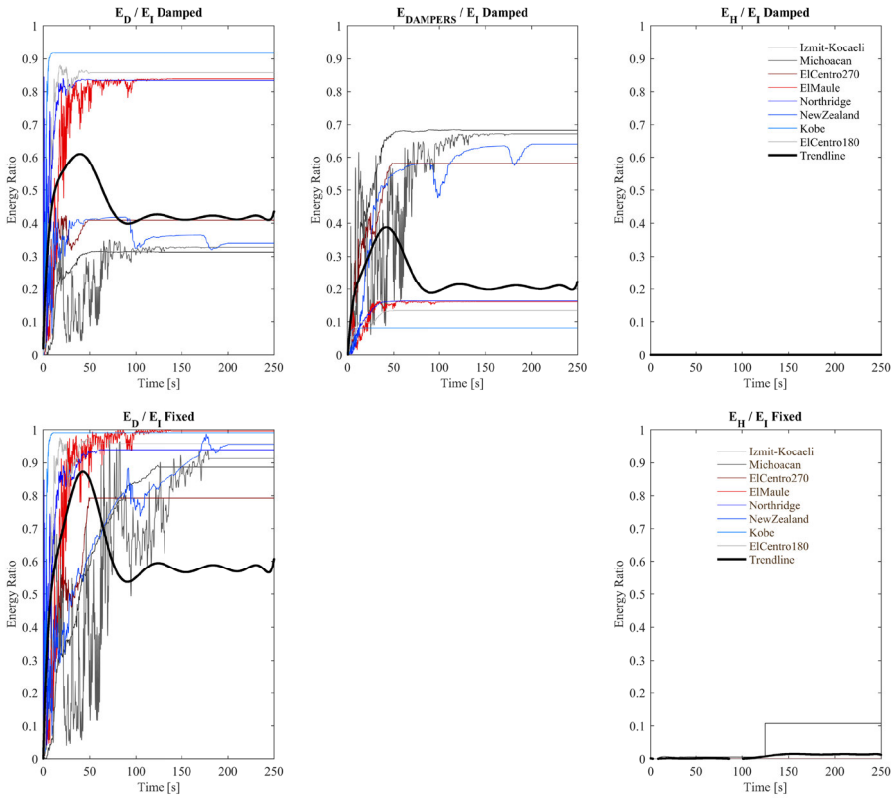

FIGURE 5.17 Energy ratios of the outrigger systems under moderate earthquake levels

§ 5.5.2 Inelastic response

The addition of supplemental damping by using viscous dampers reduces the absorbed energy in the host structure, if compared to a conventional outrigger (Figure 5.18). Since dampers increase the dissipative action of energy by damping, the energy that must be absorbed by hysteresis of the structure is reduced. This does not mean that the addition of viscous dampers directly eliminates energy dissipation by plastic deformations in the structure, but it certainly aids in its reduction (Figure 5.19). Moreover, the fact that only in this case the hysteretic energy is larger than in the fixed case, supports the observation that to avoid damage the optimal design of the damped outrigger must be based on the balanced increase of both E_D/E_I and $E_{dampers}/E_I$ ratios.

Finally, plots also show that the more damage the structure undergoes, the lesser the energy the dampers dissipate.

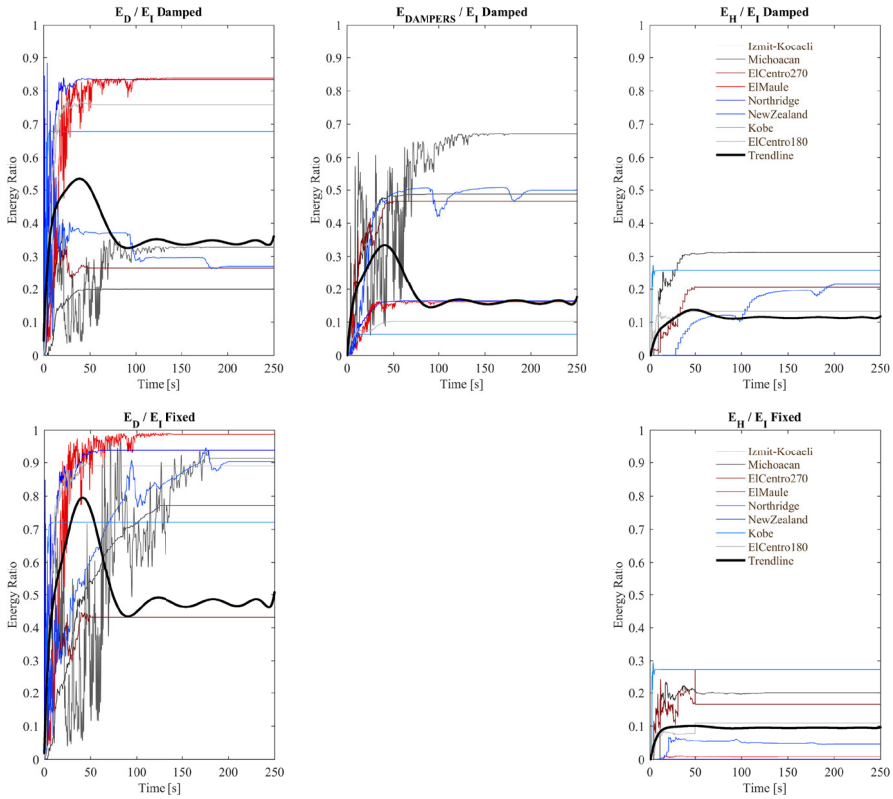

FIGURE 5.18 Energy ratios of the outrigger systems under strong earthquake levels

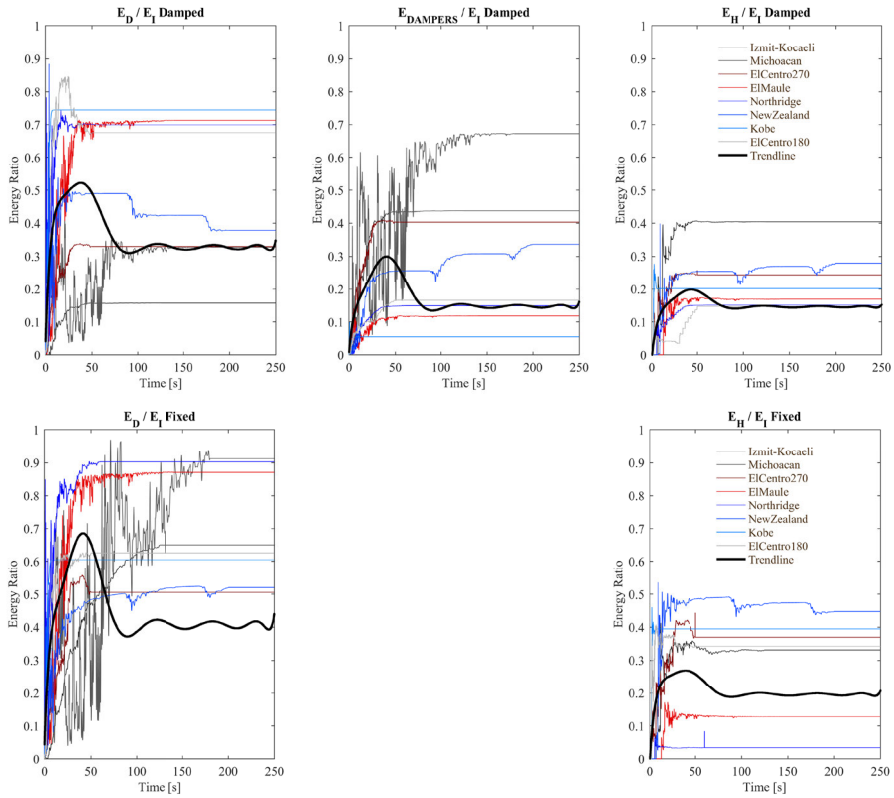

FIGURE 5.19 Energy ratios of the outrigger systems under severe earthquake levels

§ 5.6 Seismic energy distribution per element

The sources of the energy dissipations are vital to understand the role of dampers, core and outriggers in the energy dissipative function. Whereas in the case of the dampers energy, it is linked to the viscosity of the oil dampers, in the case of the damping energy, the distribution needs to be examined more in detail.

§ 5.6.1 Core

Despite of the relatively small decrease in the hysteretic energy displayed in the previous results (Section 5.5.2), the damage in the core –the only source of hysteresis in the cases studied here, is reduced to a half when using viscous dampers instead of fixed outriggers. In Figure 5.20, depicting the damping outrigger performance, it can noted that peak hysteretic energy is about 1E+7 kN-m, at the ground floor, under severe ground motions. The same location, under same conditions but now for the fixed outrigger system (Figure 5.21), displays a peak hysteretic energy of about 1.9E+7 kN-m, i.e. almost twice as larger the previous one. All the damage induced by the different levels of earthquake in the outriggers equipped with dampers is concentrated in the core, provoked by the overpass of the tensile strength, i.e. by yielding of the longitudinal reinforcement. As expected, the plastic region defined between 1st and 6th floor concentrated most of the damage (Figure 5.22).

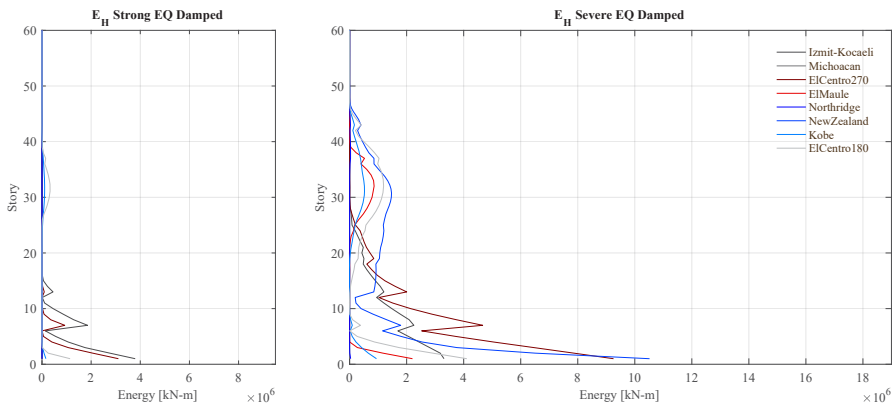

FIGURE 5.20 Distribution of the hysteretic energy dissipated by the core of the damped outrigger

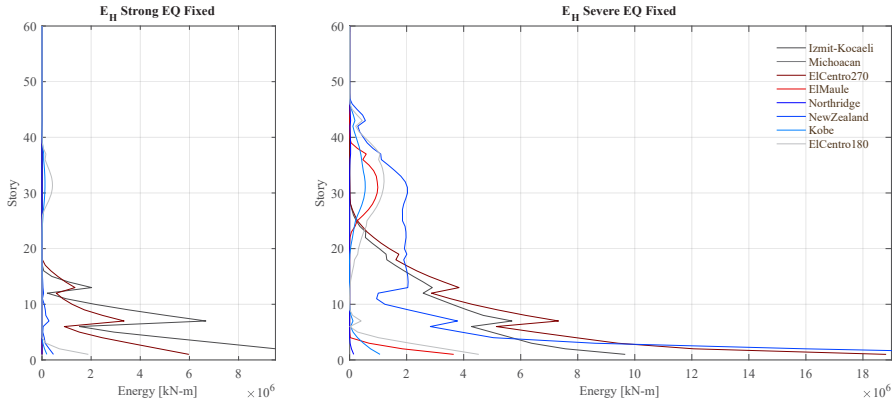

FIGURE 5.21 Distribution of the hysteretic energy dissipated by the core of the fixed outrigger

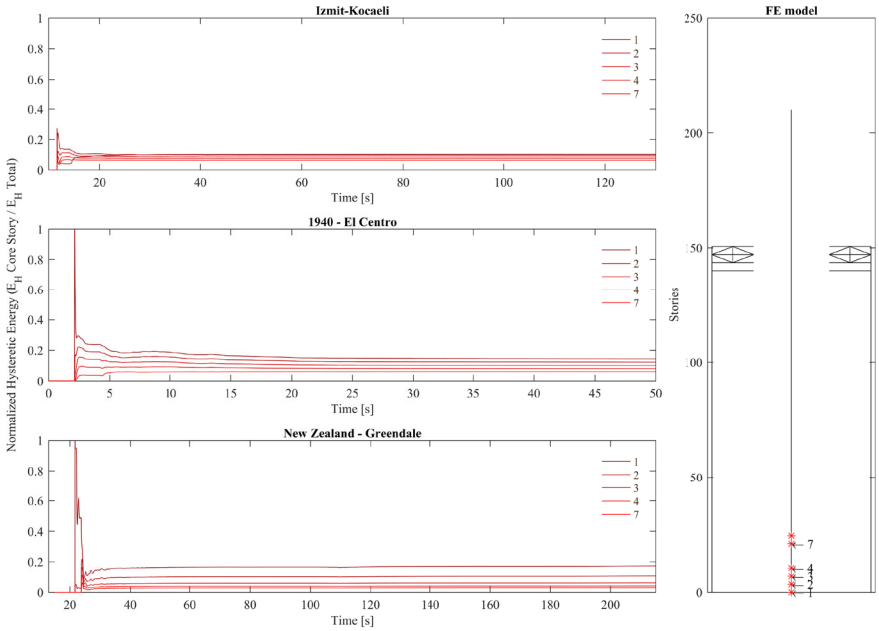

FIGURE 5.22 Normalized hysteretic energy dissipated by the core under severe level of Izmit-Kocaeli, 1940 El Centro, and New Zealand earthquakes. The five core elements displayed dissipated up to 50, 51 and 41% of the total hysteretic energy for each earthquake, respectively. (C_d= 1.18E+05kN-s/m, λ=0.7 and ζ=2.0%)

§ 5.6.2 Outriggers

In Figure 5.23, it can be notice that the contribution of the outrigger to the dissipative function by inherent damping is comparatively small. This fact also explains the lack of hysteresis in the outrigger, during the strong and severe earthquake motion, when all energy dissipated by inelastic deformations occurs at the core elements (Figure 5.24).

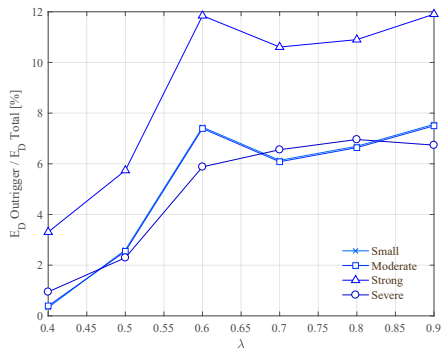

FIGURE 5.23 Damping energy (in %) dissipated only by the outriggers, under the combined influence of **λ** and different earthquake levels of 1940 El Centro earthquake; C_d= 1.18E+05kN-s/m and **ζ**=2.0%.

Under careful observation of the responses under strong earthquake level, it is clear that the addition of dampers will slightly reduce the damping participation ratio of the outrigger, if the average is considered (Figure 5.25). Although this may suggest that outriggers do not dissipate energy as their function is replaced by the viscous dampers, it is more likely that the participation of the outrigger seems to decrease because with the addition of dampers the overall damping ratio would be reduced anyway.

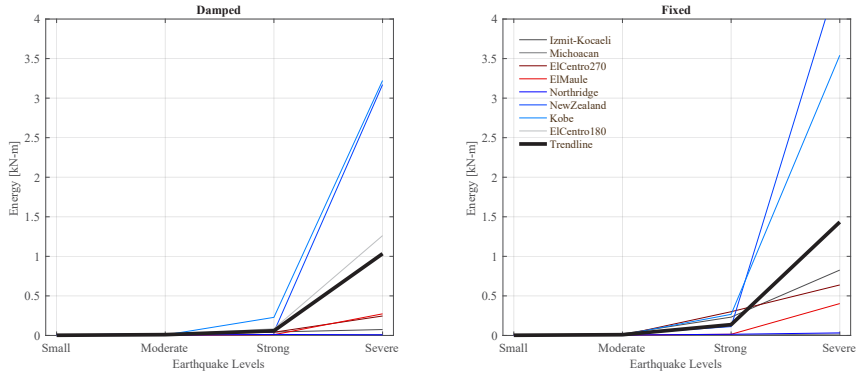

FIGURE 5.24 Damping energy dissipated by the outrigger in the damped (left) and fixed (right) system

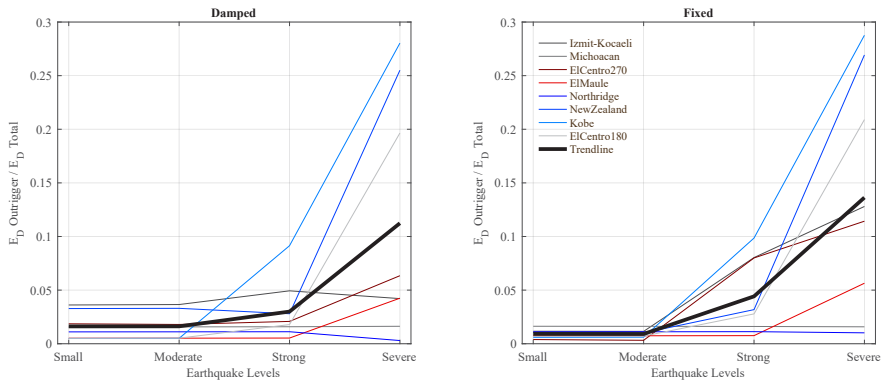

FIGURE 5.25 Percentage of the total damping energy that is dissipated by the outrigger in the damped (left) and fixed (right) system

§ 5.7 Comparative performance fixed – damped outrigger systems

§ 5.7.1 Inter-storey drift

The addition of supplemental damping in the outriggers may not significantly decrease inter-storey drift response as depicted in Figure 5.26, where the differences between fixed and damped responses are not significant.

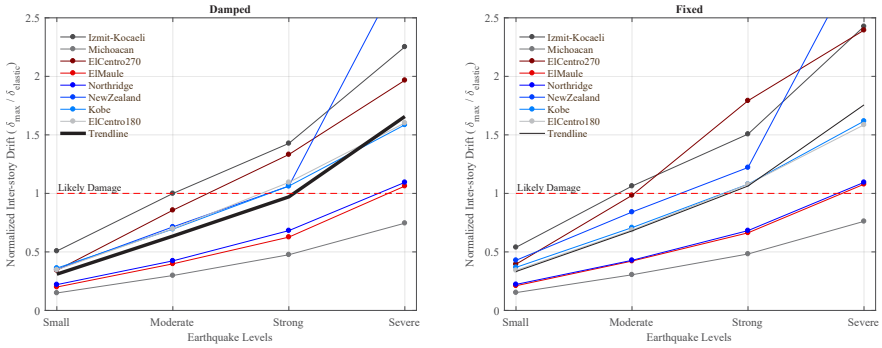

FIGURE 5.26 Normalized peak inter-storey drifts of the studied outrigger configurations

§ 5.7.2 Peak accelerations

Display of the peak accelerations for all levels of the selected suite of ground motions, show that no significant variation can be noted between the damped and fixed outrigger systems (Figure 5.27).

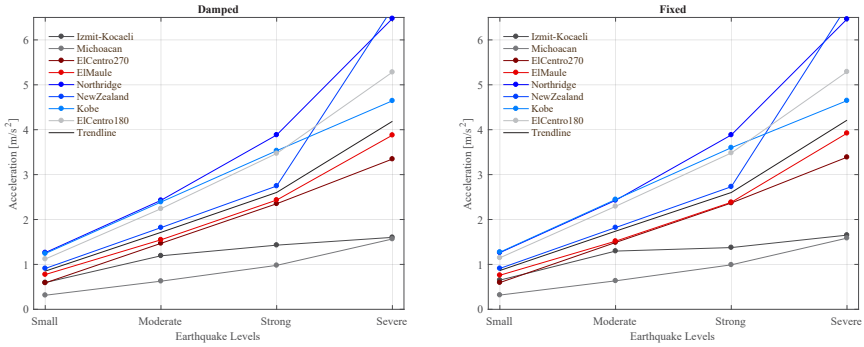

FIGURE 5.27 Peak accelerations of the studied outrigger configurations

§ 5.7.3 Base shear

The base shear plots resulting from the different configurations subjected to all levels of the selected ground motions are displayed in Figure 5.28. Base shear was normalized by the total seismic mass (W) of each configuration. As depicted in Figure 5.28, results display a similar fixed-damped trend. Nevertheless, given the fact that aforementioned plots display the results of optimal outrigger structures, it seems clear that neither inter-storey drifts nor base shear are substantially reduced with the addition of viscous dampers to the outriggers.

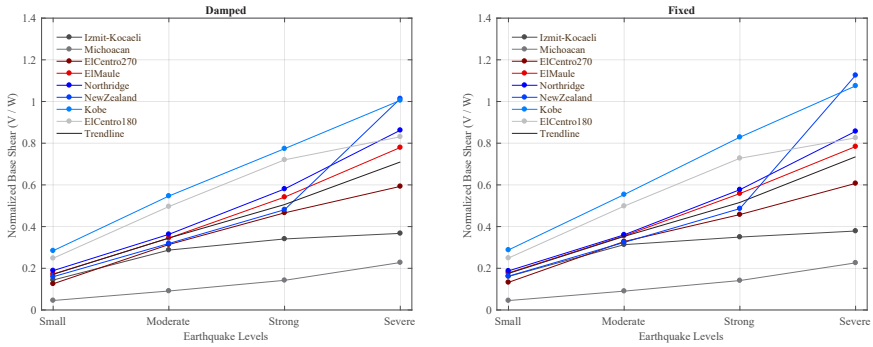

FIGURE 5.28 Normalized base shear (V/W) of the studied outrigger structures subjected to four earthquake levels of all ground motions

§ 5.7.4 Overturning moment versus yielding stress

Although peak overturning moment and stresses might not occur at the same instant during the earthquake motion, plots displaying the relationship between these two peaks were elaborated to study whether the addition of dampers help to reduce the structural response. From the plots displayed in Figure 5.29-Figure 5.32, it is clear that, under optimal design conditions, the addition of viscous dampers reduces both the overturning moment and overall stresses in core, outriggers and perimeter columns. Moreover, by helping to reduce the overall stress, the use of viscous dampers prevents the extension of damage as the ground motion grows larger, if compared with the response of the fixed outrigger.

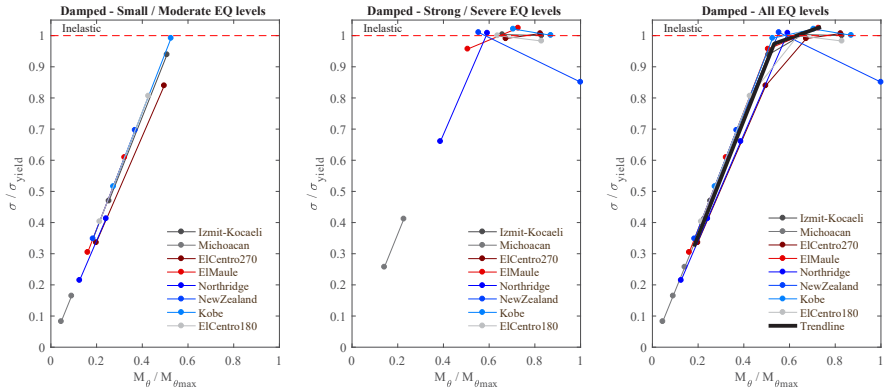

FIGURE 5.29 Normalized *core* stress (σ/σ_{yield}) to normalized overturning moment ($M\theta/M\theta\text{-}_{max}$) of the damped outrigger configurations subjected to four earthquake levels of all ground motions

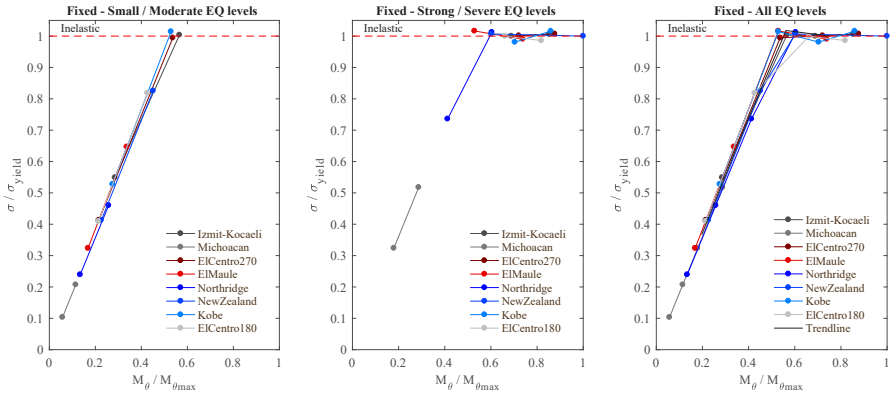

FIGURE 5.30 Normalized *core* stress (σ/σ_{yield}) to normalized overturning moment ($M\theta/M\theta_{max}$) of the fixed outrigger configurations subjected to four earthquake levels of all ground motions

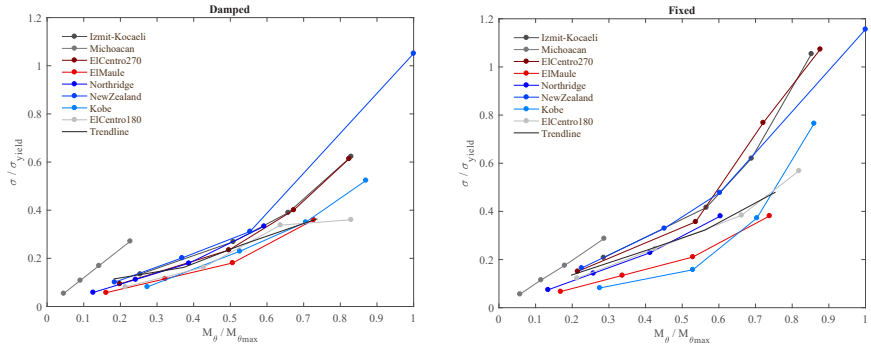

FIGURE 5.31 Normalized *outrigger* stress (σ/σ_{yield}) to normalized overturning moment ($M\theta/M\theta_{max}$) of the studied outrigger configurations subjected to four earthquake levels of all ground motions

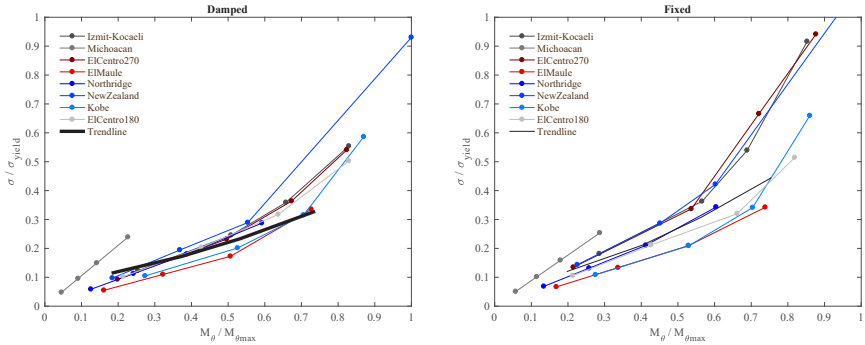

FIGURE 5.32 Normalized *column* stress (σ/σ_{yield}) to normalized overturning moment ($M\theta/M\theta_{-max}$) of the studied outrigger configurations subjected to four earthquake levels of all ground motions.

§ 5.8 Discussion

§ 5.8.1 Distribution of energy in conventional and damped outriggers

The addition of supplemental damping by using viscous dampers reduces the absorbed energy in the host structure, if compared to a conventional outrigger (Table 5.2). Since dampers increase the dissipative action of energy by damping, the energy that must be absorbed by hysteresis of the structure is reduced. This does not mean that the addition of viscous dampers directly eliminates energy dissipation by plastic deformations in the structure, but it certainly aids in its reduction (Figure 5.33). This later conclusion is in agreement with Zhou and Li (2013), who developed an experimental investigation using a 7.2m mock-up of a high-rise steel column-tube structure equipped with two sets of outrigger attached at roof and middle height, respectively. They concluded that the negative effect of the abrupt change of stiffness between fixed outrigger storeys and adjacent storeys in the inter-storey drifts is decreased due to the lower stiffness of the damped outrigger.

		E_I	E_D	E_H	$E_{dampers}$	E_S	E_K
small	damped	2.53E+02	1.56E+02	0	9.19E+01	2.76E+01	3.01E+01
	fixed	2.46E+02	2.20E+02	0	0	4.36E+01	4.45E+01
moderate	damped	9.98E+02	6.12E+02	0	3.66E+02	1.10E+02	1.20E+02
	fixed	9.70E+02	8.65E+02	2.38E+01	0	1.74E+02	1.78E+02
strong	damped	3.14E+03	1.54E+03	6.10E+02	9.01E+02	2.65E+02	2.86E+02
	fixed	3.11E+03	2.13E+03	5.98E+02	0	4.02E+02	4.13E+02
severe	damped	7.45E+03	3.92E+03	1.74E+03	1.72E+03	6.92E+02	6.58E+02
	fixed	7.83E+03	5.00E+03	2.68E+03	0	9.55E+02	9.25E+02

TABLE 5.2 Distribution of seismic energy [kN-m] in the studied outrigger configurations

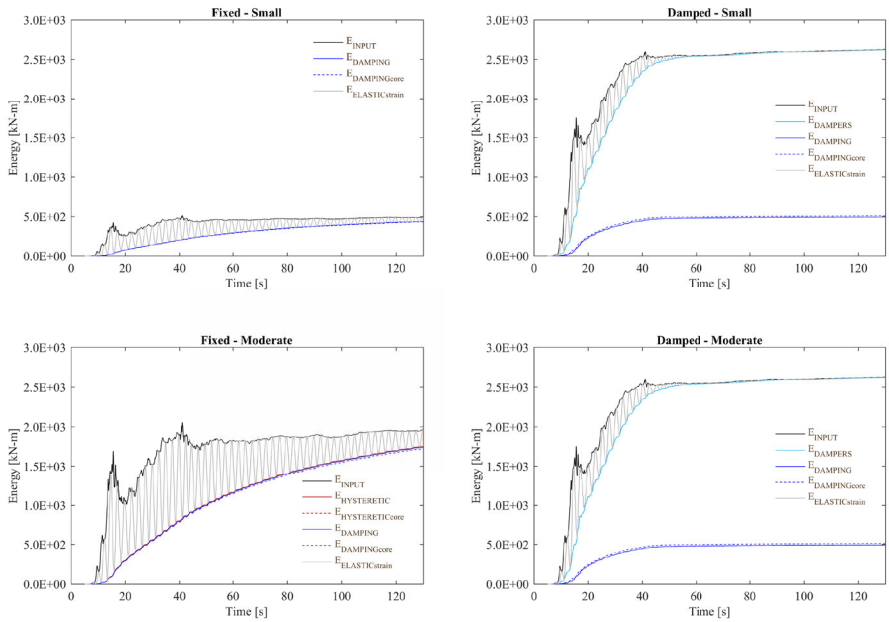

FIGURE 5.33 Energy distribution of the fixed and 1.18E+05kN-s/m damped outrigger structures under small and moderate levels of Izmit-Kocaeli earthquake (λ=0.7 and ζ=2.0%).

By only considering the distribution of damping energy between core and outrigger (columns were not considered as discussed previously), and plotting only the portion taken by the outriggers, it can be noted the increasing role of the outrigger in the dissipation of energy as the ground motion becomes stronger (Figure 5.34). Moreover, the fact that only in this case the hysteretic energy is larger than in the fixed case, supports the observation that to avoid damage the optimal design of the damped outrigger must be based on the balanced increase of both E_D/E_I and $E_{dampers}/E_I$ ratios.

Finally, plots also show that the more damage the structure undergoes, the lesser the energy the dampers dissipate.

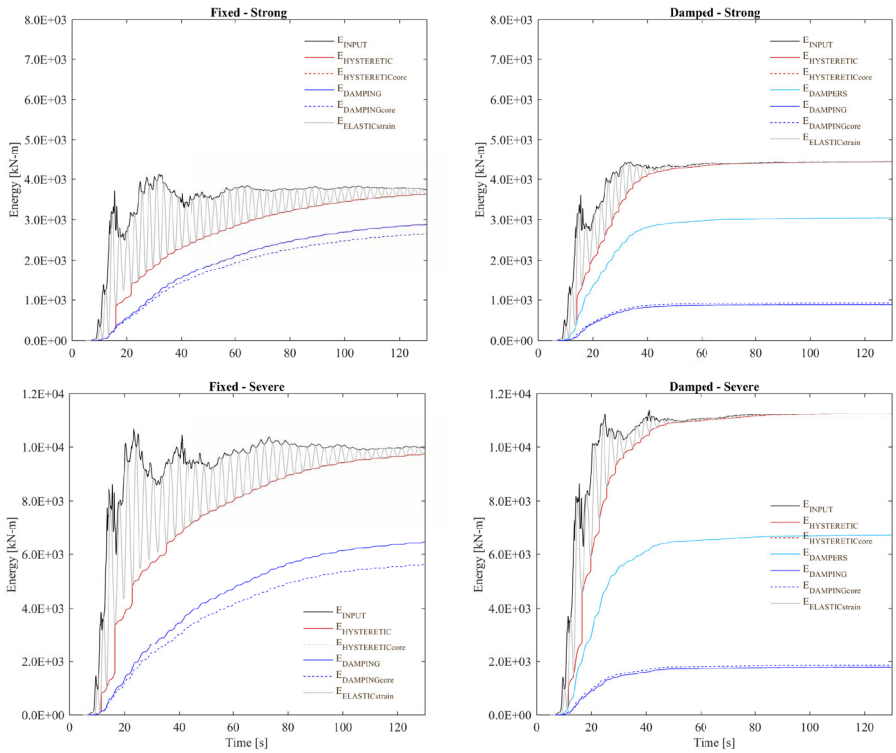

FIGURE 5.34 Energy distribution of the fixed and 1.18E+05kN-s/m damped outrigger structures under strong and severe levels of Izmit-Kocaeli earthquake (λ=0.7 and ζ=2.0%).

§ 5.8.2 Distribution of energy under strong earthquakes

When subjected to strong ground motion, the building was modelled to undergo damage so the mechanisms of dissipating energy by hysteresis of its elements can be assessed. The appearance of plastic hinges in the structure seems to be inevitable under these types of earthquakes because as it is with the structural damping itself, the dissipation of energy by dampers increases over time. Hence the maximum level of energy dissipation provided by dampers tends to occur towards the end of the motion,

whereas kinetic energy (thus large demands over the structural flexural behaviour) occurs at the beginning of the strong motion. Assuming that parameters λ, ρ_{cto} and ρ_{ctc} are defined to deliver a design performing within the optimal threshold –in terms of energy-based performance, by the end of a given earthquake motion is expected that inherent structural damping and supplemental damping energies are balanced.

In the specific case of the time-history energy ratios depicted in Figure 5.35-left, the elastic response of the damped outrigger shows that during half of the motion, both damping and dampers were equally dissipating seismic energy with an increase of the dampers energy towards the end. Whereas this information is useful to determine how much energy the dampers are dissipating, it does not give any information of how such energy is distributed during the first moments of the strong motions, which is when usually the structural damage tend to be produced. A second energy ratio, based on the summation of damping, dampers and hysteretic energies, is then proposed to give information about these initial distributions. In Figure 5.35-right, the same previously described time-history is depicted in terms of this relative energy ratio. Here, it can be seen the formation of 'crosses' between the energy plots showing that during the motion, the energy is not constantly dissipating by one mechanism, but it alternates between damping and dampers. Perhaps not surprisingly, these crosses seem to be also related to the incursion of the structure in nonlinear behaviour, i.e. with the dissipation of energy by hysteresis (Figure 5.36). These results suggest that an adequate balance between the E_D/E_I and $E_{dampers}/E_I$ ratios is required to avoid plastic incursions of the structural elements during the strong motion (Table 5.3). If the dampers dissipate the energy at expense of decreasing the inherent structural damping, the excessive stress occurring in the core and outrigger will provoke damage anyway.

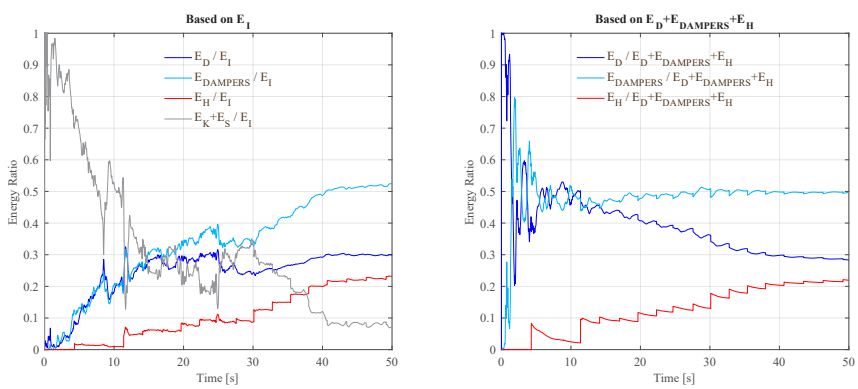

FIGURE 5.35 Energy ratios based on E_I and $E_D+E_{dampers}+E_H$, for the damped outrigger under strong earthquake level of 1940 El Centro earthquake; C_d= 1.18E+05kN-s/m, λ=0.7 and ζ=2.0%.

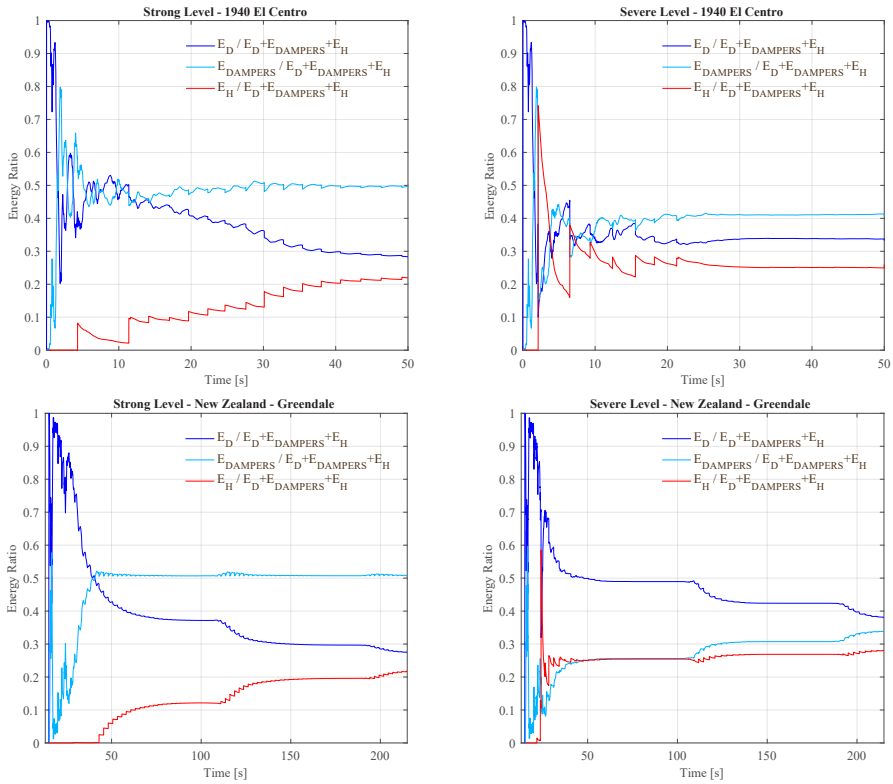

FIGURE 5.36 Energy Ratios of the damped outrigger (C_d= 1.18E+05kN-s/m, λ=0.7 and ζ=2.0%), under strong and severe levels of 1940 El Centro and New Zealand – Greendale earthquakes

		E_D/E_I	$E_{dampers}/E_I$	E_H/E_I
small	damped	0.44	0.22	-
	fixed	0.61	-	-
moderate	damped	0.44	0.22	-
	fixed	0.61	-	0.01
strong	damped	0.36	0.18	0.12
	fixed	0.51	-	0.10
severe	damped	0.35	0.16	0.15
	fixed	0.44	-	0.20

TABLE 5.3 Energy Ratios of the damped and fixed outrigger systems

Hence, the core is the main dissipative source of both damping and hysteretic energy. With the addition of viscous dampers the outrigger has a minor load-bearing role, so plastic hinges concentrate on the lower zone of the core due to the action of bending and certainly the contribution of 2nd order effects (such as P-Δ). If, for example, due to ductility demands plastic hinges need to be concentrated in the outrigger, its general sections can be reduced provided that the dampers will account for the extra flexibility of the outrigger structure. The main advantage of adding viscous dampers to the outriggers is the overall reduction of stress in the members, thus increasing ductility in the structure. This leads to the conclusion that achieving elastic response under strong earthquake motions by the use of viscous dampers also requires an increase of the overall strength of the host structure. A possible solution to avoid damaging the core when employing dampers with lower damping coefficient is to increase the thickness of the core walls towards the base of the building. This common practice in the design of tall buildings' core not only avoids plasticity of the lower regions of the shear walls but also increases its flexural ductility (Willford and Smith, 2008).

§ 5.8.3 Hysteretic energy and frequency content of the ground motions

In order to explore possible links between the hysteretic behaviour of the outrigger systems and the characteristics of the ground motions, the plots of both critical acceleration and input energy are sorted according the level of damage, as measured by the E_H/E_I ratio (Table 5.4). The ground acceleration is considered critical when it provokes damage in the structure. The input energy was computed for a SDOF with mass=1 ton, and ζ=2% only for illustration purposes.

Under Izmit-Kocaeli, ElMaule and Northridge, the use of viscous dampers attached to the outrigger increased the damage. This seems to be the result of the decrease in the first period of the fixed outrigger after the addition of viscous dampers (from 5.10 to 4.99 s). However, no correlation can be observed between the amount of input energy at the first mode and the level of damage that the structure experiences under a specific ground motion. For example, if the energy plots of Kobe and ElCentro270 are observed, it can be noted that their energy input at the first mode period are 0.2 and 1.2 approximately. If the level of damage would be correlated with this mode, their level of damage (E_H/E_I) would express similar tendency. The hysteretic ratios are fairly similar, though (0.20 to 0.23). Moreover, Michoacan earthquake has an energy input at the first mode of about 0.6, hence larger than Kobe; unlikely, under Michoacan earthquake the structure did not present any nonlinearity.

A feasible explanation to these apparent inconsistencies is that the hysteresis behaviour is dominated by the second mode. Although both the second and third mode remains almost the same between fixed and damped (0.85 to 0.82 and 0.29 to 0.30, respectively), small variations in the period can affect largely the input energy, due to the steepness of the plot. This hypothesis helps to explain the relative large structural damage under Kobe and El Centro180, but it raises questions on the reasons for the low damage under El Maule earthquake. A more comprehensible explanation comes from the outrigger location, which is in the optimal position to control the predominance of first mode responses. Since there is no second outrigger to control other modal responses, in some cases, these higher modes have a larger influence.

EQ (STRONG/ SEVERE)	GROUND ACCELERATION	CORRESPONDING SDOF INPUT ENERGY	FEM	STRONG		SEVERE	
				Peak$_t$ [sec]	E_H/E_I	Peak$_t$ [sec]	E_H/E_I
Izmit-Kocaeli (strong)	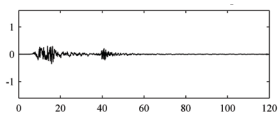	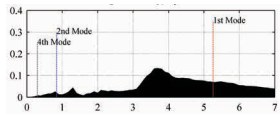	F	7.3	0.18	6.6	0.31
			D	9.2	0.31	6.6	0.40
Kobe (strong)	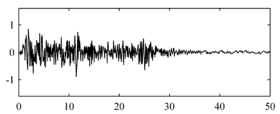	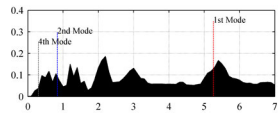	F	2.1	0.24	2.0	0.39
			D	2.1	0.23	2.0	0.20
ElCentro270 (strong)	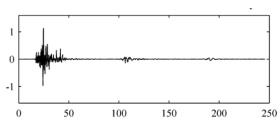	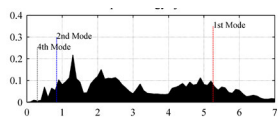	F	4.3	0.27	2.1	0.36
			D	4.3	0.21	2.1	0.23
ElCentro180 (strong)	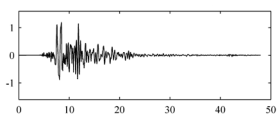	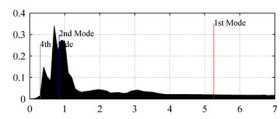	F	2.4	0.10	2.2	0.34
			D	2.4	0.13	2.2	0.15
NewZealand (strong)	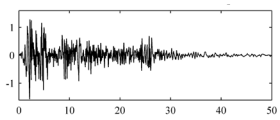	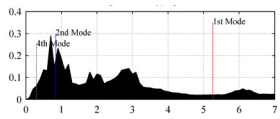	F	11.9	0.05	8.9	0.21
			D	14.0	0.21	9.3	0.18
ElMaule (severe)	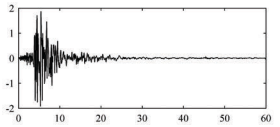	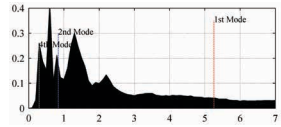	F	14.9	0.01	12.7	0.13
			D	0.0	0.00	12.7	0.17
Northridge (severe)	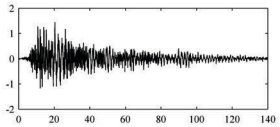	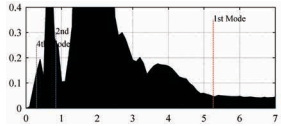	F	0.0	0.00	5.3	0.06
			D	0.0	0.00	5.3	0.13
Michoacan (severe)	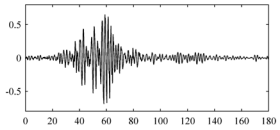	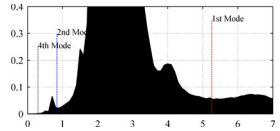	F	0.0	0.00	0.0	0.00
			D	0.0	0.00	0.0	0.00

TABLE 5.4 Ground motions organized from most to less damaging and their corresponding hysteretic and input energies. F and D are fixed and damped outrigger systems, respectively.

§ 5.8.4 Comparative performance between fixed and damped outriggers

As previously discussed, the addition of supplemental damping in the outriggers may not significantly decrease the building response in terms of peak responses. This is the case for the normalized inter-storey drifts as well as the accelerations as the differences between fixed and damped responses are not significant. In the case of the base shear, results display a similar fixed-damped trend. These results suggest that neither accelerations, inter-storey drifts nor base shear are substantially reduced with the addition of viscous dampers to the outriggers. On the other hand, according to the study described herein, it is clear that under optimal design conditions, the addition of viscous dampers reduces both the overturning moment and overall stresses in core, outriggers and perimeter columns. Moreover, by helping to reduce the overall stress, the use of viscous dampers prevents the extension of damage as the ground motion grows larger, if compared with the response of the fixed outrigger. Finally, all the damage induced by the different levels of earthquake in the outriggers equipped with dampers is concentrated in the core, provoked by the overpass of the tensile strength, i.e. by yielding of the longitudinal reinforcement. In the case of damage in the outrigger, the compressive strength was overpassed producing buckling in some of the braces and/or chords (Table 5.5).

	DAMPED	FIXED
small	2%	1%
moderate	2%	1%
strong	3%	4%
severe	8%	12%

TABLE 5.5 % of damping energy absorbed by the outrigger in the studied configurations

§ 5.9 Conclusions

Although most of the conclusions obtained are only applicable to the specific cases described in this paper, general observations can be derived from the numerical studies presented herein, as follows:

- Generally, as the ground motion becomes stronger, viscous dampers effectively reduce the potential of damage in the structure if compared to conventional outriggers. Under some earthquakes, nevertheless, viscous dampers can increase the damage potential.
- The results of this study suggest that neither inter-storey drifts, peak accelerations nor base shear are substantially reduced with the addition of viscous dampers to the outriggers.
- The addition of viscous dampers to the outriggers, under optimal design conditions, reduce the overturning moments and stresses of the main components of the system, i.e. core, outriggers and perimeter columns, under strong earthquakes –if compared to a conventional outrigger.
- Dampers cannot, however, reduce completely the damage under critical earthquakes because the peak E_H/E_I usually precedes the peak $E_{dampers}/E_I$.
- Hysteretic energy is concentrated in the core, whose damage is provoked by the overpass of the tensile strength.
- It can be assumed that viscous damper outrigger structures exhibit a comparatively improved performance if subjected to long-period ground motions. Nevertheless, this preliminary conclusion must be further investigated by extending the analyses under an extended set of ground motion records.

References

Asai, T., Chang, C.-M., Phillips, B. M. and Spencer Jr, B. F. 2013. Real-time hybrid simulation of a smart outrigger damping system for high-rise buildings. Engineering Structures. 57: 177-188. http://dx.doi.org/10.1016/j.engstruct.2013.09.016

Bojórquez, E., Reyes-Salazar, A., Terán-Gilmore, A. and Ruiz, S. 2010. Energy-based damage index for steel structures. Steel and Composite Structures. 10: 331-348.

Bruneau, M. and Wang, N. 1996. Some aspects of energy methods for the inelastic seismic response of ductile SDOF structures. Engineering Structures. 18: 1-12. http://dx.doi.org/10.1016/0141-0296(95)00099-X

Chang, C.-M., Wang, Z., Spencer Jr, B. F. and Chen, Z. 2013. Semi-active damped outriggers for seismic protection of high-rise buildings. Smart Structures and Systems. 11: 435-451.

Chopra, A. K. 2007. Dynamics of structures: theory and applications to earthquake engineering. Prentice-Hall:

Khashaee, P., Mohraz, B., Sadek, F., Lew, H. and Gross, J. L. 2003. Distribution of earthquake input energy in structures. U.S. Department of Commerce

Smith, R. 2016. The Damped Outrigger-Design and Implementation. International Journal of High-Rise Buildings. 5: 63-70.

Uang, C.-M. and Bertero, V. V. 1990. Evaluation of seismic energy in structures. Earthquake Engineering & Structural Dynamics. 19: 77-90. 10.1002/eqe.4290190108

Willford, M. and Smith, R. 2008. Performance based seismic and wind engineering for 60 story twin towers in Manila

Zhou, Y. and Li, H. 2013. Analysis of a high-rise steel structure with viscous damped outriggers. The Structural Design of Tall and Special Buildings. 23: 963-979. 10.1002/tal.1098

6 Energy dissipation and performance assessment of double damped outriggers in tall buildings under strong earthquakes

§ 6.1 Summary

The use of a set of outriggers equipped with oil viscous dampers increases the damping ratio of tall buildings in about 6-10%, depending on the loading conditions. However, if a single damped outrigger structure is designed for an optimal damping ratio, could this ratio still be increased by the addition of another set of outriggers? Should this additional set be equipped with dampers too? In order to answer these questions, several double damped outrigger configurations for tall buildings are investigated and compared to an optimally designed single damped outrigger, located at elevation 0.7 of the total building's height (h). Using free vibration analyses, double outrigger configurations increasing damping up to a ratio equal to the single-based optimal are identified. Next, selected configurations are subjected to small, moderate, strong, and severe earthquake levels of eight ground motions to compare their capability for dissipating energy and thus avoiding damage under critical excitations. Last, a simplified economic analysis highlights the advantages of each optimal configuration in terms of steel reinforcement savings versus damper cost. The results show that combining a damped outrigger at 0.5 h with a conventional outrigger at 0.7 h is more effective in reducing hysteretic energy ratios and economically viable if compared to a single damped outrigger solution.

Chapter 6 is based on the paper 'Energy distributions and performance assessment of double damped outriggers in tall buildings under strong earthquakes', submitted to *The Structural Design of Tall and Special Buildings*.

§ 6.2 Introduction

Since the previous chapters showed that the energy dissipation capacity of a single set of outrigger will not prevent damage under strong earthquakes, this chapter provides an analytical framework to comparatively assess the distribution of seismic energy in tall buildings equipped with double viscous damped outriggers, i.e. with two sets of outriggers having viscous dampers installed between their ends and the perimeter columns. By mean of a numerical study, in Chapter 5 we concluded that the use of a single set of outriggers equipped with oil viscous dampers increases the damping ratio of tall buildings subjected to strong ground motion, in the order of 8%. However, if a single damped outrigger structure is designed to reach an optimal damping ratio, could this damping ratio still be increased by the addition of another set of outriggers? Should this additional set of outriggers be equipped with dampers too? In order to investigate the benefit of an extra set of damped outriggers, a comparative study is presented, wherein several double set of outrigger configurations for tall buildings are investigated and compared to an optimally designed single damped outrigger, located at elevation 0.7 of the total building's height (h). First, using free vibration analyses, those double outrigger configurations increasing damping up to a ratio equal or larger than that of the optimal single outrigger, are identified. Second, all these hereafter optimal configurations are subjected to small, moderate, strong, and severe earthquake levels of eight ground motions to critically compare the capability of such configurations for dissipating seismic energy and thus avoiding extended damage under critical excitations.

Finally, since practice has shown that with the addition of supplemental damping construction costs are reduced (Willford and Smith, 2008), a simplified economic analysis is applied to investigate possible advantages of each optimal configuration in terms of steel reinforcement savings versus damper cost, as a consequence of the reduction in overturning moment and base shear. The results show that combining a damped outrigger at 0.5 h with a conventional outrigger at 0.7 h is both more effective in reduce hysteretic energy ratios under strong earthquakes and economically viable if compared to a single damped outrigger solution.

§ 6.3 Methodology

§ 6.3.1 Analytical models

The analytical models used in this study are based on the model described in Chapter 5, to which a new set of outriggers was attached (see Parametric FE model of the double outrigger structures). The 2D models described here consider only two and four outriggers per side, each pair modelled as a single 7 meters-height outrigger, as displayed in Figure *6.1*. In the models, both building plan and distribution of resistant elements are symmetrical so the lateral stiffness in two orthogonal directions is assumed equal. Nodal masses were added to account for the load of secondary structural components, such as slabs and steel frames. The core is an 18m x 18m reinforced concrete tube, with a constant thickness of 0.75m. The FE model of the core is modelled as a Bernoulli-Euler cantilever beam type, i.e. dominated by bending deformation. The area of the reinforced concrete perimeter columns is 1.30 m^2.

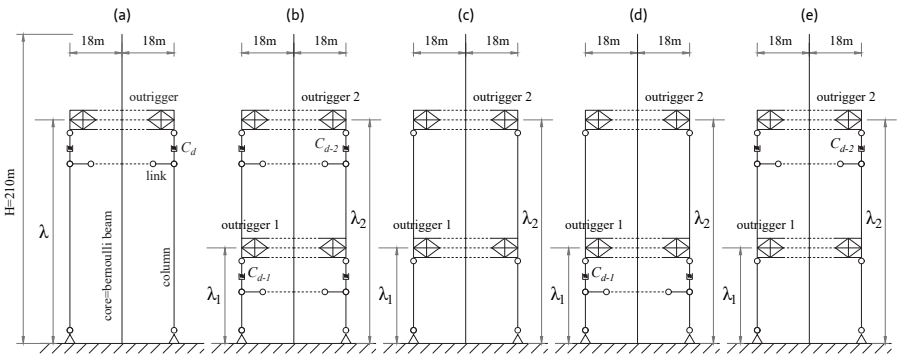

FIGURE 6.1 Analytical outrigger building models: (a) single damped; (b) double damped; (c) double fixed; (d) combined damped and fixed; and, (e) combined fixed and damped.

The total strain crack model is used to define the nonlinear behaviour of the concrete, based on a bi-linear stress-strain relationship as defined in Eurocode 2 (1992-1-1, 2004). Both the influence of the lateral confinement and the lateral influence of cracking in the reduction of strength after cracking are considered. The reduction of the Poisson effect after cracking is also considered since such effect ceases to exist when

the material cracks. Maximum longitudinal reinforcement was provided only over the lower section of the building (six floors) and decreased towards the upper levels. This distribution was defined following the capacity flexural strength design envelope as proposed by Boivin and Paultre (2012), with a minimum reinforcement ratio = 0.25% (Applied Technology Council, 2010). In the case of steel, the plasticity model of Von Mises and an ideal elasto-plastic model are considered for its constitutive behaviour, i.e. strain hardening effect is not taken into account. This is considered as a post-yield reserve of ductility. Properties of the steel are derived from Eurocode 3 (1993-1-1, 2004).

§ 6.3.2 Optimal increase of inherent damping ratio (ζ) through free vibration analyses

In order to set a valid comparative framework, all models present configurations that are optimal from the perspective of increasing the inherent damping ratio (ζ) of the bare structure, i.e. 2%. Sensitivity analyses were conducted on several configurations where both outrigger locations (λ) and dampers' damping coefficient (C_d) were systematically modified in order to obtain significant increases of ζ. A logarithmic decrement technique, under free vibration, was used to determine such optimal ζ.

For simplicity, λ is defined as multiplicand of the total height H, ranging between 0.1 and 1.0 at intervals of 0.1. The variation of C_d, nonetheless, is less straightforward and requires performing sensitivity analyses before defining a range of feasible values. For example, in the case of a single damped outrigger, values smaller than 1.5E+03kN-s/m have no influence and the building behaves as a cantilever beam, i.e. without the contribution of the outriggers; values larger than 1.5E+06kN-s/m dynamically stiffen the damper and the building behaves similarly to one equipped with fixed (or *undamped*) outriggers. Whilst the optimal value for a single damped outrigger is about 1.2E+05kN-s/m, the variation in the response does not linearly follow the variation at regular intervals, departing from this optimal C_d. It was found that a range between 2.4E+04 and 6.72E+5, using intervals of 7.2E+04kN-s/m produces substantial variations in the building's response without incrementing the number of computational simulations. Evidently, this range is the same for all the studied models.

§ 6.3.3 Energy balance equations

The equation governing the dynamic response of a multi-degree of freedom (MDOF), such as a tall building, can be expressed in terms of the relative energy balance equation as follows

$$\int_0^t \dot{x}^T M\ddot{x}dt + \int_0^t \dot{x}^T C\dot{x}dt + \int_0^t \dot{x}^T \Lambda C_d \dot{x}_d{}^{\kappa}\ d + \int_0^t \dot{x}^T Kxdt = -\int_0^t \dot{x}^T M\Gamma\ddot{x}_g dt \tag{6.1}$$

where M and K are the diagonal lumped mass and stiffness matrices, respectively; C is the damping matrix computed considering Rayleigh damping; x is the column vector of relative displacements of the node mass with respect to ground; $\ddot{x}_g$ is the one-dimensional ground acceleration; Γ is coefficient vector for ground accelerations; Λ is the location matrix of the dampers –associated to the outrigger location λ, C_d is the damping coefficient of the viscous dampers, $\dot{x}_d$ is the velocity across the damper and κ is the exponent value that controls the linear/nonlinear behaviour of the damper. In this case, $\kappa = 1$.

All terms in Eq. 6.1 can be written separately as

$$E_K = \int_0^t \dot{x}^T M\ddot{x}\ dt = \frac{1}{2}\dot{x}^T M\dot{x} \quad ; \quad E_D = \int_0^t \dot{x}^T C\dot{x}\ dt \quad ; \quad E_{dampers} = \int_0^t \dot{x}^T \Lambda C_d \dot{x}_d{}^{\kappa}\ dt$$
$$E_A = \int_0^t \dot{x}^T Kx\ dt \quad ; \quad E_I = -\int_0^t \dot{x}^T M\Gamma\ddot{x}_g\ dt \tag{6.2}$$

where E_K, E_D, $E_{dampers}$, E_A, E_I are the kinetic, (inherent) damping, dampers (supplemental damping), absorbed and input energy, respectively. Moreover, since the structure absorbs energy by a combination of elastic and inelastic mechanisms, E_A can also be defined as

$$E_A = E_S + E_H \quad ; \quad E_S = \frac{1}{2}\dot{x}^T Kx \quad ; \quad E_H = \int f_s(x - x_{yield})\ dx + \int M_b(\theta - \theta_{yield})\ d\theta \tag{6.3}$$

where E_S and E_H are the elastic strain and hysteretic energy, respectively; f_s is the restoring force, M_b is the bending moment, and θ is the associated angle of rotation. Due to the assumption of a Bernoulli beam in the modelling of the core and the outrigger frame, stresses and strains derived from shear forces are not considered in the derivation of E_H.

Finally, replacing Eq. 6.2-6.3 in Eq. 6.1, the energy balance equation for a MDOF system is given by

$$E_K + E_D + E_{dampers} + E_S + E_H = E_I \tag{6.4}$$

§ 6.3.4 Assessment of the distribution of seismic energy in a tall building

According to Eq. 6.4, the distribution of seismic energy is based on the demand of total input energy – E_I, using relative coordinates since internal forces within a structure are frequently computed using relative displacements and velocities. Nonetheless, kinetic and elastic strain energies tend to zero at the end of the vibration, whilst its maximum values take place at the beginning of the earthquake motion. Hence, they are not affected by the duration of strong motion (Khashaee *et al.*, 2003) and it is valid to assume that, by the end of the motion, E_I is mostly defined by the combined effect of damping energies (E_D + $E_{dampers}$) and hysteretic energy (E_H) dissipation. On the other hand, maximum damping and hysteretic energies show the energy dissipation capacity which can be used to enhance the design and limit the structural damage. Therefore, insights on how these energies are related may be more significant for the assessment of the seismic energy distribution in the damped outriggers, than spotting single-based performances. These relationships can be expressed by (a) the ratio of hysteretic-to-input energy, defined as the hysteresis energy ratio E_H/E_I; (b) the ratio of damping-to-input energy, defined as the inherent viscous damping energy ratio E_D/E_I; and (c) the ratio of dampers-to-input energy, defined as the supplemental damping ratio $E_{dampers}/E_I$. Whereas $E_H/E_I = 1$ implies that the total change in input energy is dissipated by extended damage and/or failure of the structure, a value of zero implies no structural damage (Bojórquez *et al.*, 2010). Furthermore, $E_H/E_I = 0$ implies elastic behaviour in all the elements of the structure, during the entire ground motion. Since this latter case is highly unlikely under strong and severe earthquake levels, the purpose of the following studies is to determine which outrigger configurations extend the threshold where energy dissipation due to hysteresis can be fully replaced by energy dissipated through the action of viscous dampers.

§ 6.3.5 Earthquake Levels

Eight earthquake records were used in the analysis. These records were scaled down/up based on peak-ground-velocity (PGV) rather than on peak-ground-acceleration (PGA). This is because a velocity-based assessment framework is considered to be more meaningful for structures whose expected improved performance relies on the addition of velocity-dependent devices. The elastic threshold was set at velocity amplitudes around 0.9 m/s. Ground velocity amplitudes up to 0.5, 1.0, 1.5 m/s and beyond, were classified as small, moderate, strong and severe earthquakes, respectively (Table 6.1). Strong levels of five ground motions that induced damage in the structures are displayed in Figure 6.2; there, alongside the plot of the accelerations, the input energy spectrum relative to each ground motion is also displayed. These spectra allow a comparison among the levels of input energy that is introduced to a single degree of freedom system, with mass = 1kN, inherent damping ratio (ζ) = 2%, fundamental period T ranging between 0.1 and 7 s, and subjected to different ground motions. Severe levels of the remaining three ground motions are displayed in Figure 6.3 and Figure 6.4. The damage threshold of the structures seems to be associated with the high levels of input energy introduced by the first period of vibration (Izmit-Kocaeli), by both the first and second periods (El Centro-270 and New Zealand), or by the second period (Kobe, El Centro-180, Northridge, and El Maule). Note that the latter earthquake did not produce any damage to the structures at all. These earthquake records were downloaded via the Strong-motion Virtual Data Center (CESMD).

NO	EVENT/STATION/COMPONENT	PGA (G)	PGV (M/S)	PGA/PGV	FACTORS TO SCALE EARTHQUAKES TO:			
					Small	Moderate	Strong	Severe
1	Izmit-Kocaeli, Yarimca, 90	0.230	0.91	2.54	0.50	1.00	1.50	2.50
2	Michoacan, SCT1, N90W	0.158	0.57	2.76	0.80	1.60	2.50	4.00
3	El Centro, No.117, 270	0.210	0.37	5.69	1.25	2.50	4.00	6.70
4	El Maule, Concepcion, Long.	0.393	0.68	5.81	0.70	1.40	2.20	3.60
5	Northridge, Newhall - County Fire, 90	0.580	0.75	7.75	0.65	1.25	2.00	3.30
6	New Zealand, Greendale, N55W	0.738	0.95	7.81	0.50	1.00	1.50	2.50
7	Kobe, KJMA, 90	0.600	0.74	8.07	0.65	1.25	2.00	3.30
8	El Centro, No.117, 180	0.342	0.33	10.22	1.40	2.80	4.40	7.00

TABLE 6.1 Selected ground motions and factors chosen to scale them to the four earthquake levels used in this study.

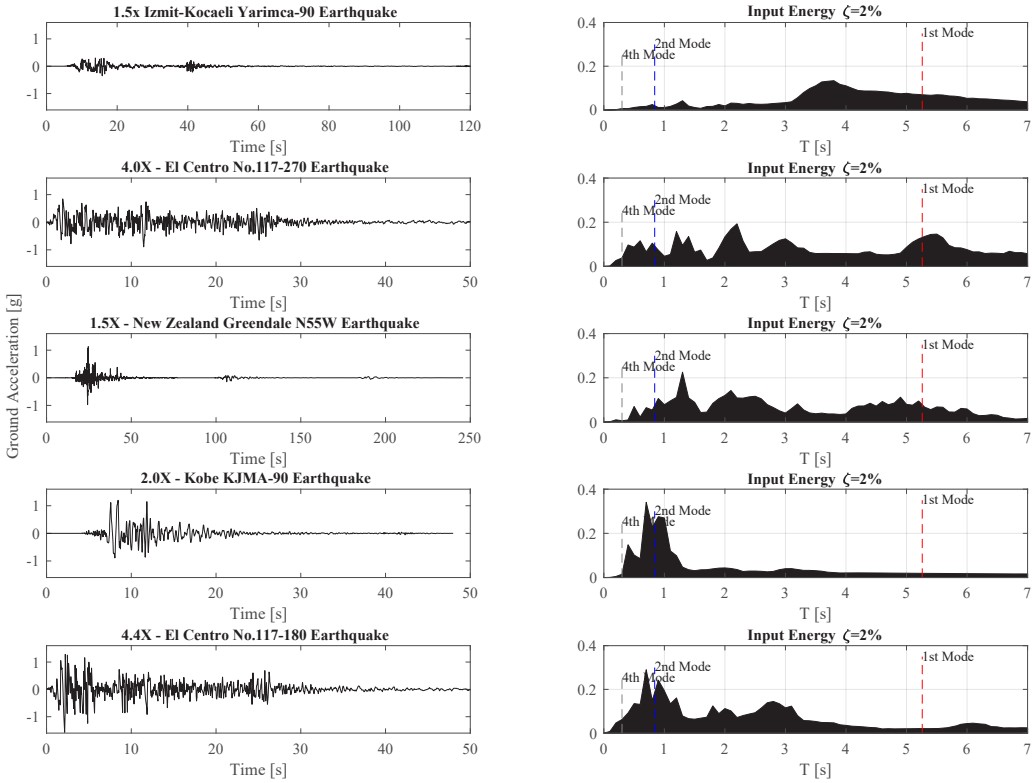

FIGURE 6.2 Five (out of eight) scaled ground motion records used in this study. Displayed accelerations, corresponding to strong earthquake level, caused damage to the single damped outrigger structure.

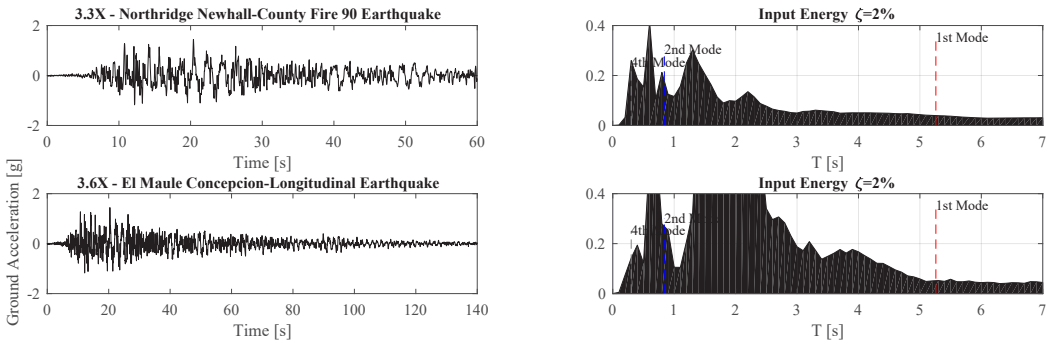

FIGURE 6.3 Two (out of eight) scaled ground motion records used in this study. Displayed accelerations, corresponding to severe earthquake level, caused damage to the single damped outrigger structure.

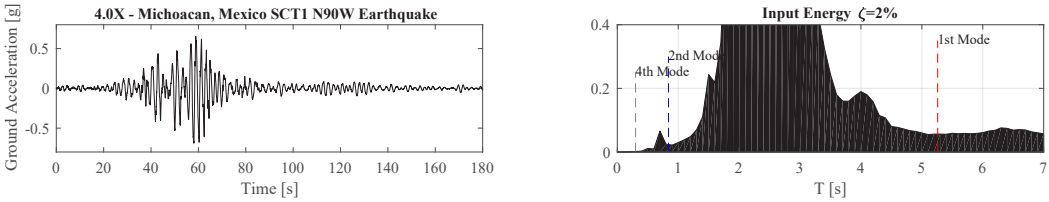

FIGURE 6.4 One of the eight scaled ground motion records used in this study. Displayed accelerations, corresponding to severe earthquake level, did not cause damage to any of the outrigger structures.

§ 6.4 Optimal damping ratio (ζ) under fee vibration

All the optimal inherent damping ratios described hereafter are in absolute values, i.e. the original damping ratio = 2% is included in these optimal ratios. Hence an optimized ζ = 8% represents a gain of 6% in damping.

§ 6.4.1 Single damped outrigger

Optimized ζ = 8% is obtained when the single damped outrigger is at λ=0.7-0.8, and C_d =9.60E+04kN-s/m (Figure *6.5*).

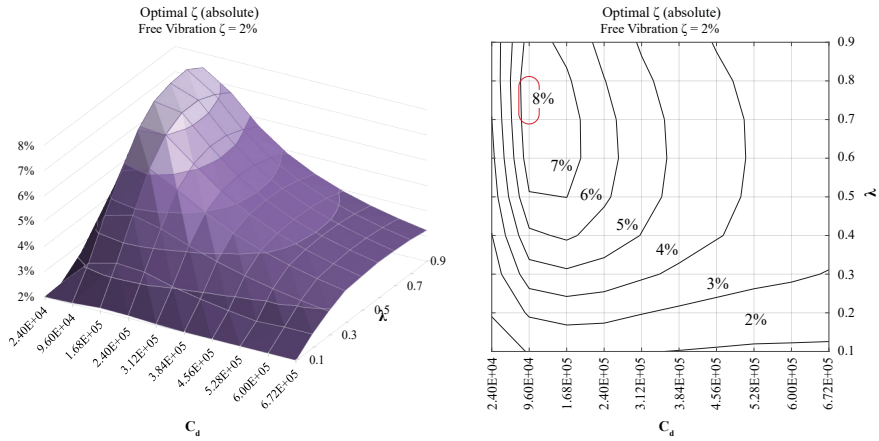

FIGURE 6.5 Optimal ζ in absolute values under a single damped outrigger configuration

§ 6.4.2 Double damped outriggers

Optimized ζ = 8.8% is obtained when the first set of damped outriggers (outrigger 1) is at λ=0.5 and the second one (outrigger 2) at λ=0.7-0.8 (Figure *6.6*). The C_d of the dampers attached to outrigger 1 is 1.68E+05kN-s/m, whereas C_d of outrigger 2 are 3.84E+05 and 4.56E+05kN -s/m, for λ=0.8 and 0.7, respectively. Since it is assumed that a lower C_d implies the use of less devices, the optimal double damped outriggers structure attaches the second set of outriggers at λ=0.8.

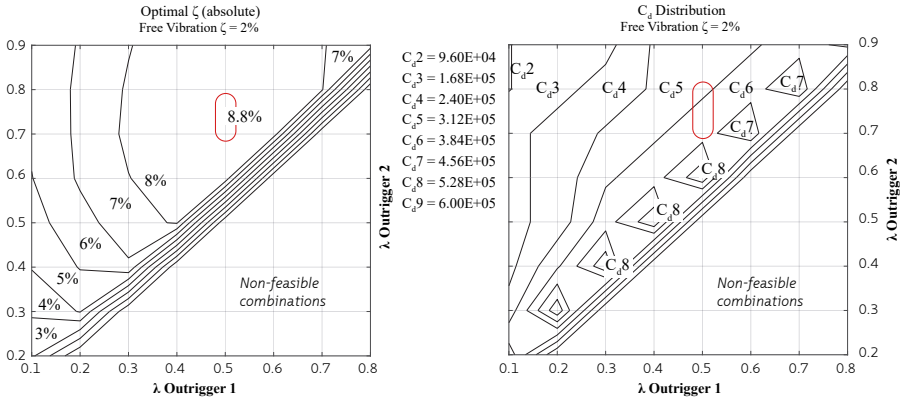

FIGURE 6.6 Optimal ζ (absolute values) under a double damped outrigger configuration (C_d outrigger 1 = 1.68E+05kN-s/m) and C_d distribution according to optimal λ combinations.

§ 6.4.3 Double fixed outriggers

Compared with ζ=2% given by the cantilevered core wall, the use of two sets of fixed outriggers is decreasing the damping to 1.4-1.8%, depending on the combination of outriggers' locations (Figure *6.7*). In this context, the optimized ζ = 1.8% is obtained when the first set of fixed outriggers (outrigger 1) is at λ=0.8 and the second one (outrigger 2) at λ=0.9. The result shows that the optimum position for the two fixed outriggers are very close to each other. This basically indicates that a single fixed outrigger would be enough and possibly more economical than implementing two fixed outriggers in the structure.

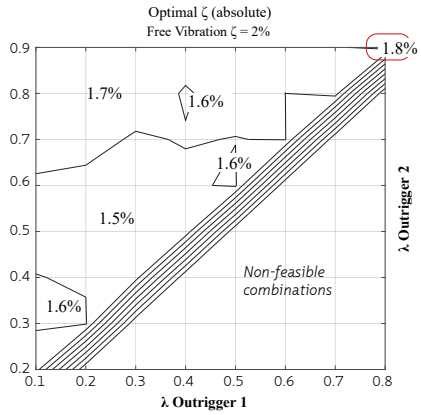

FIGURE 6.7 Optimal ζ (absolute values) under a double fixed outrigger configuration

§ 6.4.4 Combined damped and fixed outriggers

Optimized ζ = 8.6% is obtained when the lower set of damped outriggers is at λ_1=0.5 and the second set of fixed outriggers is at λ_2=0.7 (Figure *6.8*). C_d of the dampers attached to outrigger 1 is 1.68E+05kN-s/m.

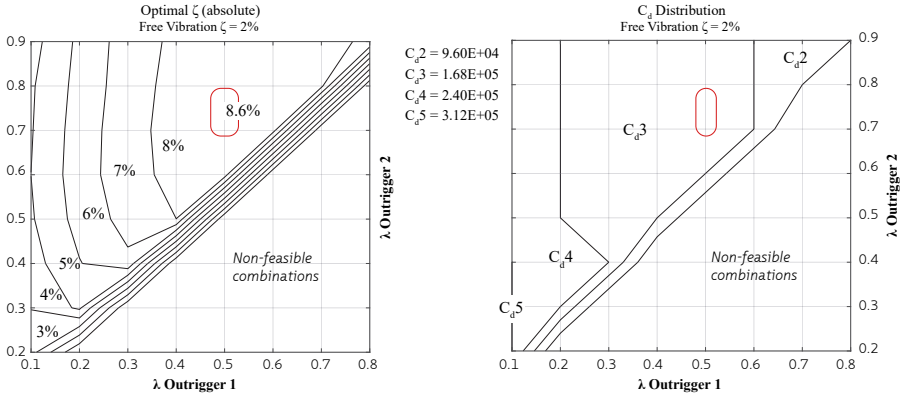

FIGURE 6.8 Optimal ζ (absolute values) under a combined damped (λ_1) and fixed outrigger (λ_2) configuration and C_d distribution according to optimal λ combinations

§ 6.4.5 Combined fixed and damped outriggers

Optimized ζ = 6.2% is obtained when the lower set of fixed outriggers is at λ_1=0.1 and the second set of damped outriggers is at λ_2=0.7, which is slightly better than that at 0.6 (Figure 6.9). C_d of the dampers attached to outrigger 2 is 9.60E+04kN-s/m. This result can be compared with that displayed in Figure 6.5 in which the structure involves only one damped outrigger, and hence, leading to the thought that the configuration of a fixed and a damped outrigger is not economical.

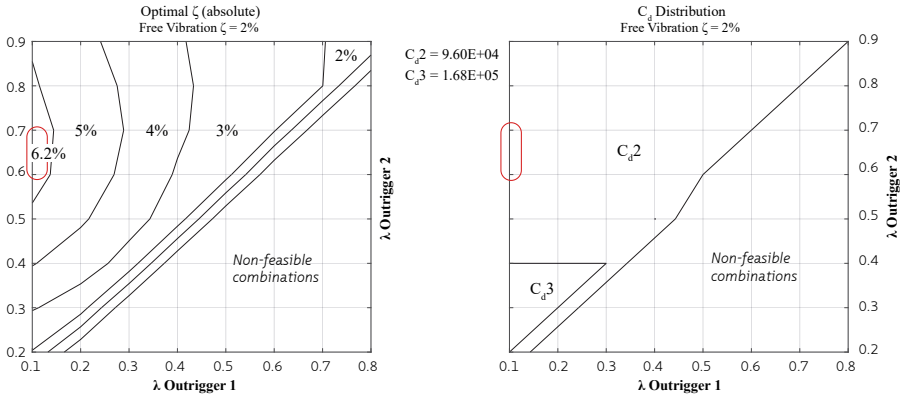

FIGURE 6.9 Optimal ζ (absolute values) under a combined fixed (λ_1) and damped outrigger (λ_2) configuration and C_d distribution according to optimal λ combinations

§ 6.5 Energy dissipation under strong earthquakes

Due to space constraints, only optimal configurations –based on increased ζ – were further studied. Hereafter, *single* damped, *double* damped and *combined* damped and fixed outriggers refer to a single damped outrigger at λ=0.7, to a set of double damped outriggers at λ=0.5 and 0.8, and to a combined damped outrigger (λ=0.5) plus a fixed outrigger (λ=0.7), respectively.

In order to generate a valid parameter of comparison, the scattered data produced by the energy-based assessment of the structures subjected to each earthquake record, were fitted into a trend line using the function *polyfit* and *polyval* in Matlab (MATLAB, 2013).

§ 6.5.1 Single damped outriggers

Despite the variations displayed by the individual plots – corresponding to each earthquake, the trend lines of E_D/E_I and $E_{DAMPERS}/E_I$ are almost equal for the severe and strong levels of the selected ground motions (Figure 6.10). Hysteretic energy distribution presents, nevertheless, a small increase (from 0.14 to 0.19) under severe levels due to the additional nonlinear performance of the structure under El Maule and Northridge earthquakes. Michoacan earthquake did not produce structural damage.

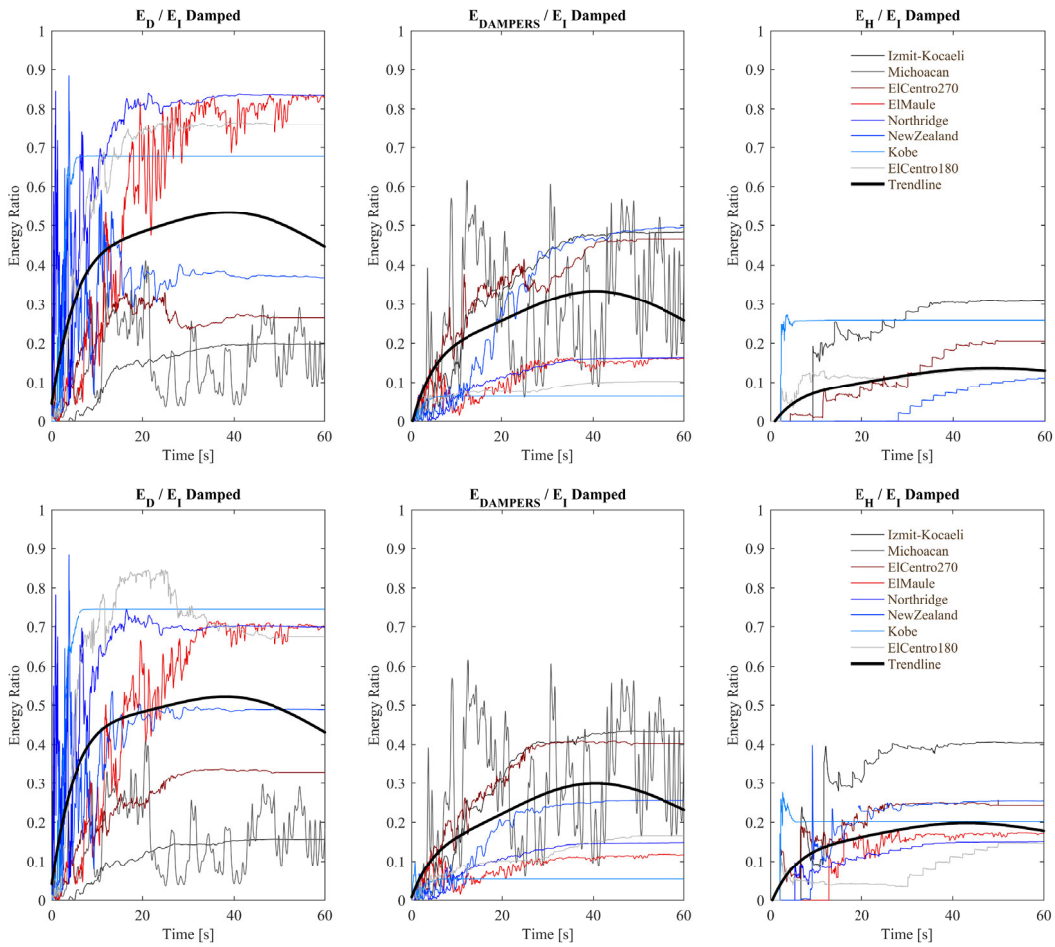

FIGURE 6.10 Energy dissipation ratios of the *single* damped outrigger under strong (upper row) and severe (lower row) levels of the selected eight earthquakes.

§ 6.5.2 Double damped outriggers

When increasing the ground motion from strong to severe levels (Figure 6.11), the use of a double set of damped outriggers do not present significant differences in the average energy dissipation due to structural damping (~45%), dampers (~40%), and hysteresis (~13%). However, if compared with the average energy dissipated by the single damped outrigger, it can be noticed a decrease from 0.19 to 0.13 in

the hysteretic energy dissipation and an increase from 0.30 to 0.40 in the dampers energy dissipation. Whereas the increase in the energy dissipated by the action of the viscous dampers may be explained by the extra number of dampers, the reduction in the average hysteretic energy is derived from the individual reduction in the hysteretic energy ratio of the structure under each earthquake. In this sense, notorious is the fact that under severe levels of El Maule and Northridge earthquakes, E_H/E_I is very small if compared to similar response of the single configuration. In simple words, under severe levels of certain earthquakes, the double damped outrigger reduces the damage to a minimum.

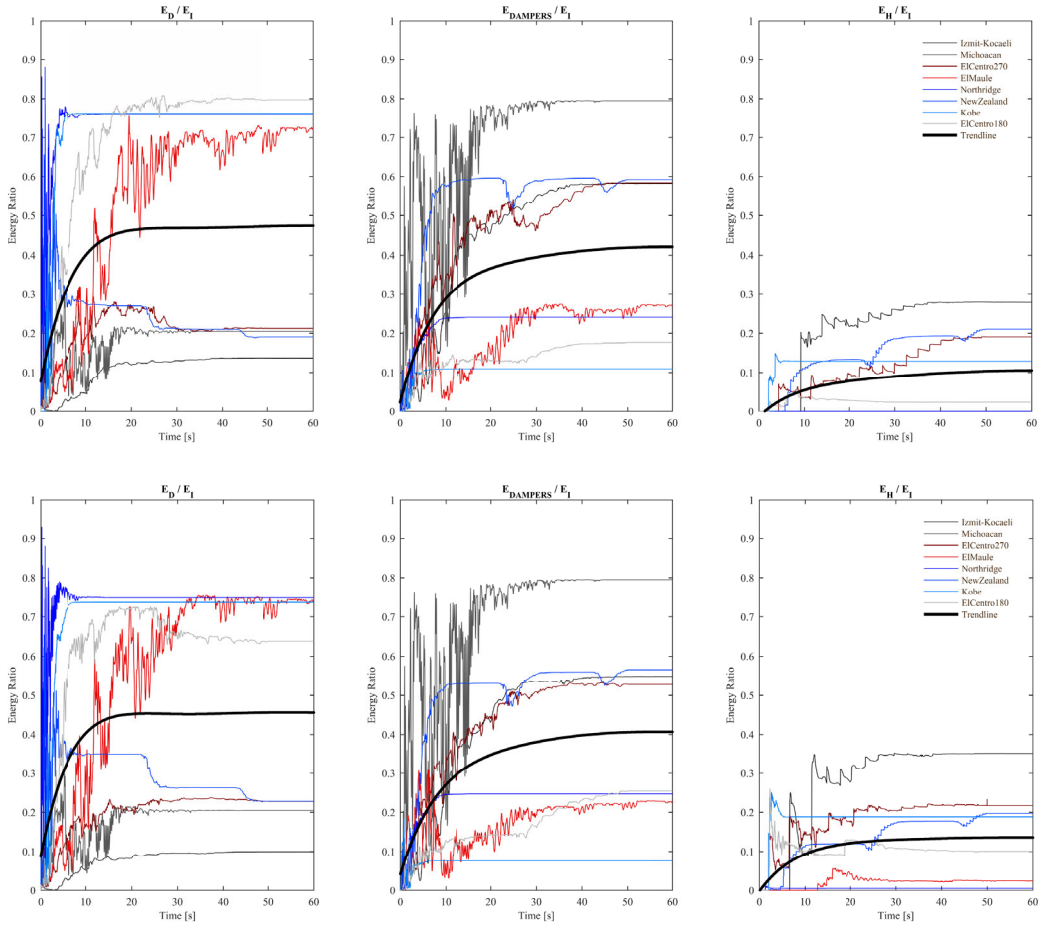

FIGURE 6.11 Energy dissipation ratios of the *double* damped outrigger under strong (upper row) and severe (lower row) levels of the selected eight earthquakes.

§ 6.5.3 Combined damped and fixed outriggers

In similar fashion with the previous two configurations, when the level of ground motions increases from strong to severe, the combined damped and fixed outriggers configuration does not present significant variations in the energy dissipation ratios (Figure 6.12). If compared with the single configuration, nevertheless, there is a reduction in the average energy dissipation due to hysteresis from 0.19 to 0.15, in the case of the severe level. As in the double damped case, this reduction can be attributed to the small contribution of the hysteretic energy of the structure when subjected to severe level of El Maule and Northridge earthquakes.

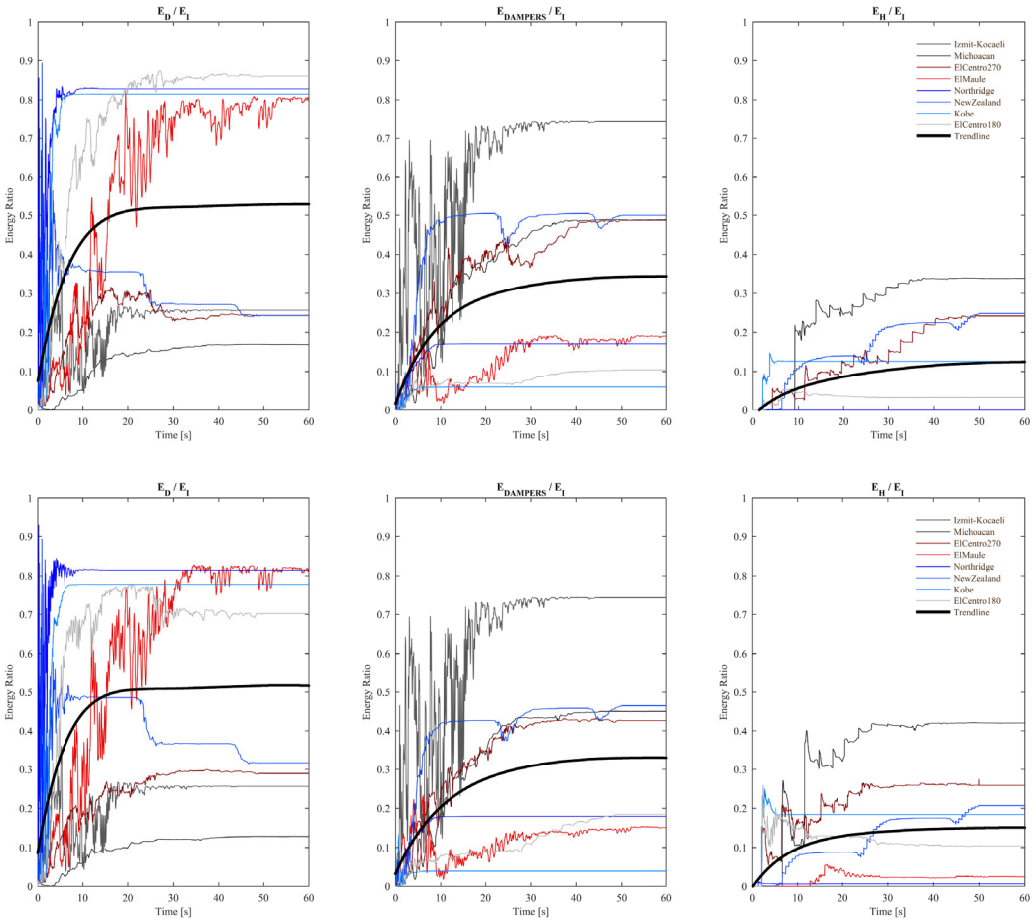

FIGURE 6.12 Energy dissipation ratios of the *combined* damped and fixed outrigger under strong (upper row) and severe (lower row) levels of the selected eight earthquakes.

§ 6.6 Decrease in structural response

§ 6.6.1 Peak inter-storey drift

The inter-storey drift was normalized by the target drift = $h_s/555$, where h_s = storey height. Values larger than 1.0 are assumed to likely produce damage in the structure. The displayed trend line in Figure 6.13 is the average of the peak inter-storey drift of the structures subjected to the four different earthquake levels. Despite small variations in the plots, there are no significant differences between *single*, *double* and *combined* configurations in terms of reducing drifts. Moreover, the locations of these maxima values –except for two specific cases, are always among the five upper floors, i.e. between the 55th and 60th floor (see Appendix E - Peak inter-storey drift response locations). The two exceptions are the single and combined configurations, under the severe level of Michoacan earthquake, whose peak inter-storey drifts occur at the 53rd and 54th floor, respectively.

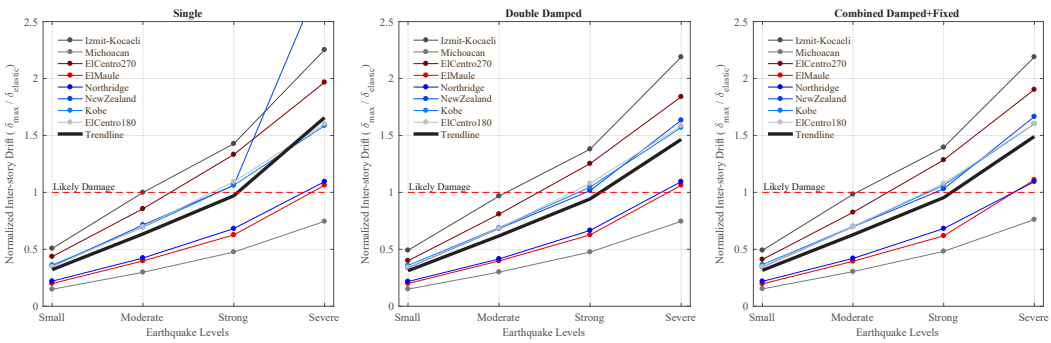

FIGURE 6.13 Normalized peak inter-storey drifts of the studied outrigger configurations.

§ 6.6.2 Peak accelerations

Despite some individual variations (e.g., severe level of Northridge case), the average normalized peak accelerations remain fairly invariable for all the studied cases (Figure 6.14). Equally steady is the location of the peak acceleration at the building's roof, except for the severe level of Kobe earthquake, under which the peak acceleration takes place at the 32nd floor (see Appendix E - Peak acceleration response locations).

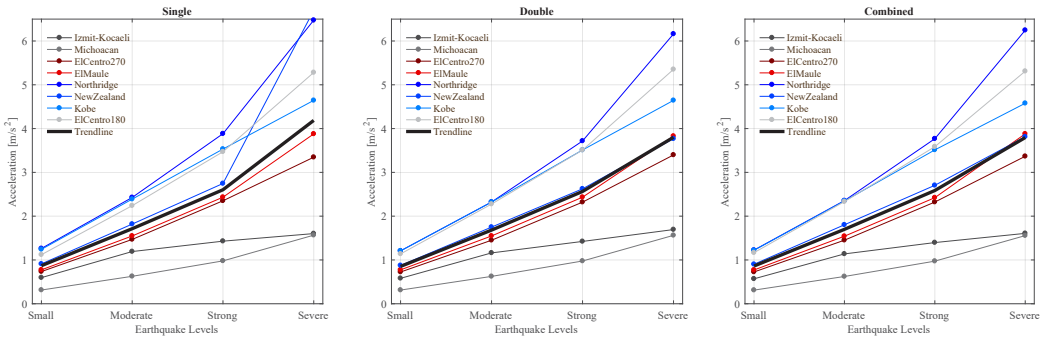

FIGURE 6.14 Normalized peak accelerations of the studied outrigger configurations.

§ 6.6.3 Base shear

The base shear plots resulting from the different configurations subjected to all levels of the selected ground motions are displayed in Figure 6.15. Base shear was normalized by the total seismic mass (W) of each configuration: 8.05 E+04, 8.10E+04, and 8.08E+04 tons for single, double, and combined outriggers, respectively. Despite the individual variations, the trend lines in each plot of Figure 6.15 do not reveal substantial variation between the different configurations evaluated.

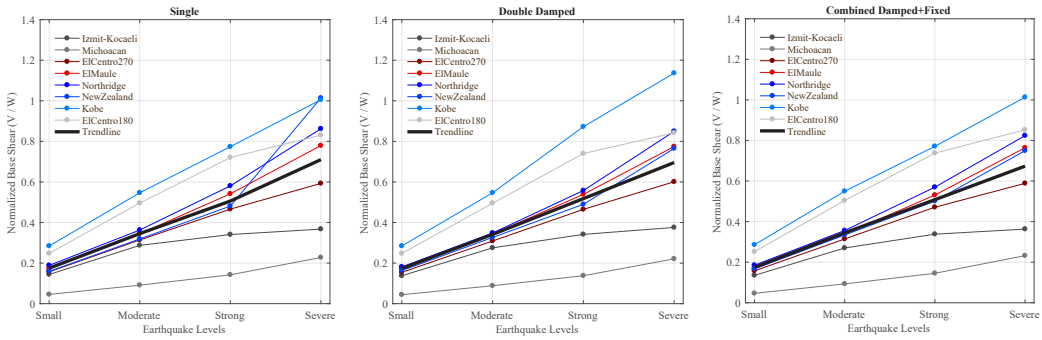

FIGURE 6.15 Normalized base shear (V/W) of the studied outrigger structures subjected to four earthquake levels of all ground motions.

§ 6.6.4 Stresses and overturning moment

Although peaks of overturning moment and stresses might not occur at the same instant of the time-history of an earthquake, plots addressing the relationship between these peaks were elaborated to study their mutual influence in the nonlinear structural response. Peak overturning moments were normalized by the maximum overturning moment produced by a ground motion (Kobe earthquake in all cases); maximum stresses were normalized by the yielding stress, thus $\sigma/\sigma_{yield} = 1$ represents the inelastic threshold. From the plots displayed in Figure 6.16 it can be noticed that (1) there is no substantial difference between the response trend lines (average) of each configuration, and (2) inelastic responses are triggered when peak overturning moments are ~60% of the maximum overturning moment, for all the evaluated configurations.

In addition, all the nonlinear responses induced in the single, double, and combined configurations by the strong and severe level of the selected earthquakes were provoked by the overpass of the core's tensile strength, i.e. by yielding of the longitudinal reinforcement. As expected, all nonlinearities –for all the cases- took place in the plastic hinge region of the core, i.e. between the 1st and 6th floor.

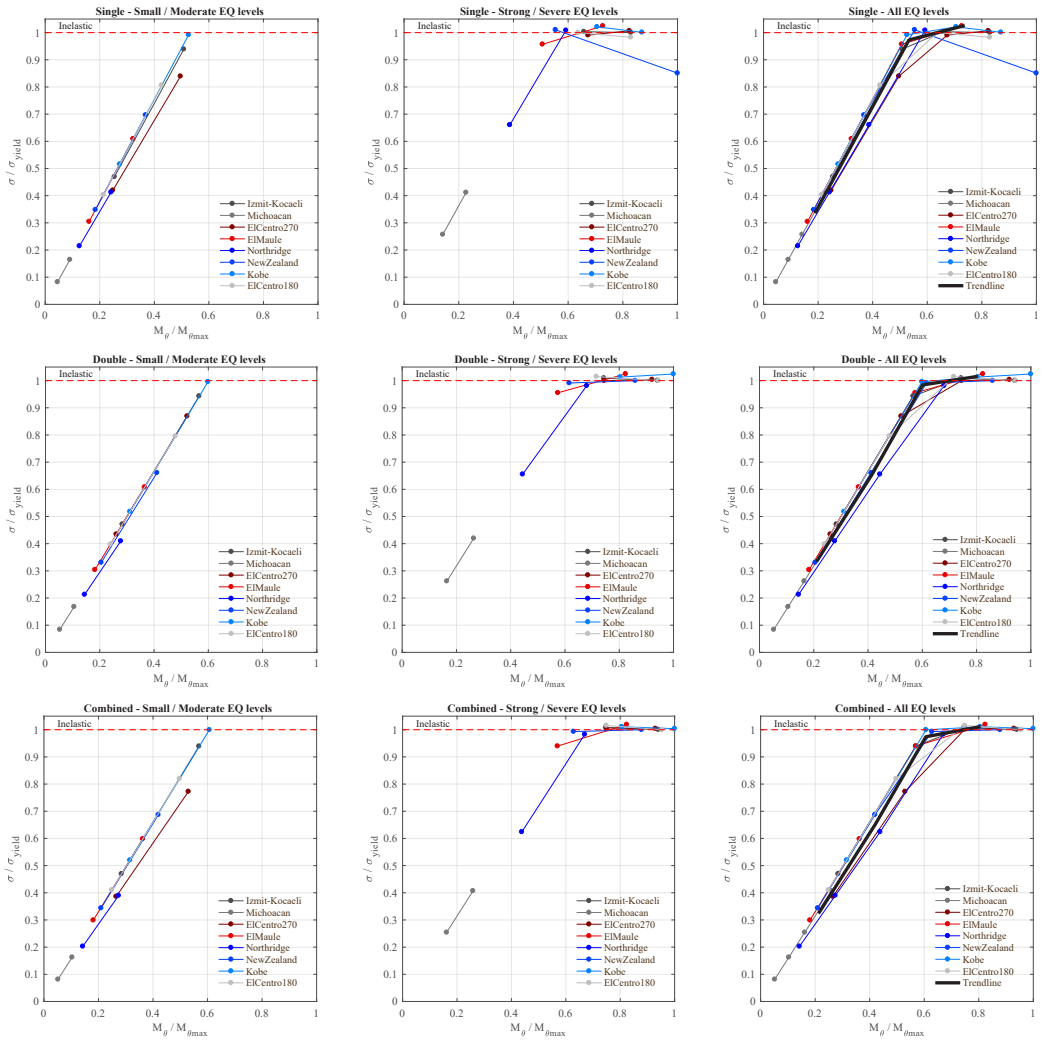

FIGURE 6.16 Normalized *core* stress (σ/σ_{yield}) to normalized overturning moment ($M\theta/M\theta_{-max}$) of the single (upper row), double (middle row) and combined (lower row) outrigger configurations subjected to four earthquake levels of all ground motions.

In the case of the outrigger frame structure, composed of I steel profiles, the response remains elastic, regardless of the level and the ground motion applied (Figure 6.17). However, compared to the single damped outrigger, there is a clear decrease in the stress levels of the outrigger frame in both double and combined configurations. When the ratio $M\theta/M\theta_{-max}$ is ~0.6 (inelastic threshold of the core), in the double configuration there is a change in slope of the trend line, indicating that some of the stress is reduced due to the core's damage.

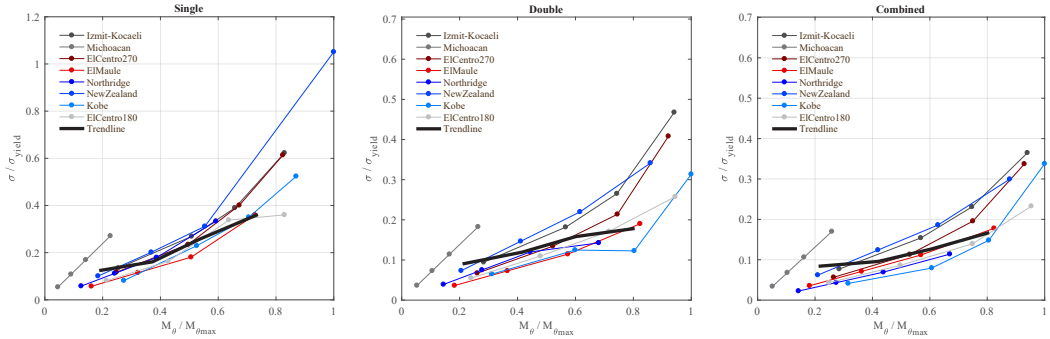

FIGURE 6.17 Normalized *outrigger* stress (σ/σ_{yield}) to normalized overturning moment ($M\theta/M\theta_{-max}$) of the studied outrigger configurations subjected to four earthquake levels of all ground motions.

In the case of the perimeter columns (Figure 6.18), there is a substantial increase in the stress levels when two sets of damped outriggers are used. At the same time, there is no difference between stress levels of the columns between the single and combined configurations. This phenomenon can be explained by the dynamic stiffness provided by the addition of several viscous dampers, which increases the rotational stiffness of the core by increasing the axial forces over the perimeter columns.

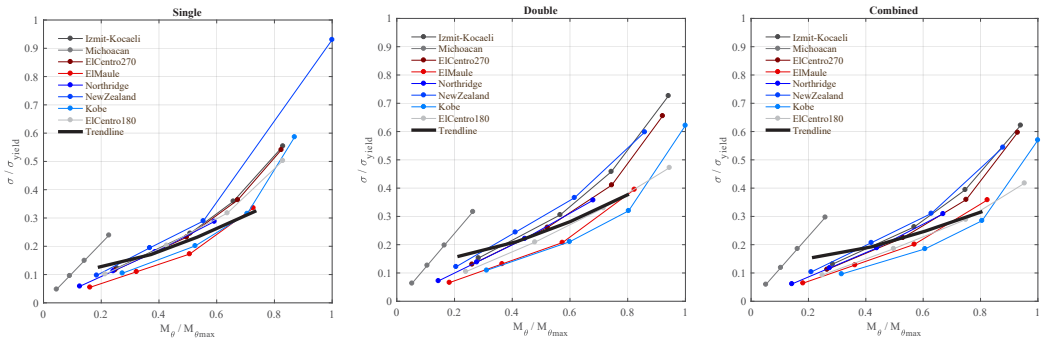

FIGURE 6.18 Normalized *column* stress (σ/σ_{yield}) to normalized overturning moment ($M\theta/M\theta_{-max}$) of the studied outrigger configurations subjected to four earthquake levels of all ground motions.

§ 6.7 Simplified economic evaluation

Practical relevance of the current work was studied by conducting a simple economic evaluation of the analytical models, which possess altered number of outriggers and viscous damper configurations. The alternative hypothesis was; using outriggers combined with oil viscous dampers causes a significant reduction in the amount of required reinforcement steel at the building core, which in turn will also cause a decrease in reinforcement steel costs. Nevertheless, the additional costs incurred through introduction of oil viscous dampers to the structural system must be addressed as well. Therefore, in this simplified approach, the current work solely considered the trade-off between the material costs of reinforcement steel at the building core against the costs of viscous dampers. Acknowledging such costs as the number of workers, the social security contributions, and earthquake losses through life cycle of the building were not taken into account.

To determine the cost of reinforcement steel required in each alternative, first, the base shear and overturning moment (OTM) envelopes were determined by modal analysis (see Appendix E - Storey shear and overturning moment envelopes). The five predominant modes -equivalent to 90% of the seismic mass in horizontal direction (Table 6.2), were combined using square-root-of-sum-of-squares (SRSS) method, in order to obtain the modal storey shear and OTM envelopes of each configuration (Figure 6.19). Predominant modes in vertical direction were not considered (Table 6.3). Second, the ratio (%) of reinforcement steel to the vertical and horizontal sections of the building core was calculated according to the capacity flexural strength design envelope, for a non-conservative case, as proposed by Boivin and Paultre (2012). In accordance with Eurocode (1992-1-1, 2004), the calculated vertical reinforcement ratios below the threshold level were replaced with the minimum reinforcement ratio requirement of 0.25%. Next, using these values and simple geometry, the total volume of reinforcement steel for each alternative was calculated. Multiplying these values with the density of the reinforcement steel provided the total weight in tons. In this work, market price of reinforcement steel per ton was assumed as $ 600.

MODE		1	2	4	5	7
T	single	5.26	0.84	0.30	0.17	0.16
	double	5.27	0.85	0.31	0.20	0.16
	combined	5.26	0.84	0.30	0.16	0.12
Effective Mass-X (kN)	single	4.98E+04	1.51E+04	5.02E+03	1.99E-01	2.63E+03
	double	4.98E+04	1.53E+04	5.09E+03	5.25E+01	2.55E+03
	combined	4.97E+04	1.53E+04	5.07E+03	2.57E+03	1.75E-02
Cumulative %	single	62	80	86	86	90
	double	62	80	87	87	90
	combined	62	80	87	90	90

TABLE 6.2 Effective modal mass participation in X direction

MODE		3	6	8
T	single	0.39	0.17	0.13
	double	0.39	0.20	0.13
	combined	0.39	0.13	0.12
Effective Mass-Y (kN)	single	6.50E+04	8.22E+02	7.21E+03
	double	6.55E+04	6.49E-01	7.23E+03
	combined	6.53E+04	6.95E+03	5.72E+02
Cumulative %	single	80	81	90
	double	81	81	90
	combined	81	89	90

TABLE 6.3 Effective modal mass participation in Y direction

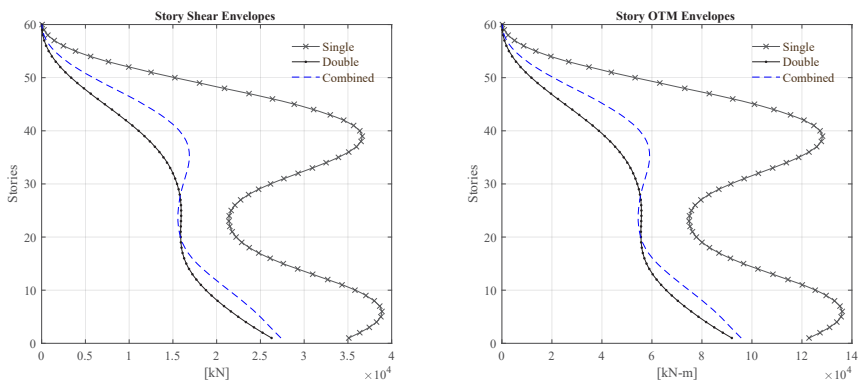

FIGURE 6.19 SRSS modal storey shear and OTM moment envelopes for the three configurations of outriggers.

Gidaris and Taflanidis (2015), provided an empirical cost estimation model for oil viscous dampers based on maximum force capacity $F_{ud,j}$, as $96.88(F_{ud,j})^{0.607}$. In the current work, two different commercially available oil viscous damper types were used based on the required damping coefficient. Maximum force capacity of selected dampers is 2000 kN, and therefore the cost of one damper is estimated as 9,771.46.

§ 6.7.1 Results of economic evaluation

The current work considered three alternatives of outriggers with oil viscous dampers. The calculated values are compared then to the results obtained from the alternative using conventional outriggers, called fixed, whose reinforcement demand was computed using a conservative approach. For each alternative, computed horizontal and vertical steel reinforcement values as required solely in the building core, are outlined in Table 6.4 and Table 6.5, respectively.

NO. STOREY	REQUIRED REINFORCEMENT STEEL RATIOS				REQUIRED REINFORCEMENT STEEL WEIGHT (KG)			
	Fixed	Single	Double	Combined	Fixed	Single	Double	Combined
1-6	0.50%	0.26%	0.19%	0.20%	44,510	22,699	16,994	17,686
7-12	0.44%	0.22%	0.17%	0.17%	39,168	19,862	14,870	15,476
13-18	0.37%	0.19%	0.14%	0.15%	32,937	17,025	12,746	13,265
19-24	0.31%	0.16%	0.12%	0.12%	27,596	14,188	10,621	11,054
25-30	0.25%	0.13%	0.10%	0.10%	22,255	11,350	8,497	8,843
31-36	0.25%	0.13%	0.10%	0.10%	22,255	11,350	8,497	8,843
37-42	0.25%	0.13%	0.10%	0.10%	22,255	11,350	8,497	8,843
43-48	0.25%	0.13%	0.10%	0.10%	22,255	11,350	8,497	8,843
49-54	0.25%	0.13%	0.10%	0.10%	22,255	11,350	8,497	8,843
55-60	0.25%	0.13%	0.10%	0.10%	22,255	11,350	8,497	8,843
Total weight (tons)					277.74	141.87	106.21	110.54

TABLE 6.4 Required *horizontal* reinforcement steel values in the building core

NO. STOREY	REQUIRED REINFORCEMENT STEEL RATIOS				REQUIRED REINFORCEMENT STEEL WEIGHT (KG)			
	Fixed	Single	Double	Combined	Fixed	Single	Double	Combined
1-6	1.00%	0.93%	0.70%	0.73%	85,310	79,472	59,499	61,922
7-12	0.85%	0.84%	0.63%	0.65%	72,513	71,525	53,549	55,730
13-18	0.76%	0.75%	0.56%	0.58%	64,836	63,578	47,599	49,538
19-24	0.65%	0.65%	0.49%	0.51%	55,451	55,631	41,649	43,345
25-30	0.56%	0.56%	0.42%	0.44%	47,774	47,683	35,699	37,153
31-36	0.51%	0.41%	0.31%	0.32%	43,508	35,195	26,349	27,423
37-42	0.46%	0.32%	0.25%	0.25%	39,243	27,248	21,327	21,230
43-48	0.37%	0.25%	0.25%	0.25%	31,565	21,327	21,327	21,327
49-54	0.25%	0.25%	0.25%	0.25%	21,327	21,327	21,327	21,327
55-60	0.25%	0.25%	0.25%	0.25%	21,327	21,327	21,327	21,327
Total weight (tons)					482.85	444.31	349.65	360.32

TABLE 6.5 Required *vertical* reinforcement steel values in the building core

As previously defined, the terms *fixed*, *single*, *double*, and *combined* correspond to structural design alternatives that possess no outriggers, a single set of outriggers with dampers, two sets of outriggers with dampers, and two outriggers where one is fixed and one has dampers, respectively. In line with the provided definitions, the required number of dampers employed in *single*, *double*, and *combined* alternatives were computed as 8, 40, and 8, respectively (Table 6.6). These dampers are commercially available in seven sizes ranging from 1.25E+04 to 8.75E+04 kN. Hence, except for the case of the upper outrigger in the double alternative, one damper per outrigger is enough to provide the required supplemental damping. Two dampers were not yet enough for the upper outrigger in the double alternative (1.92E+05/2 > 8.75E+04, i.e. demand > supply), thus four dampers were necessary to provide the required damping. Recall that, market price of reinforcement steel per ton was assumed as $ 600 and the cost of one viscous damper was estimated as $ 9,771.46. The results of comparative cost analysis among structural design alternatives considered in this work are given in Table 6.7.

DAMPING COEFFICIENT [*KN*]					NO. DAMPERS	
		Required at damping point*	type	Supplied per damper	per outrigger	per set of out-riggers
single		4.80E+04	B4	5.00E+04	1	8
double	lower	8.40E+04	B7	8.75E+04	1	8
	upper	1.92E+05	B4	5.00E+04	4	32
combined		8.40E+04	B7	8.75E+04	1	8

** equals to the optimal C_d divided by two, as two outriggers were modelled as one.*

TABLE 6.6 Supply of dampers according to the required damping coefficients (C_d's)

DESIGN ALTER-NATIVE	TOTAL REINFORCE-MENT COST	CHANGE COMPARED TO FIXED MODEL (%)	COST OF DAMPERS	TOTAL COST	CHANGE COMPARED TO FIXED MODEL (%)
Fixed	$ 456,356		$ -	$ 456,356	
Single	$ 351,712	-23%	$ 78,172	$ 429,883	-06%
Double	$ 273,521	-40%	$ 390,858	$ 664,380	+46%
Combined	$ 282,519	-38%	$ 78,172	$ 360,690	-21%

TABLE 6.7 Comparative cost analysis among structural design alternatives

The results suggest provision of the single outrigger system with dampers to the structural design of the hypothetical building core under the identical design loads, caused 23% reduction in the reinforcement steel costs. The cost reduction became more significant at the level of 40% and 38% when double outrigger configurations were considered. Nevertheless, due to the high number of required dampers in the design alternative *double* it is economically non-viable, as the total costs, defined as the sum of reinforcement steel cost and dampers cost, were 46% higher than the *fixed* design. One can deduce that high number of required dampers and their associated costs surpasses the economic gains obtained from the reinforcement steel savings. *Single* and *combined* alternatives, on the other hand, presented an opposite figure. A relatively lower number of dampers required in the design of these alternatives kept the required dampers costs at the reasonable levels. Therefore, in these alternatives the economic benefits obtained from reduction in the required reinforcement steel amount exceeded the economic losses caused by inclusion of dampers in the structural design. In particular, design alternative *combined* demonstrated a significant decrease in the total construction cost at the level of 21% when compared to *fixed* design, and therefore proposed the most viable option, economically speaking. It should be noted, nonetheless, that the placement of the outrigger in the building was not considered in the cost analysis. Had it been so, the single outrigger structure might have presented advantages –from an economic perspective, over multiple outrigger structures.

§ 6.7.2 Pushover Analyses

In order to ensure that the previous distribution of reinforcement ratios provided an adequate level of ductility and strength, the design of the shear core wall was revised and evaluated by nonlinear static analyses, i.e. using pushover method. The final design followed the requirements defined in Eurocode 2 (1992-1-1, 2004).

With this purpose, a 3D model of the 60-storey building core was created in SAP2000 (CSI, 2004). Since the outriggers do not affect the lateral stiffness of the building, they were not considered in this model. Concrete strength class is C35/45 and reinforcement steel bars are 400MPa. The reinforcement ratios were applied by considering the cross sectional area of the core versus the number of bars along both 3-dir face (2) and 2-dir face (60). For example, if the longitudinal reinforcement ratio is considered (1%) the formula is 18000mm x 750mmx0.01 = 135000mm^2. By using 2 and 60 layers for perpendicular directions yields 1125mm^2, equivalent to a φ38 bars. For the transversal reinforcement, the number of bars and their diameters were computed by considering a relative cross section of 750mmx1000mm. This yielded the use of a minimum confinement bar size = φ8, with longitudinal spacing = 0.15cm, and a number of confinement bars in 3-dir and 2-dir, equal to 10 and 2, respectively. A plastic hinge was assigned to the core end.

As in the model developed in Diana (DIANA-FEA, 2017), nodal masses were applied to account for the floor live and dead loads. The settings for the pushover analysis considered several load combinations, according to Eurocode 2, and the alternative whether to consider geometric nonlinearities (P-Δ effects). The lateral load pattern was derived from the modes 1 and 2.

The results of the pushover analyses show no difference between the curves with and without P-Delta effects (Figure 6.20). This makes sense as P-delta effects tend to affect perimeter columns and slender elements. When the pushover curves corresponding to the modes 1 and 2 are compared (Figure 6.21), it can be noticed that 2nd mode-base shear is about three times larger than that resulting from the 1st mode, whereas the inverse trend is observe in the case of the top storey displacements. In other words, it seems that the building undergo larger displacements with less base shear forces. This phenomenon is explained by the modal shapes: since the mode 2 is less unbalanced around the building axis, the base shear reaches larger values with smaller top storey displacements. This explanation is supported by the fact that whilst the plasticity for mode 2 is located in the middle height, for mode 1 is located at the bottom.

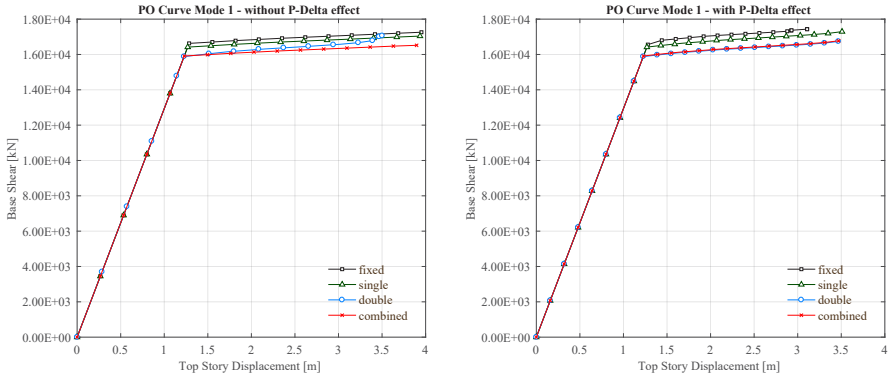

FIGURE 6.20 Pushover (PO) curves for Mode 1 with and without P-Delta effects

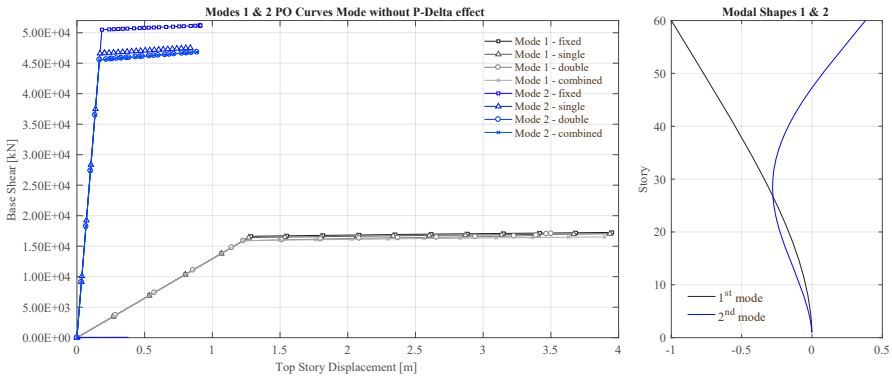

FIGURE 6.21 Comparison between pushover (PO) curves - Modes 1 & 2, without P-Delta effect

§ 6.8 Discussion

§ 6.8.1 Optimal configurations for increasing the inherent damping ratio ζ

In terms of ζ only a double set of damped outriggers and the combined damped and fixed outriggers (attaching viscous dampers in the lower set of outriggers) displays larger increase than that of the single damped outrigger. Optimized ζ of the former two are 8.8 and 8.6%, respectively, which is in practical terms, almost the same but with the double damped outrigger requiring more dampers. Nevertheless, from an economical point of view, the use of combined damped and fixed outriggers is not only equally optimal but cheaper than its counterpart using a double set of damped outriggers.

In addition, it should be noticed, that whereas a single damped outrigger exhibits optimal ζ only at λ=0.7-0.8, both double and combined outrigger configurations exhibit broader display of optimal combinations (*Figure 6.6* and *Figure 6.8*), which offer flexibility of design to the high-rise architecture and distributions of building systems. It is worth to notice that the use of multiple outriggers is desired in tall buildings (Smith, 2016) and that their final locations depends on both the availability of space, say mechanical floors, and the influence of the outrigger members' size (Choi and Joseph, 2012).

§ 6.8.2 Optimal configurations for reducing the hysteretic energy

From the average ratios E_D, $E_{DAMPERS}$, and E_H to E_I of the three studied configurations in Table 6.8, it is clear that both double damped and combined damped and fixed outriggers are reducing the hysteretic energy ratio (E_H/E_I), and hence becoming more effective in reducing structural damage under strong earthquake motions. However, as mentioned before, the double damped configuration requires the use of more dampers and hence it is assumed to be comparatively more expensive. The combined damped and fixed configuration, compared with the single damped one, is effectively reducing the hysteretic energy and maintaining the levels of energy dissipated by both inherent damping and viscous dampers.

Although a single set of conventional outriggers without dampers (fixed) was not included among the initial studied configurations, it was added for framing a valid performance bound. Thus, by observing the column E_H/E_I in Table 6.8, it can be noticed that the reduction in the hysteretic energy due to the addition of supplemental damping is not significant. For instance, no change and a decrease from 0.23 to 0.14 under strong and severe motion, respectively, are the results of comparing the cases of the fixed and double damped configurations. This relatively small decrease in E_H/E_I may be explained by two observations: (1) as indicated by the results of the studies described in Chapters 4 and 5, the dampers' damping coefficient (C_d) and the outrigger's location (λ) are the parameters that most influence the tall building's response. Since these two parameters have been already optimized in each of the studied configurations, further improvements –beyond each optimal, are unlikely to take place; (2) as suggested by columns E_D/E_I and $E_{DAMPERS}/E_I$, most of the energy dissipated by the dampers seems to be partially subtracted from that dissipated from the inherent structural damping.

Finally, the fact that the rows of energy dissipation ratios for the *single*, *double*, and *combined* configurations add up to 100% (column *Sum*, Table 6.8), indicates that these configuration are effective for reducing the building's response by the end of the ground motion. To the contrary, the fixed outrigger will continue vibrating beyond the end of the ground motion and thus, part of the input energy will be dissipated as strain elastic energy.

		E_D/E_I	$E_{DAMPERS}/E_I$	E_H/E_I	SUM
Fixed	small	0.93	-	0	0.93
	moderate	0.93	-	0.01	0.94
	strong	0.82	-	0.10	0.92
	severe	0.72	-	0.23	0.95
Single	small	0.61	0.39	0	1.00
	moderate	0.61	0.39	0	1.00
	strong	0.52	0.33	0.14	0.99
	severe	0.50	0.31	0.19	1.00
Double	small	0.52	0.48	0	1.00
	moderate	0.52	0.48	0	1.00
	strong	0.47	0.42	0.10	0.99
	severe	0.45	0.41	0.14	1.00
Combined	small	0.59	0.41	0	1.00
	moderate	0.59	0.41	0	1.00
	strong	0.53	0.34	0.12	0.99
	severe	0.51	0.33	0.15	0.99

TABLE 6.8 Peak energy dissipation ratios (trend line-based), for each configuration under all earthquake levels.

§ 6.8.3 Hysteretic energy and frequency content of the ground motions

In order to explore possible links between the hysteretic behaviour of the outrigger systems and the characteristics of the ground motions, the plots of both critical acceleration and input energy of all configurations studied are sorted according the level of damage, as measured by the E_H/E_I ratio (Table 6.9). The ground acceleration is considered critical when it provokes damage in the structure. The input energy was computed for a SDOF with mass=1 ton, and ζ=2% only for illustration purposes.

As remarked in Chapter 5, the fact that under certain earthquakes the use of viscous dampers attached to the outrigger increased the damage seems to be related to the predominance of the second mode. Furthermore, this hypothesis is reinforced by the effect of both number and location of the outrigger. Since in a single fixed and damped outrigger systems there is no second outrigger to control other modal responses, higher modes may have a larger influence over the response when subjected to certain earthquakes. The fact that double configurations were quite successful in reducing damage under Northridge and El Maule earthquakes proves that by adding a second

set of outrigger the influence of the second mode was further controlled. Following the same logic, since Michoacan earthquake does not introduce large energy inputs at any of the predominant modes, no damage was produced neither the performance of the damped outriggers was required.

EQ (STRONG/ SEVERE)	GROUND ACCELERATION	CORRESPONDING SDOF INPUT ENERGY	FEM	STRONG		SEVERE	
				Peak$_t$ [sec]	E_H/E_I	Peak$_t$ [sec]	E_H/E_I
Izmit-Ko-caeli (strong)	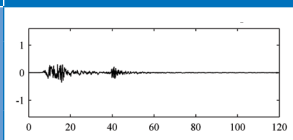	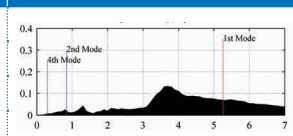	F	7.3	0.18	6.6	0.31
			D	9.2	0.31	6.6	0.40
			d	9.2	0.28	6.6	0.35
			c	9.2	0.34	6.6	0.42
Kobe (strong)	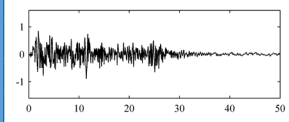	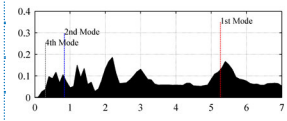	F	2.1	0.24	2.0	0.39
			D	2.1	0.23	2.0	0.20
			d	2.1	0.11	2.0	0.19
			c	2.1	0.11	2.0	0.18
ElCentro270 (strong)	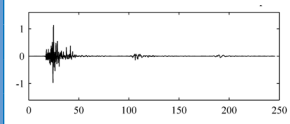	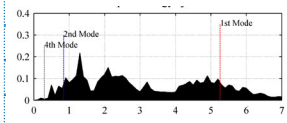	F	4.3	0.27	2.1	0.36
			D	4.3	0.21	2.1	0.23
			d	4.3	0.19	2.1	0.23
			c	4.3	0.24	2.1	0.27
ElCentro180 (strong)	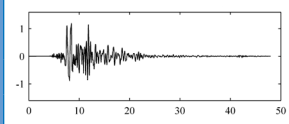	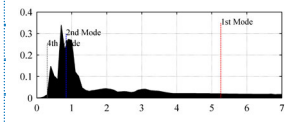	F	2.4	0.10	2.2	0.34
			D	2.4	0.13	2.2	0.15
			d	2.4	0.02	2.2	0.10
			c	2.4	0.03	2.2	0.10
NewZealand (strong)	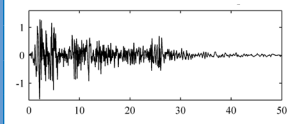	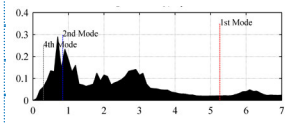	F	11.9	0.05	8.9	0.21
			D	14.0	0.21	9.3	0.18
			d	14.0	0.21	9.3	0.20
			c	12.0	0.25	9.3	0.21
ElMaule (severe)	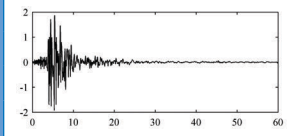	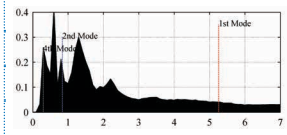	F	14.9	0.01	12.7	0.13
			D	0.0	0.0	12.7	0.17
			d	0.0	0.0	12.7	0.02
			c	0.0	0.0	12.8	0.02
Northridge (severe)	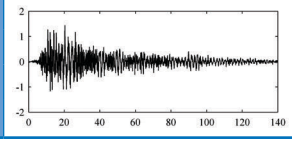	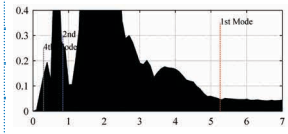	F	0.0	0.0	5.3	0.06
			D	0.0	0.0	5.3	0.13
			d	0.0	0.0	5.3	0.004
			c	0.0	0.0	5.3	0.004

TABLE 6.9 Ground motions organized from most to less damaging and their corresponding hysteretic and input energies. F, D, d, and c are fixed, damped, double, and combined outrigger systems, respectively.

§ 6.8.4 Optimal configurations for reducing the overall structural response

Inter-storey drift can be reduced by adding outriggers and it is been suggested that the effect of two sets of outriggers is, in this regard, better than one (Zhou *et al*. (2011), as cited in Zhou and Li (2014)). However, according to the results tabulated in Table 6.10, this is not necessarily the case when using damped outriggers. Whereas both double and combined outrigger solutions slightly reduce the maxima inter-storey drifts when compared with the single configuration, the decrease is comparatively very small. This may be explained by the comparatively large influence of the outrigger location in the reduction of the inter-storey drift; since there is no substantial difference in the location of the outriggers between both configurations, the inter-storey drift is not affected largely. This seems to suggest that configurations with optimal ζ might not be further optimized for inter-storey drifts reductions.

	SMALL	MODERATE	STRONG	SEVERE
fixed	0.34	0.68	1.06	1.62
single	0.32	0.64	0.97	1.50
double	0.31	0.62	0.94	1.46
combined	0.32	0.63	0.95	1.49

TABLE 6.10 Average Normalized Peak Inter-storey Drifts

The almost non-existent variation among the peak acceleration response of all the configurations can also be explained by the difficulty of a further optimization after a damping ratio-based optimized design. Moreover, neither the addition of an extra set of outriggers nor viscous dampers will modify the seismic mass of the building substantially. Hence the no variation in the peak values of acceleration (Table 6.11).

The fact that under the severe level of the Kobe ground motion, the system will experience its peak acceleration around half way of the height (see Appendix E - Peak acceleration response locations), seems to indicate that –when subjected to this earthquake- the second mode shape has a larger influence in the response of the building. This observation is supported by the findings of Sun *et al.* (2017). In their experimental study on seismic resonant behaviour of core-outrigger structure, the authors observed that large accelerations on the upper and middle floors resulted from the second-period resonant ground motion.

	SMALL	MODERATE	STRONG	SEVERE
fixed	0.88	1.74	2.60	3.84
single	0.87	1.71	2.60	3.83
double	0.85	1.68	2.56	3.80
combined	0.86	1.70	2.59	3.79

TABLE 6.11 Average Normalized Peak Accelerations

The same steady trend is observed in the results of normalized base shear in Table 6.12, wherein variations are fairly minimal. However, if the large variation of the average values for each earthquakes is considered (as displayed in Figure 6.13 and Figure 6.15 for inter-storey drifts and base shear, respectively), it seems that earthquake characteristics have a larger influence than outrigger configurations in the response of tall buildings.

	SMALL	MODERATE	STRONG	SEVERE
fixed	0.18	0.36	0.52	0.69
single	0.17	0.35	0.50	0.68
double	0.17	0.34	0.52	0.70
combined	0.17	0.34	0.51	0.67

TABLE 6.12 Average Normalized Peak Base Shear

Considering the results described in previous chapters, it is clear that under optimal design conditions, the addition of viscous dampers reduces both the overturning moment and overall stresses in the core, outriggers and perimeter columns.

As it can be seen in Table 6.13, all damage produced by strong and severe earthquake levels, in the three studied configurations, is concentrated in the core. Due to the stress reduction in the outrigger's frame elements of the double and combined configurations, higher levels of axial stress appear in the perimeter columns. Moreover, by helping to reduce the overall stress, the use of viscous dampers prevents the extension of damage as the ground motion grows larger, if compared with the response of the fixed outrigger. As mentioned before, inelastic responses are triggered when peak overturning moments are ~60% of the maximum overturning moment, for all the evaluated configurations (Table 6.14).

From these results it is not possible to conclude which configuration seems to be the optimal to reduce the overall structural response.

		SMALL	MODERATE	STRONG	SEVERE
core	fixed	0.37	0.74	1.02	1.00
	single	0.34	0.68	0.97	1.00
	double	0.33	0.66	0.98	1.02
	combined	0.32	0.65	0.97	1.01
outrigger	fixed	0.14	0.24	0.33	0.55
	single	0.14	0.17	0.26	0.36
	double	0.09	0.12	0.16	0.18
	combined	0.08	0.10	0.13	0.17
column	fixed	0.12	0.21	0.31	0.49
	single	0.13	0.18	0.24	0.34
	double	0.16	0.21	0.28	0.38
	combined	0.15	0.19	0.25	0.32

TABLE 6.13 Average Normalized Peak Stresses

	SMALL	MODERATE	STRONG	SEVERE
fixed	0.23	0.46	0.64	0.83
single	0.22	0.43	0.61	0.81
double	0.21	0.42	0.60	0.80
combined	0.21	0.42	0.61	0.81

TABLE 6.14 Average Normalized Peak Overturning Moment

§ 6.9 Conclusions

Although most of the conclusions obtained are only applicable to the specific cases described in this paper, general observations can be derived from the numerical studies presented herein:

- Among the studied outrigger configurations, only a double set of damped outriggers and the combined damped and fixed outriggers (attaching viscous dampers in the lower set of outriggers) display larger increase of ζ than the 8% of the single damped outrigger. Optimized ζ of the former two are 8.8 and 8.6%, respectively.
- A double set of outriggers including dampers only in the upper set, will result in a lower damping ratio than that obtained with a damped outrigger alone. In simple words, attaching a conventional outrigger below the damped outrigger will decrease the structure's damping capability.
- Whereas a single damped outrigger exhibits optimal ζ only at λ=0.7-0.8, both double and combined damped and fixed outriggers exhibit broader display of optimal combinations, which offer flexibility of design to the high-rise architecture and distributions of building systems.
- Both double damped and combined damped and fixed outriggers are reducing the hysteretic energy ratio (E_H/E_I). The double damped outrigger is more effective for reducing the damage in the structure when subjected to strong and severe earthquake levels.
- Given the C_d values involved in these optimal designs, and assuming the building costs mostly influenced by the amount of reinforcement steel and viscous dampers, the extra costs due to the double damped are about 50% more expensive than the single damped solution. To the contrary, the additional costs due to the combined damped and fixed solutions are about 16% cheaper than the single damped solution.
- The addition of a second set of outriggers may help to reduce the structural response under the second mode. This seems to be the reason for the important reduction in damage when the building was subjected to Kobe earthquake.

References

1992-1-1, E. 2004. Eurocode 2: Design of concrete structures - Part 1-1: General rules and rules for buildings

1993-1-1, E. 2004. Eurocode 3: Design of steel structures - Part 1-1: General rules and rules for buildings

Applied Technology Council (ATC 72-1), 2010. Modeling and Acceptance Criteria for Seismic Design and Analysis of Tall Buildings, Report No. PEER/ATC-72-1, CA, 242 pp.

Boivin, Y. and Paultre, P. (2012). Seismic force demand on ductile reinforced concrete shear walls subjected to western North American ground motions: Part 2 — new capacity design methods. *Canadian Journal of Civil Engineering*. **39:** 738-750.

Bojórquez, E., Reyes-Salazar, A., Terán-Gilmore, A. and Ruiz, S. (2010). Energy-based damage index for steel structures. *Steel and Composite Structures*. **10:** 331-348.

CESMD, Strong-motion Virtual Data Center. 2014. (Accessed Sep-2014 ww.strongmotioncenter.org)

Choi, H. S. and Joseph, L. 2012. Outrigger system design considerations. International Journal of High-Rise Buildings. 1: 237-246.

CSI (Computers and Structures Inc.).SAP2000 v10 Integrated Finite Element Analysis and Design of Structures. CSI, Berkeley, 2004

DIANA FEA, DIANA (Displacement Analyzer), Version 10.1. User manual. Delft, Netherlands; 2017.

Gidaris, I. and Taflanidis, A. A. 2015. Performance assessment and optimization of fluid viscous dampers through life-cycle cost criteria and comparison to alternative design approaches. Bulletin of Earthquake Engineering. 13: 1003-1028.

Khashaee, P., Mohraz, B., Sadek, F., Lew, H. and Gross, J. L. (2003). Distribution of earthquake input energy in structures. U.S. Department of Commerce

MATLAB R2013b The MathWorks, Inc. Natick, Massachusetts, United States.

Smith, R. 2016. The Damped Outrigger-Design and Implementation. International Journal of High-Rise Buildings. 5: 63-70.

Sun, F., Hu, Z., Chen, G., Xie, L. and Sheng, L. 2017. Shaking table test on seismic resonant behavior of core-outrigger structure. The Structural Design of Tall and Special Buildings. 26: 1-16. 10.1002/tal.1349

Willford, M. and Smith, R. (2008). Performance based seismic and wind engineering for 60 story twin towers in Manila. Proceedings of the 14th World Conference on Earthquake Engineering, (14WCEE), Beijing, China

Zhou, Y. and Li, H. (2014). Analysis of a high-rise steel structure with viscous damped outriggers. *The Structural Design of Tall and Special Buildings*. **13**: 963-979.

7 Integrated discussion: towards an energy-based seismic design of tall buildings with damped outriggers

§ 7.1 Summary

This chapter discusses the main aspects of a design method for outrigger structures using viscous dampers, by integrating the results obtained in the analyses described in chapters 4, 5, and 6.

§ 7.2 Introduction

In seismic engineering, when designing structures incorporating passive dampers it is assumed that the supplemental damping provided by these devices will reduce the structural response and, eventually, damage. This assumption implies that, under strong earthquakes, the host structure will remain elastic whereas dampers will absorb most of the energy that otherwise will be dissipated by extended damage. One of the main questions of this research is whether that assumption is correct, and rather important, what are the boundaries of the cases wherein such assumption can be correctly assumed. Hence, the parametric investigations described in Chapter 4, focused on the aspects of the modelling and structural parameters influencing the behaviour of tall building equipped with fixed and damped outriggers. The main parameters subjected to evaluation were the core-to-column and core-to-outrigger stiffness ratios, location and number of the outriggers, viscous damping coefficient of the dampers, natural frequency of the building, and frequency content of the seismic motion. The optimization of these parameters defined pseudo-optimal configurations, which were further are assessed in terms of response reduction, namely displacement, acceleration, base shear, base moment and stress distribution; and, in terms of energy distributions.

In Chapter 5, the concept of *optimal* configurations was explored in terms of reducing the total input energy introduced by an earthquake. This chapter discussed to which extent the use of passive viscous damped outriggers can avoid damage of the host structure when subjected to strong earthquake motion. The distribution of seismic energy and responses between fixed and damped outrigger structures, subjected to different levels of peak ground accelerations (PGA), was comparatively evaluated. This energy-based assessment relied on the damping-to-input (E_D/E_I), dampers' damping-to-input ($E_{DAMPERS}/E_I$), and hysteretic-to-input (E_H/E_I) energy ratios as parameters for finding optimal configurations.

Since the results obtained from the time-history analyses of a single damped outrigger system showed that only a portion of the earthquake energy will be absorbed by the viscous dampers, the next step was the study of design strategies to improve that linear threshold. Since it was found that with the use of a set of viscous damped outriggers the damping ratio increases in about 6-10%, the natural question was: Could this ratio still be increased by the addition of another set of outriggers? Furthermore, should this additional set be equipped with dampers too? In Chapter 6, therefore, several double damped outrigger configurations for tall buildings are investigated and compared to an optimally designed single damped outrigger in order to find some answers. Using free vibration analyses, double outrigger configurations increasing damping up to a ratio equal to the single-based optimal were first identified. Next, selected configurations were subjected to small, moderate, strong, and severe earthquake levels of eight ground motions to compare their capability for dissipating energy and thus avoiding damage under critical excitations. Last, a simplified economic analysis highlighted the advantages of each optimal configuration in terms of steel reinforcement savings versus damper cost. The results showed that combining a damped outrigger at 0.5 h with a conventional outrigger at 0.7 h is more effective in reducing hysteretic energy ratios and economically viable if compared to a single damped outrigger solution.

Despite the advantages provided by double damped outriggers, these systems could not yet avoid structural damage under strong ground motions.

§ 7.3 Parameters influencing the distribution of energy in an outrigger system

§ 7.3.1 Damping coefficient of the dampers

Frequency response analyses were executed using damping coefficients ranging between 1.5E+02 and 1.5E+08kN-s/m. These values are arbitrary and were found by conducting sensitive analyses through a process of trial and error. It was observed that when C_d < 1.5E+02, the system remains only damped by the core, i.e. without any contribution of the outrigger whatsoever. Beyond 1.5E+08 the structure behaves the same as with fixed outriggers. When C_d=1.5E+03, the dynamic stiffness of the dampers is not enough to combine the axial stiffness given by the columns and the bending stiffness created by the core. When C_d=1.5E+06, the high dynamic stiffness 'ties' the column to the outrigger so vertically they displace the same amount, i.e. as if the structure had only conventional outriggers. The optimal value lies between 1.5E+04 and 1.5E+05 kN-s/m. Given the optimization of additional parameters, such as the outrigger location and stiffness core-to-column and core-to-outrigger ratios, this optimal C_d was found to be 1.18E+08 N-s/m.

Although this optimal value may certainly change for other buildings, a numerical value helps to illustrate the practical implications associated with providing the demanded supplemental damping. For example, commercially-available viscous dampers feature C_d values in the order of 1.5E+03 kN-s/m, hence providing insufficient damping force for the aforementioned case. Alternatively, the number of dampers could be increased according to the space availability in the outrigger (Figure 7.1). Since the number of dampers per outrigger cannot be likely increased beyond eight, the available supplemental damping may not match the optimal supplemental damping. However, the gap between available and optimal supplemental damping ould be yet reduced by modifying the stiffness properties of the key elements of the system, namely, core, outriggers and perimeter columns, as discussed in the next sections.

When introducing more dampers, in the case of double or combined damped outrigger systems, the costs related to the implementation of such a high number of devices may become a valid concern. However, given the C_d values involved in these optimal designs, and assuming the building costs mostly influenced by the amount of reinforcement steel and viscous dampers, the extra costs due to the double damped are about 50% more expensive than the single damped solution. On the contrary, the additional costs

due to the combined damped and fixed solutions are about 16% cheaper than the single damped solution.

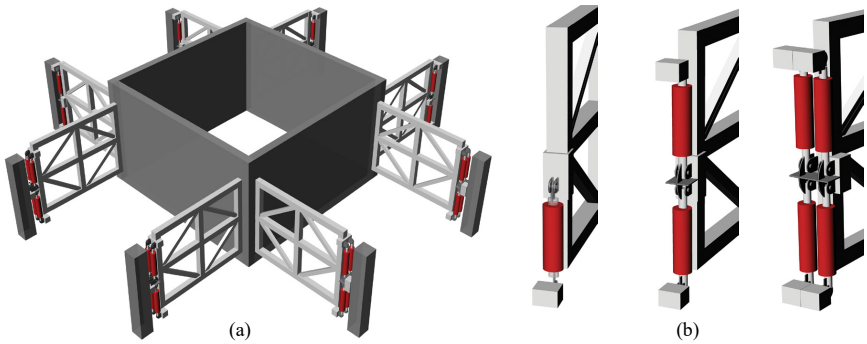

FIGURE 7.1 Typical arrangement of frame outrigger used in this research (a) and possible combinations of dampers (b).

§ 7.3.2 Number and position of the outriggers

The influence of the outrigger location in the increase of the inherent damping ratio ζ was studied by assuming a range of locations between 0.1 and 0.9 of the total height of the building, under free-vibration analyses. The outrigger location is described in terms of a non-dimensional parameter λ, such that location of the outrigger = λ*H, hence λ=0.1 – 0.9.

When optimal dampers size are considered, the optimal $\zeta$is achieved when λ=0.6 – 0.8. Without considering optimal dampers sizes, λ < 0.4 has less effect on improving the overall damping ratio of the building, if compared to values of λ >= 0.4. This observation is in agreement with other studies (Huang and Takeuchi, 2017), and suggests that such optimal location of the outrigger is somewhere between 0.4 and 0.9. However, no further modification of the design parameters have any influence on the frequency shift of the damped outrigger, when λ<0.6. Frequency shifts become more significant as the outrigger approaches the roof.

Double and combined damped + fixed outriggers exhibit broader display of optimal combinations, where the lower set of outrigger is at λ=0.5 and the upper one at λ=0.7 and 0.8, respectively.

§ 7.3.3 Modal damping and damping ratios

Inherent damping ratio ζ, assumed as equivalent viscous damping coefficient, was calculated using Rayleigh damping with values = 1.5, 2.0, and 2.5%. The increase in the optimal damping ratio was proportional to the inherent initial damping ratio.

A single damped outrigger displays a ζ = 8%. Optimal double set of damped outriggers and the combined damped + fixed outriggers (attaching viscous dampers in the lower set of outriggers) display ζ equal to 8.8 and 8.6%, respectively. A double set of outriggers including dampers only in the upper set, will result in a lower damping ratio than that obtained with a damped outrigger alone. In simple words, attaching a conventional outrigger below the damped outrigger will decrease the structure's damping capability.

Optimal damping coefficient C_d and optimal location λ have a major influence in the optimal damping ratio ζ. It was found, nevertheless, that the optimal damping varies with the mode, so no single outrigger location will lead to reduce the response of all the modes to its minimum. This is in agreement with other studies (Chen *et al.*, 2010).

§ 7.3.4 Stiffness core-to-columns and core-to-outriggers ratios

The initial FE models considered a core design about 2.5 times stiffer than the combined bending and shear stiffness of the outrigger, i.e. ρ_{cto} ~=2.5. The core bending stiffness was about 2.25 times stiffer than the axial stiffness of the perimeter columns, i.e. ρ_{ctc} ~= 2.3. Sensitivity analyses extended these ratios over a range between one and four. Values of ρ_{ctc} smaller than one are not practical as they would demand the use of columns with comparatively large cross sections in combination with a core of comparatively small wall dimensions. Values of ρ_{ctc} > 4, on the other hand, imply that the axial stiffness of perimeter columns is less than 25% of the bending stiffness of the core. Moreover, according to the study of Tan *et al.* (2014), ρ_{ctc} 'should not be larger than four to achieve a supplementary 5% damping level'. The results of analyses showed that effect of ρ_{ctc} is limited to a general 1% increase of ζ, for a given λ and C_d. However, when λ and C_d approximate to the optimal values, the effect of ρ_{ctc} may imply an overall ζ increase in 7%. This suggests that if required dampers sizes are not be available, a modification in the ratio ρ_{ctc} may help to increase the overall damping ratio. It should be noted that such increase will only occurs if ρ_{ctc} decreases.

Eigen-frequency analyses were conducted using fixed and damped outriggers to understand to which extent the combined parameters ρ_{cto} and ρ_{ctc} modify the building's fundamental frequency. The results showed that frequency shift is larger in the fixed outrigger (about 0.10Hz), compared to that of the damped outrigger (about 0.6Hz). In addition, in the case of the damped outrigger, the influence of ρ_{cto} is almost none and the frequency shift is due almost exclusively to the variation of ρ_{ctc}. With the increase in λ, the outrigger exerts major influence in the frequency shift, reaching its maximum around λ=0.8-0.9 in both fixed and damped outriggers. Hence that none of the parameters λ, ρ_{ctc} and ρ_{cto}, have any influence in the frequency shift of the damped outrigger, when λ<0.6. The fact that frequency shifts become more significant as the outrigger approaches the roof, and that only ρ_{ctc} has influence of such frequency shifts, supports the conclusion that both λ and ρ_{ctc} exert their influence by modifying the building's natural frequency. The fact that ρ_{cto} does modifies the response but not the frequency, suggests that its influence is closely related to the effect of the viscous dampers.

The influence of the combined parameters ρ_{cto} and ρ_{ctc} on the seismic energy distributions was studied through time-history analyses of the damped outrigger. The results showed that when the outrigger is flexible (ρ_{cto} =4), E_I is comparatively large regardless the modification of ρ_{ctc}, under all earthquake levels except severe. Under this last one, the use of a rigid outrigger (ρ_{cto} =1) implies larger amount of input energy in the system. This sudden shift may be related to the assumption of the linear behaviour of the dampers: under small, moderate, and strong earthquakes, the velocities across the damper might not be large and hence the damping forces benefit from a rigid outrigger. Under severe earthquakes, the damping forces will be proportionally increased to the now large velocities and hence damping forces are amplified by the effect of a rigid outrigger.

§ 7.3.5 Feasibility of supplying the required control force

The exponent K determines the sensitivity of the damper, as a damping system, to the magnitude of the motion to which the system is subjected. According to the literature reviewed in Chapter 2, range of k is often set between 0.1 and 2. With high exponents (k>1), the damping forces will be amplified by the exponential increase of the velocity across the damper. The inverse effect occurs when low exponents (k<1) are used. A unit exponent (k=1) obviously implies a linear effect in the resulting damping force, as a consequence of the neither increase nor decrease of the velocity across the damper. Also suggested by the previously revised literature, a k=>1 is been suggested for wind

applications, whereas lower values (k~=0.2) is been suggested for seismic control. This is because a low exponent *k* guarantees that the high velocity amplitudes produced in a structure by strong earthquakes, will not be proportionally translated to large damping forces. This suggestion comes, on the one hand, from the technical limitation of commercially available dampers to produce the comparatively very large damping forces resulting from seismic-induced motion. On the other hand, large damping forces could damage the host structure to which the damper is attached too, at a local level, hence demanding an increase in stiffness of the surrounding elements.

Despite these disadvantages, in this study an exponent $k=1$ has been used. In order to prove whether damping energy can overcome hysteretic energy, damping forces need to be kept at a realistic level, from a technical point of view. This does not mean to use a safety valve to reduce the damping force in case of an excessive outcome, but to assume that damping forces will not conveniently increased ($k>1$) or safely reduced ($k<1$), i.e. the exponent $k=1$.

§ 7.3.6 Optimal design of damped outriggers

As the effectiveness of energy-dissipating outrigger systems as they are installed at very specific locations on the building structure is bound to specific design conditions, the host structure has to meet some requisites for ensuring a proper application. Nevertheless, a tentative methodology for the optimal design of damped outriggers may follow these steps:

1. Design the outrigger, core and column using stiffness ratios of 2-2.5 approximately. This ensures that both core and outriggers possess adequate flexibility. In order to provide an adequate margin of safety, the outrigger strength must be twice as larger as the maximum damping force provided by the dampers attached to it. Once the strength is guaranteed, and if different configurations are available, the selected outrigger configuration must provide a comparative larger displacement, i.e. it must be flexible to ensure adequate ductility.
2. Through sensitivity analyses, study the optimal location of the outrigger for increasing the damping ratio, the damping coefficient, and rather important: the performance target;
3. Define the damper size (damping coefficient) and study the feasibility in the number of the dampers;
4. Define the optimal location and study the influence of the stiffness ratios in the structural performance.

§ 7.4 Assessment of the energy demands due to strong-earthquake induced motion

Initially it was assumed that viscous damped outrigger structures would exhibit a comparatively improved performance if subjected to long-period ground motions. For this reason earthquake records displaying a PGA/PGV ratio below 8 were selected to conduct the studies. It was expected that lower PGA/PGV ratios were indicative of a better chance for the damped outrigger to eliminate, or at least largely reduce, damage due to strong ground motions. However, on the light shed by the simulations, it seems clear that the solely use of this ratio is not enough; because in tall buildings higher modes may become predominant during the transient response, a good indicator of the building performance is the plot of energy input (E_I) for different fundamental periods (T). For example, in Figure 7.2a, given the three main modes it is clear that most of the energy input –hence the energy demand- must be dissipated by the first mode of the building. However, in the studies conducted in this research, larger demands of input energy (and damage) occurred when the building was subjected to Kobe earthquake (Figure 7.2b); this proves that actually the second mode was influencing the response. The fact that double configurations were quite successful in reducing damage under Northridge and El Maule earthquakes (Figure 7.2c), proves that by adding a second set of outrigger the influence of the second mode was further controlled. Following the same logic, since Michoacan earthquake (Figure 7.2d) does not introduce large energy inputs at any of the predominant modes, no damage was produced neither the performance of the damped outriggers was required.

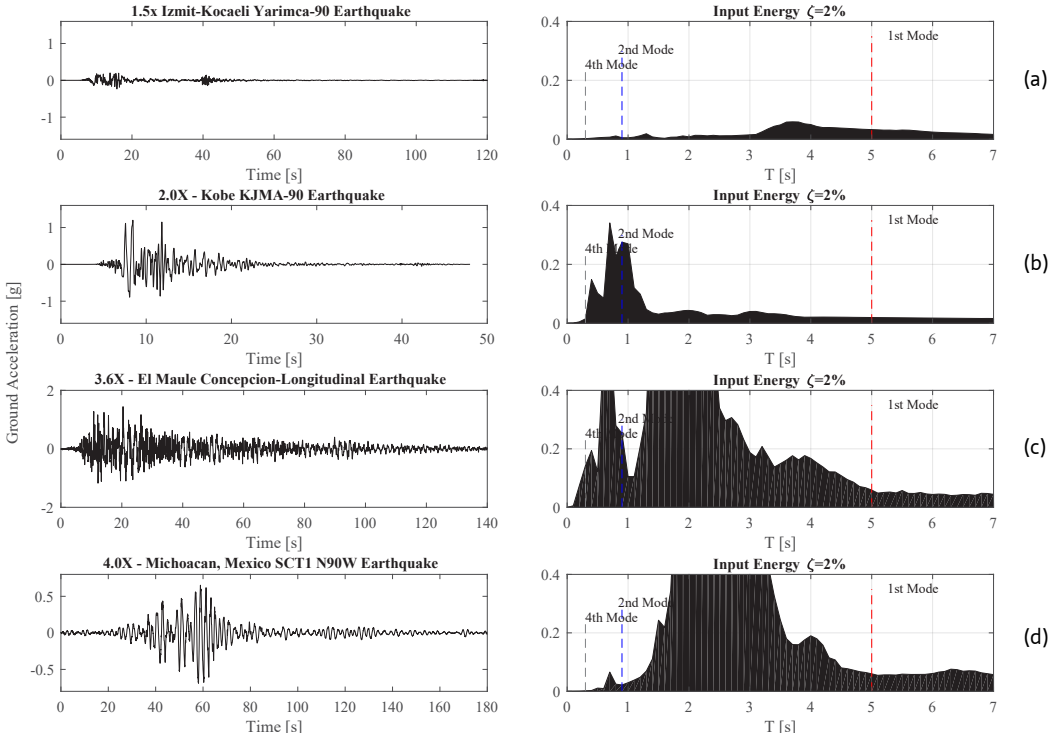

FIGURE 7.2 Scaled ground motions and their corresponding input energy (E_I), displaying the three main periods of the structures studied.

§ 7.5 Assessment of the energy capacity of tall buildings with damped outriggers

§ 7.5.1 Energy dissipated by the core

The core is the main source of seismic energy dissipation in a tall building. Despite that some studies have pointed out the formation of plastic hinges at the regions adjacent to outriggers (Beiraghi and Siahpolo, 2017), in the studies undertaken in this research, plasticity was confined almost exclusively to the plastic hinge area, located at the base zone, between the 1st and 6th floor. The plastic hinges concentrated on the lower zone of the core due to the action of bending and certainly the contribution of 2nd order effects (such as P-Δ). Since it is been demonstrated that the distribution of inelastic energy along the building's height is strongly related to the amount of plastic hinges used in the modelling of the core (Beiraghi *et al.*, 2016), the analytical models considered the use of general nonlinear material models throughout almost the whole finite element model. Analyses based on this modelling, allowed determining that the core is the main dissipative source of both damping and hysteretic energy.

Modelling the core with and without a uniform distribution of longitudinal reinforcement affected the energy distribution. Under severe earthquake levels, damping energy (E_D) and input energy (E_I) vary in about 10%, dampers energy ($E_{dampers}$) in almost a 20% and hysteretic energy (E_H), in more than 25%.

A possible solution to avoid damaging the core when employing dampers with lower damping coefficient is to increase the thickness of the core walls towards the base of the building. This common practice in the design of tall buildings' core not only avoids plasticity of the lower regions of the shear walls but also increases its flexural ductility (Willford and Smith, 2008). Introducing a second set of outriggers does not change the fact of the core dissipating most of the energy, as in double and combined damped+fixed outrigger configurations, all damage produced by strong and severe earthquake levels, was too concentrated in the core.

§ 7.5.2 Energy dissipated by the outrigger

Both core and outrigger were modelled using nonlinear settings, as they are expected to be the major sources of hysteretic energy dissipation. However, with the addition of viscous dampers the outrigger has a minor load-bearing role. Hence if, due to ductility demands, plastic hinges need to be concentrated in the outrigger, its general sections can be reduced provided that the dampers will account for the extra flexibility of the outrigger structure.

By only considering the distribution of damping energy taken by the outriggers, it can be noted the increasing role of the outrigger in the dissipation of energy as the ground motion becomes stronger. When the outrigger is flexible (ρ_{cto} =4), E_I is comparatively large regardless ρ_{ctc}, under all earthquake levels except by severe. Under this latter, the use of a rigid outrigger (ρ_{cto} =1) implies larger amount of input energy in the system. This shift may be the result of large damping forces being linearly amplified by the high velocities of the severe motions.

§ 7.5.3 Energy dissipated by the perimeter columns

Perimeter columns, on the contrary, were modelled with elastic elements. Unless the use of a small cross-sectional area is combined with a large core bending deformation, column strength demand can be safely expected to be smaller than 70% of the yielding strength, even under severe earthquake loading, and thus remaining within the elastic threshold (Figure 7.3).

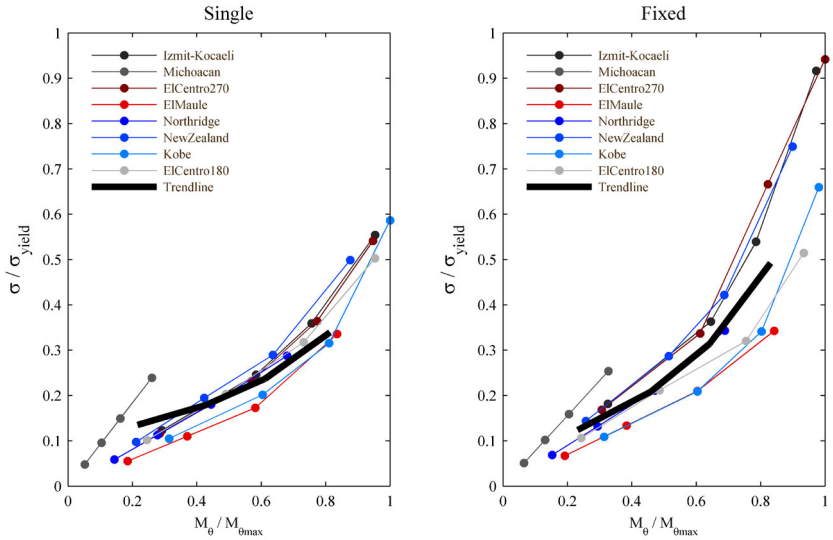

FIGURE 7.3 Normalized *column* stress (σ/σ_{yield}) to normalized overturning moment ($M\theta/M\theta_{-max}$) of the studied outrigger configurations subjected to four earthquake levels of all ground motions.

Although due to the stress reduction in the outrigger's frame elements of the double and combined configurations, higher levels of axial stress appear in the perimeter columns, these are not yet high enough as for provoking the columns to yield.

§ 7.5.4 Energy dissipated by the dampers

As the ground motion becomes stronger, viscous dampers effectively reduce the potential of damage in the structure if compared to conventional outriggers. Nevertheless, the contribution of the viscous dampers to the improved structural response seems to follow a twofold mechanism: One is direct, i.e., by explicitly increasing the amount of input energy dissipated by the action of the damping force in the structure. According to energy equations derived in Chapter 3, the energy dissipated by the dampers is proportional to the product of C_d and the velocity across the damper, modified by the exponent κ. In the parametric study, however, *k* was taken equals to one since comparatively excessive damping forces may help to understand the role of the outrigger's bending and shear stiffness in the distribution of seismic energy in the building structure. Since the resulting forces were indeed large, the use of a relief valve was introduced in the magneto-rheological damped outriggers.

Second one is indirect, i.e. by helping the reduction of stress or response. The addition of viscous dampers to the outriggers, under optimal design conditions, reduce the overturning moments and stresses of the main components of the system, i.e. core, outriggers and perimeter columns, under strong earthquakes –if compared to a conventional outrigger. Hence, by helping to reduce the overall stress, the use of viscous dampers prevents the extension of damage as the ground motion grows larger, if compared with the response of the fixed outrigger. This leads to the conclusion that achieving elastic response under strong earthquake motions by the use of viscous dampers also requires an increase of the overall strength of the host structure. Moreover, the fact that only in this case the hysteretic energy is larger than in the fixed case, supports the observation that to avoid damage the optimal design of the damped outrigger must be based on the balanced increase of both E_D/E_I and $E_{dampers}/E_I$ ratios.

§ 7.6 Research question revisited: design for elasticity?

§ 7.6.1 Damping (f)or damage?

The addition of supplemental damping in the outriggers may not significantly decrease the building response in terms of peak responses, either. This is the case for the normalized inter-storey drift and base shear response as the differences between fixed and damped responses are not significant. On the other hand, according to the study described herein, under optimal design conditions, the addition of viscous dampers reduces both the overturning moment and overall stresses in core, outriggers and perimeter columns. Moreover, by helping to reduce the overall stress, the use of viscous dampers prevents the extension of damage as the ground motion grows larger, if compared with the response of the fixed outrigger.

Using viscous dampers reduces the absorbed energy in the host structure, if compared to a conventional outrigger. Since dampers increase the dissipative action of energy by damping, the energy that must be absorbed by hysteresis of the structure is reduced. This does not mean that the addition of viscous dampers directly eliminates energy dissipation by plastic deformations in the structure, but it certainly aids in its reduction.

An apparent reason for the dampers being unable to completely reduce the damage under critical earthquakes because the peak E_H/E_I usually precedes the peak $E_{dampers}/E_I$. This is due to the fact that all the damage induced by the different levels of earthquake in the outriggers equipped with dampers is concentrated in the core, provoked by the overpass of the tensile strength, i.e. by yielding of the longitudinal reinforcement. In the case of damage in the outrigger, the compressive strength was overpassed producing buckling in some of the braces and/or chords

By observing at the regions under the curves displayed in Figure 7.4, one could deduce that the addition of supplemental damping, in the form of viscous dampers in the tips of the cantilevered outriggers, is more effective in reducing the total energy in the system than relying on an increase in the overall stiffness. Preliminarily, the conclusion that increasing dynamic stiffness is more effective than simply increasing stiffness seems to be proved by these numerical and simple models. Nonetheless, previous research studies using FE models support these general conclusions. For example, since the input energy has been reduced, it is possible to conclude that additional damping not only relaxes the demand over structural damping [ref to previous article] but also decreases the region of elastic strain and kinetic energies.

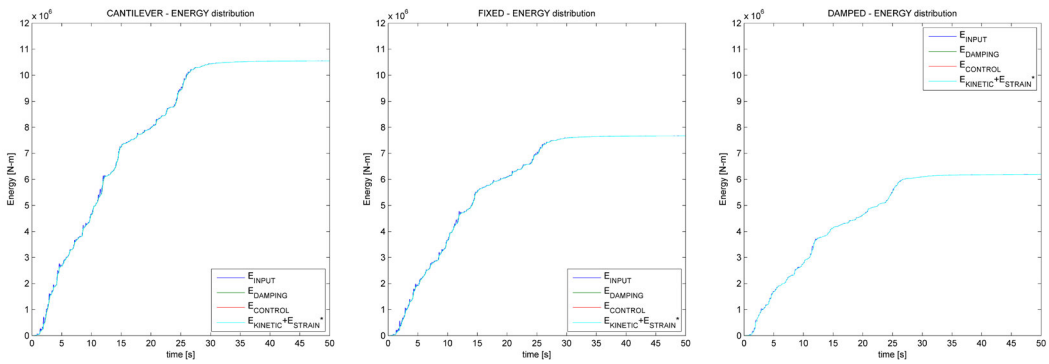

FIGURE 7.4 Distribution of seismic input energy in the cantilever, fixed, and damped outrigger models

§ 7.6.2 Strategies to extend the elastic response threshold of viscous damped outrigger systems

Once optimized the reduction in the hysteretic energy due to the addition of supplemental damping to conventional outriggers is not significant. This relatively small decrease in E_H/E_I may be explained by two observations: (1) the dampers' damping coefficient (C_d) and the outrigger's location (λ) are the parameters that most influence the tall building's response. Since these two parameters have been already optimized in the studied configurations, further improvements –beyond each optimal, are unlikely to take place; (2) as suggested by columns E_D/E_I and $E_{DAMPERS}/E_I$, most of the energy dissipated by the dampers seems to be partially subtracted from that dissipated from the inherent structural damping. However, these configurations are indeed effective for reducing the building's response by the end of the ground motion.

In terms of ζ only a double set of damped outriggers and the combined damped and fixed outriggers (attaching viscous dampers in the lower set of outriggers) displays larger increase than that of the single damped outrigger. Optimized ζ of the former two are 8.8 and 8.6%, respectively, which is in practical terms, almost the same but with the double damped outrigger requiring more dampers. Nevertheless, from an economical point of view, the use of combined damped and fixed outriggers is not only equally optimal but cheaper than its counterpart using a double set of damped outriggers.

From the average ratios E_D, $E_{DAMPERS}$, and E_H to E_I of the three above described configurations, it can be stated that both double damped and combined damped and fixed outriggers are reducing the hysteretic energy ratio (E_H/E_I), and hence becoming more effective in reducing structural damage under strong earthquake motions. However, as the double damped configuration requires the use of more dampers, it is assumed to be comparatively more expensive. The combined damped and fixed configuration, compared with the single damped one, is effectively reducing the hysteretic energy and maintaining the levels of energy dissipated by both inherent damping and viscous dampers.

§ 7.7 Slenderness and plan design of tall buildings with damped outriggers

§ 7.7.1 Slenderness and aspect ratio of tall buildings

The core needs to be designed with a certain degree of flexibility: a large relative motion between perimeter columns and outrigger is necessary for the dampers to dissipate energy. Slenderness guarantees that the building's design is controlled by bending and axial stress rather than by shear deformation. The aspect ratio, i.e. the ratio height/width of the building, should be equal or larger than 5, in order to obtain a slender structure[20]. However, this slender or tall building cannot be so high, because beyond 250m height is unrealistic to suppose only an earthquake-based scenario inducing the dynamic response of the building. Consequently, to ensure both the slenderness and a realistic earthquake-exclusive scenario, the height of the building should be around 200m (50 storeys). Such a realist earthquake-exclusive scenario can be only observed in countries where hazards due to strong winds are not comparable, neither in frequency nor level of damages, to those derived from the occurrence of earthquakes. For instance, in Chile there is no statistical data about string winds, nor a norm method for calculating wind forces in function of the building height. The reason seems to be the complete absence of such strong winds in the country. However, for the design of the two tallest buildings in Chile, *Titanium* (200 m) and *Costanera Center* (300 m), wind tunnel tests were required to assess the influence of the neighbour buildings over the wind pressure in the respective buildings[21]. According to these studies it was concluded that the response is mixed: stress and loading in foundations is dominated by the seismic action, while in the upper third of the building height, results from the application of seismic and wind loading are similar. Consequently, lateral displacements due to wind action should not be neglected.

20 There is no agreement about this value though; Smith and Coull (1991), in the context of the use of dynamic methods in wind loading analysis, and citing UBC, pointed out the validity of such methods for "exceptionally tall, slender, or vibration-prone buildings. Those may be defined (...) as those of height greater than 400ft (123m), or of a height greater than five times their width, or those with structures that are sensitive to wind-excited oscillations". Some authors suggest higher values, such as 8 or 10.

21 Guendelman, T. Personal communication

§ 7.7.2 Building plan incorporating outriggers

In office buildings, the design of the core has to be sized according functional requirements, such as number of lifts, stairs, circulations, etc. According to the three references displayed in Figure 7.5 and Table 7.1, the average size of the core in office buildings is about 420m^2, which gives a square dimension of 20.5m (Table 7.2). The usable average space between core and perimeter columns must be defined according to the actual location of the building. For instance, in Germany and the Netherlands, such span is 7 meters, whereas in UK and USA it ranges between 9 and 12 meters. In Chile such span is not regulated by norm, but common practice has defined this span in about 10 meters, including perimeter columns (see Appendix F: Average distance between central core and perimeter columns in Chilean office buildings).

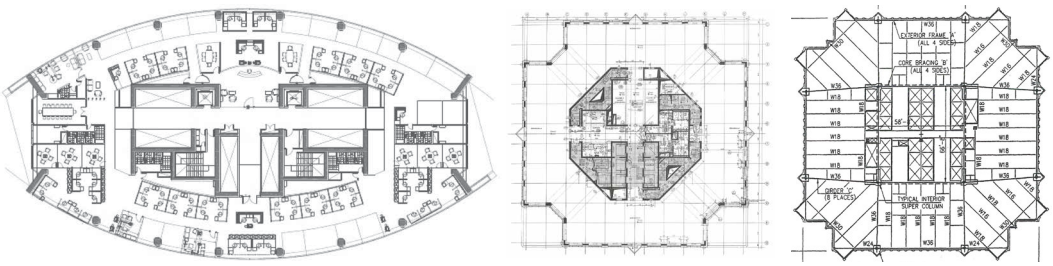

(a) (b) (c)

FIGURE 7.5 Floor plans of Titanium (a), Messeturm (b), and Nations Bank Plaza (c) buildings.

STOREY PLAN DISPLAYED	TYPICAL FLOOR	48TH - 56TH FLOOR	TYPICAL FLOOR
country	Chile	Germany	USA
building name	*titanium*	*messeturm*	*nations bank plaza*
height (m)	190	228	227
storeys	52	63	55
storey area (m2)	1729	1490	2387
core area (m2)	441	465	364
square core equivalence (m)	21 x 21	21.5 x 21.5	19 x 19

TABLE 7.1 Comparative core sizes in 200m office buildings, located in Chile, Germany and USA.

LOCATION CRITERIA	CORE WIDTH	USABLE DEPTH	BUILDING WIDTH	ASPECT RATIO	SLENDER?
Chile	20.5	9	38.5	5.19	yes
Germany / the Netherlands		7	34.5	5.80	yes
USA		12	44.5	4.49	no

TABLE 7.2 Usable space depth according to the location of the building

§ 7.8 Conclusions

From the overall discussion presented in this chapter, the following general conclusions can be obtained. These will be further addressed in Chapter 8.

- Optimal damping coefficient C_d and optimal location λ are the most influential design parameters
- There is no optimal design for all the cases
- Viscous damped outrigger systems reduce the damage potential under strong earthquakes
- No optimal damped outrigger configuration can reduce completely the damage during strong earthquakes
- The main source of hysteretic energy dissipation is the core
- Under certain conditions, double damped outriggers overpass the performance of single damped outriggers
- Optimal double damped outrigger systems offer flexibility of design and cost-saving

References

Beiraghi, H., Kheyroddin, A. and Kafi, M. A. 2016. Energy dissipation of tall core-wall structures with multi-plastic hinges subjected to forward directivity near-fault and far-fault earthquakes. The Structural Design of Tall and Special Buildings. 25: 801-820. 10.1002/tal.1284

Beiraghi, H. and Siahpolo, N. 2017. Seismic assessment of RC core-wall building capable of three plastic hinges with outrigger. The Structural Design of Tall and Special Buildings. 26: e1306-n/a. 10.1002/tal.1306

Chen, Y., McFarland, D., Wang, Z., Spencer, B. and Bergman, L. 2010. Analysis of Tall Buildings with Damped Outriggers. Journal of Structural Engineering. 136: 1435-1443. 10.1061/(ASCE)ST.1943-541X.0000247

Huang, B. and Takeuchi, T. 2017. Dynamic Response Evaluation of Damped-Outrigger Systems with Various Heights. Earthquake Spectra. 33: 665-685. 10.1193/051816EQS082M

Prieto Hoces, A. 2011. Interfaz ambiental en edificios de oficina: envolvente de espesor programático variable como sistema de mediación ambiental pasivo

Tan, P., Fang, C. and Zhou, F. 2014. Dynamic characteristics of a novel damped outrigger system. Earthquake Engineering and Engineering Vibration. 13: 293-304. 10.1007/s11803-014-0231-3

Willford, M. and Smith, R. 2008. Performance based seismic and wind engineering for 60 story twin towers in Manila

8 Conclusions

§ 8.1 Summary

This chapter provides the conclusions of the research presented in the previous chapters. It includes conclusions from the parametric analyses, and energy-based assessment of single and double viscous damped outrigger systems. Finally, recommendations for future research are also given.

§ 8.2 Introduction

From the numerical investigations performed in this research is concluded that among several design parameters, damping coefficient C_d and outrigger location λ have a major influence in the obtaining of an optimal damping ratio ζ. This optimal damping ratio may not necessarily imply a significant reduction in the overall response of the outrigger structure. Complementary modification of the stiffness ratios may help to improve the effect of the viscous damped outriggers in the reduction of response of the building. When subjected to strong motion, it was found that the use of viscous damped outriggers effectively reduce the potential of damage in the structure if compared to conventional outriggers. The addition of viscous dampers to the outriggers, under optimal design conditions, reduce the overturning moments and stresses of the main components of the system, i.e. core, outriggers and perimeter columns, under strong earthquakes –if compared to a conventional outrigger. Dampers cannot, however, reduce completely the damage under critical earthquakes because the peak E_H/E_I usually precedes the peak $E_{DAMPERS}/E_I$; Hysteretic energy is concentrated in the core, whose damage is provoked by the overpass of the tensile strength. Addition of another set of outriggers and combination of conventional with damped outriggers may improve the reduction of response and the occurrence of damage, under certain conditions. From the numerical analyses with double damped and combined damped and fixed outriggers, it is concluded that both system are effective for further reduction of the hysteretic energy ratio (E_H/E_I). The double damped outrigger is more effective for

reducing the damage in the structure when subjected to strong and severe earthquake levels. A combined conventional and damped outrigger system may not only offer a larger versatility for architectural considerations, but also some economic savings.

§ 8.3 Conclusions from the parametric analyses

§ 8.3.1 Optimal damping coefficient C_d and optimal location λ are the most influential design parameters

From the numerical analyses using FE models with conventional and damped outrigger systems, under free vibration, it is concluded that optimal damping coefficient C_d and optimal location λ have a major influence in the optimal damping ratio ζ and, thus, in the overall response of the outrigger structure. In addition, when λ and C_d approximate to the optimal values, the effect of ρ_{ctc} may imply an overall ζ increase in 7%. This suggests that if required damper sizes are not available, a modification in the ratio ρ_{ctc} will help to increase the overall damping ratio. It should be noted that such increase occurs only if ρ_{ctc} decreases.

Both λ and ρ_{ctc} exert their influence by modifying the building's natural frequency. The fact that ρ_{cto} does modifies the response but not the frequency, suggests that its influence is closely related to the effect of the viscous dampers. None of the parameters under discussion, namely λ, ρ_{ctc} and ρ_{cto}, have any influence on the frequency shift of the damped outrigger, when $\lambda<0.6$. Frequency shifts become more significant as the outrigger approaches the roof.

Finally, when the outrigger is flexible (ρ_{cto} =4), E_I is comparatively large regardless ρ_{ctc}, under all earthquake levels except by severe. Under this latter, the use of a rigid outrigger (ρ_{cto} =1) implies larger amount of input energy in the system. This shift may be the result of large damping forces being linearly amplified by the high velocities of the severe motions.

§ 8.3.2 There is no optimal design for all the cases

From the parametric analyses, it is obtained that regardless C_d, $\lambda < 0.4$ has less effect on improving the overall damping ratio of the building, if compared to values of $\lambda >= 0.4$. This suggests that optimal λ is somewhere between 0.4 and 0.9. Nevertheless, the optimal damping varies with the mode, so no single outrigger location will lead to reduce the response of all the modes to its minimum.

§ 8.3.3 The distribution of energy is determined by the type of nonlinear modelling

The use of a model without the influence of either the lateral confinement or the lateral may fail to define to which extent the non-accounted increase of the wall strength would influence the energy dissipation mechanisms of the structure, especially after cracking. Nonetheless, in the cases studied here, it can be noticed that the use of lateral confinement does not substantially modify the distribution of input energy (variation < 0.0000001%).

In the case of modifications in the distribution of longitudinal steel reinforcement of the core along the height will do affect the energy distribution. Modelling the core with and without a uniform distribution of longitudinal reinforcement affects the energy distribution. Under severe earthquake levels, damping energy (E_D) and input energy (E_I) vary in about 10%, dampers energy ($E_{dampers}$) in almost a 20% and hysteretic energy (E_H), in more than 25%.

Physically and geometrically nonlinear effects were considered in the analyses in Diana. The total strain crack model is used to define the nonlinear behaviour of the concrete, which is characterized by tensile cracking and compressive crushing. This constitutive model is based on total strain and describes the tensile and compressive behaviour of the concrete based on a bi-linear stress-strain relationship. In the case of the outrigger, two models of plasticity are considered: ideal elastoplastic (also called elastic-perfectly-plastic [EPP]) or bilinear model and the other including a strain hardening slope. Both were defined by using Von Mises plasticity models. The reason for using these two models is that bilinear models allows for a primary assessment of the steel stress-strain relationship without the extra reserve of ductility given by the hardening post-yield and thus increasing the safety factor in the design. For instance, results using similar modelling parameters but different material definition (bilinear and strain hardening) showed that outrigger's strength increased with the addition of the post-yield strain

hardening, whereas the curve force-displacement maintained the same shape. The use of these plasticity models explains the bilinear structural response and distribution of energy.

It is worth to mention here that despite 3D models were built for the initial analyses, 2D models were used latter on as they save computational time, reduce considerable the error margin by reducing the amount of DOFs involved and are as accurate as a 3D model can be.

§ 8.4 Conclusions from the analyses of viscous damped outrigger systems

§ 8.4.1 Viscous damped outrigger systems reduce the damage potential under strong earthquakes

From the numerical analyses using FE models with conventional and damped outrigger systems, subjected to four levels of ground motions, it was concluded that as the ground motion becomes stronger, viscous dampers effectively reduce the potential of damage in the structure if compared to conventional outriggers. The results confirm that increasing dynamic stiffness by using dampers is more effective than simply increasing stiffness by adding outriggers to reduce the overall response of core structures. The use of dampers in the outrigger seems to be effective in reducing both kinetic and strain energies, which also explains the overall decrease in the accelerations.

In addition, the use of viscous damped outriggers, under optimal design conditions, reduces the overturning moments and stresses of the main components of the system, i.e. core, outriggers and perimeter columns, under strong earthquakes –if compared to a conventional outrigger. Nevertheless, the results of this study also suggested that neither inter-storey drifts, peak accelerations nor base shear are substantially reduced with the addition of viscous dampers to the outriggers. These results reinforce the conclusion that no optimal configuration can be considered optimal for reducing all structural responses.

§ 8.4.2 No optimal damped outrigger configuration can reduce completely the damage during strong earthquakes

From the numerical analyses using FE models with conventional and damped outrigger systems, subjected to four levels of ground motions, it was concluded that damped outriggers cannot reduce completely the structural damage under critical earthquakes because the peak E_H/E_I usually precedes the peak $E_{dampers}/E_I$. This occurs because the maximum level of energy dissipation provided by dampers tends to occur towards the end of the motion, whereas hysteretic energy (or damage) tends to occur at the beginning of the strong motion. On the other hand, since dampers increase the dissipative action of energy by damping, the energy that must be absorbed by hysteresis of the structure is reduced. This does not mean that the addition of viscous dampers directly eliminates energy dissipation by plastic deformations in the structure, but it certainly aids in its reduction. Finally, the results showed that the overall reduction in the overturning moments and stresses of the main components of the system under strong earthquakes, compared to a conventional outrigger, extends the elastic threshold of the tall building structure wich depends then on the characteristics of the ground motion.

§ 8.4.3 The main source of hysteretic energy dissipation is the core

Hysteretic energy is concentrated in the core, whose damage is provoked by the overpass of the tensile strength. Hence, the core is the main dissipative source of both damping and hysteretic energy. With the addition of viscous dampers the outrigger has a minor load-bearing role, so plastic hinges concentrate on the lower zone of the core due to the action of bending and certainly the contribution of 2nd order effects (such as P-Δ). If, for example, due to ductility demands plastic hinges need to be concentrated in the outrigger, its general sections can be reduced provided that the dampers will account for the extra flexibility of the outrigger structure. The main advantage of adding viscous dampers to the outriggers is the overall reduction of stress in the members, thus increasing ductility in the structure.

§ 8.5 Conclusions from the analyses of double damped outrigger systems

§ 8.5.1 Under certain conditions, double damped outriggers overpass the performance of single damped outriggers

From the analyses of several configurations of double damped and combined fixed+damped outrigger systems described in Chapter 6, under free vibration, it is concluded that only a double set of damped outriggers and the combined damped and fixed outriggers (attaching viscous dampers in the lower set of outriggers) display larger increase of ζ than the 8% of the single damped outrigger. Optimized ζ of the former two are 8.8 and 8.6%, respectively.

Despite this increase of ζ, double and combined outrigger solutions do not present further reduction of peak inter-storey drifts when compared with the single configuration. This seems to suggest that configurations with optimal ζ might not be further optimized for inter-storey drifts reductions. From these results it is not possible to conclude which configuration seems to be the optimal to reduce the overall structural response. However, it should be noted that a double set of outriggers including dampers only in the upper set, will result in a lower damping ratio than that obtained with a damped outrigger alone. In simple words, attaching a conventional outrigger below the damped outrigger will decrease the structure's damping capability.

From the analyses of optimal double set of damped outriggers and the combined damped and fixed outriggers, subjected to eight different ground motions, it is concluded that these configurations reduced the hysteretic energy ratio (E_H/E_I). In addition, the double damped outrigger is more effective for reducing the damage in the structure when subjected to strong and severe earthquake levels. However, such reduction in the hysteretic energy provided by the supplemental damping is not significant. This relatively small decrease in E_H/E_I may be explained by the fact that optimal configurations can hardly be subjected to further level of optimizations.

From all the time-history analyses using a set of eight earthquake records, it can be concluded that viscous damper outrigger structures exhibit a comparatively improved performance if the use of two outriggers matches the predominance of the 2nd mode of vibration, given by the ground motion frequency.

§ 8.5.2 Optimal double damped outrigger systems offer flexibility of design and cost-saving

From the analyses of several configurations of double damped and combined fixed+damped outrigger systems, it is concluded that both double and combined damped and fixed outriggers can reach optimal values of ζ, by displaying a broad display of optimal combinations. These quasi-optimal configurations have an advantage over a single damped outrigger, as they offer flexibility of design to the high-rise architecture and distributions of building systems. It is worth to notice that the use of multiple outriggers is desired in tall buildings.

From the simplified economic analyses of optimal double set of damped outriggers and the combined damped and fixed outriggers, it is concluded that the extra costs due to the double damped are about 50% more expensive than the single damped solution. This is valid within the framework given by the C_d values involved in these optimal designs, and assuming the building costs mostly influenced by the amount of reinforcement steel and viscous dampers. To the contrary, the additional costs due to the combined damped and fixed solutions are about 16% cheaper than the single damped solution. It should be noted, nonetheless, that the placement of the outrigger in the building was not considered in the cost analysis. Had it been so, the single outrigger structure might have presented advantages –from an economic perspective, over multiple outrigger structures.

§ 8.6 Recommendations

A number of topics are recommended from future research on the subject addressed in this research. These topics are investigations using large-scale experimental mock-ups, architectural considerations in the implementation of damped outrigger systems, topology optimization of damped outriggers, and further investigations on semiactive control of damped outrigger systems.

§ 8.6.1 Large scale experimental testing

The numerical studies developed in this research are bound by the limitations of the analytical models. Large scale testing would allow validating results in terms of energy distributions. Aspects such as the efficiency of the damped outriggers to reduce hysteresis in the core and/or optimization of the outrigger design to improve the damping capacity of viscous dampers can be further studied through experimental settings. Last but not least, a large scale testing model would allow to determine the influence of near/fault earthquakes in the distribution of seismic energy through the host structure and the role of the dampers in dissipating such energy.

§ 8.6.2 Architectural considerations

The use of single or multiple outriggers in a building depends on much more factors than those related to their structural performance. All the optimal design parameters obtained in this research may be useless if architectural considerations are not considered. For example, the design of the core has to be sized according functional requirements, such as number of lifts, stairs, circulations, etc., which are required according the main function of the building. The length of the outrigger arm depends on the usable average space between core and perimeter columns, which changes according to the location of the building. In seismic countries, such as USA and Chile, that space ranges between 9 and 12 meters. The number of outrigger sets and their final locations mostly depends on the need of mechanical floors, which will provide the availability of space to install the outriggers.

Furthermore, qualitative research is suggested as future studies on this subject. Through this, architects, engineers, stakeholders and clients could be interviewed on the aspects of the realization of damped outriggers for tall buildings.

§ 8.6.3 Topology optimization of damped outriggers

In this research, dampers were connected in series with the columns. Dampers can also be installed in the diagonals of the braced outriggers. Given the state-of-the-art in topology optimization of frame and trussed structures, a further level of research is the study of possible optimal designs where dampers can be integrated as *part* of the structural system and not as an attached component. This research demonstrated that optimal designs parameters can improved the performance of the damped outriggers. However, parameters as the core thickness and size of the outrigger elements were rather defined through a stochastic search. A topology-based approach opens the possibility of further optimizations of those parameters excluded in this research. This may lead to further improvements of the performance of damped outrigger systems.

Appendix A Strain and hysteretic energy stored by elements under shear forces

The elastic strain energy stored by an element subjected to shear forces is given as

$$ds = \frac{Q}{2} * \Delta_{shear} \tag{APP.1}$$

where Q is the shear force and Δ is the associated lateral deformation. Using the following relationship

$$G = \frac{Q}{A_r} \Big/ \frac{\Delta_{shear}}{l_n} \tag{APP.2}$$

where A_r is the effective shear area of the cross section and l_n is the length of the element, the strain energy can be formulated as

$$ds = \frac{Q}{2} * \frac{Ql_n}{A_r G} \Rightarrow \frac{Q^2 l_n}{2A_r G} \tag{APP.3}$$

Thus, the total elastic strain energy stored by a structure under shear forces is equal to

$$E_S = \sum \frac{Q^2 l_n}{2A_r G} \tag{APP.4}$$

In the presence of nonlinearities, the inelastic strain energy dissipated by damage (hysteresis) of an element under shear forces (Figure APP.A.1) can be computed as

$$ds_P = Q_{yield}(\Delta - \Delta_{yield}) \tag{APP.5}$$

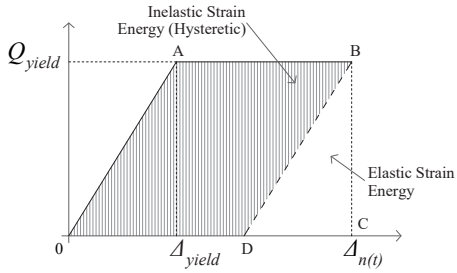

FIGURE APP.A.1 Strain energy for an inelastic system defined by Q -Δ

Thus, the total hysteretic energy dissipated by a structure under shear forces is equal to

$$E_H = \sum Q_{yield}(\Delta - \Delta_{yield}) \qquad \text{(APP.6)}$$

Appendix B Comparative floor-by-floor seismic equivalent lateral forces

		NCH433 2010			UBC 1994			
		PGA (g)		0.4	PGA (g)		0.4	0.8
		OTM (kN*m)		1.23E+07	OTM (kN*m)		5.53E+06	1.10E+07
Storey	h_i	$A_k = \sqrt{\left(1-\frac{h_i-1}{L}\right)} - \sqrt{\left(1-\frac{h_i}{L}\right)}$	A_k*h_i	F_i	$w*h_i$	$\Sigma w*h$	F_i	F_i
60	210	1.0000	9210.60	22638.18	4606400.40	0.03279	10647.02	21294.04
59	206.5	0.1291	1898.15	4665.35	4529627.06	0.03224	522.51	1045.02
58	203	0.0535	786.24	1932.45	4452853.72	0.03169	513.65	1027.31
57	199.5	0.0410	603.30	1482.82	4376080.38	0.03115	504.80	1009.59
56	196	0.0346	508.61	1250.08	4299307.04	0.03060	495.94	991.88
55	192.5	0.0305	448.09	1101.34	4222533.70	0.03005	487.08	974.17
54	189	0.0276	405.11	995.69	4145760.36	0.02951	478.23	956.46
53	185.5	0.0253	372.53	915.63	4068987.02	0.02896	469.37	938.74
52	182	0.0236	346.75	852.25	3992213.68	0.02842	460.52	921.03
51	178.5	0.0221	325.67	800.45	3915440.34	0.02787	451.66	903.32
50	175	0.0209	308.03	757.08	3838667.00	0.02732	442.80	885.61
49	171.5	0.0199	292.97	720.08	3761893.66	0.02678	433.95	867.90
48	168	0.0190	279.93	688.03	3685120.32	0.02623	425.09	850.18
47	164.5	0.0183	268.49	659.91	3608346.98	0.02568	416.24	832.47
46	161	0.0176	258.35	634.98	3531573.64	0.02514	407.38	814.76
45	157.5	0.0170	249.28	612.68	3454800.30	0.02459	398.52	797.05
44	154	0.0164	241.10	592.58	3378026.96	0.02404	389.67	779.34
43	150.5	0.0159	233.67	574.33	3301253.62	0.02350	380.81	761.62
42	147	0.0154	226.90	557.67	3224480.28	0.02295	371.96	743.91
41	143.5	0.0150	220.68	542.39	3147706.94	0.02240	363.10	726.20
40	140	0.0146	214.94	528.29	3070933.60	0.02186	354.24	708.49
39	136.5	0.0143	209.63	515.24	2994160.26	0.02131	345.39	690.77
38	133	0.0139	204.70	503.11	2917386.92	0.02077	336.53	673.06
37	129.5	0.0136	200.09	491.80	2840613.58	0.02022	327.68	655.35
36	126	0.0133	195.79	481.22	2763840.24	0.01967	318.82	637.64
35	122.5	0.0130	191.75	471.30	2687066.90	0.01913	309.96	619.93
34	119	0.0128	187.95	461.96	2610293.56	0.01858	301.11	602.21
33	115.5	0.0125	184.37	453.16	2533520.22	0.01803	292.25	584.50

>>>

32	112	0.0123	180.99	444.84	2456746.88	0.01749	283.39	566.79
31	108.5	0.0121	177.78	436.97	2379973.54	0.01694	274.54	549.08
30	105	0.0119	174.75	429.50	2303200.20	0.01639	265.68	531.37
29	101.5	0.0117	176.08	432.77	2226426.86	0.01585	256.83	513.65
28	98	0.0115	173.26	425.84	2149653.52	0.01530	247.97	495.94
27	94.5	0.0113	166.48	409.19	2072880.18	0.01475	239.11	478.23
26	91	0.0112	163.98	403.04	1996106.84	0.01421	230.26	460.52
25	87.5	0.0110	161.59	397.15	1919333.50	0.01366	221.40	442.80
24	84	0.0108	159.29	391.52	1842560.16	0.01311	212.55	425.09
23	80.5	0.0107	157.10	386.12	1765786.82	0.01257	203.69	407.38
22	77	0.0105	154.99	380.93	1689013.48	0.01202	194.83	389.67
21	73.5	0.0104	152.96	375.95	1612240.14	0.01148	185.98	371.96
20	70	0.0103	151.01	371.16	1535466.80	0.01093	177.12	354.24
19	66.5	0.0101	149.14	366.55	1458693.46	0.01038	168.27	336.53
18	63	0.0100	147.33	362.11	1381920.12	0.00984	159.41	318.82
17	59.5	0.0099	145.58	357.82	1305146.78	0.00929	150.55	301.11
16	56	0.0098	143.90	353.68	1228373.44	0.00874	141.70	283.39
15	52.5	0.0097	142.27	349.69	1151600.10	0.00820	132.84	265.68
14	49	0.0096	140.70	345.82	1074826.76	0.00765	123.99	247.97
13	45.5	0.0095	139.18	342.08	998053.42	0.00710	115.13	230.26
12	42	0.0094	137.71	338.46	921280.08	0.00656	106.27	212.55
11	38.5	0.0093	136.28	334.96	844506.74	0.00601	97.42	194.83
10	35	0.0092	134.90	331.56	767733.40	0.00546	88.56	177.12
9	31.5	0.0091	133.55	328.26	690960.06	0.00492	79.70	159.41
8	28	0.0090	132.25	325.05	614186.72	0.00437	70.85	141.70
7	24.5	0.0089	130.99	321.94	537413.38	0.00383	61.99	123.99
6	21	0.0088	129.76	318.92	460640.04	0.00328	53.14	106.27
5	17.5	0.0087	128.56	315.98	383866.70	0.00273	44.28	88.56
4	14	0.0087	127.40	313.12	307093.36	0.00219	35.42	70.85
3	10.5	0.0086	126.26	310.34	230320.02	0.00164	26.57	53.14
2	7	0.0085	125.16	307.63	153546.68	0.00109	17.71	35.42
1	3.5	0.0084	124.09	304.99	76773.34	0.00055	8.86	17.71
			Σ Fi =	58493.97		Σ Fi =	26322.28	52644.57

Appendix C Matlab scripts

All the following scripts were written by the author

Studies on lateral confinement / reinforcement distribution / outrigger location under free-vibration

```
%%%% script prepared to run set1: CORE / OUTRIGGER / DAMPER variables
%% define parametric variables
core_mod={'ln','nn','nu','lu'}; % 'ln' was tested in the first set of simulations
dat_lcon=[310,326,341,356,371,386,401,416];
dat_unif=[307,323,338,353,368,383,398,413];
min_dc=9.6e+7;delta_dc=7.2e+7; max_dc=2.4e8;
damp_coeff=min_dc:delta_dc:max_dc;
lambda=0.1:0.1:0.9;
S1_All=cell(length(core_mod),6);
S1_resD=zeros(length(lambda),length(damp_coeff));
S1_resDX=zeros(length(lambda),length(damp_coeff));
S1_resDH=zeros(length(lambda),length(damp_coeff));
S1_resV=zeros(length(lambda),length(damp_coeff));
S1_resVX=zeros(length(lambda),length(damp_coeff));
S1_resVH=zeros(length(lambda),length(damp_coeff));
outrigger(1:20,1)=(62:81)';
outrigger(1:20,2)=[9.500000E+00; 1.425000E+01; 1.900000E+01; -1.900000E+01;...
  -1.425000E+01; -9.500000E+00; -1.900000E+01; -1.425000E+01; -9.500000E+00;...
  9.500000E+00; 1.425000E+01; 1.900000E+01; -1.900000E+01; -1.425000E+01;...
  -9.500000E+00; 9.500000E+00; 1.425000E+01; 1.900000E+01; -1.900000E+01;...
  1.900000E+01];
for cm=1:length(core_mod);
  if strncmp(core_mod{cm}, 'n', 1)==1
    D{1}=':  CNFCRV  VECCHI';
    D{2}=':  REDCRV  VC1993';
    for jj=1:8 %because there are 8 'core' material properties sections
      fid = fopen('Parametric.dat','r+');
      ii=dat_lcon(jj);
      for k=1:ii-1
        fgetl(fid);
      end
      fseek(fid, 0, 'cof');
      fprintf(fid,'%s\r\n', D{1:2});
      fclose(fid);
    end
  else
    D{1}='   CNFCRV  VECCHI';
```

```
    D{2}='   REDCRV  VC1993';
    for jj=1:8 %because there are 8 'core' material properties sections
      fid = fopen('Parametric.dat','r+');
      ii=dat_lcon(jj);
      for k=1:ii-1
        fgetl(fid);
      end
      fseek(fid, 0, 'cof');
      fprintf(fid,'%s\r\n', D{1:2});
      fclose(fid);
    end
  end
  if strncmp(core_mod{cm}, 'nu', 2)==1 || strncmp(core_mod{cm}, 'lu', 2)==1
    E ='   TENSTR  7.20000E+06';
    for jj=1:8 %because there are 8 'core' material properties sections
      fid = fopen('Parametric.dat','r+');
      ii=dat_unif(jj);
      for k=1:ii-1
        fgetl(fid);
      end
      fseek(fid, 0, 'cof');
      fprintf(fid,'%s\r\n', E);
      fclose(fid);
    end
  end
  for n=1:length(lambda); % loop for selected outrigger locations
    outrigger(1:6,3)=210*lambda(n);
    outrigger(7:12,3)=210*lambda(n)+3.5;
    outrigger(13:18,3)=210*lambda(n)-3.5;
    outrigger(19:20,3)=210*lambda(n)-7;
%% modify DIANA input file Parametric.dat in outrigger-line LAMBDA
    A=cell(20,1);
    for jj=1:20
      if outrigger(jj,2)>0
        A{jj}=['  ',num2str(outrigger(jj,1)),'   ',num2str(outrigger(jj,2),'%10.6E\n'),'
',num2str(outrigger(jj,3),'%10.6E\n')];
      else
        A{jj}=['  ',num2str(outrigger(jj,1)),'   ',num2str(outrigger(jj,2),'%10.6E\n'),'
',num2str(outrigger(jj,3),'%10.6E\n')];
      end
    end
    A=A';
    fid = fopen('Parametric.dat','r+');
    ii=71;
    for k=1:ii-1
      fgetl(fid);
    end
    fseek(fid, 0, 'cof');
    fprintf(fid,'%s\r\n', A{1:20});
    fclose(fid);
    H{1}=['  84   -9.500000E+00   ',num2str(outrigger(20,3),'%10.6E\n')];
    H{2}=['  85   9.500000E+00   ',num2str(outrigger(20,3),'%10.6E\n')];
    fid = fopen('Parametric.dat','r+');
    ii=95;
    for k=1:ii-1
```

```
      fgetl(fid);
    end
    fseek(fid, 0, 'cof');
    fprintf(fid,'%s\r\n', H{1:2});
    fclose(fid);
%% modify DIANA input in ELEMENTS connectivity + story 'beams' at the dampers level
    if lambda(n)==0.1
      F{1}=['  70   ',num2str(lambda(n)*60+2),' DX=9.5'];
      F{2}=['  71   ',num2str(lambda(n)*60+2),' DX=-9.5'];
      F{3}=['  67   ',num2str(lambda(n)*60+1),' DX=9.5'];
      F{4}=['  62   ',num2str(lambda(n)*60+1),' DX=-9.5'];
      F{5}=['  76   ',num2str(lambda(n)*60),' DX=9.5'];
      F{6}=['  77   ',num2str(lambda(n)*60),' DX=-9.5'];
      F{7}=['  84   ',num2str(lambda(n)*60-1),' DX=9.5'];
      F{8}=['  85   ',num2str(lambda(n)*60-1),' DX=-9.5'];
    else
      F{1}=['  70  ',num2str(lambda(n)*60+2),' DX=9.5'];
      F{2}=['  71  ',num2str(lambda(n)*60+2),' DX=-9.5'];
      F{3}=['  67  ',num2str(lambda(n)*60+1),' DX=9.5'];
      F{4}=['  62  ',num2str(lambda(n)*60+1),' DX=-9.5'];
      F{5}=['  76  ',num2str(lambda(n)*60),' DX=9.5'];
      F{6}=['  77  ',num2str(lambda(n)*60),' DX=-9.5'];
      F{7}=['  84  ',num2str(lambda(n)*60-1),' DX=9.5'];
      F{8}=['  85  ',num2str(lambda(n)*60-1),' DX=-9.5'];
    end
    fid = fopen('Parametric.dat','r+');
    ii=475; %before it was 471
    for k=1:ii-1
      fgetl(fid);
    end
    fseek(fid, 0, 'cof');
    fprintf(fid,'%s\r\n', F{1:8});
    fclose(fid);
%% modify damping coefficient in DIANA input file
    for dc=1:length(damp_coeff); % inner loop for selected damper's damping coefficient
      C=['   DAMP   ',num2str(damp_coeff(dc),'%10.5E\n')];
      fid = fopen('Parametric.dat','r+');
      ii=284;
      for k=1:ii-1
        fgetl(fid);
      end
      fseek(fid, 0, 'cof');
      fprintf(fid,'%s\r\n', C);
      fclose(fid);
    %% run DIANA
      command =dos('command.cmd'); % works inside matlab
      heading=['S1-',core_mod{cm},num2str(lambda(n)),'H',num2str(damp_coeff(dc),'%10.2e\n')];
      [count]=renameOUT(heading);  % changing files names
      d = 7; nod = 61; [tDX,~,tVX,~]=freq_resp(d,nod,heading);
      [~,~,nd,nv]=theXmen(nod,tDX,tVX);  %function to pick the peaks
      if length(nd)~=1;
        fid=fopen([num2str(nd(1)),'_',heading,'.dat'],'w');
        fprintf(fid,'%12.8f\r\n',tVX(nd(1),:));
        fclose(fid);
        fid=fopen([num2str(nd(2)),'_',heading,'.dat'],'w');
```

```
        fprintf(fid,'%12.8f\r\n',tVX(nd(2),:));
        fclose(fid);
        nd=nd(1);
      end
      if length(nv)~=1;
        fid=fopen([num2str(nv(1)),'_',heading,'.dat'],'w');
        fprintf(fid,'%12.8f\r\n',tVX(nv(1),:));
        fclose(fid);
        fid=fopen([num2str(nv(2)),'_',heading,'.dat'],'w');
        fprintf(fid,'%12.8f\r\n',tVX(nv(2),:));
        fclose(fid);
        nv=nv(1);
      end
      [~,~,zeta_D,zetaX_D,zetaH_D]=log_decayD(nd,tDX);
      [~,~,zeta_V,zetaX_V,zetaH_V]=log_decayV(nv,tVX);
      S1_resD(n,dc)=zeta_D; S1_resDX(n,dc)=zetaX_D; S1_resDH(n,dc)=zetaH_D;
      S1_resV(n,dc)=zeta_V; S1_resVX(n,dc)=zetaX_V; S1_resVH(n,dc)=zetaH_V;
      %% move *.tb files to the tab folder
      movefile('*.tb','P Set1 DianaTabs')
    end
  end
  S1_All{cm,1}=S1_resD; S1_All{cm,2}=S1_resDX; S1_All{cm,3}=S1_resDH;
  S1_All{cm,4}=S1_resV; S1_All{cm,5}=S1_resVX; S1_All{cm,6}=S1_resVH;
end
namefile=num2str([min_dc, delta_dc, max_dc],'%10.2E');

function [theDman,theVman,nd,nv]=theXmen(nod,tDX,tVX)
theDman=zeros(nod,1);theVman=zeros(nod,1);%theAman=zeros(nod,1);
tt=10; % maximum values after 1 step
for ii=1:nod
  theDman(ii)=max(abs(tDX(ii,tt:end))); theVman(ii)=max(abs(tVX(ii,tt:end)));
end
[theDman,nd]=max(theDman); [theVman,nv]=max(theVman);
if nd~=61
  nd=[61,nd];
end
if nv~=61
  nv=[61,nv];
end

% Get all files in the current folder clear all;
function[count]=renameOUT(heading)
files = dir('*.tb');
% Loop through each
count=0;
for id = 1:length(files)
 % Get the file name (minus the extension)
  [~, f] = fileparts(files(id).name);
  if strncmp(f, 'EQ ', 3)==1
    A=textscan(f,'%s');
    oldfile=[f, '.tb']; newfile=[heading,A{1}{2},'.tb'];
    movefile(oldfile,newfile) % must create 'my folder' first
    count=count+1;
  end
end
```

```
%%% computing damping ratio from the logarithmic decay
function[N,P_pos,zeta,zetaX,zetaH]=log_decayD(nd,tDX)
D=zeros(2*length(nd),length(tDX(1,:)));
bump_D=cell(2*length(nd),1);
for ii=1:length(nd)
  jj=nd(ii);
  for k=1:length(tDX(1,:))
    if sign(tDX(jj,k))==1
      D(2*ii-1,k)=tDX(jj,k);
    else
      D(2*ii,k)=tDX(jj,k);
    end
  end
end
for ii=1:2*length(nd)
  % from http://stackoverflow.com/questions/27076618/how-to-split-vector-by-zeros-in-matlab
  v=D(ii,:);
  w = [false v~=0 false]; %// "close" v with zeros, and transform to logical
  starts = find(w(2:end) & ~w(1:end-1)); %// find starts of runs of non-zeros
  ends = find(~w(2:end) & w(1:end-1))-1; %// find ends of runs of non-zeros
  bump_D{ii,1} = arrayfun(@(s,e) v(s:e), starts, ends, 'uniformout', false); %// build result
end
N=length(bump_D{1,1});
P_pos=zeros(length(nd),N);  % only positive side will be considered
for ii=1:length(nd)
  for jj=1:N
    P_pos(ii,jj)=max(bump_D{2*ii-1,1}{1,jj});
  end
end
delta=zeros(length(nd),1); zeta=zeros(length(nd),1);
deltaX=zeros(length(nd),1); zetaX=zeros(length(nd),1);
deltaH=zeros(length(nd),1); zetaH=zeros(length(nd),1);
for ii=1:length(nd)
  bump=5; delta(ii,1)=(1/(N-bump-1))*log(P_pos(ii,bump)/P_pos(ii,end-1)); % counting from the 5th bump
  if rem(N,2)==0
    deltaX(ii,1)=log(P_pos(ii,(N/2)-1)/P_pos(ii,(N/2)));
  else
    deltaX(ii,1)=log(P_pos(ii,((N+1)/2)-1)/P_pos(ii,((N+1)/2)));
  end
  deltaH(ii,1)=log(P_pos(ii,bump)/P_pos(ii,bump+1));
  zeta(ii,1)=delta(ii,1)/sqrt(4*pi+delta(ii,1)^2); % https://www.youtube.com/watch?v=W42QXas4yII
  zetaX(ii,1)=(deltaX(ii,1)/(2*pi))/sqrt(1+(deltaX(ii,1)/(2*pi))^2);
  zetaH(ii,1)=deltaH(ii,1)/(2*pi);
end
```

Studies on lateral confinement / reinforcement distribution / outrigger location under earthquake motion

Only new lines are showed

```
%%%% script prepared to run set2: CORE / OUTRIGGER / EQ levels
%% define parametric variables
clc,clear
tic
mkdir('P Set2rev DianaTabs') % folder to move *.tb diana files in
%% VARIABLE input data
% CORE modeling properties
.
.
.
% outrigger locations
lambda=0.4:0.1:0.9; %
% earthquake ground motion
earthquake='elcentro-270'; Ts=0.0050; EQ='Ce-'; scale_factor=[1,2.5,4,6.7]; freq_fact=50; count=10000;
%% FIXED input data
% building properties
story_h=3.5; bldg_h=210;  no=61;           % number of nodes whose response is read
mm(1)=0; mm(2:61)=0.797E+08/(no-1); % linear distribution of mass per story
%% material properties - element sections VARIABLE
BPROF=[4.00000E-01   4.08000E-01   4.08000E-01 2.10000E-02   2.10000E-02   2.10000E-02];
VPROF=[4.98000E-01   4.32000E-01   4.32000E-01 7.00000E-02   7.00000E-02   4.50000E-02];
HPROF=[4.98000E-01   4.32000E-01   4.32000E-01 7.00000E-02   7.00000E-02   4.50000E-02];
[AsB,AsV,AsH]=AsTruss(BPROF,VPROF,HPROF); % function to compute cross-sectional areas of profiles
lnB=5.9; lnV=3.5; lnH=4.75;
As(1:60,1)=47.71; ln(1:60,1)=3.5;  % cross-sectional core 40.59? + length element
As(61:72,1)=AsH; ln(61:72,1)=lnH;
As(73:80,1)=AsV; ln(73:80,1)=lnV;
As(81:88,1)=AsB; ln(81:88,1)=lnB;
clear BPROF VPROF HPROF lnB lnV lnH AsB AsV AsH
% Tensile / Compressive Strengths
% core non-uniform vertical reinforcement distribution
tenstr(1:6,1)=7.20000E+06; tenstr(7:12,1)=6.00000E+06; tenstr(13:18,1)=5.36000E+06;
tenstr(19:24,1)=5.16000E+06; tenstr(25:30,1)=5.24000E+06; tenstr(31:36,1)=5.24000E+06;
tenstr(37:42,1)=5.04000E+06; tenstr(43:48,1)=4.68000E+06; tenstr(49:54,1)=4.20000E+06;
tenstr(55:60,1)=4.20000E+06;
tenstr(61:88,1)=3.55000E+08;
comstr(1:60,1)=-4.30000E+07; comstr(61:88,1)=-3.55000E+08; % compressive strength core : outrigger elements
%% storing matrices and cell arrays
S_energyEQ=zeros(12,length(scale_factor)); % 12 energies
S_dispEQ=zeros(count,length(scale_factor));
S_veloEQ=zeros(count,length(scale_factor));
S_acceEQ=zeros(count,length(scale_factor));
Nd=zeros(1,length(scale_factor)); Nv=zeros(1,length(scale_factor)); Na=zeros(1,length(scale_factor));
lg_input2=cell(1,length(scale_factor));
Dr=zeros(3,length(scale_factor)); Dr2=zeros(3,length(scale_factor));  % 3 ratios
S_maxR=zeros(10,4*length(scale_factor));  % for storing max_response (10,4) per each EQ
```

```
%% FE model data
.
.
.
% for cm=1:length(core_mod);
.
.
.
  for n=1:length(lambda); % loop for selected outrigger locations
    outrigger(1:6,3)=210*lambda(n);
    outrigger(7:12,3)=210*lambda(n)+3.5;
    outrigger(13:18,3)=210*lambda(n)-3.5;
    outrigger(19:20,3)=210*lambda(n)-7;
%% modify DIANA input file Parametric.dat in outrigger-line LAMBDA
.
.
.
%% modify earthquake ground motion levels
    for s_f=1:length(scale_factor)
      [xg,time]=groundmotion(earthquake,Ts,scale_factor(s_f));
      S=sprintf('%.4f ',xg');
      G=[ ' FACTOR ',cellstr(S),' / '];
      fid = fopen('Parametric.dat','r+');
      ii=492; %before it was 486
      for k=1:ii-1
        fgetl(fid);
      end
      fseek(fid, 0, 'cof');
      fprintf(fid,'%s', G{1:3});
      fclose(fid);
    %% run DIANA
      command =dos('command.cmd'); toc % works inside matlab
      heading=['S2rev-',num2str(lambda(n)*10),'H','0',num2str(scale_factor(s_f)*100),'x',EQ];
      [fname,fname0,fname1,fname2,fname3,fname4,fname5,...
        fname7,fname8,fname9,fname10,fname12,fname13]=renameOUT(heading);
      %% Stresses + Strains
      d = 7; node = 2; intpoint = 9; % number of integration points (L7BEN has 9)
      noe = 88; % No elements whose response is retrieved FIXED = 90 (1-60:core +61-88:outrigger)
      [SXX,~,EIN,stap]=SSread(d,noe,node,intpoint,fname); clear fname
      %% CRACK Strains
      d=6; noecore = 60; % 1-60:core
      [pEknn,Eh_story,Eh1]=crack_strain(As,ln,tenstr,d,noecore,node,intpoint,stap,fname2); clear fname2%
      %% Crack Energy Distribution
      if max(Eh1)~=0
        [bb,hyst_stories]=sort(Eh_story(:,end),'descend');
        hyst_distribution=bb.*inv(sum(bb));
        hyst_dist=zeros(size(Eh_story));
        for jj=1:length(Eh_story(1,:))
          aa=sum(Eh_story(:,jj));
          for ii=1:length(Eh_story(:,1))
            if aa~=0
              hyst_dist(ii,jj)=Eh_story(ii,jj).*inv(aa);
            end
          end
        end
```

```
        figure; plot(time(1:10000),hyst_dist);hold all; legend(num2str(hyst_stories));
        tail=['Eh_Story Distribution - Outrigger@',num2str(60*lambda(n))];lg_location='NorthEast'; xy_
label={'time [s]','Normalized Hysteretic Energy'}; WH=[17.88, 5.96]; %WH=[17.88, 11.92];
        lg_input={num2str(hyst_stories(1:10))};
        save_TIFF(heading,tail,lg_input,lg_location,xy_label,WH,h);
        dlmwrite([heading,'Eh_Story Distribution.dat'],[hyst_distribution;hyst_stories],'delimiter','\
t','precision','%s\r\n')
      end
      %% Plastic Strains
      d=7; noe = 88;
      [~,Ehdis2,Eh2]=Pstrain(As,ln,comstr,tenstr,d,noe,node,intpoint,stap,fname3); clear fname3
      %% sTRESS COLUMN total
      d = 7; node = 2; intpoint = 1; noe =1;
      [CSXX,~]=CSSread(d,noe,node,intpoint,fname13); clear fname13
      %% RESPONSES
      d = 7; nod = 81; % number of nodes whose response is retrievd 81 = DAMPED cause no-DOF supports
      [TrDtX,~,TVtX,TVtY,TAtX,~,FrDX,FrDY]=readDIANA2(d,nod,fname5,fname7); clear fname5 fname7
      fix_sup=2; nodrot=nod-fix_sup;
      [MrDZa,TVrZa]=dvrotaread2(d,nodrot,fname8); clear fname8
      TVrZ=[TVrZa;zeros(fix_sup,length(TVrZa(1,:)))];MrDZ=[MrDZa;zeros(fix_sup,length(MrDZa(1,:)))]; clear MrDZa
TVrZa
      %% FORCES
      d=7; nod2 = 3;[FrBXR,~]=baseforce(d,nod2,fname9); clear fname9
      %% MOMENTS
      d=7; [MrBZR]=basemoment(d,fname10); clear fname10
      %% Cumulative Energy from DIANA
      noecore=60; d=6;intpoint=9;
      [Wn_dis]=Wnread(d,noecore,node,intpoint,stap,fname0); clear fname0
      Wn=zeros(1,stap);
      for dt=1:stap
        Wn(dt)=sum(abs(Wn_dis(:,dt)));
      end
      %% Damping FORCE at dampers
      d = 8; noddamp=2; [FEDYa,~]=dampdamp(d,noddamp,fname1); clear fname1
      %% Node forces Axial global
      d = 7; noe=83; [FrNX,FrNY]=nodeforce(d,noe,stap,fname4); clear fname4
      %% MAXIMUM RESPONSES
      [max_response]=max_responses(story_h,bldg_h,TrDtX,TVtX,TAtX,FrBXR,MrBZR,SXX,EIN,CSXX);
      %% clearing non-used variables
      clear d dt fix_sup intpoint noddamp node nodrot noe noecore
%      [theDman,theVman,theAman,nd,nv,na]=theXmen(nod,tDX,tVX,tAX);  %function to pick the peaks
      [~,~,~,nd,nv,na]=theXmen(nod,TrDtX,TVtX,TAtX);  %function to pick the peaks
      if length(nd)~=1;
        [nd]=manypeaks(nd,heading,TrDtX); %function to save peaks in *.dat
      end
      if length(nv)~=1;
        [nv]=manypeaks(nv,heading,TVtX); %function to save peaks in *.dat
      end
      if length(na)~=1;
        [na]=manypeaks(na,heading,TAtX); %function to save peaks in *.dat
      end
      %% Energy Distribution
[Ei,Ek,ED,Edampers,Ea,Edx,Edy,xg,time]=energy_dis(xg,time,stap,mm,TVtX,FrDX,FrDY,MrDZ,TVrZ,FrNX,FrNY,FEDYa,TVtY);
      Eh_crackcore=Eh1*1e-3; Eh=(Eh1+Eh2)*1e-3;
      % according to the elastic cat's theory
```

```
    if max(Eh)==0
      Es=Ea-Edampers-Edy;
      Ei_ind=Ea+Ek+Edx;
    else
      Esh=Ea-ED;
      [Eh,Es,Wn]=Eh_area(Eh,Esh,Wn);
      Ei_ind=Ek+ED+Es+Eh;
    end
    Ed=ED-Edampers;
    Eh_plast_core=sum(Ehdis2(1:1080,:))*1e-3;Eh_plast_out=sum(Ehdis2(1081:end,:))*1e-3;
    S_energyEQ(:,s_f)=[Ei(end),Ek(end),max(Ed),max(Edampers),Es(end),max(Eh),...
      max(Edx),max(Edy),max(Eh_crackcore),max(Eh_plast_core),max(Eh_plast_out),Ei_ind(end)];
    % plot normal
    figure
    plot(time,Ei) ; hold all % Relative
    plot(time,Ek) ; hold all % Relative
    plot(time,Edx) ; hold all
    plot(time,Edampers) ; hold all
    plot(time,Es) ; hold all
    plot(time,Eh) ; hold all
    h=0;
    tail='E_dis';lg_location='NorthWest'; xy_label={'time [s]','Energy [kN-m]'}; WH=[17.88, 11.92];       lg_
input={'E_I_N_P_U_T','E_K_I_N_E_T_I_C','E_D_A_M_P_I_N_G',
'E_D_A_M_P_E_R_S','E_S_T_R_A_I_N','E_H_Y_S_T_E_R_E_T_I_C'};
    save_TIFF(heading,tail,lg_input,lg_location,xy_label,WH,h);
    % Bertero-type plot
    [l1,l2,l3,l4,l5,l6,l7]=bertero_plot(Ei_ind,Ed,Ek,Es,Edx,Eh,Eh_plast_out,time);
    if max(Eh)==0
      h=[12 13];
    else
      h=0;
    end
    tail='BERTERO-E_dis';lg_location='NorthWest'; xy_label={'time [s]','Energy [kN-m]'}; WH=[17.88, 11.92];
    lg_input={'E_I_N_P_U_T','E_H_Y_S_T_E_R_E_T_I_C','E_H_Y_S_T_E_R_E_T_I_C_c_o_r_e',...
      'E_D_A_M_P_E_R_S','E_D_A_M_P_I_N_G','E_D_A_M_P_I_N_G_c_o_r_e','E_E_L_A_S_T_I_C_s_t_r_a_i_n'};
    save_TIFF(heading,tail,lg_input,lg_location,xy_label,WH,h);
    % energy ratios
    damping_ratio=Ed./Ei; damping_ratio(1)=0;
    dampers_ratio=Edampers./Ei; dampers_ratio(1)=0;
    hysteretic_ratio=Eh./Ei; hysteretic_ratio(1)=0;
    Dr(:,s_f)=[damping_ratio(end);dampers_ratio(end);hysteretic_ratio(end)];
    figure; plot(time,damping_ratio,time,dampers_ratio,time,hysteretic_ratio); hold all
    tail='E_ratios';lg_location='Best'; xy_label={'time [s]',' '}; WH=[17.88, 11.92];
    h=0; lg_input={'ratio E_D / E_I','ratio E_D_A_M_P_E_R_S / E_I','ratio E_H / E_I'};
    save_TIFF(heading,tail,lg_input,lg_location,xy_label,WH,h);
    % energy ratios II
    Eddh=ED+Eh;
    damping_ratio2=Ed./Eddh; damping_ratio2(1)=0;
    dampers_ratio2=Edampers./Eddh; dampers_ratio2(1)=0;
    hysteretic_ratio2=Eh./Eddh; hysteretic_ratio2(1)=0;
    Dr2(:,s_f)=[damping_ratio2(end);dampers_ratio2(end);hysteretic_ratio2(end)];
    figure; plot(time,damping_ratio2,time,dampers_ratio2,time,hysteretic_ratio2); hold all
    tail='E_ratios2';lg_location='Best'; xy_label={'time [s]',' '}; WH=[17.88, 11.92];
    h=0; lg_input={'ratio E_D / E_D+E_D_A_M_P_E_R_S+E_H','ratio E_D_A_M_P_E_R_S / E_D+E_D_A_M_P_E_R_
S+E_H','ratio E_H / E_D+E_D_A_M_P_E_R_S+E_H'};
```

```
      save_TIFF(heading,tail,lg_input,lg_location,xy_label,WH,h);
      %% Fast Fourier Transformation
      min_freq=0; max_freq=30; WH=[17.88, 11.92];
      fft_plotting(TVtY,TrDtX,min_freq,max_freq,freq_fact,Ts,time,heading,WH);
      min_freq=0; max_freq=5; WH=[17.88, 11.92]; heading2=[heading,'close-up'];
      fft_plotting(TVtY,TrDtX,min_freq,max_freq,freq_fact,Ts,time,heading2,WH);
      close all
      %% matrices for saving max. responses
      S_dispEQ(:,s_f)=TrDtX(nd,:)'; S_veloEQ(:,s_f)=TVtX(nv,:)'; S_acceEQ(:,s_f)=TAtX(na,:)';
      Nd(s_f)=nd; Nv(s_f)=nv; Na(s_f)=na;
      S_maxR(:,4*s_f-3:4*s_f)=max_response;
      %% saving data
  movefile('*.xls','P Set2rev DianaTabs')
% end
```

Studies on damping ratio / outrigger location under free vibration / core-to-outrigger and core-to-column stiffness ratios

Only new lines are showed

```
%%%%%%%%%%%%%%%%%%%%%%%%%%%     finding EIGEN-FREQUENCIES
.
.
.
% DAMPER - damper coefficient
min_dc=2.4e+7;delta_dc=7.2e+7; max_dc=6.72e8;
damp_coeff=min_dc:delta_dc:max_dc;
% COLUMN - rigidity ratio-core-to-column
h=18; b=18; t=0.75;
Icore=(b*h^3)/12-((b-2*t)*(h-2*t)^3)/12;
lo=9.5; r=lo+b/2; clear b h t lo
rho_now=Icore/(2*1.3*r^2);
% rho_ctc=[1,2,rho_now,3,4];
rho_ctc=[1,2,2.5,3,4];
% computing As columns according to rho_ctc;
As_column=zeros(1,length(rho_ctc));
for ii=1:length(rho_ctc)
  As_column(ii)=Icore/(2*rho_ctc(ii)*r^2);
end
%% storing matrices and cell arrays
S3eig_lambda=cell(1,length(lambda));
S3DtXY_lambda=cell(1,length(lambda));
S3eig_damp_rho=cell(length(damp_coeff),length(rho_ctc));
S3DtXY_damp_rho=cell(length(damp_coeff),length(rho_ctc));
S3_eig=zeros(length(damp_coeff),length(rho_ctc));
%% FE model data
.
.
.
```

```
%% modify DIANA input file Parametric.dat in outrigger-line LAMBDA
.
.
.
%% modify DIANA input in ELEMENTS connectivity + story 'beams' at the dampers level
.
.
.
%% modify damping coefficient in DIANA input file
    for dc=1:length(damp_coeff); % inner loop for selected damper's damping coefficient
      C=['   DAMP   ',num2str(damp_coeff(dc),'%10.5E\n')];
      fid = fopen('Parametric.dat','r+');
      ii=284;
      for k=1:ii-1
        fgetl(fid);
      end
      fseek(fid, 0, 'cof');
      fprintf(fid,'%s\r\n', C);
      fclose(fid);
      for rho2=1:length(As_column)
        G=['   RECTAN  ',num2str(As_column(rho2),'%10.5E\n'),'    ',num2str(As_column(rho2),'%10.5E\n')];
        fid = fopen('Parametric.dat','r+');
        ii=440; %before it was 436
        for k=1:ii-1
          fgetl(fid);
        end
        fseek(fid, 0, 'cof');
        fprintf(fid,'%s\r\n', G);
        fclose(fid);
      %% run DIANA
        command =dos('command.cmd'); % works inside matlab
        heading=['Sf',num2str(lambda(n)*10),num2str(damp_coeff(dc),'%10.2e\n'),num2str(rho_ctc(rho2))];
        [count]=renameOUT(heading);  % changing files names
        d=6;nodes=81;modes=17;
        [eigen,mode_shape]=eigen_freq(d,nodes,modes,[heading,'eigen']);
        S3eig_damp_rho{dc,rho2}=eigen;
        S3DtXY_damp_rho{dc,rho2}=mode_shape;
        S3_eig(dc,rho2)=eigen(1);
      end
    S3eig_lambda{n}=S3eig_damp_rho;
    S3DtXY_lambda{n}=S3DtXY_damp_rho;
  end
  save('S3eig_lambda','S3eig_lambda')
  save('S3DtXY_lambda','S3DtXY_lambda')

%%%% script prepared to run set3: CORE-zeta / OUTRIGGER-lambda/rho_out /
%%%% DAMPER-damper_coeff / COLUMN-rho_ctc
%%%% Set3b: CORE-zeta / OUTRIGGER-lambda + rho_cto / COLUMN-rho_ctc
%% VARIABLE input data
% CORE damping ratio
zeta_ratios=[1.5,2,2.5];  % damping ratios
%%% NOTE: before running this script, PAfrequency_set3b must be used to determine
%%% the eigen frequencies of the system as PARAMETRICALLY designed
load('S3eig_lambda');
zeta_rayleigh=cell(1,3);
```

```
ray_damp=cell(size(S3eig_lambda));
% OUTRIGGER - locations
lambda=0.1:0.1:0.9; % set l shows few improvement between 0.1-0.3
%% OUTRIGGER - rigidity ratio-core-to-outrigger (rho_out)
lnB=5.9; lnV=3.5; lnH=4.75;
h=18; b=18; t=0.75;
Icore=(b*h^3)/12-((b-2*t)*(h-2*t)^3)/12;
lo=9.5; r=lo+b/2; clear b h t lo
rho_out= [1,2,2.5,3,4];
BPROF=zeros(length(rho_out),6); VPROF=zeros(length(rho_out),6);
HPROF=zeros(length(rho_out),6);
for ii=1:length(rho_out)
AsB=2*3.40000E+10*Icore*r/(((2*2.10000E+11*2*lnV*((2*lnH)^2)/
(lnB^3))+(2.10000E+11*2*((2*lnV)^2)*7.385/2))*210*rho_out(ii));
  AsV=AsB; AsH=AsV;
  [BPROF(ii,:),VPROF(ii,:),HPROF(ii,:)]=RevAsTruss(AsB,AsV,AsH); % compute the profiles from cross-sectional
areas
end
clear AsB AsV AsH lnB lnH lnV
% COLUMN - rigidity ratio-core-to-column
rho_ctc=[1,2,2.5,3,4];
% computing As columns according to rho_ctc;
As_column=zeros(1,length(rho_ctc));
for ii=1:length(rho_ctc)
  As_column(ii)=Icore/(2*rho_ctc(ii)*r^2);
end
%% storing matrices and cell arrays
S3_Zeta=cell(1,length(zeta_ratios));
S3_All=cell(length(lambda),6);
S3_resD=zeros(length(rho_out),length(rho_ctc));
S3_resDX=zeros(length(rho_out),length(rho_ctc));
S3_resDH=zeros(length(rho_out),length(rho_ctc));
S3_resV=zeros(length(rho_out),length(rho_ctc));
S3_resVX=zeros(length(rho_out),length(rho_ctc));
S3_resVH=zeros(length(rho_out),length(rho_ctc));
%% FE model data
.
.
.
%% Begin iteration
for z=1:length(zeta_ratios);  %loop for damping ratios
  zeta=zeta_ratios(z);
  for n=1:length(lambda); % loop for selected outrigger locations
    outrigger(1:6,3)=210*lambda(n);
    outrigger(7:12,3)=210*lambda(n)+3.5;
    outrigger(13:18,3)=210*lambda(n)-3.5;
    outrigger(19:20,3)=210*lambda(n)-7;
%% modify DIANA input file Parametric.dat in outrigger-line LAMBDA
.
.
.
%% modify DIANA input in ELEMENTS connectivity + story 'beams' at the dampers level
.
.
.
```

```
    for rho1=1:length(rho_out)
      N{1}='  1 NAME   BPROF';
      N{2}=['   ISHAPE  ',num2str(BPROF(rho1,1),'%10.5E\n'),'   ',num2str(BPROF(rho1,2),'%10.5E\n'),'
',num2str(BPROF(rho1,3),'%10.5E\n'),];
      N{3}=['       ',num2str(BPROF(rho1,4),'%10.5E\n'),'   ',num2str(BPROF(rho1,5),'%10.5E\n'),'
',num2str(BPROF(rho1,6),'%10.5E\n'),];
      N{4}='  2 NAME   VPROF';
      N{5}=['   ISHAPE  ',num2str(VPROF(rho1,1),'%10.5E\n'),'   ',num2str(VPROF(rho1,2),'%10.5E\n'),'
',num2str(VPROF(rho1,3),'%10.5E\n'),];
      N{6}=['       ',num2str(VPROF(rho1,4),'%10.5E\n'),'   ',num2str(VPROF(rho1,5),'%10.5E\n'),'
',num2str(VPROF(rho1,6),'%10.5E\n'),];
      N{7}='  3 NAME   HPROF';
      N{8}=['   ISHAPE  ',num2str(HPROF(rho1,1),'%10.5E\n'),'   ',num2str(HPROF(rho1,2),'%10.5E\n'),'
',num2str(HPROF(rho1,3),'%10.5E\n'),];
      N{9}=['       ',num2str(HPROF(rho1,4),'%10.5E\n'),'   ',num2str(HPROF(rho1,5),'%10.5E\n'),'
',num2str(HPROF(rho1,6),'%10.5E\n'),];
      fid = fopen('Parametric.dat','r+');
      ii=424; %
      for k=1:ii-1
        fgetl(fid);
      end
      fseek(fid, 0, 'cof');
      fprintf(fid,'%s\r\n', N{1:9});
      fclose(fid);
      P=['   RAYLEI  ',num2str(outrigger_beta(1,rho1),'%10.5E\n'),'  ',num2str(outrigger_
beta(2,rho1),'%10.5E\n')];
      fid = fopen('Parametric.dat','r+');
      ii=294; %
      for k=1:ii-1
        fgetl(fid);
      end
      fseek(fid, 0, 'cof');
      fprintf(fid,'%s\r\n', P);
      fclose(fid);
%% modify damping coefficient in DIANA input file
.
.
.
      for rho2=1:length(As_column)
        G=['   RECTAN  ',num2str(As_column(rho2),'%10.5E\n'),'   ',num2str(As_column(rho2),'%10.5E\n')];
        fid = fopen('Parametric.dat','r+');
        ii=440;
        for k=1:ii-1
          fgetl(fid);
        end
        fseek(fid, 0, 'cof');
        fprintf(fid,'%s\r\n', G);
        fclose(fid);
        %% NOW RAYLEIGH DAMPING
        w = 2*pi*S3eig_lambda{1,n}{rho1,rho2}(1:2); % NATURAL FREQUENCIES
        beta=[2*w(1)*w(2)*(zeta*0.01*w(2)-zeta*0.01*w(1))/(w(2)^2-w(1)^2)
          2*(zeta*0.01*w(2)-zeta*0.01*w(1))/(w(2)^2-w(1)^2)];
        ray_damp{1,n}{rho1,rho2}=beta;
        O=['   RAYLEI  ',num2str(beta(1),'%10.2E\n'),' ',num2str(beta(2),'%10.2E\n')];
        for jj=1:8 %because there are 8 'core' material properties sections
```

```
          fid = fopen('Parametric.dat','r+');
          ii=raylei_core(jj);
          for k=1:ii-1
            fgetl(fid);
          end
          fseek(fid, 0, 'cof');
          fprintf(fid,'%s\r\n', O);
          fclose(fid);
        end

      %% run DIANA
        command =dos('command.cmd'); % works inside matlab
.
.
.
    end
    dlmwrite([num2str(lambda(n)*10),'-test.dat'],S3_resD,'delimiter','\t','precision','%.5f')
    S3_All{n,1}=S3_resD; S3_All{n,2}=S3_resDX; S3_All{n,3}=S3_resDH;
    S3_All{n,4}=S3_resV; S3_All{n,5}=S3_resVX; S3_All{n,6}=S3_resVH;
  end
  zeta_rayleigh{z}=ray_damp;
  S3_Zeta{z}=S3_All;
  for ii=1:length(S3_All)
    namefile=[num2str(zeta_ratios(z)*10),num2str(lambda(ii)*10),'rho_cto+rho_ctc'];
    for jj=1:length(S3_All(1,:))
      xlswrite(['S3b-',namefile,'.xlsx'],S3_All{ii,jj},jj)
    end
  end
end
```

Main Matlab script for running Diana time-history analyses

```
%%%% script prepared to run set5
%%%% Set5: Energy / Response only by EQ-scale_factor
% lateral confinement + non uniform vertical reinforcement distribution
% optimal lambda / optimal Cd
%% define parametric variables
% +loop confinement: CONF
clc,clear
tic
% earthquake ground motion
EQlevel{1}='small';EQlevel{2}='moderate';EQlevel{3}='strong';EQlevel{4}='severe';
earthquake{1}='elcentro-270'; Ts(1)=0.0050; EQ{1}='Ce-'; scale_factor(1,1:4)=[1.25,2.5,4,6.7]; freq_fact(1)=50;
count(1)=10000; %scale_factor(1,1:4)=[1,2.5,4,6.7];
earthquake{2}='NZ_Greendale-N55W'; Ts(2)=0.020; EQ{2}='Nz-'; scale_factor(2,1:4)=[0.05,0.1,0.15,0.25]; freq_
fact(2)=240; count(2)=10000; %scale_factor(2,1:4)=[0.05,0.1,0.25,0.5];
earthquake{3}='izmit_270'; Ts(3)=0.0050; EQ{3}='Iz-'; scale_factor(3,1:4)=[0.5,1,1.5,2.5]; freq_fact(3)=135;
count(3)=25000; % scale_factor(3,1:4)=[0.5,1,1.5,2]
```

```
earthquake{4}='kobe_90'; Ts(4)=0.020; EQ{4}='Ko-'; scale_factor(4,1:4)=[0.65,1.25,2,3.3]; freq_fact(4)=100;
count(4)=2400;
earthquake{5}='northridge_newhall_90'; Ts(5)=0.020; EQ{5}='Nr-'; scale_factor(5,1:4)=[0.65,1.25,2,3.3]; freq_
fact(5)=100; count(5)=3000;
earthquake{6}='Mexico_n90w'; Ts(6)=0.020; EQ{6}='Mx-'; scale_factor(6,1:4)=[0.8,1.6,2.5,4]; freq_fact(6)=100;
count(6)=9000;
earthquake{7}='concepcion-longitudinal'; Ts(7)=0.0050; EQ{7}='Mc-'; scale_factor(7,1:4)=[0.7,1.4,2.2,3.6]; freq_
fact(7)=100; count(7)=28000;
earthquake{8}='elcentro-180'; Ts(8)=0.0050; EQ{8}='Ce2-'; scale_factor(8,1:4)=[1.4,2.8,4.4,7]; freq_fact(8)=50;
count(8)=10000;
%% FIXED input data
% building properties
story_h=3.5; bldg_h=210;  no=61;           % number of nodes whose response is read
mm(1)=0; mm(2:61)=0.797E+08/(no-1); % linear distribution of mass per story
%% material properties - element sections VARIABLE
BPROF=[4.00000E-01   4.08000E-01   4.08000E-01 2.10000E-02   2.10000E-02   2.10000E-02];
VPROF=[4.98000E-01   4.32000E-01   4.32000E-01 7.00000E-02   7.00000E-02   4.50000E-02];
HPROF=[4.98000E-01   4.32000E-01   4.32000E-01 7.00000E-02   7.00000E-02   4.50000E-02];
[AsB,AsV,AsH]=AsTruss(BPROF,VPROF,HPROF); % function to compute cross-sectional areas of profiles
lnB=5.9; lnV=3.5; lnH=4.75;
As(1:60,1)=47.71; ln(1:60,1)=3.5;  % cross-sectional core
ln(61:72,1)=lnH;
ln(73:80,1)=lnV;
ln(81:88,1)=lnB;
As(61:72,1)=AsH; ln(61:72,1)=lnH;
As(73:80,1)=AsV; ln(73:80,1)=lnV;
As(81:88,1)=AsB; ln(81:88,1)=lnB;
clear BPROF VPROF HPROF lnB lnV lnH AsB AsV AsH
% Tensile / Compressive Strengths
% core non-uniform vertical reinforcement distribution
tenstr(1:6,1)=7.20000E+06; tenstr(7:12,1)=6.00000E+06; tenstr(13:18,1)=5.36000E+06;
tenstr(19:24,1)=5.16000E+06; tenstr(25:30,1)=5.24000E+06; tenstr(31:36,1)=5.24000E+06;
tenstr(37:42,1)=5.04000E+06; tenstr(43:48,1)=4.68000E+06; tenstr(49:54,1)=4.20000E+06;
tenstr(55:60,1)=4.20000E+06;
tenstr(61:88,1)=3.55000E+08;
comstr(1:60,1)=-4.30000E+07; comstr(61:88,1)=-3.55000E+08; % compressive strength core : outrigger elements
  %% storing matrices and cell arrays
  S_energyEQ=zeros(12,length(scale_factor(1,:))); % 12 energies
  Nd=zeros(1,length(scale_factor(1,:))); Nv=zeros(1,length(scale_factor(1,:))); Na=zeros(1,length(scale_
factor(1,:)));
  lg_input2=cell(1,length(scale_factor(1,:)));
  Dr=zeros(3,length(scale_factor(1,:))); Dr2=zeros(3,length(scale_factor(1,:)));  % 3 ratios
  S_maxR=zeros(10,4*length(scale_factor(1,:)));  % for storing max_response (10,4) per each EQ
%% Begin iteration
for n_eq=1:8
  %% storing matrices and cell arrays
  S_dispEQ=zeros(count(n_eq),length(scale_factor(1,:)));
  S_veloEQ=zeros(count(n_eq),length(scale_factor(1,:)));
  S_acceEQ=zeros(count(n_eq),length(scale_factor(1,:)));
%% modify earthquake ground motion levels
      for s_f=1:length(scale_factor(n_eq,:))
        [xg,time]=groundmotion(earthquake{n_eq},Ts(n_eq),scale_factor(n_eq,s_f));
        if n_eq==2
          time=time(750:end,1); xg=xg(750:end,1);
        end
```

```
        if n_eq==3
          time=time(1000:end,1); xg=xg(1000:end,1);
        end
        if n_eq==4
          xg=xg*980; % original record is in gal units
        end
        if n_eq==7
          time=time(1:28338,1); xg=xg(1:28338,1);
        end
        S=sprintf('%.4f ',xg');
        G=[ ' FACTOR ',cellstr(S),' / '];
        fid = fopen('Parametric.dat','r+');
        ii=492; %before it was 486
        for k=1:ii-1
          fgetl(fid);
        end
        fseek(fid, 0, 'cof');
        fprintf(fid,'%s', G{1:3});
        fclose(fid);
    %% run DIANA
        command =dos('command.cmd'); toc % works inside matlab
        heading=['S5-damped-',num2str(scale_factor(n_eq,s_f)*100),'x',EQ{n_eq}];
        [fname,fname0,fname1,fname2,fname3,fname4,fname5,...
          fname7,fname8,fname9,fname10,~,fname13]=renameOUT(heading);
      %% Stresses + Strains
        d = 7; node = 2; intpoint = 2; % DIANA 10 number of integration points (L7BEN has 9)
        noe = 88; % No elements whose response is retrieved FIXED = 90 (1-60:core +61-88:outrigger)
        [SXX,~,EIN,stap]=SSread(d,noe,node,intpoint,fname); clear fname
      %% CRACK Strains
        d=6; noecore = 60; % 1-60:core
        [~,Eh_story,Eh1]=crack_strain(As,ln,tenstr,d,noecore,node,intpoint,stap,fname2); clear fname2%
      %% Crack Energy Distribution
        if max(Eh1)~=0
          [bb,hyst_stories]=sort(Eh_story(:,end),'descend');
          hyst_distribution=bb.*inv(sum(bb));
          hyst_dist=zeros(size(Eh_story));
          for jj=1:length(Eh_story(1,:))
            aa=sum(Eh_story(:,jj));
            for ii=1:length(Eh_story(:,1))
              if aa~=0
                hyst_dist(ii,jj)=Eh_story(ii,jj).*inv(aa);
              end
            end
          end
          figure; plot(time(1:count(n_eq)),hyst_dist);hold all; legend(num2str(hyst_stories));
          tail='Eh_Story Distribution-AsOut';lg_location='NorthEast'; xy_label={'time [s]','Normalized
Hysteretic Energy'}; WH=[17.88, 5.96]; %WH=[17.88, 11.92];
          h=0; lg_input={num2str(hyst_stories(1:10))};
          save_TIFF(heading,tail,lg_input,lg_location,xy_label,WH,h);
          dlmwrite([heading,'Eh_Story Distribution.dat'],[hyst_distribution;hyst_stories],'delimiter','\
t','precision','%s\r\n')
        end
      %% Plastic Strains
        d=7; noe = 88; intpoint = 9;
        [~,Ehdis2,Eh2]=Pstrain(As,ln,comstr,tenstr,d,noe,node,intpoint,stap,fname3); clear fname3
```

```
%% sTRESS COLUMN total
  d = 7; node = 2; intpoint = 1; noe =1;
  [CSXX,~]=CSSread(d,noe,node,intpoint,fname13); clear fname13
%% RESPONSES
   d = 7; nod = 81; % number of nodes whose response is retrievd 81 = DAMPED cause no-DOF supports
  [TrDtX,~,TVtX,TVtY,TAtX,~,FrDX,FrDY]=readDIANA2(d,nod,fname5,fname7); clear fname5 fname7
  fix_sup=2; nodrot=nod-fix_sup;
  [MrDZa,TVrZa]=dvrotaread2(d,nodrot,fname8); clear fname8
  TVrZ=[TVrZa;zeros(fix_sup,length(TVrZa(1,:)))];MrDZ=[MrDZa;zeros(fix_sup,length(MrDZa(1,:)))];
%% FORCES
  d=7; nod2 = 3;[FrBXR,~]=baseforce(d,nod2,fname9); clear fname9
%% MOMENTS
  d=7; [MrBZR]=basemoment(d,fname10); clear fname10
%% Cumulative Energy from DIANA
  noecore=60; d=6;intpoint=9;
  [Wn_dis]=Wnread(d,noecore,node,intpoint,stap,fname0); clear fname0
  Wn=zeros(1,stap);
  for dt=1:stap
    Wn(dt)=sum(abs(Wn_dis(:,dt)));
  end
%% Damping FORCE at dampers
  d = 8; noddamp=2; [FEDYa,~]=dampdamp(d,noddamp,fname1); clear fname1
%% Node forces Axial global
  d = 7; noe=83; [FrNX,FrNY]=nodeforce(d,noe,stap,fname4); clear fname4
%% MAXIMUM RESPONSES
  [max_response]=max_responses10(story_h,bldg_h,TrDtX,TVtX,TAtX,FrBXR,MrBZR,SXX,EIN,CSXX);
%% clearing non-used variables
  clear d dt fix_sup intpoint noddamp node nodrot noe noecore
  [~,~,~,nd,nv,na]=theXmen(nod,TrDtX,TVtX,TAtX);  %function to pick the peaks
  if length(nd)~=1;
    [nd]=manypeaks(nd,heading,TrDtX); %function to save peaks in *.dat
  end
  if length(nv)~=1;
    [nv]=manypeaks(nv,heading,TVtX); %function to save peaks in *.dat
  end
  if length(na)~=1;
    [na]=manypeaks(na,heading,TAtX); %function to save peaks in *.dat
  end
%% Energy Distribution
[Ei,Ek,ED,Edampers,Ea,Edx,Edy,xg,time]=energy_dis(xg,time,stap,mm,TVtX,FrDX,FrDY,MrDZ,TVrZ,FrNX,FrNY,FEDYa,TVtY);
  Eh_crackcore=Eh1*1e-3; Eh=(Eh1+Eh2)*1e-3;
% according to the elastic cat's theory
  if max(Eh)==0
    Es=Ea-Edampers-Edy;
    [amp,stup]=max(Es); Wn=Wn*(amp/Wn(stup));
    clear amp stup
    Es=Wn;
    Ei_ind=Ea+Ek+Edx;
    Eh_plast=0;
  else
    if Ea(end)> ED(end)
      Esh=Ea-ED;
    elseif Ea(end)> Edx(end)
      Esh=Ea-Edx;
      heading=[heading,'S5-dampedX-basedHYST-'];
```

```
          else
            Esh=Ea-Edy;
            heading=[heading,'S5-dampedY-basedHYST-'];
          end
            [Eh,Eh_plast,Es,Wn]=Eh_plast_area(Eh1,Eh2,Esh,Wn);
            Ei_ind=Ek+ED+Es+Eh;
        end
        Ed=ED-Edampers;
        for ii=1:length(Ed);
          if Ed(ii)<0
            Ed(ii)=0;
          end
        end
        if max(Eh_plast)==0
          Eh_plast_core=0;
          Eh_plast_out=0;
        else
          Eh_plast_core=Eh_plast*max(sum(Ehdis2(1:1080,:)))/
(max(sum(Ehdis2(1:1080,:)))+max(sum(Ehdis2(1081:end,:))));
          Eh_plast_out=Eh_plast-Eh_plast_core;
        end
        S_energyEQ(:,s_f)=[Ei(end),Ek(end),max(Ed),max(Edampers),Es(end),max(Eh),...
          max(Edx),max(Edy),max(Eh_crackcore),max(Eh_plast_core),max(Eh_plast_out),Ei_ind(end)];
      % plot normal
        figure
        plot(time,Ei) ; hold all % Relative
        plot(time,Ek) ; hold all % Relative
        plot(time,Ed) ; hold all
        plot(time,Edampers) ; hold all
        plot(time,Es) ; hold all
        plot(time,Eh) ; hold all
        h=0;
        tail='E_dis';lg_location='NorthWest'; xy_label={'time [s]','Energy [kN-m]'}; WH=[17.88, 11.92];
lg_input={'E_I_N_P_U_T','E_K_I_N_E_T_I_C','E_D_A_M_P_I_N_G',
'E_D_A_M_P_E_R_S','E_S_T_R_A_I_N','E_H_Y_S_T_E_R_E_T_I_C'};
        save_TIFF(heading,tail,lg_input,lg_location,xy_label,WH,h);
      % Bertero-type plot
        [l1,l2,l3,l4,l5,l6,l7]=bertero_plot(Ei_ind,Ed,Ek,Es,Edx,Eh,Eh_plast_out,time);
        if max(Eh)==0
          h=[l2 l3];
        else
          h=0;
        end
        tail='BERTERO-E_dis';lg_location='NorthWest'; xy_label={'time [s]','Energy [kN-m]'}; WH=[17.88, 11.92];
        lg_input={'E_I_N_P_U_T','E_H_Y_S_T_E_R_E_T_I_C','E_H_Y_S_T_E_R_E_T_I_C_c_o_r_e',...
'E_D_A_M_P_E_R_S','E_D_A_M_P_I_N_G','E_D_A_M_P_I_N_G_c_o_r_e','E_E_L_A_S_T_I_C_s_t_r_a_i_n'};
        save_TIFF(heading,tail,lg_input,lg_location,xy_label,WH,h);
      % energy ratios
        damping_ratio=Ed./Ei; damping_ratio(1)=0;
        dampers_ratio=Edampers./Ei; dampers_ratio(1)=0;
        hysteretic_ratio=Eh./Ei; hysteretic_ratio(1)=0;
        Dr(:,s_f)=[damping_ratio(end);dampers_ratio(end);hysteretic_ratio(end)];
        figure; plot(time,damping_ratio,time,dampers_ratio,time,hysteretic_ratio); hold all
        tail='E_ratios';lg_location='Best'; xy_label={'time [s]',' '}; WH=[17.88, 11.92]; %WH=[17.88, 11.92];
        h=0; lg_input={'ratio E_D / E_I','ratio E_D_A_M_P_E_R_S / E_I','ratio E_H / E_I'};
```

```
        save_TIFF(heading,tail,lg_input,lg_location,xy_label,WH,h);
      % energy ratios II
        Eddh=ED+Eh;
        damping_ratio2=Ed./Eddh; damping_ratio2(1)=0;
        dampers_ratio2=Edampers./Eddh; dampers_ratio2(1)=0;
        hysteretic_ratio2=Eh./Eddh; hysteretic_ratio2(1)=0;
        Dr2(:,s_f)=[damping_ratio2(end);dampers_ratio2(end);hysteretic_ratio2(end)];
        figure; plot(time,damping_ratio2,time,dampers_ratio2,time,hysteretic_ratio2); hold all
        tail='E_ratios2';lg_location='Best'; xy_label={'time [s]',' '}; WH=[17.88, 11.92];
        h=0; lg_input={'ratio E_D / E_D+E_D_A_M_P_E_R_S+E_H','ratio E_D_A_M_P_E_R_S / E_D+E_D_A_M_P_E_R_
S+E_H','ratio E_H / E_D+E_D_A_M_P_E_R_S+E_H'};
        save_TIFF(heading,tail,lg_input,lg_location,xy_label,WH,h);
      %% Fast Fourier Transformation
        min_freq=0; max_freq=30; WH=[17.88, 11.92];
        fft_plotting(TVtY,TrDtX,min_freq,max_freq,freq_fact,Ts(n_eq),time,heading,WH);
        min_freq=0; max_freq=5; WH=[17.88, 11.92]; heading2=[heading,'close-up'];
        fft_plotting(TVtY,TrDtX,min_freq,max_freq,freq_fact,Ts(n_eq),time,heading2,WH);
        close all
      %% matrices for saving max. responses
        S_dispEQ(:,s_f)=TrDtX(nd,:)'; S_veloEQ(:,s_f)=TVtX(nv,:)'; S_acceEQ(:,s_f)=TAtX(na,:)';
        Nd(s_f)=nd; Nv(s_f)=nv; Na(s_f)=na;
        S_maxR(:,4*s_f-3:4*s_f)=max_response;
      %% saving data
        df_name=['S5-',EQ{n_eq},EQlevel{s_f}];
        save(df_name)
      end
end
toc
```

Appendix D Diana files

Input file Diana 10.1 - reduced

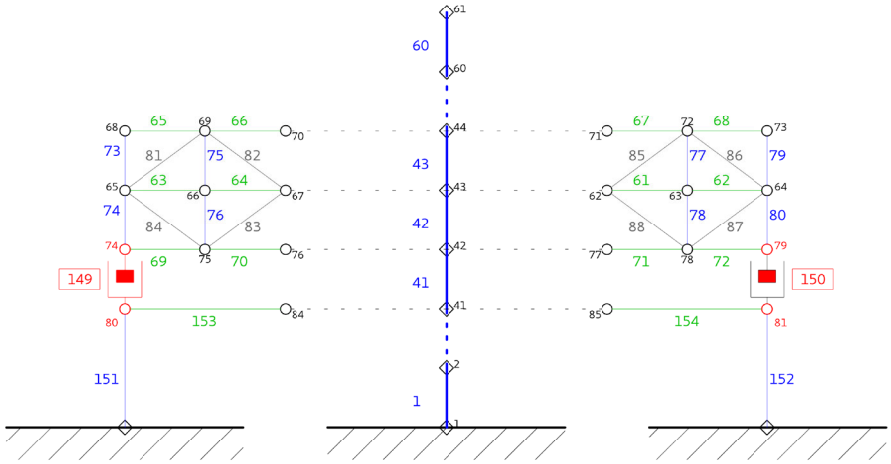

FIGURE APP.D.1 FE model of the single damped outrigger configuration

: DIANA datafile written by DIANA 10.1 (latest update: 2016-09-27)
FEMGEN MODEL : DAMP2DBUILD
ANALYSIS TYPE : Structural 2D
'UNITS'
[...]
'COORDINATES' DI=2
1 0.000000E+00 0.000000E+00
[..]
61 0.000000E+00 2.100000E+02
: OUTRIGGER + dampers
62 9.000000E+00 1.470000E+02
[...]
81 1.900000E+01 1.400000E+02
: + columns
82 -1.900000E+01 0.000000E+00
83 1.900000E+01 0.000000E+00

```
: story beams slave nodes 0.5*H
84 -9.000000E+00 1.400000E+02
85 9.000000E+00 1.400000E+02
'ELEMENTS'
CONNECTIVITY
1 L7BEN 1 2
[...]
88 L7BEN 78 62
89 PT3T 2
[...]
148 PT3T 61
149 SP2TR 74 80
150 SP2TR 79 81
151 L4TRU 80 82
152 L4TRU 81 83
: + story 'beams' at the dampers level
153 L6BEN 80 84
154 L6BEN 81 85
MATERIALS
/ 1-6 / 7
[...]
/ 153 154 / 5
GEOMETRY
/ 1-60 / 5
[...]
/ 153 154 / 4
'MATERIALS'
1 NAME REDCON
[...]
14 NAME CONCR7
'GEOMETRY'
1 NAME BPROF
[...]
6 NAME CROSSE
'GROUPS'
ELEMEN
1 VERT / 73-80 /
[...]
12 DAMP_N / 74 79-81 /
'SUPPORTS'
[...]
'TYINGS'
[...]
'LOADS'
CASE 1
BASE
1 1.00
: Izmit-Kocaeli Koer-90 Earthquake time steps=0.0050 s; 26164 data: 60s = 12000 steps
'TIMELO'
LOAD 1
TIMES 0.000 0.005
[...]
FACTOR -0.0006 -0.0003
[...]
'DIRECTIONS'
```

```
1 1.000000E+00 0.000000E+00 0.000000E+00
2 0.000000E+00 1.000000E+00 0.000000E+00
3 0.000000E+00 0.000000E+00 1.000000E+00
'END'
```

Analysis command file

```
*FILOS
INITIA
*INPUT
*NONLIN LABEL="Structural nonlinear"
BEGIN TYPE
GEOMET
BEGIN TRANSI
METHOD NEWMAR
BEGIN DYNAMI
MASS LUMPED
DAMPIN
RELBAC ON
END DYNAMI
END TRANSI
END TYPE
BEGIN EXECUT
BEGIN TIME
BEGIN STEPS
BEGIN ITERAT
INISIZ 0.005
NSTEPS 25000
END ITERAT
END STEPS
END TIME
ITERAT METHOD SECANT LINEAR
LOGGIN REPORT FULL
END EXECUT
SOLVE AUTOMA
BEGIN OUTPUT
:damping force+displacements
[...]
END OUTPUT
BEGIN OUTPUT
:velocity+accelerations
[...]
END OUTPUT
BEGIN OUTPUT
: dampers cd
[...]
END OUTPUT
BEGIN OUTPUT
: base shear
```

```
[...]
END OUTPUT
BEGIN OUTPUT
: overturning moment
[...]
END OUTPUT
BEGIN OUTPUT
: local stress-strain core+outrigger
[...]
END OUTPUT
BEGIN OUTPUT
:cumulative energy
[...]
END OUTPUT
BEGIN OUTPUT
: local stress-strain columns
[...]
END OUTPUT
BEGIN OUTPUT
:strain crack core"
[...]
END OUTPUT
BEGIN OUTPUT
plastic strain core-outrigger
[...]
END OUTPUT
BEGIN OUTPUT
: node forces
[...]
END OUTPUT
*END
```

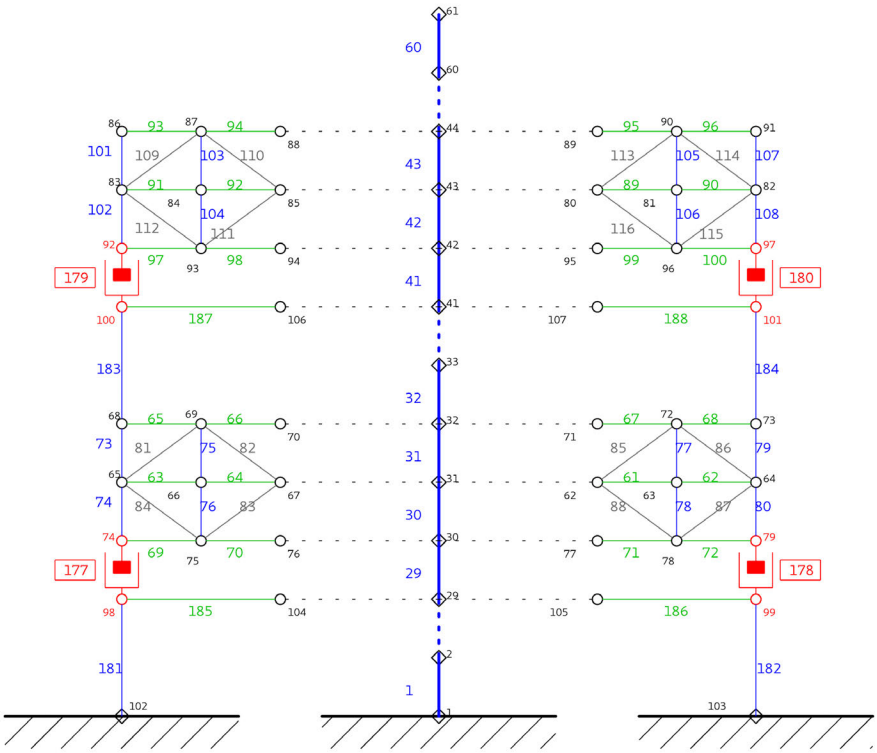

FIGURE APP.D.2 FE model of the double damped outrigger configuration

: Diana Datafile written by Diana 10.1
FEMGEN MODEL : DAMP2DBUILD
ANALYSIS TYPE : Structural 2D
'MODEL'
...
'COORDINATES'
1 0.00000E+00 0.00000E+00 0.00000E+00
...
107 9.00000E+00 1.61000E+02 0.00000E+00
'MATERI'
...
'GEOMET'
...
'ELEMENTS'

```
CONNECT
1 L7BEN 1 2
...
188 L6BEN 101 107
'LOADS'
CASE 1
BASE
1 1.00000E+00
'SUPPOR'
...
'TYINGS'
...
'TIMELO'
LOAD 1
TIMES 0.00000E+00 ... 5.37300E+01 /
FACTOR 5.90000E-02 ... 1.80000E-02 /
'END'
```

Appendix E Peak responses – Single, double and combined damped outrigger systems

Peak inter-storey drift response locations

	STOREY				TIME (S)			
EQ \ EQ LEVEL	Small	Moderate	Strong	Severe	Small	Moderate	Strong	Severe
Izmit-Kocaeli	59	59	58	59	9.9	9.9	9.9	10.0
Michoacan	58	58	60	53	60.1	60.1	60.1	60.1
El Centro - 270	59	57	59	59	9.9	9.9	9.9	13.6
El Maule	58	59	60	57	14.5	14.5	14.5	22.4
Northridge	59	59	58	57	7.7	7.8	7.7	7.8
New Zealand	57	57	58	59	16.6	16.6	16.6	17.2
Kobe	58	58	60	60	9.0	9.0	9.1	9.1
El Centro - 180	59	58	60	56	2.8	2.8	2.8	2.8

TABLE APP.E.1 Peak inter-storey drift response locations - Single Damped Outrigger

	STOREY				TIME (S)			
EQ \ EQ LEVELS	Small	Moderate	Strong	Severe	Small	Moderate	Strong	Severe
Izmit-Kocaeli	58	60	59	57	9.9	9.9	9.9	10.0
Michoacan	59	60	59	57	60.1	60.1	60.1	58.9
El Centro - 270	59	55	59	60	9.9	9.9	9.9	13.5
El Maule	58	60	59	58	14.5	14.5	14.5	22.4
Northridge	60	60	60	60	7.8	7.7	7.7	7.8
New Zealand	60	59	55	59	16.6	16.6	16.6	17.1
Kobe	57	58	57	58	9.0	9.0	9.0	9.1
El Centro - 180	59	56	58	59	2.8	2.8	2.8	2.8

TABLE APP.E.2 Peak inter-storey drift response locations - Double Damped Outrigger

	STOREY				TIME (S)			
EQ \ EQ LEVELS	Small	Moderate	Strong	Severe	Small	Moderate	Strong	Severe
Izmit-Kocaeli	60	57	60	59	9.8	9.9	9.9	10.0
Michoacan	58	58	56	54	60.1	60.1	60.1	59.0
El Centro - 270	60	55	59	59	9.9	9.9	10.0	13.5
El Maule	60	60	59	59	14.5	14.5	14.5	22.4
Northridge	58	57	59	57	7.8	7.8	7.7	7.8
New Zealand	59	56	58	60	14.5	14.5	16.6	17.2
Kobe	58	60	56	58	9.0	9.0	9.0	9.1
El Centro - 180	58	59	60	56	2.8	2.8	2.8	2.8

TABLE APP.E.3 Peak inter-storey drift response locations - Combined Damped + Fixed Outrigger

Peak acceleration response locations

Node number corresponds to the upper node of the element representing the core portion of a storey. Hence 61 is the roof of the 60th storey and 32, the floor between 31st and 32nd storeys.

	NODE				TIME (S)			
EQ \ EQ LEVELS	Small	Moderate	Strong	Severe	Small	Moderate	Strong	Severe
Izmit-Kocaeli	61	61	61	61	12.0	12.0	12.0	10.0
Michoacan	61	61	61	61	58.8	58.8	58.8	58.8
El Centro - 270	61	61	61	61	2.7	2.7	2.7	2.7
El Maule	61	61	61	61	14.9	14.9	14.9	20.6
Northridge	61	61	61	61	5.7	5.7	5.7	5.7
New Zealand	61	61	61	61	9.8	9.8	0.0	9.8
Kobe	61	61	32	32	9.9	9.9	8.6	8.6
El Centro - 180	61	61	61	61	4.1	4.1	4.1	2.3

TABLE APP.E.4 Peak acceleration response locations – Single Damped Outrigger

	NODE				TIME (S)			
EQ \ EQ LEVELS	Small	Moderate	Strong	Severe	Small	Moderate	Strong	Severe
Izmit-Kocaeli	61	61	61	61	11.9	11.9	12.0	10.0
Michoacan	61	61	61	61	58.8	58.8	58.8	58.8
El Centro - 270	61	61	61	61	2.7	2.7	2.7	2.7
El Maule	61	61	61	61	14.9	14.9	14.9	14.9
Northridge	61	61	61	61	5.7	5.7	5.7	5.7
New Zealand	61	61	61	61	9.8	9.8	9.8	9.9
Kobe	61	61	32	32	8.7	8.7	8.6	8.6
El Centro - 180	61	61	61	61	4.1	4.1	4.1	4.2

TABLE APP.E.5 Peak acceleration response locations - Double Damped Outrigger

	NODE				TIME (S)			
EQ \ EQ levels	Small	Moderate	Strong	Severe	Small	Moderate	Strong	Severe
Izmit-Kocaeli	61	61	61	61	12.0	12.0	12.0	10.0
Michoacan	61	61	61	61	58.8	58.8	58.8	58.8
El Centro - 270	61	61	61	61	2.7	2.7	2.7	2.7
El Maule	61	61	61	61	14.9	14.9	14.9	20.6
Northridge	61	61	61	61	5.7	5.7	5.7	5.7
New Zealand	61	61	61	61	9.8	9.8	9.8	9.8
Kobe	61	61	32	32	8.7	8.7	8.6	8.6
El Centro - 180	61	61	61	61	4.1	4.1	4.1	4.2

TABLE APP.E.6 Peak acceleration response locations - Combined Damped + Fixed Outrigger

Distribution of peak levels of stress in outrigger and core elements

T and *C* are tensile and compressive stress, respectively.

EQ LEVELS	SMALL		MODERATE		STRONG		SEVERE	
EQ	T	C	T	C	T	C	T	C
Izmit-Kocaeli	67	66	67	66	66	66	66	82
Michoacan	66	67	66	67	67	67	67	85
El Centro - 270	67	66	67	66	66	82	67	85
El Maule	67	66	67	66	67	66	67	67
Northridge	67	66	67	66	67	66	66	66
New Zealand	66	67	66	67	66	67	66	82
Kobe	66	67	66	66	67	67	66	67
El Centro - 180	66	67	66	67	67	67	66	82

TABLE APP.E.7 Distribution of peak stress levels in the outrigger elements - Single Damped Outrigger

EQ LEVELS	SMALL		MODERATE		STRONG		SEVERE	
EQ	T	C	T	C	T	C	T	C
Izmit-Kocaeli	80	80	80	66	80	66	74	82
Michoacan	80	74	80	74	80	74	80	74
El Centro - 270	80	74	80	74	80	74	66	80
El Maule	74	80	74	80	74	80	80	74
Northridge	74	80	74	80	74	74	80	74
New Zealand	80	74	80	74	80	67	74	66
Kobe	70	71	70	71	74	80	71	70
El Centro - 180	80	74	80	74	71	74	74	74

TABLE APP.E.8 Distribution of peak stress levels in the outrigger elements - Double Damped Outrigger

EQ LEVELS	SMALL		MODERATE		STRONG		SEVERE	
EQ	T	C	T	C	T	C	T	C
Izmit-Kocaeli	80	74	80	74	74	74	74	82
Michoacan	80	74	80	74	80	74	80	74
El Centro - 270	80	74	80	74	80	74	80	74
El Maule	74	80	74	80	74	80	80	74
Northridge	80	74	80	74	80	74	80	74
New Zealand	74	74	74	80	74	74	74	74
Kobe	71	70	71	70	71	74	71	88
El Centro - 180	71	70	71	70	71	80	74	74

TABLE APP.E.9 Distribution of peak stress levels in the outrigger elements - Combined Damped + Fixed Outrigger

	SINGLE				DOUBLE				COMBINED			
EQ LEVELS	Strong		Severe		Strong		Severe		Strong		Severe	
EQ	T	C	T	C	T	C	T	C	T	C	T	C
Izmit-Kocaeli	5	1	6	1	4	1	6	1	4	1	6	1
Michoacan	1	1	1	1	1	1	1	1	1	1	1	1
El Centro - 270	6	1	6	1	5	1	6	1	6	1	6	1
El Maule	1	1	1	1	1	1	1	1	1	1	1	1
Northridge	1	1	1	1	1	1	1	1	1	1	1	1
New Zealand	1	1	6	1	1	1	6	1	1	1	6	1
Kobe	1	1	1	1	1	1	1	1	1	1	1	1
El Centro - 180	3	1	6	1	1	1	5	1	4	1	4	1

TABLE APP.E.10 Distribution of peak stress levels in the core elements

Peak core stress was concentrated in the element 1 for the small and moderate levels of all earthquakes.

Storey shear and overturning moment envelopes

	SINGLE		DOUBLE		COMBINED	
STOREY	V [kN]	OTM [kNm]	V [kN]	OTM [kNm]	V [kN]	OTM [kNm]
1 - 6	7.55E+04	2.09E+05	5.65E+04	1.56E+05	5.88E+04	1.63E+05
7	7.39E+04	2.05E+05	5.53E+04	1.54E+05	5.76E+04	1.60E+05
8	7.23E+04	2.02E+05	5.41E+04	1.51E+05	5.63E+04	1.57E+05
9	7.07E+04	1.98E+05	5.30E+04	1.49E+05	5.51E+04	1.55E+05
10	6.92E+04	1.95E+05	5.18E+04	1.46E+05	5.39E+04	1.52E+05
11	6.76E+04	1.91E+05	5.06E+04	1.43E+05	5.27E+04	1.49E+05
12	6.60E+04	1.88E+05	4.94E+04	1.41E+05	5.14E+04	1.46E+05
13	6.45E+04	1.84E+05	4.83E+04	1.38E+05	5.02E+04	1.44E+05
14	6.29E+04	1.81E+05	4.71E+04	1.36E+05	4.90E+04	1.41E+05
15	6.13E+04	1.78E+05	4.59E+04	1.33E+05	4.78E+04	1.38E+05
16	5.97E+04	1.74E+05	4.47E+04	1.30E+05	4.65E+04	1.36E+05
17	5.82E+04	1.71E+05	4.35E+04	1.28E+05	4.53E+04	1.33E+05
18	5.66E+04	1.67E+05	4.24E+04	1.25E+05	4.41E+04	1.30E+05
19	5.50E+04	1.64E+05	4.12E+04	1.22E+05	4.29E+04	1.27E+05
20	5.35E+04	1.60E+05	4.00E+04	1.20E+05	4.16E+04	1.25E+05
21	5.19E+04	1.57E+05	3.88E+04	1.17E+05	4.04E+04	1.22E+05
22	5.03E+04	1.53E+05	3.77E+04	1.15E+05	3.92E+04	1.19E+05
23	4.87E+04	1.50E+05	3.65E+04	1.12E+05	3.80E+04	1.17E+05
24	4.72E+04	1.46E+05	3.53E+04	1.09E+05	3.67E+04	1.14E+05
25	4.56E+04	1.43E+05	3.41E+04	1.07E+05	3.55E+04	1.11E+05
26	4.40E+04	1.39E+05	3.30E+04	1.04E+05	3.43E+04	1.08E+05
27	4.24E+04	1.36E+05	3.18E+04	1.02E+05	3.31E+04	1.06E+05
28	4.09E+04	1.32E+05	3.06E+04	9.90E+04	3.18E+04	1.03E+05
29	3.93E+04	1.29E+05	2.94E+04	9.64E+04	3.06E+04	1.00E+05
30	3.77E+04	1.25E+05	2.82E+04	9.38E+04	2.94E+04	9.76E+04
31	3.77E+04	1.10E+05	2.82E+04	8.23E+04	2.94E+04	8.56E+04
32	3.77E+04	1.06E+05	2.82E+04	7.97E+04	2.94E+04	8.29E+04
33	3.77E+04	1.03E+05	2.82E+04	7.71E+04	2.94E+04	8.02E+04
34	3.77E+04	9.94E+04	2.82E+04	7.45E+04	2.94E+04	7.75E+04
35	3.77E+04	9.60E+04	2.82E+04	7.18E+04	2.94E+04	7.48E+04
36	3.77E+04	9.25E+04	2.82E+04	6.92E+04	2.94E+04	7.21E+04
37	3.77E+04	8.90E+04	2.82E+04	6.66E+04	2.94E+04	6.94E+04
38	3.77E+04	8.55E+04	2.82E+04	6.40E+04	2.94E+04	6.66E+04

>>>

	SINGLE		DOUBLE		COMBINED	
STOREY	V [kN]	OTM [kNm]	V [kN]	OTM [kNm]	V [kN]	OTM [kNm]
39	3.77E+04	8.20E+04	2.82E+04	6.14E+04	2.94E+04	6.39E+04
40	3.77E+04	7.86E+04	2.82E+04	5.88E+04	2.94E+04	6.12E+04
41	3.77E+04	7.51E+04	2.82E+04	5.62E+04	2.94E+04	5.85E+04
42	3.77E+04	7.16E+04	2.82E+04	5.36E+04	2.94E+04	5.58E+04
43	3.77E+04	6.81E+04	2.82E+04	5.10E+04	2.94E+04	5.31E+04
44	3.77E+04	6.46E+04	2.82E+04	4.84E+04	2.94E+04	5.04E+04
45	3.77E+04	6.12E+04	2.82E+04	4.58E+04	2.94E+04	4.77E+04
46	3.77E+04	5.77E+04	2.82E+04	4.32E+04	2.94E+04	4.49E+04
47	3.77E+04	5.42E+04	2.82E+04	4.06E+04	2.94E+04	4.22E+04
48	3.77E+04	5.07E+04	2.82E+04	3.80E+04	2.94E+04	3.95E+04
49	3.77E+04	4.72E+04	2.82E+04	3.54E+04	2.94E+04	3.68E+04
50	3.77E+04	4.38E+04	2.82E+04	3.28E+04	2.94E+04	3.41E+04
51	3.77E+04	4.03E+04	2.82E+04	3.02E+04	2.94E+04	3.14E+04
52	3.77E+04	3.68E+04	2.82E+04	2.75E+04	2.94E+04	2.87E+04
53	3.77E+04	3.33E+04	2.82E+04	2.49E+04	2.94E+04	2.60E+04
54	3.77E+04	2.98E+04	2.82E+04	2.23E+04	2.94E+04	2.32E+04
55	3.77E+04	2.64E+04	2.82E+04	1.97E+04	2.94E+04	2.05E+04
56	3.77E+04	2.29E+04	2.82E+04	1.71E+04	2.94E+04	1.78E+04
57	3.77E+04	1.94E+04	2.82E+04	1.45E+04	2.94E+04	1.51E+04
58	3.77E+04	1.59E+04	2.82E+04	1.19E+04	2.94E+04	1.24E+04
59	3.77E+04	1.24E+04	2.82E+04	9.31E+03	2.94E+04	9.69E+03
60	3.77E+04	8.95E+03	2.82E+04	6.70E+03	2.94E+04	6.97E+03

Appendix F Average distance between central core and perimeter columns in Chilean office buildings

The following table has been prepared based on the information given by Prieto Hoces (2011).

BUILDING NAME	STOREYS	AVERAGE DISTANCE CORE - BUILDING ENVELOPE (M)
cruz del sur	21	8.4
isidora 3000	31	9
metropolis	22	8.15
matta	22	10.6
edificio de las artes	22	11.1
parque sur	22	12.2
isidora foster	23	9.2
parque andino	22	9.8
neruda	24	9.9
isidora magdalena	26	10.5
mistral	23	10
corp-group	24	10
titanium	52	10
	average	9.91

TABLE APP.F.1 Average distance core-perimeter columns in Chilean office buildings

Curriculum Vitae

Mauricio Morales-Beltran was born on June 27, 1974 in Santiago de Chile. In 1999, he graduated as an Architect in *Universidad Catolica del Norte* (UCN), in Antofagasta, Chile. His graduation project dealt with the relationship between technology and architectural design in extreme environments. He continued the explorations in the bound architecture-structure as lecturer in the same faculty he graduated from (UCN). There he delivered courses about structures and participated in design studios as instructor, along free-lance activities as architect. In 2006, in parallel to his work as lecturer, Mauricio started his master studies in Universidad Mayor in Santiago de Chile. In 2008 he graduated in Seismic Design of Buildings. Shortly after, he began working as structural engineer in a few projects led by his former architect colleagues.

In 2011, Mauricio moved to the Netherlands, to integrate the former Architectural Engineering chair, in BK at TU Delft. During the first two years of PhD studies, he conducted research in the field of adaptive structures in a seismic context. In 2013, due to the move of his former supervisor and the incorporation of a new one, the topic of the research shifted to the use of innovative passive and semiactive strategies for seismic control of buildings. During this period, Mauricio collaborated in a few master

theses as technical mentor. In 2014, while continuing his PhD research, he moved to Turkey to join the Faculty of Architecture at Yaşar University in Izmir, as a senior lecturer teaching undergraduate design studios and courses about structures.

Apart from all this academic performance, Mauricio likes to practice outdoor activities. Between 1995 and 2000, he performed several bike trips through the Atacama Desert (Chile) and amateur climbing activities in the same area. In 2001, he joined the UCN mountaineering club, becoming team leader of about 20 expeditions and director of the club between 2003 and 2006. Until 2010, when he left the club, he had climbed more than 50 mountains in the Andes, most of them with more than 6,000m altitude and some of them, in solitary. After moved to NL, Mauricio found no mountains but plenty of cycle paths, so he decided to travel everywhere –literally- by using a bike. In 2011, he toured the circuit The Hague – Mons – Paris – Basel – Karlsruhe – Keulen – Monchengladbach (~400km, 29 days), breaking the bicycle in this last city. In July 2013, he travelled Delft- Roermond – Koblenz – Stuttgart – Kempten – Imst – Nauders – Bozen – Cortina d'ampezzo – Venice – Ancona – Bari – Corfu island (Ferry) – Igoutmenitsa – Metsovo – Meteora – Larisa (~1,600km, 46 days), breaking the bicycle near the last city, again. Both trips were made alone and without GPS.

List of publications

Journal articles

Morales-Beltran M, Turan G, Dursun O, Nijsse R. (2018) Energy dissipation and performance assessment of double damped outriggers in tall buildings under strong earthquakes, under review in *The Structural Design of Tall and Special Buildings*

Morales-Beltran M, Turan G, Yildirim U, Paul J. (2018) Distribution of strong earthquake input energy in tall buildings equipped with damped outriggers. *The Structural Design of Tall and Special Buildings*; e1463. *https://doi.org/10.1002/tal.1463*

Morales-Beltran M, Paul J. (2015) Technical note: Active and semi-active strategies to control building structures under large earthquake motion, *Journal of Earthquake Engineering*, Volume 19, Issue 7 *http://dx.doi.org/10.1080/13632469.2015.1036 26*

Morales-Beltran M, Teuffel P. (2013) Towards smart building structures: adaptive structures in earthquake and wind loading control response – a review, *Intelligent Buildings International*, Volume 5, Issue 2 *http://dx.doi.org/10.1080/17508975.20 3.778193*

Book chapter

Cevizci E, Kutucu S, Morales-Beltran M, Ekici B, Tasgetiren M. F. (2018) *Structural Optimization for Masonry Shell Design Using Multi-Objective Evolutionary Algorithms*, accepted for publication in "Optimization in Industry - Present Practices and Future Scopes" by S. Datta and J. P. Davim Editors, Series: Management and Industrial Engineering, Springer.

Conference articles

Morales-Beltran M, Turan G, Yildirim U. Distribution of earthquake input energy in high-rise buildings with viscously damped outriggers, *4th International Conference on Earthquake Engineering and Seismology,* 12pp, Eskisehir, Turkey, October 11-13, 2017 http://www.tdmd.org.tr/TR/Genel/4UDMSK/pdf2017/3245.pdf

Morales-Beltran M, Turan G, Yildirim U. Distribution of large-earthquake input energy in viscous damped outrigger structures, Proceedings of the *16th World Conference on Earthquake Engineering, (16WCEE),* 13pp, Santiago, Chile, January 9-13, 2017 uuid:8b881f19-d32e-4053-a8d2-f92a8dd74a0e

Morales-Beltran M. Effective integration architecture-seismic design in teaching practice: elementary school design as case study, Proceedings of the *16th World Conference on Earthquake Engineering, (16WCEE)*, 10pp, Santiago, Chile, January 9-13, 2017

Morales-Beltran M. Integrating architectural and seismic design of buildings in teaching practice, *3rd Turkish Conference on Earthquake Engineering and Seismology*, 10pp, Izmir, Turkey, October 14-16, 2015. http://www.tdmd.org.tr/TR/Genel/pdf2015/TDMSK_243.pdf

Mostafavi S, Morales-Beltran M, Biloria N. Performance driven design and design information exchange, *Computation and Performance – Proceedings of the 31st International Conference on education and research in Computer Aided Architectural Design in Europe (eCAADe)*(ed. R. Stouffs and S. Sariyildiz), Volume 2, pp. 117 – 126, TU Delft, the Netherlands, 18-20 September 2013. uuid:63b06620-8753-4db7-ab6b-f36f9636bd69

Morales-Beltran M, Teuffel P. Towards adaptive structures: State-of-the-art in active structures for seismic response, *Smart Structures: Proceedings of the 5th European Conference on Structural Control (EACS)* (ed. A. Del Grosso and P. Basso), 13pp, Genoa, Italy, June 2012

Morales-Beltran M, Borgart A. Teaching Structures with Models: Experiences from Chile and The Netherlands, *IASS-APCS 2012 Symposium: From Spatial Structures to Space Structures*, 11pp, Seoul, Korea, 2012. uuid:0013b5e1-cb91-485f-b43d-04ab35aedb09

Morales-Beltran M, Teuffel P. Adaptable earthquake-resistant structural building system, *IABSE- IASS 2011 Symposium: Taller, Longer, Lighter: Meeting growing demand with limited resources*, 8pp, London, UK, 2011